University of Namur

THESIS / THÈSE

**DOCTOR OF SCIENCES**

# Small molecules as therapeutic options for Parkinson's disease case of modulators of UCH-L1 and GLP-1 receptor

Mambourg, Kalina

*Award date:*
2022

*Awarding institution:*
University of Namur

Link to publication

UNIVERSITÉ
DE NAMUR

FACULTÉ
DES SCIENCES

# Small molecules as therapeutic options for Parkinson's disease: case of modulators of UCH-L1 and GLP-1 receptor

A thesis submitted by **Kalina MAMBOURG**
for the fulfilment of the requirements
for the degree of Doctor in Sciences

**Thesis Committee:**

Dr. Catherine Michaux (Université de Namur, president of the thesis committee)

Prof. Johan Wouters (Université de Namur, advisor)

Dr. Javier Garcia-Ladona (Abaxys Therapeutics S.A.)

Prof. Tom Leyssens (Université Catholique de Louvain-La-Neuve)

Prof. Steve Lanners (Université de Namur)

**March 2022**

Université de Namur
FACULTE DES SCIENCES
Rue de Bruxelles, 61 – 5000 Namur, Belgique

# Petites molécules comme agents thérapeutiques contre la maladie de Parkinson : cas des modulateurs d'UCH-L1 et du récepteur de GLP-1

par **Kalina Mambourg**

## Résumé

La maladie de Parkinson (PD) est une maladie neurodégénérative progressive du système nerveux central qui induit une perturbation des fonctions motrices du corps humain. Les traitements actuels sont effectifs uniquement contre les symptômes moteurs et ne limitent pas la progression de la maladie. Il est donc très important d'identifier des nouveaux traitements qui modifient la progression de PD. La présente thèse de doctorat a centré la recherche sur deux cibles thérapeutiques : la déubiquitinase UCH-L1 et le récepteur GLP-1 (GLP-1R). UCH-L1 est impliquée dans le système ubiquitine-protéasome, étroitement liée à la modification des protéines cellulaires et a été associée génétiquement à PD. Le GLP-1R est un modulateur du métabolisme glucidique par la sécrétion d'insuline et dont l'activité a démontré des effets neuroprotecteurs dans les modèles PD. L'utilisation de composés actifs pour ces protéines pourrait réduire la progression de PD. L'objectif de cette thèse est d'identifier et d'étudier les propriétés et les interactions moléculaires de petites molécules modulatrices d'UCH-L1 et de GLP-1R, deux protéines cibles impliquées dans le développement de PD.

La recherche conduite dans le présent travail a permis de :
(i) Synthétiser et formuler un dérivé du 1,2,4-oxadiazole, agoniste du GLP-1R, en présence de saccharine et acide citrique résultant en un système co-amorphe.

(ii) Etudier l'interaction *in silico* et *in vitro* des composés dérivés d'alanylpipéridine avec UCH-L1. La salification de ces composés a ensuite été utilisée comme méthode pour moduler la solubilité.

(iii) Caractériser *in silico* et *in vitro* un orthologue de la protéine UCH-L1 humaine, UCH-L1 *zébrafish*, et d'étudier les comportements de ces deux protéines vis-à-vis d'une même liste de ligands.

Dissertation doctorale en Sciences Chimiques

**Namur, Mars 2022**

Université de Namur
FACULTE DES SCIENCES
Rue de Bruxelles, 61 – 5000 Namur, Belgium

# Small molecules as therapeutic options for Parkinson's disease: case of modulators of UCH-L1 and GLP-1 receptor

by **Kalina Mambourg**

## Abstract

Parkinson's disease (PD) is a chronic and progressive neurodegenerative disorder of the central nervous system inducing severe motor disturbance. The current available treatments are effective for relieving motor symptoms but they do not alter the progression of the disease. Subsequently, there is an urgent need to develop disease modifying therapies that address the neurodegenerative processes. During the present PhD thesis, we have been investigating: the deubiquitinase UCH-L1 and GLP-1 receptor (GLP-1R). UCH-L1 is involved in the ubiquitin-proteasome system modulating the integrity of cellular proteins. The GLP-1R promotes insulin secretion and has shown neuroprotective properties in PD models. Combining ligands with these proteins can impact the progression of PD. Therefore, the objective of this thesis is to study small molecules acting as ligands of UCH-L1 and GLP-1R, two protein targets that are involved in the development of PD.

The research conducted during this work allowed us to:
(i) Synthesize and formulate a derivative of 1,2,4-oxadiazole, an agonist of GLP-1R, as a co-amorphous system with saccharin or citric acid.

(ii) Investigate alanylpiperidine derivatives as activators of UCH-L1 *in silico* and *in vitro*. The salification of these compounds was then studied in order to increase their solubility.

(iii) Characterize *in silico* et *in vitro* an ortholog of UCH-L1 human protein, zebrafish UCH-L1, and to study the behavior of these proteins towards similar ligands.

PhD thesis in Chemistry

**Namur, March 2022**

*To Мария*

*At the end of this thesis, I would like to take the opportunity to thank all people who in one way or another have contributed to the thesis work.*

*First of all, I would like to thank my supervisor* **Prof. Johan Wouters** *for not only providing me with the opportunity to work in the CBS lab but also for all his support and his guidance on the project.*

*My gratitude also goes to* **Dr. Javier-Garcia Ladona** *of Abaxys Therapeutics for mentoring me and actively participating in this work.*

*To* **Prof. Steve Lanners***, member of my advisory committee who supervised me during my work in organic chemistry, I extend my gratitude for the fruitful discussions and good advice.*

*I would like to thank the member of my thesis jury for the discussions and most importantly all their advice during the private defense. I also thank them for their careful reading of the thesis (***Dr. Catherine Michaux***,* **Prof. Johan Wouters***,* **Dr. Javier Garcia-Ladona***,* **Prof. Tom Leyssens** *and* **Prof. Steve Lanners***).*

*Furthermore, I thank the URBM for letting us work in their lab. Especially, I thank* **Françoise***,* **Aurélie** *and* **Mathieu** *who always helped us when needed and also Régis Hallez's students for their good mood. Our colleague in the IT department,* **Laurent***, I thank for his precious help and for providing us with a homeworking possibility during the covid lockdown period.*

*Many thanks to* **Corry** *for guidance and support with the electronic microscope SEM as well as the* $PC^2$ *platform for access to all the instrumentation throughout these three years of PhD.*

*I thank also* **Nikolay** *and* **Laurie** *for their help and advice on single-crystal or powder X-ray diffraction results.*

*Thank you to the members of the COS laboratory for warmly welcoming me in the lab as if I was still one of theirs.*

*I would also like to thank the 5th floor for welcoming me during lunches and for the celebrations as if I was one of theirs.*

*What would a PhD be without the coworkers? Many thanks to all my fellow CBS lab coworkers (past and present) for the pleasant time spent together and the food related discussions we regularly had. To* **Marie** *and* **Laurie***, the inseparable two who assisted me in my coffee addiction.* **Mégane***, for her patience towards me, her office neighbor, throughout these three years and for sharing my sense of humor.* **Manon***, who I knew from KFS but who I came to know better, I would like to thank for all the good time in the lab (and elsewhere). Finally, I would like to thank* **Elise***, my buddy since first year of chemistry, who made this journey funnier; for all the laughter and chats in the lab but also for her support during this work.*

*I would also like to thank the students present in the lab during my last year of PhD for the lovely atmosphere that they brought with them (hihi). It helped me during the writing process, not only to distract me but also to motivate me as the end got nearer.*

*I would like to thank the students that contributed to this work. First, **Simon** with his enthusiasm that made the teaching easy. Second, I thank **Gilles**, a toddler that grew to become a teenager during his master thesis. As he said to me at the first opportunity when he was drunk «Finalement, les mémorants ont tous trouvé une mamancadrante qui leur convenait parfaitement.»*

*I especially thank my friends for all the good moments spent together and for letting me feel surrounded, especially during the covid period. A special thanks to **Myriam**, my best friend who shared with me this journey from the first year of bachelor in chemistry up to the end of the PhD, by way of the presidency of the JC-SRC, SANA project, and many other activities together.*

*Many thanks to **Frida, Sami and Samer** for their support especially during the writing process but also **Shadi** for proofreading the manuscript.*

*I also thank from the bottom of my heart my family, **my parents** and **my brother**, for believing in me and motivating me during all my cursus in chemistry.*

*I would like to finish these acknowledgements with the most important one for me, my husband-to-be **Tarek**. I thank him for his support during the though moments but also for the celebrations when needed. Most importantly, I thank him for bearing with me during all this time and for making me laugh during all the short breaks (it was practical to work in the same building).*

# ABBREVIATIONS

| | |
|---|---|
| ACN | Acetonitrile |
| AD | Alzheimer's Disease |
| Ad | Autosomal dominant |
| API | Active Pharmaceutical Ingredient |
| Ar | Autosomal recessive |
| AS | Allosteric Site |
| ATP | Adenosine TriPhosphate |
| BBB | Blood-Brain Barrier |
| Boc | *tert*-butyloxycarbonyl |
| CA | Citric Acid |
| CAM | Co-AMorphous system |
| CNS | Central Nervous System |
| COMT | Catechol-OMethylTransferase |
| COSY | Correlated Spectroscopy |
| CSD | Cambridge Structural Database |
| Cy | Cyclohexane |
| Da | Daltons |
| DIPEA | *N*,*N*-Diisopropylethylamine |
| DJ-1 | Daisuke-Junko-1 |
| DMSO | DiMethyl SulfOxide |
| DPP-4 | DiPeptidyl Peptidase-IV |
| DSC | Differential Scanning Calorimetry |
| DUB | Deubiquitinase |
| DVS | Dynamic Vapor Sorption |
| EAFUS | Everything Added to Food in the United States |
| ESI | ElectroSpray Ionization |
| eq. | Equivalent |
| $E_1$ | Ubiquitin-activating enzyme |
| $E_2$ | Ubiquitin-conjugating enzyme |
| $E_3$ | Ubiquitin-protein ligase |
| FDA | Food and Drug Administration |
| GLP-1 | Glucagon-Like Peptide-1 |
| GLP-1R | Glucagon-Like Peptide-1 Receptor |
| GOLD | Genetic Optimization for Ligand Docking |
| GRAS | Generally Recognized As Safe |
| GST | Glutathione S-Transferase |
| HBP | Hydrogen Bond Propensity |
| HMBC | Heteronuclear Multiple Bond Correlation |
| HMQC | Heteronuclear Multiple Quantum Coherence |
| HPLC | High Performance Liquid Chormatography |
| HRMS | High Resolution Mass Spectrometry |
| hUCH-L1 | *Homo sapiens* Ubiquitin C-terminal Hydrolase L1 |
| $IC_{50}$ | Half maximal inhibitory concentration |
| IR | InfraRed |
| $k_{cat}$ | Catalytic constant |

| | |
|---|---|
| $K_i$ | Inhibition constant |
| $K_m$ | Michaelis constant |
| LAG | Liquid Assisted Grinding |
| LB | Lewis Body |
| L-DOPA | Levodopa |
| LE | Ligand Efficiency |
| LRRK2 | Leucine-Rich Repeat Kinase 2 |
| MM-GBSA | Molecular Mechanics/Generalized Born Surface Area |
| MOA | MonoAmine Oxidase |
| Mp | Melting point |
| MPTP | 1-methyl-4-phenyl-1,2,3,6-tetrahydropyridine |
| MS | Mass Spectroscopy |
| MW | Molar Weight |
| NG | Neat Grinding |
| NMR | Nuclear Magnetic Resonance |
| PD | Parkinson’s Disease |
| PDB | Protein Data Bank |
| Ph | Phenyl |
| PINK1 | PTEN-Induced Putative Kinase 1 |
| ppm | Part per million |
| PXRD | Powder X-Ray Diffraction |
| $R_f$ | Retention factor |
| RMSD | Root-Mean-Square Deviation |
| rt | Room temperature |
| ROS | Reactive Oxygen Species |
| SA | Saccharin |
| SCXRD | Single Crystal X-Ray Diffraction |
| SDS-PAGE | Sodium Dodecyl Sulphate–PolyAcrylamide Gel Electrophoresis |
| SEM | Scanning Electron Microscopy |
| SNCA | SyNuClein Alpha |
| SNpc | *Substantia Nigra pars compacta* |
| SOSA | Selective Optimization of Side Activities |
| TCID | Tetrachloro-1,3-indandione |
| $T_g$ | Glass transition temperature |
| TGA | ThermoGravimetric Analysis |
| THF | TetraHydroFuran |
| TLC | Thin Layer Chromatography |
| TFA | TriFluoroacetic Acid |
| Ub | Ubiquitin |
| Ub-AMC | Ubiquitin 7-Amino-4-MethylCoumarin |
| Ub-Rho | Ubiquitin Rhodamine 110 |
| UbVMe | Ubiquitin VinylMethylester |
| UCH-L1 | Ubiquitin C-terminal Hydrolase L1 |
| UPS | Ubiquitin Proteasome System |
| UV | UltraViolet |
| zUCH-L1 | *Danio rerio* Ubiquitin C-terminal Hydrolase L1 |

**Table 1 -** Natural amino acid residues, three and one letter code.

| One letter code | Three letter code | Name | One letter code | Three letter code | Name |
|---|---|---|---|---|---|
| A | Ala | Alanine | L | Leu | Leucine |
| R | Arg | Arginine | K | Lys | Lysine |
| N | Asn | Asparagine | M | Met | Methionine |
| D | Asp | Aspartate | F | Phe | Phenylalanine |
| C | Cys | Cysteine | P | Pro | Proline |
| E | Glu | Glutamate | S | Ser | Serine |
| Q | Gln | Glutamine | T | Thr | Threonine |
| G | Gly | Glycine | W | Trp | Tryptophan |
| H | His | Histidine | Y | Tyr | Tyrosine |
| I | Ile | Isoleucine | V | Val | Valine |

# TABLE OF CONTENTS

# PREFACE

The following thesis focuses on UCH-L1 and GLP-1R, two proteins implicated in Parkinson's disease (PD). The main part of the research work aimed UCH-L1 that was strengthen by a second part related to GLP-1R. As a chemist, my work focused on molecules that have activation properties on UCH-L1 and GLP-1R. The following manuscript details the results generated through the past three years of doctorate study. It consists of an introduction that first discusses and details the main information about Parkinson's disease. The deeper clinical and biological domains of the disease were not specified here so as to avoid drowning the reader in information not related to the study conducted hereafter. If the reader wishes to obtain further information about the disease, I invite them to pursue the references:1–6. The introduction thereafter focuses on the two proteins and their activators. It ends with an explanation of the modulation of the physical and chemical properties of active pharmaceutical ingredients (APIs). The experimental results generated in this work are then divided in three parts. Part I details the results gathered on the small molecules – their synthesis and the interaction study with their respective protein. Then, the modulation of their physical and chemical properties is assessed in Part II. Finally, Part III consists in the study of zUCH-L1 protein as a model to investigate modulators of UCH-L1. The manuscript ends with a conclusion that includes outlooks for future work.

This thesis was carried out in close collaboration with Abaxys Therapeutics S.A. This collaboration allowed me to understand the benefits and constraints that can result from the collaboration with an industrial partner. Indeed, handling the confidentiality became one the challenges of this collaboration. Through this challenge, I managed to develop my communication skills towards the general and scientific public while maintaining the integrity and the confidential aspects of the project. Secondly, the transfer of the knowhow and some materials, including UCH-L1 activator compound described in the literature, was conducted.

I conclude by thanking Dr. Javier Garcia-Ladona for the scientific exchanges and Abaxys Therapeutics S.A. and the University of Namur for the financial support. I would also like to thank Valérie Troonbeeckx for the "Parkinson & Young" grant. Finally, I thank all authors of the publications and the different collaborators that helped achieve the intended goals of my thesis.

Enjoy the reading.

# INTRODUCTION AND AIM OF THE STUDY

It has been more than two hundred years since the first ever detailed clinical features of Parkinson's disease (PD) were published as "An essay on the shaking palsy".[7] Yet, PD, named after the writer of the essay, continues to be a major age-related health problem due to the general demographic composition of the population. Despite effective treatment of motor symptoms, there is no robust treatment today to cure or prevent PD-related degeneration; the full pathogenesis remains to be elucidated in the pursuit for effective prevention and treatment in the future.

## 1. PARKINSON'S DISEASE

### 1.1 Introduction

Parkinson's disease (PD) is a chronic and progressive neurodegenerative disorder of the central nervous system which gives rise to motor disturbances. It is the second most common neurodegenerative disorder in the world after Alzheimer's disease (AD). The median age of onset is around 60-65 years old but it is estimated that 10% of people diagnosed with PD already had the disease onset before the age of 50 years old.[8] PD affects 1% of the population over 60 years old, with an incidence[*] that increases with age. [9,10] The prevalence[†] is 1,900 persons per 100,000 in people over the age of 80.[3] It is estimated that the number of people diagnosed with PD will double by 2030.[11]

Healthy people display a slow and progressive loss of dopamine with age. However, PD patients show a severe depletion of dopamine due to the degeneration of the dopaminergic neurons (**Figure 1**). PD is essentially defined by two hallmarks: (i) the progressive and irreversible loss of the dopaminergic neurons in the *substantia nigra pars compacta* (SNpc) and (ii) the presence of abnormal aggregates of proteins that are developed inside the nerve cell, called Lewis bodies (LB).[9] Dopamine is a neurotransmitter serving as chemical signaling from one neuron to the other by travelling through the synapse[‡].[12] The dopaminergic neuronal network in the brain controls body motor function, thus a deficit in the signaling pathways induces multiple motor symptoms such as slowness of movement, resting tremor, muscular rigidity, akinesia and dystonia. In addition, deficits on the dopaminergic innervation reaching the limbic system leads to non-motor impairments and neurological disturbances such as anxiety, depression, sleep disorders, cognitive deficits, weight loss and digestive disorders.[8] The depletion of dopamine leads also to dysfunction of other basal ganglia neurotransmitter

---

[*] The newly diagnosed cases.

[†] The number of persons affected by a medical condition at a particular time.

[‡] The region of interaction between two nerve cells allowing the transmission of a signal.

systems and pathways such as the cholinergic, serotonergic, glutamatergic and noradrenergic pathways.[13] Generally, motor symptoms appear when almost 80% of dopaminergic neurons in SNpc perished.[14] The rate of progression and the severity of the disease differ from one person to another due to genetic and environmental factors.[15] The diagnosis of PD is based on two observations: (i) neurological signs and (ii) brain imaging.

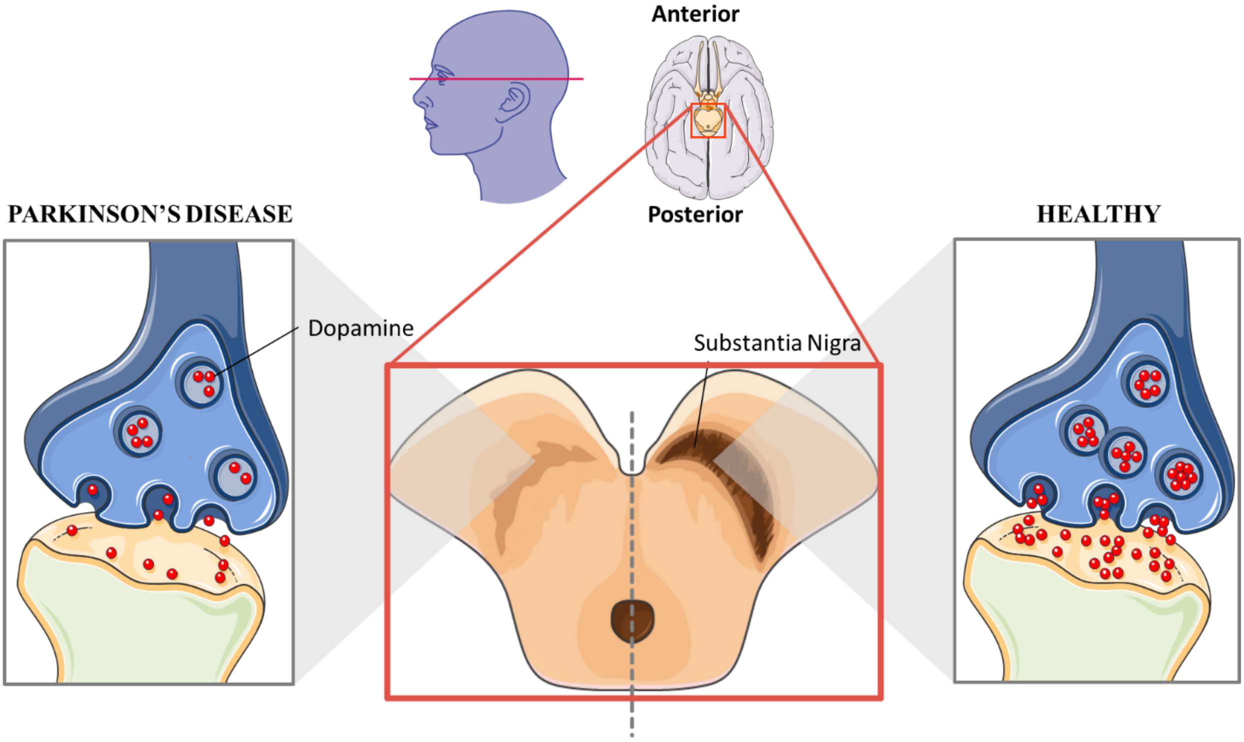

**Figure 1** - Cross-section of the midbrain in a patient with Parkinson's disease (left) and in the case of a healthy person (right). (Adapted from BioRender templates)

Most of PD cases are known as idiopathic possibly induced by environmental factors. Studies suggest that several pathogenic pathways are implicated in the occurrence of PD, thus mutually reinforcing the final mechanisms that lead to neuronal cell death.[5,16] Among these, oxidative stress associated with mitochondrial dysfunction, neuroinflammation and proteolytic stress are observed. However, a small portion of PD cases are caused by genetic factors that are usually inherited and cause the commonly named familial PD.

## 1.2 Forms of the disease

### 1.2.1 Familial PD

Familial PD represents about 5% of PD cases generally presenting an early-onset PD due to the specific gene mutation the patients have inherited.[6] At present, twenty gene mutations grouped in the PARK family have been associated to PD. The most commonly known ones are gathered in **Table 2**.

**Table 2** - Genes implicated in PD. Ar: autosomal recessive and Ad: autosomal dominant.[1,17]

| Gene | Protein Name | Inheritance | Function | Reference |
|---|---|---|---|---|
| PARK1 | α-synuclein | Ad | Regulation of the dopamine release in the synapse | 18–20 |
| PARK2 | Parkin | Ar | E3 Ubiquitin ligase | 18 |
| PARK5 | UCH-L1 | Ad | Deubiquitinating enzyme | 18 |
| PARK6 | PINK1 | Ar | Serine/threonine protein kinase | 9,21,22 |
| PARK7 | DJ-1 | Ar | Chaperone protein | 23,24 |
| PARK8 | LRRK2 | Ad | GTPase and kinase functions | 25–28 |

The presence of LBs in PD allows to classify the disease as a synucleinopathy. It is a group of neurodegenerative disease characterized by distinctive intraneuronal inclusions that are composed of abnormal aggregation of proteins with the significant presence of a presynaptic neuronal protein called α-synuclein. Thus, the first discovered genetic cause of PD was PARK1 that refers to the SNCA gene encoding for α-synuclein.[19] Until now, 5 mutations have been identified.[18] Two other genes (PARK2 and PARK5) encoding for Parkin and Ubiquitin C-terminal hydrolase L1 (UCH-L1) proteins are implicated in the system in which damaged proteins are recycled. Parkin is a E3 ligase that tags proteins for degradation and UCH-L1 is a deubiquitinase (DUB) which removes the tag of the targeted protein.[18] Parkin is also involved in the maintenance of the mitochondrial function: the PINK1 protein responses to dysfunctional mitochondria and recruits Parkin which promotes mitophagy through mitochondrial protein ubiquitination. Mutation in the PINK1/Parkin signaling pathway thus affects the function of the mitochondria, a dysregulation that is also associated with amyotrophic lateral sclerosis, Huntington’s disease and eye diseases.[9,21,22] Additionally, DJ-1 is a protein associated with both forms of PD, familial and idiopathic. This protein, through its chaperone function, reduces the proteolytic stress and demonstrates antioxidative stress function.[23,29] Finally, LRRK2-PD is relatively common and most patients with it carry the Gly2019Ser mutation which manifests as a late-onset PD. Mutations in LRRK2 have been associated with both familial and idiopathic PD.[25–27]

Inherited mutations can directly cause the disease, even if the matching gene from another parent is normal; this is referred to as dominant inheritance. Recessive forms can also be observed when the disease is induced by both gene mutations from the parents. Research shows that mutations in SNCA, UCH-L1 and LRRK2 are transmitted through dominant inheritance whereas mutations in DJ-1, Parkin and PINK1 cause autosomal recessive forms of PD.[30]

### 1.2.2 Idiopathic PD

PD without a genetic background seems to be associated with different environmental factors and represent the so-called idiopathic PD. In the early 1980s, the search for environmental factors inducing PD intensified when an intermediate 1-methyl-4-phenyl-1,2,3,6-tetrahydropyridine (MPTP) due to the synthesis of an illicitly manufactured opiate (1-methyl-4-phenyl-4-propionoxy-piperidine) was correlated with symptoms associated with idiopathic PD.[31] In fact, this non-opiate intermediate is bioconverted into a toxic metabolite $MPP^+$ that inhibits the mitochondrial complex I of the respiratory chain and increases oxidative stress in SNpc neurons.[32] From there, the influence of environmental factors started being closely studied. They were suggested as possible contributing factors to PD as they affect people with gene susceptibilities.[33] Pesticides such as Rotenone and Paraquat® were shown to be potent inhibitors of the mitochondrial complex I and thus a possible cause in some cases of idiopathic PD. Neurotoxins such as iron, lead, copper and manganese were also found to induce PD by stimulation of free radicals.[34–36] Other factors of every-day life, such as coffee consumption and cigarette smoking were studied in relation to PD. Interestingly, both factors seem to have a protective effect on the risk of PD.[37,38]

## 1.3 Pathogenic cellular pathways involved in PD

Multiple studies have shown that several pathogenic mechanisms are implicated in the occurrence and progression of PD. Oxidative stress, mitochondrial dysfunction, neuroinflammation and proteolytic stress are intracellular signals that may trigger downstream molecular pathways which may ultimately be responsible for the death of dopaminergic neurons.[5,16]

The production of reactive oxygen species (ROS) occurs as a result of cellular stress taking place in mechanisms of injury and other pathological conditions.[39] This is known as **oxidative stress** which plays an important role in PD as it is linked to mitochondrial dysfunction and to neuroinflammation.

Mitochondria provide energy to power neural activity and control ROS levels, calcium homeostasis and biosynthesis of macromolecules.[21,39] **Mitochondrial dysfunction** is caused by an alteration of mitochondrial functionality or integrity that may induces ROS production that in turns alters their functionality and affects the integrity of mitochondrial DNA.[40,41] Mitochondrial dysfunction can occur through genetic (PINK1/Parkin) or environmental toxicants (MPTP, pesticides) that cause deficiencies of respiratory complex I.
ROS accumulation also induces oxidative stress that activates the inflammatory pathway. **Neuroinflammation** is a defense mechanism in response to deleterious processes such as tissue injury, cell injury and viral infection.[12] Microglial and astrocytes cells are glial cells involved in such response in the brain. These glial cells act as sentinels of the microenvironment and any noxious stimulus can activate them to react and act as macrophages. Microglial activation triggers an intracellular signal cascade and induces the release of proinflammatory mediators such as ROS, chemokines and cytokines (e.g. interferon-γ, interleukin-1, interleukin-6 and tumor necrosis factor-α).[42] Although neuroinflammation is a neuroprotective mechanism, a dysregulation or an over-activation of microglia can lead to a sustained inflammatory response which is neurotoxic and could be the origin of neurodegeneration.[43,44]

**Proteolytic stress** results from a dysfunction of the ubiquitin-proteasome system (UPS), which is essential for the regulation of protein homeostasis. It regulates the fate of damaged and unrequired proteins in eukaryotic cells. A large number of proteins (ubiquitin and deubiquitinating enzymes) are involved in the recycling of proteins into peptides or amino acids through the 26S proteasome (**Figure 2**).[45] A dysfunction of the UPS can lead to aggregation of undesired proteins.

The UPS starts with ubiquitination, a protein labelling mechanism using an ubiquitin (Ub) and leading to the degradation of the targeted protein. It is a post-translational modification catalyzed by three enzymes: ubiquitin-activating enzyme (E1), ubiquitin-conjugating enzyme (E2), and ubiquitin-protein ligase (E3). E1 activates the Ub at the expense of ATP and E2 transfers the tag. Then, E3 recognizes the protein and catalyzes the transfer of Ub from E2 through a covalent linkage. An isopeptide bond is thus formed between a lysine of the targeted protein and the carboxylic C-terminal group of Ub. Additional Ub may then be also bonded through one of the 7 internal lysines of Ub, previously attached to the targeted protein. This could lead to different Ub codes[§] which define the fate of the tagged proteins. For example, Lys11-linked and Lys48-linked polyubiquitin chains are the most common linkages for proteasomal degradation.[45–47]

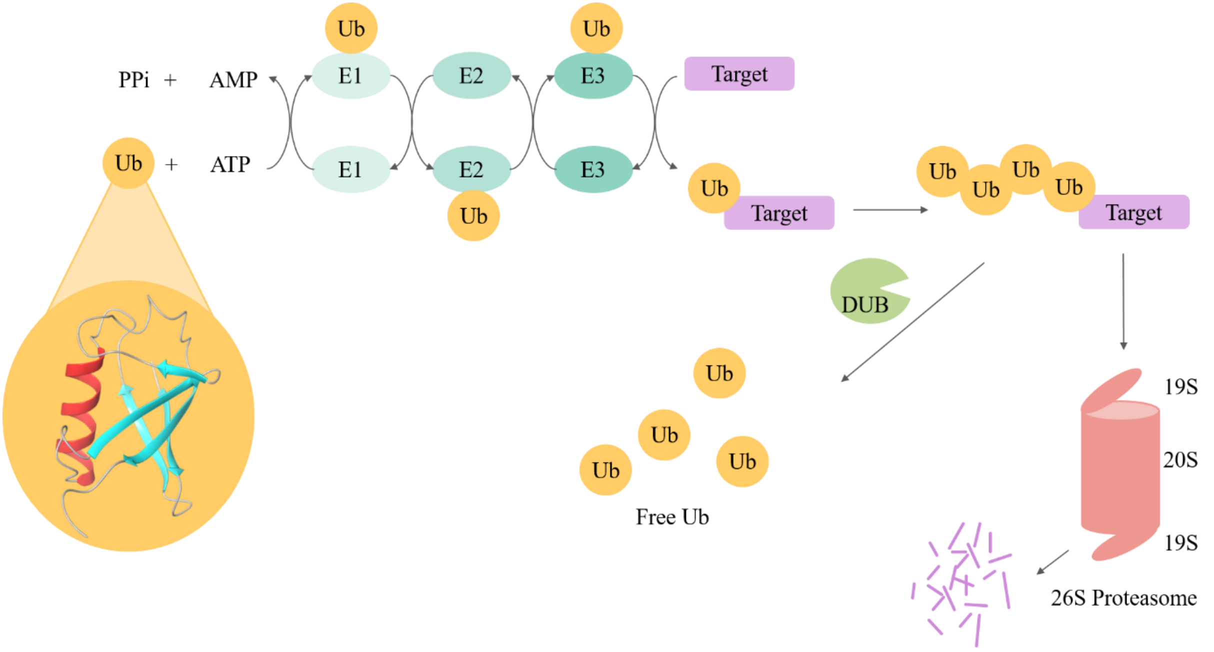

**Figure 2** - Overview of the UPS. The binding of Ub to the protein target involves the sequential actions of E1, E2 and E3 enzymes in an ATP-dependent manner. Ubiquitinated protein target is recognized by the 19S unit of the 26S proteasome. DUBs enzymes remove Ub from the protein target which will be degraded into amino acids or peptides.

The ubiquitination tagging processes of proteins are kept in balance with deubiquitinases, DUBs. This type of enzyme removes Ub from proteins by hydrolysis of the amide bond of the Ub and the lysine side chain. This allows the free Ub to be recycled and not degraded.[48] DUBs consist of approximately 100 enzymes encoded in the human genome. Most of them are cysteine proteases bearing a cysteine involved in the catalytic triad. DUBs are divided into families based on their domains: ubiquitin C-terminal hydrolases, ubiquitin-specific proteases, Machado–Joseph disease proteases, ovarian tumor proteases, motif-interacting with ubiquitin-containing novel DUB family, ubiquitin-like proteases and the JAB1/MPN/Mov34 family, the only zinc metalloprotease DUBs.[46,49]

The 26S proteasome recognizes and degrades the ubiquitinated protein. It is composed of two fragments: (i) 19S regulatory unit (one or two), responsible for substrate recognition,

---

[§] mono or poly-Ub (linear, branched, homotypic or heterotypic chains) deubiquitination and unfolding of the targeted protein and (ii) 20S core, where the protein is degraded into amino acids or small peptides.[45,50]

The association between the UPS and PD was first made through mutation in the parkin gene compromising its E3 ligase activity.[51] It was later further fueled by the discovery in siblings with inherited PD of a mutation inhibiting the activity of UCH-L1, a deubiquitinase, inhibiting its activity.[52] The last association with PD, is α-synuclein. Even if it is not a UPS member, its overexpression was demonstrated to inhibit the proteasome.[53] This genetic evidence shows that a failure in the UPS is a key factor in the disease pathway.

## 1.4 Therapeutics strategies

The advancing knowledge and understanding of PD pathology allowed an improvement of treatments. As explained above, the hallmarks of PD are dopaminergic neuron deficits and presence of LBs. Consequently, diverse treatments are currently available that are first focused on the neuron deficit. Treatments aim either the restoration of dopaminergic neuronal function by pharmacological replacement of dopamine or to compensate abnormal brain function by neurosurgical approaches. These therapies are directed to alleviate the symptoms of PD but they do not affect the neurodegenerative processes. Recently, therapies that are stopping or slowing-down the disease progression, named disease-modifying therapies, have been investigated. There are also other non-conventional therapies, such as physiotherapies, physical exercise, speech therapy and relaxation depending on the patient's needs.[54,55] An effective treatment should be personalized for the patient, according to the stage of their disease, its type, the severity of motor and non-motor symptoms as well as their PD-unrelated conditions.[3]

### 1.4.1 Neurosurgical approaches

Several neurosurgical approaches towards PD treatment exist. These help alleviate motor symptoms of the patient. Deep brain stimulation, consisting of high frequency electrical stimulations, allows the reduction of motor symptoms with few sides effects.[56] Gamma knife radiosurgery[57] and magnetic resonance imaging-guided focused ultrasound[58] are also two alternatives requiring less invasive interventions and subsequently causing less postoperative complications.[6]

Cell based therapies requiring neurosurgical intervention have been also investigated for the treatment of PD. This therapeutic approach relies on the use of undifferentiated stem cells which can be induced to differentiate in cells producing dopamine. Primary studies have shown encouraging results but more work has to be done to confirm the efficiency and safety of such a method.[5,59]

### 1.4.2 Pharmacological approach

a. L-DOPA-therapy

The first drug found to alleviate symptoms of PD was L-DOPA, 3,4-dihydroxy-L-phenylalanine or also known as levodopa. It was synthesized and isolated as pure enantiomer in the early 1900s. In the 50s, Arvid Carlsson made a discovery for which he won the Nobel Prize in 2000: dopamine is a neurotransmitter that is implicated in PD. From that, he performed clinical trials with L-DOPA in the 60s that showed motor improvement in PD patients. The Food and Drug Administration (FDA) approved the drug as a replacement of dopamine in 1970.[60] Since then, and for more than 50 years, L-DOPA has been considered the standard symptomatic therapy treatment for PD.[8] As dopamine cannot cross the blood-brain barrier (BBB), L-DOPA is considered as a good substitute as it is a precursor of dopamine. In fact, L-DOPA is bioconverted to dopamine in the blood by dopamine decarboxylase thus activating dopamine receptors and improving motor function in the CNS.[60] Several characteristic of L-DOPA compromises it use as a therapeutic agent and contribute to the need of a high amount in order to reach the therapeutic effect. L-DOPA is poorly soluble in water and has a very short biological half-life of around 1 hour. It is rapidly removed by enzymes in the blood. In order to increase its half-life, L-DOPA is administrated with decarboxylase inhibitors (e.g. Carbidopa and Benserazide) to avoid conversion to dopamine in the blood.[5] Furthermore, in long term L-DOPA-therapies a diminished effectiveness over time has been observed accompanied with the appearance of severe complications such as dyskinesia and motor fluctuations. These side effects impact negatively the patient’s quality of life and strongly complicate the clinical status and treatment of the patient. To manage these sides effects, diverse formulations of L-DOPA were developed. Since within the synapse, dopamine can be broken down by two enzymes: MonoAmine Oxidase (MAO) and Catechol-OMethyl Transferase (COMT), inhibitors of these two enzymes (e.g. Rasagiline, Selegiline for MAO and Entacapone and Tolcapone for COMT) are prescribed as a complement to L-DOPA therapy, highly improving the half-life of dopamine. They aim to inhibit the enzymes responsible of the metabolism of dopamine and thus increase its level in the synapse. However, such a strategy is still not optimal as it induces sides effects such as nausea, dry mouth, constipation and hallucinations.[3,6]

### b. Dopaminergic agonist

Another therapeutic strategy aiming the replacement of dopamine function that was proposed in the 1970s is the use of structural analogs of dopamine called dopaminergic agonists acting on dopamine receptors. Apomorphine, agnosit of receptor D1 and D2, is mostly used as an adjunct to L-DOPA in order to decrease its quantity used in the treatment and alleviate its sides effects. [61,62] Compounds agonist of the dopamine receptors D2/D3, such as Ropinirole, are also investigated as a PD treatment.[63]

### c. Non-dopaminergic agonist

Drugs acting in other non-dopaminergic neurotransmitter systems controlling brain functions have been also investigated for the treatment of PD. Among others, the compounds are targeting the glutaminergic system, such as mGluR4, mGluR5 and Amantadine, adenosine receptor 2A and serotonergic receptors.[13,64,65] Amantadine has been used for nearly 50 years due to its antidyskinetic effects on patients with PD but it has cardiovascular and psychiatric sides effects.[66,67] Natural products such as Atremorine have also been proposed with neuroprotective behavior against neuronal death.[68,69]

Most of the above-mentioned treatments evolved into complex approaches depending on the patients and the doctor following their case. The existing treatments available on the market are effective for relieving motor symptoms but they are not free of severe side effects and do not alter the progression of the disease. Subsenquently, there is an urgent need to develop neuroprotective treatments that are slowing down or stopping the disease progression. Therefore, new strategies must be put in place, like disease-modifying therapies focused on targeting specific molecular pathways implicated in PD pathogenesis. Several clinical trials are ongoing for disease-modifying drugs.[70,71] Some of the candidates are calcium channel blockers, iron chelating compounds, agonists of the GLP-1 receptor (GLP-1R) implicated in the insulin-signaling pathway or drugs that target the α-synuclein protein; its production, aggregation and degradation.[72] The UCH-L1 protein is involved in the UPS system and is closely related to the degradation of α-synucleins and some of its mutations have been associated to severe forms of PD.

In the present PhD project, small molecules modulators of UCH-L1 and GLP-1R, two potentially disease-modifying targets, have been investigated.

## 2. GLP-1/GLP-1R

### 2.1 GLP-1 in PD

Glucagon-like peptide-1 (GLP-1) through its action in GLP-1R modulates the glucose homeostasis effect and may also function as a neuropeptide in the brain.[73] In fact, GLP-1 and its receptor have both been found in the brain. Numerous *in vitro* and *in vivo* studies have demonstrated neuroprotective effects through the activation of GLP-1R in models of neurodegenerative diseases such as AD and PD.[74–80] GLP-1 analogues or dipeptidyl peptidase-IV (DPP-4) inhibitors modulates several neuropathological pathways implicated in PD as they allow the activation of GLP-1R.[78] Agonists of GLP-1R in experimental models have shown anti-inflammatory properties, such as the suppression of cytotoxic microglia and beneficial actions on the preservation of mitochondrial function.[81–83] *In vivo* studies in animal toxin models of PD showed that GLP-1 analogues can alter protein aggregation processes, resulting to an improvement in behavior and motor symptoms.[78]

### 2.2 GLP-1 and GLP-1R

GLP-1 is a peptide hormone composed of 30 amino acids. It is produced and secreted by L-cells present in the small intestine in response to food digestion and leads to an increase of the glucose amount in the plasma. This protein is an incretin: it can enhance the secretion of insulin and thereby decrease the blood sugar level.[84] GLP-1 has a short half-life as it is rapidly degraded by DPP-4 in human plasma into a peptide not active against GLP-1R.[73,85]

GLP-1 exerts its effect by binding and activating GLP-1R, a member of the class B G-protein-coupled receptor family. GLP-1R is widely expressed, most abundantly within the pancreas, gastrointestinal tract, brain, heart and kidney.[86,87] The structure of GLP-1R was completely resolved and was shown to exhibits a multi-domain architecture:[88]

- ECD amino terminal extracellular domain (represented in purple in **Figure 3**), which binds to the C-terminal GLP-1 peptide. The ECD is composed of 4 β-strains and of two α-helices,
- TMD is a transmembrane domain that binds the N-terminal part of the GLP-1 peptide (represented in red in **Figure 3**). TMD is composed of 8 α-helixes.

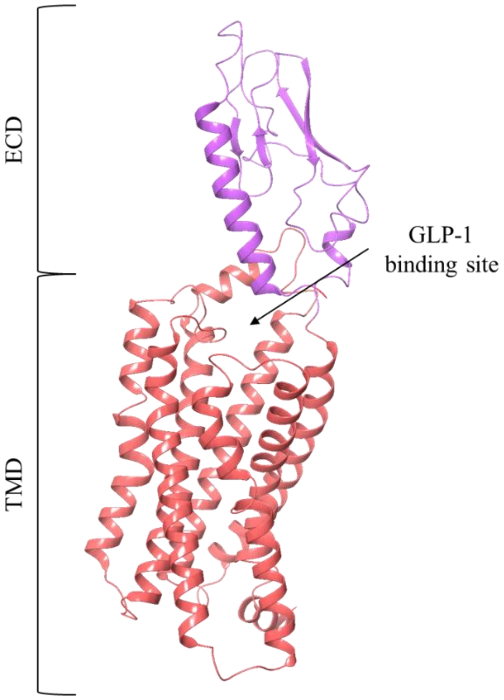

**Figure 3** - Secondary structure representation of the crystallographic structure of GLP-1R (5NX2). ECD domain highlighted in purple and TMD domain in red.

In type 2 diabetes mellitus, which accounts for 90 to 95% of all cases of diabetes, the regulatory activity of insulin is disordered and requires often interventions of glycemic control.[89,90] GLP-1 is best known for its actions in this disease as its incretin function is preserved in diabetes.[91] This fact allows the design of therapeutic strategies based on drugs that activate (directly or indirectly) GLP-1R in the pancreatic cells.

### 2.3 Modulators of GLP-1R

Therapeutic targets developed for the treatment of type 2 diabetes mellitus are divided into two classes of incretin-based therapies, (i) analogues of GLP-1 that can activate GLP-1R and (ii) inhibitors of DPP-4 that prevent the degradation of GLP-1.[78] In the first case, this leads to therapeutic design that consists of synthesizing modified peptides to improve GLP-1 stability and the duration of its action. The GLP-1R agonist mimics the glucoregulatory effects of GLP-1 **1** and thus increases the glucose-dependent insulin secretion. Currently available GLP-1R agonists are for instance Albiglutide **2**, Exenatide **3**, Lixisenatide **4**, Liraglutide **5** and Semaglutide **6** (**Figure 4**).[90,92,93] Several of these agonists can reach the CNS by crossing the BBB. The list includes Liraglutide, Lixisenatide and Exenatide. Generally speaking, Liraglutide and Lixisenatide showed better neuroprotective effects in models of PD compared to Exenatide.[74,79,80,94] In the second case, inhibitors of DPP-4 are studied as GLP-1 is rapidly degraded by DPP-4. Compounds such as Sitagliptin **7**, Saxagliptin **8**, Linagliptin **9** and

Alogliptin **10** are the most common DPP-4 small molecule inhibitors available on the market.[92,95] Among the GLP-1R agonists there is Exenatide which showed also resistance to metabolization by DPP-4.[96] Furthermore, head-to-head clinical trials between GLP-1R agonists and DPP-4 inhibitors showed a higher stimulation of GLP-1R with GLP-1R agonists.[97] Furthermore, DPP-4 inhibitors demonstrated lower penetration of the BBB.[78,98]

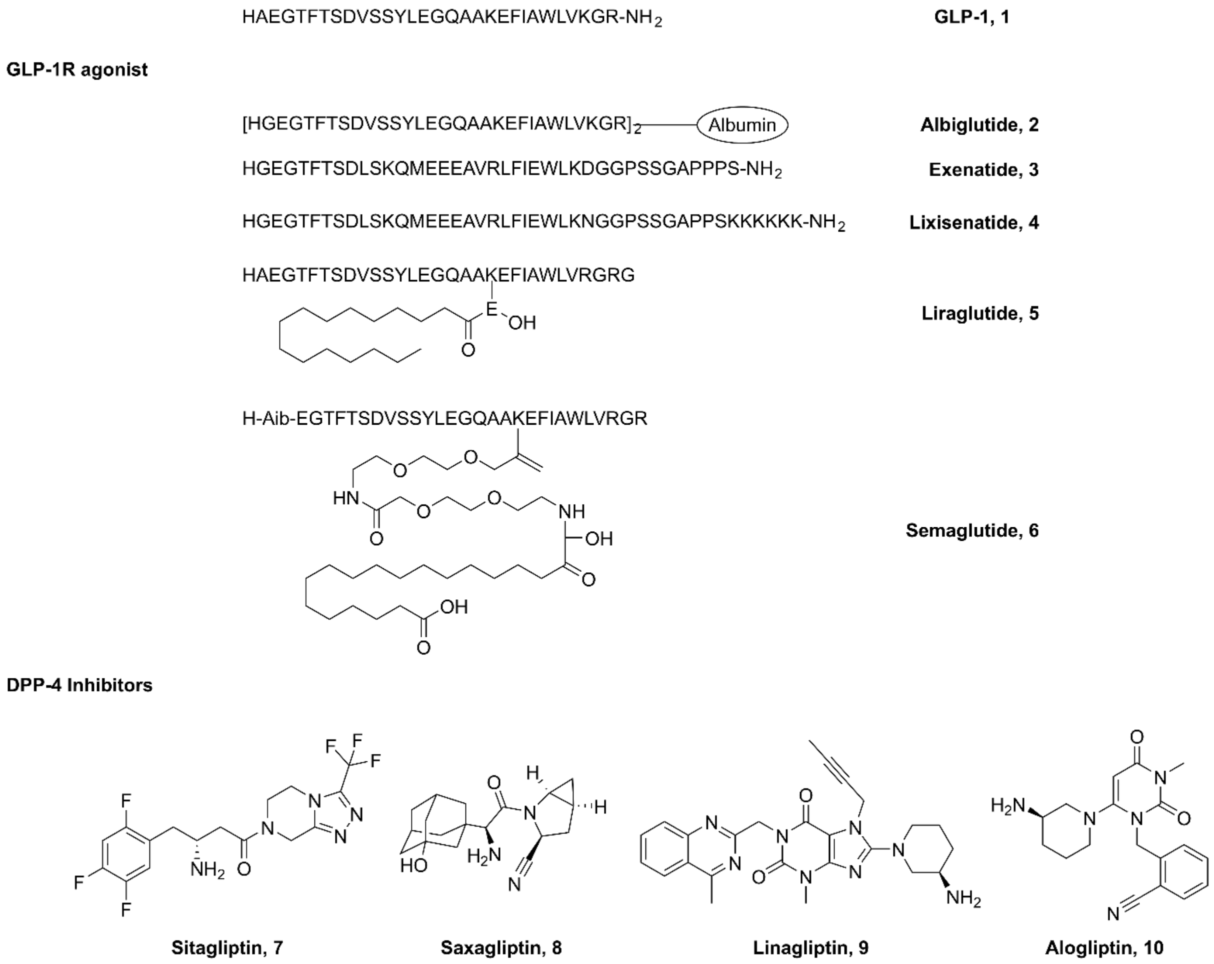

**Figure 4** - Structures of GLP-1, selected GLP-1 receptor agonists and some DPP-4 inhibitors.

GLP-1R agonists are peptides and their administration currently requires subcutaneous injections of medication that is still too expensive to produce.[99] In order to bypass these problems, the development of small molecules acting as GLP-1R agonists is highly desirable. These may constitute a significant advance due to their enhanced bioavailability, particularly oral absorption. So far, no treatment based on small molecules have been approved. However small molecules have been reported as positive allosteric modulators of GLP-1R (**Figure 5**): they potentiate GLP-1R alone or in the presence of GLP-1.[100] Screening of libraries allowed the discovery of several small molecules, such as compounds with quinoxaline scaffold **11** and pyrimidine-based molecules **12**.[100,101] A series of flavonoids were also reported to positively modulate GLP-1R activity, such as Quercetin **13**.[102] A CNS penetrant GLP-1R modulator was also reported, compound **14**.[103] In addition to that, a new class of compounds showing activity towards GLP-1R is emerging: derivatives of 1,2,4-oxadiazole that are already studied in drug design for several diseases,[104] have been investigated since 2014 as GLP-1R agonist.[105]

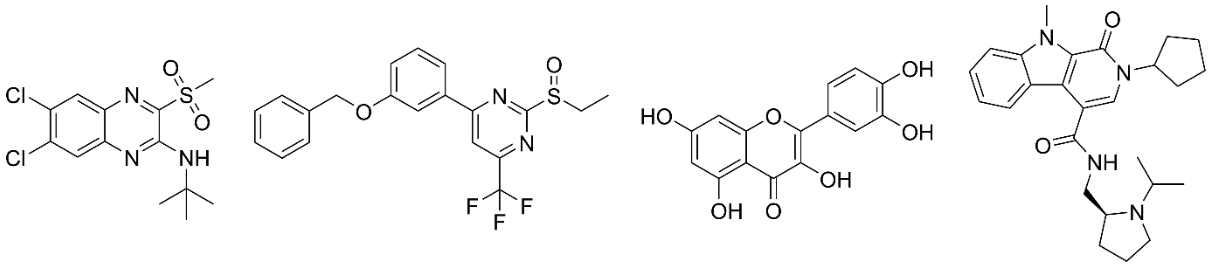

**BETP** **Quercetin** **VU0453379**

**11** **12** **13** **14**

**Figure 5** - Structures of selected small molecules positive allosteric modulators of GLP-1R.

## 3. UCH-L1

Ubiquitin C-terminal hydrolase L1 (UCH-L1) was originally discovered 40 years ago during polyacrylamide gel electrophoresis of human brain extract experiments.[106] It was first called “Protein Gene Product 9.5” for its position on the gel.

### 3.1 UCH-L1 in PD

UCH-L1 is a deubiquitinating enzyme implicated in the UPS system. Its primary function is to catalyze the hydrolysis of peptide bonds between Ub and the protein that is targeted for degradation. The involvement of UCH-L1 in PD was first reported by a genetic association study identifying mutation in familial PD. UCH-L1 was named a susceptibility gene for familial PD, as the Ile93Met mutation was discovered in four out of seven patients who developed the disease. Ile93 is located near the active site where the mutation results in the exposure of the hydrophobic core. This leads to a decrease of UCH-L1 solubility and the formation of protein aggregates.[52,107] By contrast, Ser18Tyr mutation showed neuroprotective effects against PD. Mutation Glu7Ala, was associated to early-onset PD. This mutation led to a near complete loss of the hydrolase activity *in vitro* as the position Glu7 was highlighted as required for ubiquitin binding.[108,109] Decreased levels of UCH-L1 were found in the brain of patients with AD and PD.[110] Furthermore, UCH-L1 hydrolase activity was shown inhibited by 60% due to the binding to Cys152 by dopamine derivatives.[111] Between 20 and 30% of UCH-L1 was also shown to be membrane associated through farnesylation, promoting accumulation of α-synucleins.[112]

Thus, UCH-L1 plays an important role in maintaining axon integrity and protection of neurons by removing abnormal proteins through the UPS. UCH-L1 has been studied as protein aggregates have been found to be increasingly present in such disease.[113] UCH-L1 was also identified as one of the major components in LBs.[114] The studies suggest that maintaining UCH-L1 to normal level is crucial for a normal functioning of the brain.

### 3.2 Characteristics of the protein

UCH-L1 is part of the UCH family that includes three other enzymes: UCH-L3, UCH-L5 and BAP1. UCH-L1 is a protein of interest as it has been linked to PD. It is an abundant neuronal protein that represents 2% of total proteins in the brain. It can also be found in small amounts in the reproductive tissues (ovaries and testes).[115,116] UCH-L1 is essentially found in the cytoplasm but when overexpressed it can be found in the nucleus.[117,118]

At a molecular level, UCH-L1 is a globular protein in a helix-β-helix sandwich fold (**Figure 6**). UCH-L1 can only hydrolyze small fractions of Ub because the catalytic site is not accessible to larger polymers of Ub. The protein possesses a "tunnel" that gives access to the catalytic site. The "tunnel" is closed by a loop blocking the path to larger Ub (**Figure 6**). UCH-L1 is a cysteine protease, with a catalytic triad composed of three amino acids: Cys90, His161 and Asp176.[108]

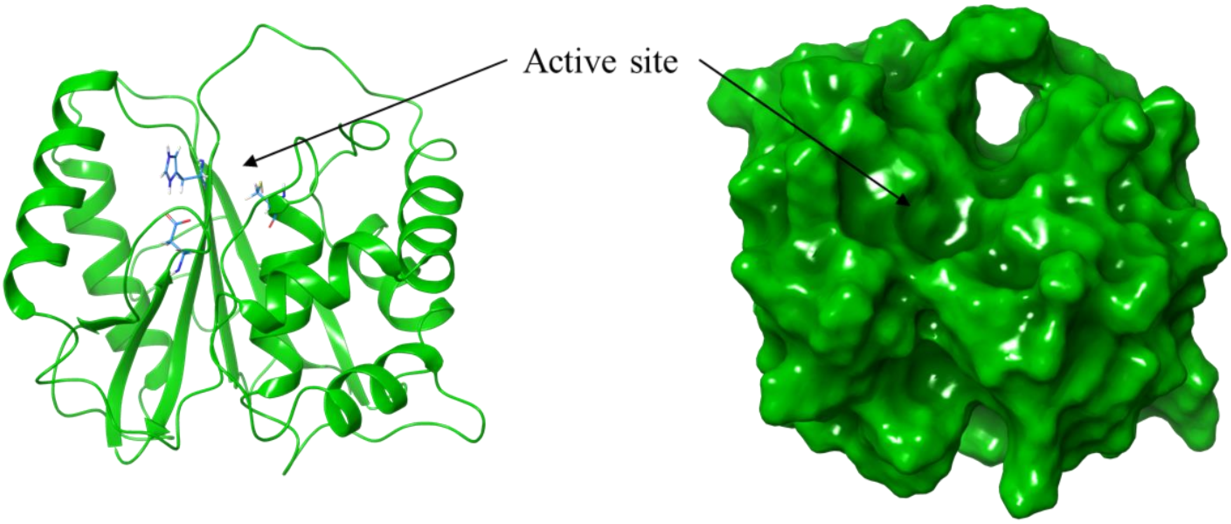

**Figure 6** - Crystal structure of UCH-L1 (2ETLa). The amino acids of the active site are highlighted in blue. Secondary structure representation (left) and surface of the protein (right).

More particularly UCH-L1 exists in two forms: an inactive one, in the absence of its substrate Ub (**Figure 6**) and an active form in the presence of Ub (**Figure 7**). The forms were determined by Das and Boudreaux's group through crystallization of the protein with and without the substrate.[108,119] The inactive form was crystallized with ubiquitin vinyl methyl ester group (UbVMe), a suicide substrate that is bound to UCH-L1 through a thioester bond (**Figure 7**).

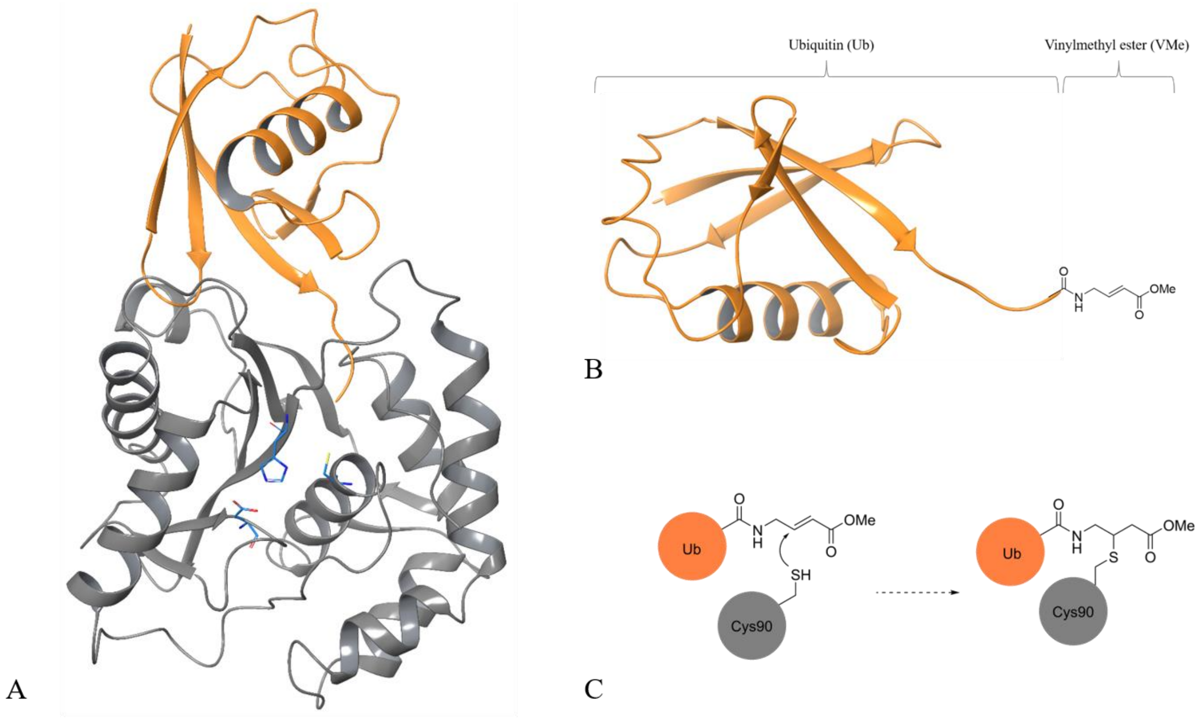

**Figure 7** - (A) Secondary structure representation of the crystal structure of hUCH-L1 with UbVMe (3KW5). The amino acids of the active site are highlighted in blue. (B) Secondary structure representation of UbVMe (3KW5b). (C) Formation of the UCH-L1-UbVMe complex by a covalent attack of the Cys90 at the α,β-unsaturated bond of the VMe moiety.

The rearrangement between both forms, represented in **Figure 8**, is induced by the β-hairpin of the amino-terminal Ub. It creates a domino effect through two phenylalanines (Phe214 and Phe53) resulting into the rearrangement of His161 brought closer to Cys90 (from 8 to 4Å). This leads to an activation of the protein.[119]

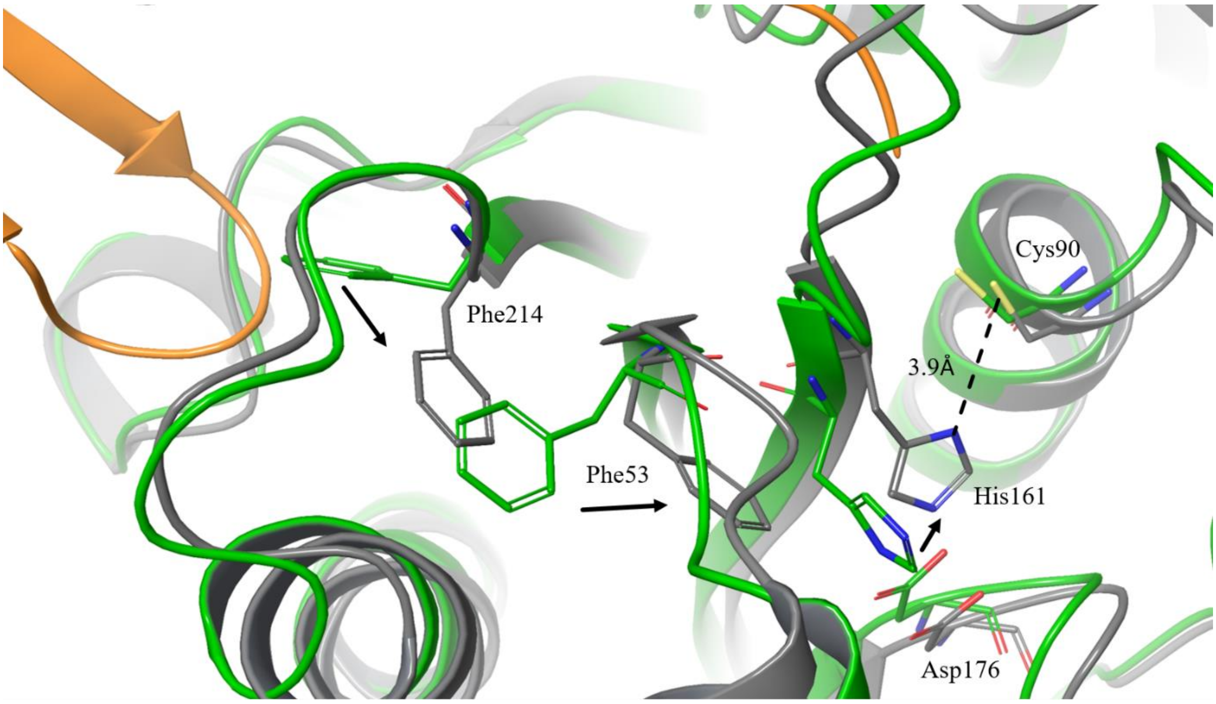

**Figure 8** - Rearrangement between inactive (green, 2ETL) and active (UCH-L1 in grey and Ub in orange, 3KW5) forms of UCH-L1. The amino acids of the catalytic triad and the ones implicated in the domino rearrangement are shown.

As mentioned, the primary function of UCH-L1 is to remove Ub from the targeted-for-degradation proteins. In the cysteine-histidine-aspartate catalytic triad implicated in the hydrolysis, Cys90 acts as the nucleophilic group, activated by His161 and Asp176. UCH-L1 removes and thus recycles Ub from degraded proteins. Consequently, UCH-L1 regulates the cellular pool in free Ub and can also stabilize them to avoid degradation by lysosomes.[108,119–122] Unlike most DUBs it was demonstrated that UCH-L1 acts as a ligase in its dimeric form.[123]

UCH-L1 function in neurons has been suggested by studies in brain injury showing axon and neuron repair by removing abnormal proteins.[124] For that purpose, it is also used as a biomarker that helps indicate the severity of injury in acute neurotrauma and CNS injury.[125,126] Although UCH-L1 is mainly expressed in neurons, it plays a crucial role in cardiac fibrosis[127] but most importantly in a number of cancers including, lymphoma,[128] lung,[129,130] colorectal,[131,132] pancreatic,[133] breast,[134,135] prostate[136] and ovarian[137,138] cancers. Expression of UCH-L1 in some cancers is correlated with an increase metastatic behavior. A depletion of UCH-L1 was proven to reduce the potential metastatic behavior.[139]

Post-translational modifications can alter the function and structure of UCH-L1. Reactive lipids from brain injury can covalently modify cysteine residues. In the case of UCH-L1, generally lipids can bind with Cys152 thus resulting in the aggregation and loss of UCH-L1 activity.[140,141]

A mutation in this site can then protect neurons from cell death. Furthermore, UCH-L1 activity can also be diminished during oxidative stress. The oxidative modifications disrupt its native structure causing it to shift from its soluble to its insoluble form.[107,142]

### 3.3 Modulators of UCH-L1

O-acyl oxime derivatives were the first class of UCH-L1 inhibitors to be identified via high-throughput screening of a ligand library.[123] In this family, one derivative stands out with high inhibition results, LDN-57444 **15** (**Figure 9**). It was found to be the most potent ($K_i$ of 400 nM) and specific to UCH-L1 in the UCH family.[123] Compound LDN-91946 **16** and TCID **17** are also two interesting inhibitors of UCH-L1 with $K_i$ of 3 µM[143] and $IC_{50}$ 75 µM[123] respectively, whereas TCID is more selective to UCH-L3 ($IC_{50}$ of 600 nM). Z-VAE(OMe)-FMK **18** was also identified as a potential irreversible inhibitor of UCH-L1. To this date, it is the only crystal structure reported of a complex ligand/UCH-L1.[144] Recently, Mission Therapeutics developed a new series of cyanopyrrolidine-based compounds such as **19** that show inhibition activity.[145,146] These compounds inhibit UCH-L1 via covalent binding of the catalytic Cys90 site by electrophilic conjugation. In the last few years, derivatives of this family, such as **20**, were synthesized by Panyain *et al*.[147] and Krabill *et al*.[148] and showed high inhibition activity.

Downregulation of UCH-L1 has been reported in neurodegenerative diseases such as PD and AD, suggesting that activators of this protein may have therapeutic effects.[110] The only activator described in the literature (**Figure 9**, **21**) was found by *in silico* screening using a virtual compound library that could bind to UCH-L1. Mitsui *et al.* found that this compound, at concentration of 63µM, can increase the hydrolase activity up to 111%.[149]

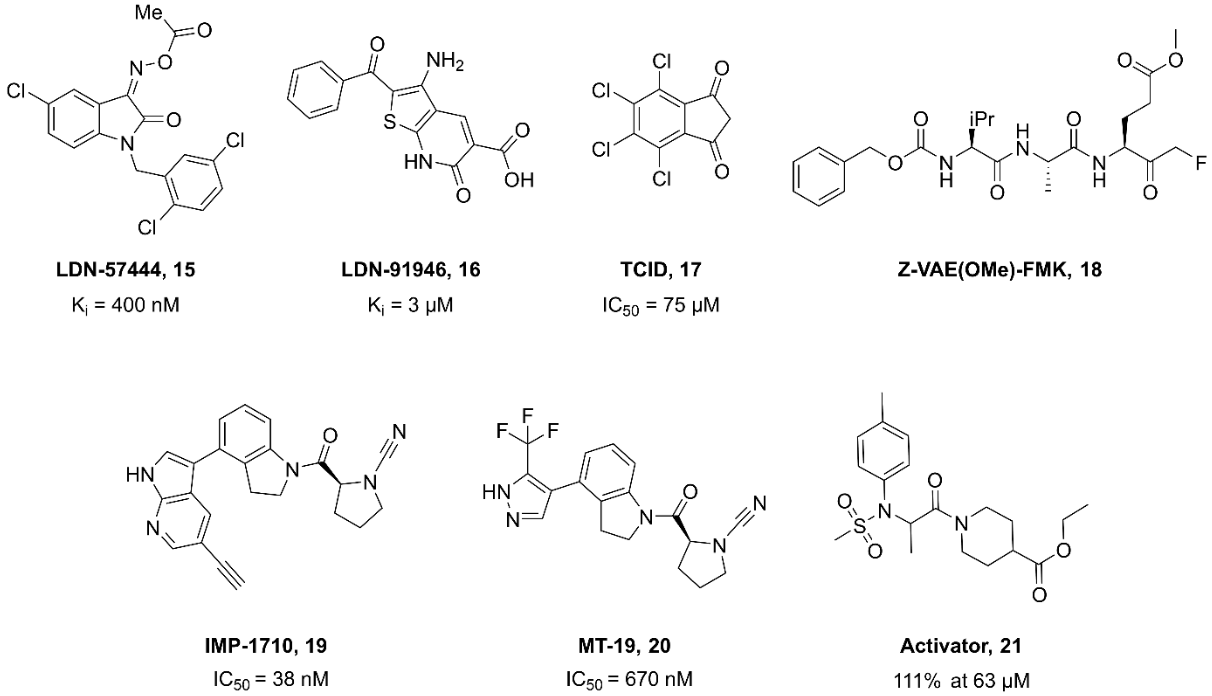

**Figure 9** - Structure of selected UCH-L1 inhibitors and activators.

## 4. MODULATION OF THE PHYSICAL AND CHEMICAL PROPERTIES OF MOLECULES

A major challenge in the treatments of brain disorder, such as PD, is the delivering of small molecules across the BBB in the brain. Several approaches to this problem are lately provided, such as the use of prodrugs or nanoparticules.[150] The most known example of PD drugs with this problem is dopamine. The molecule is too polar to cross the BBB, however its prodrug L-DOPA can cross it. As one may think that L-DOPA is too polar, its similarity to the tyrosine amino acid is the parameter that allows it to cross the BBB. The challenge of crossing the BBB is not the only one for PD drugs under development. Modulation of the physical and chemical properties of the drug is an important process. The properties that can be tuned are for instance, solubility, hygroscopicity, stability, crystal formation, melting points and impurity profile.[151] For that purpose, salt formation is a commonly used approaches for tailoring the physical and chemical properties without altering the drug molecule. Indeed, several PD drugs currently available on the market are in salt form, such as Benserazide.HCl, Apomorphine.HCl, Selegiline.HCl, Rasagiline mesylate and Amantadine.HCl.[3] In the latter example, Amantadine free base exhibit low solubility in water.[152] Thus, the compound was obtained in a salt form with hydrochloric acid in order to increase its solubility. Rasagiline is available as a mesylate salt, not to improve the solubility but this time to increase the stability upon storage.[153]

Salt formation involves an acid-base reaction, a proton transfer between the API and a counter ion. The latter has to be capable of donating or accepting a proton. When trying to achieve salt formation between drug combination, other phenomena can be obtained: co-crystallization (solvated or hydrated forms) or polymorphs. Depending on these forms different physical and chemical properties can be reached. Co-crystallization addresses physical and chemical properties of non-ionizable compounds. It is the combination of two entities, the API and a co-former, in the same crystal lattice through non-ionizable interactions, mostly hydrogen bonds.[154] Recently, to resolve a racemic mixture of drug substance or to modulate the drug-drug formulation, co-crystallization has been shown to be effective.[155] In the search for a suitable counter ion the ΔpKa (pKa of the base – pKa of the acid) is a valuable parameter to take into account:[156]

- if ΔpKa is higher or equal to 3: salt formation occurs.
- if ΔpKa is lower than 0: co-crystal formation occurs.
- if ΔpKa is comprised between 0 and 3: a formation of either a salt or co-crystal occurs.

Co-crystallization can now be predicted by several knowledge-based methods.[157] One of these methods is hydrogen bond propensity (HBP) that relies on the probabilities of hydrogen bonding formation between the API and the compounds included in the Cambridge Structural Database (CSD). The HBP method is a statistical analysis which estimates the donors and the acceptors of hydrogen bonds between the API and the possible co-former.[158]

On the other hand, crystalline solids are not the only possible way to modulate the physical and chemical properties of APIs. The amorphous solid state such as in co-amorphous systems (CAM) can enhance the solubility, dissolution rate and the physical stability of the API.[159–161] The CAM systems are like co-crystals differentiated by the lack of recurrence in the lattice. It is a multi-component single amorphous solid system with intermolecular interactions between the components. The CAM system was found first as an alternative approach to the use of polymeric amorphous solid dispersion. The difference is that the API is not stabilized by a polymer but by an excipient (drug-excipient CAM) or a low-molecular-weight drug (drug-drug CAM).

Furthermore, the counter ion/co-former used for the crystalline or amorphous solid formulation has to be pharmacologically acceptable. Specifically, the compound is usually chosen from lists complied by the FDA: either the “Generally Recognized as Safe” list (GRAS, https://www.cfsanappsexternal.fda.gov/scripts/fdcc/ index.cfm?set=GRASNotices) or the “Substances Added to Food” list (formerly called “Everything Added to Food in the United

States", EAFUS, https://www.cfsanappsexternal.fda.gov/scripts/ fdcc/index.cfm?set=FoodSubstances).[162] Other parameters can be taken into account when one is searching for a suitable counter ion/co-former, such as its solubility[163] or toxicity[164]. For the latter, the maximum daily dose or the median lethal dose ($LD_{50}$) can be a good choice of parameter to consider.

Several techniques can be used for the salt, co-crystals and CAM formation. They are divided in two categories: solvent-based and solid-state. The latter will be carried out in this work through mechanochemistry. It is a green method with a chemical transformation that consists of a solvent-free grinding process (NG) or with very small amount of solvent (LAG), in order to increase the molecular mobility and thus accelerate the reaction.[165–168]

# 5. AIM OF THE STUDY

The principal goal of this thesis was to study small molecules as ligands of UCH-L1 and GLP-1R, two protein targets that are involved in the development of PD. In that respect, the thesis is divided in three sections, described in **Figure 10**.

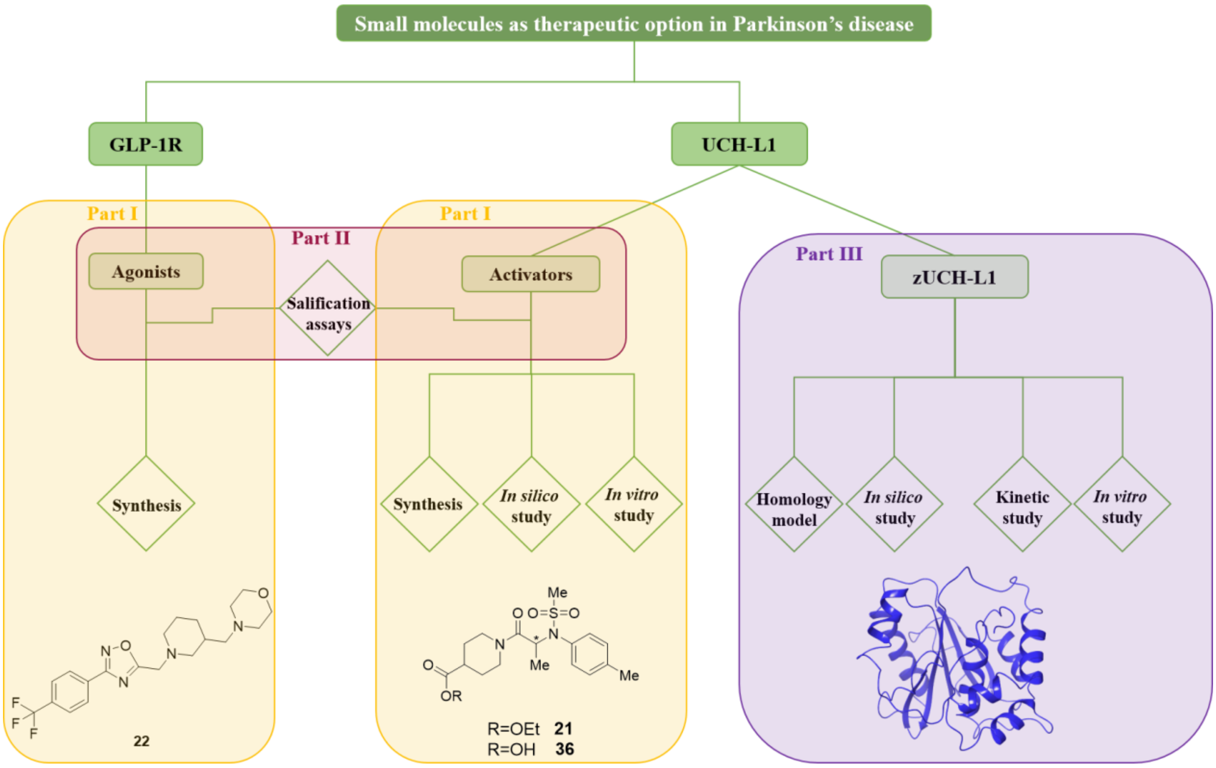

**Figure 10** - Representation of the strategy adopted in this thesis to find and study ligands of GLP-1R and UCH-L1 proteins.

Firstly, a special attention was first given to a GLP-1R small molecule agonist and more specifically to a derivative of 1,2,4-oxadiazole (ABXY-3) that was subject of a preliminary study by the company Abaxys Therapeutics, our collaborator **Figure 10**, Part I). The above-mentioned compound was synthesized so as to conduct a deeper study of its effect on the GLP-1R activity. Then, the research focused on identifying activators of UCH-L1 as the protein was proven to be downregulated in PD which renders studying its activators highly interesting.[110] In order to find new activators, a virtual screening was performed and the hits were assessed *in vitro* on hUCH-L1. Additionally, the activator described in the literature by Mitsui *et al.*[149] was studied. Further derivatives from Mitsui's compound are also investigated as potential activators (ABXY-1). These compounds were first studied *in silico* (by docking) and then *in vitro* on hUCH-L1.

The second part of the thesis consists in the modulation of the physical and chemical properties of the above-mentioned small molecules (**Figure 10**, Part II). Salification assays were carried out so as to change the physical aspect of the GLP-1R agonist and to modulate the solubility of an activator of UCH-L1.

Finally, we also investigated the UCH-L1 protein of zebrafish (*Danio rerio*) zUCH-L1 (**Figure 10**, Part III). It was carefully investigated with a view to study the modulators on zebrafish *in vivo* models. In fact, in the last few years, zebrafish species have gained popularity as *in vivo* models for use in the modeling of neurodegenerative diseases because of the accessibility of the embryos, their transparency allowing the use of non-invasive imaging and especially because of their genetic similarity to humans.[169,170] As UCH-L1 is related to neurodegenerative diseases, zebrafish has been used as *in vivo* model to study UCH-L1 modulators. Since the zUCH-L1 protein has not yet been described or studied in the literature, a special interest was dedicated to it in this thesis. The behavior of the protein regarding similar ligands was therefore studied and compared to *Homo sapiens* UCH-L1 (hUCH-L1) in order to verify whether a similarity exists between both the zebrafish and the human UCH-L1. For that purpose, a first comparison *in silico* was realized and after production and purification of zUCH-L1, it was followed by an *in vitro* study of the zebrafish protein. A comparison of its enzymatic activity regarding already described modulators of hUCH-L1 was also carried out.

# RESULTS AND DISCUSSION

# PART I:

# SMALL MOLECULES AS THERAPEUTIC OPTIONS IN PARKINSON'S DISEASE

This chapter is dedicated to the study of two targeted small molecules derived from alanylpiperidine and 1,2,4-oxadiazole. They were both synthesized in the laboratory but the physical state of the 1,2,4-oxadiazole compound rendered it difficult to achieve a deeper study on it. Therefore, our main focus was on the alanylpiperidine derivative. After a structural characterization, the interactions between this compound and UCH-L1 protein were preliminarily investigated. An *in silico* study was performed and the influence on the enzymatic activity of UCH-L1 was assessed. As very little is known about activators of UCH-L1, a virtual screening was performed so as to find new potentially interesting molecules.

## 1. 1,2,4-OXADIAZOLE DERIVATIVE AS AGONIST OF GLP-1R

GLP-1R is a promising therapeutic approach for PD as its activation showed neuroprotective effects.[77] There are already several identified agonists of GLP-1R, however, the most promising ones are peptides that are highly expensive to produce.[99] Therefore, there is a real need for small molecule activators to overcome the problemes faced with peptide compounds. Several groups have already started investigating the use of some small molecules.[100–103] In this section, we will focus our attention on the 1,2,4-oxadiazole derivatives, since the collaborators we are working with on this project obtained 4-1-3-4-(trifluoromethyl)phenyl-1,2,4-oxadiazol-5-ylmethylpiperidin-3-ylmethylmorpholine (**22** in **Figure 11**) as a compound of interest for GLP-1R. They performed a screening on GLP-1R with an in-house database and obtained this particular molecule as a hit. This family of 1,2,4-oxadiazole derivatives is not insignificant since Rodriguez's group has already demonstrated that these compounds are interesting as activators of GLP-1R.[105]

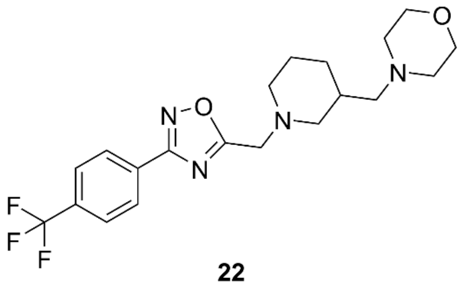

22

**Figure 11** - Structure of 4-1-3-4-(trifluoromethyl)phenyl-1,2,4-oxadiazol-5-ylmethylpiperidin-3-ylmethylmorpholine **22** (ABXY-3).

The molecule in **Figure 11** was first studied as a racemic mixture. The convergent synthesis of compound **22**, depicted in **Scheme 1**, consists of six steps with an overall yield of 68% corresponding to the largest linear sequence starting from compound **23**.

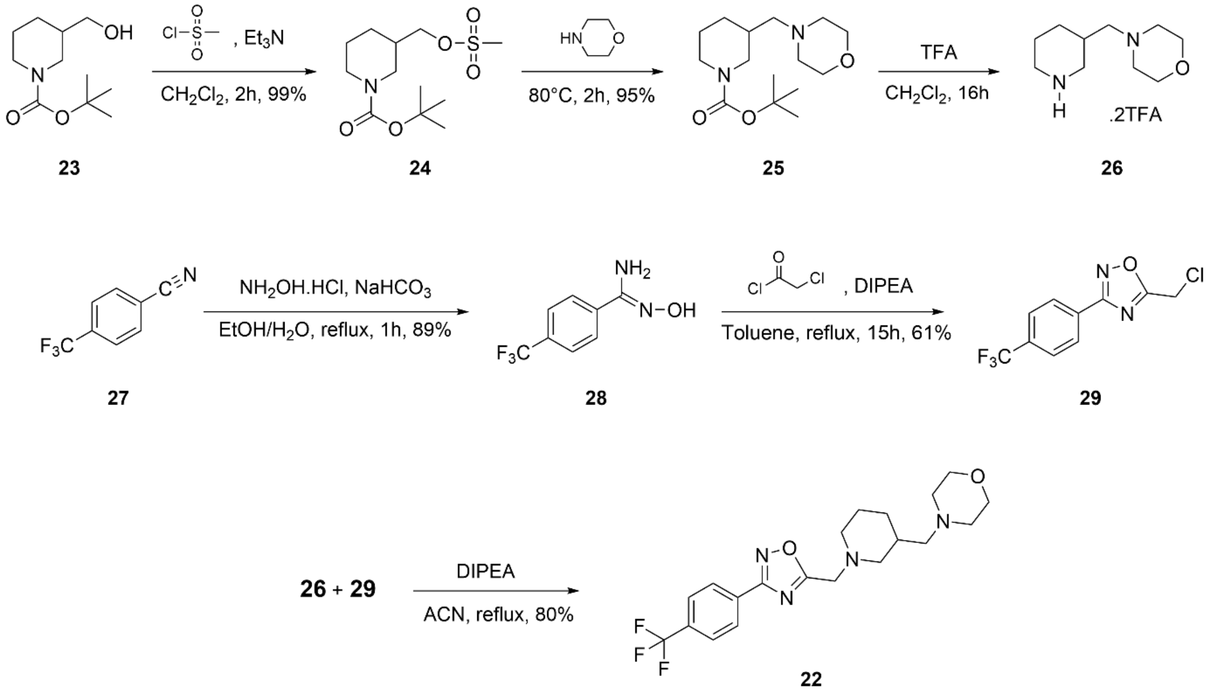

**Scheme 1** - Synthesis of compound **22**.

The strategy adopted consisted of a convergent synthesis conducted in three parts. First, the synthesis of the intermediate piperidine **26** was carried out uneventfully. Alcohol compound **23** was transformed into the corresponding mesylate **24** following the same conditions as described in the literature.[171] A nucleophilic substitution reaction was then performed with morpholine to yield molecule **25**. The last step was performed to remove the Boc protecting group. It was not possible to calculate the yield of this step because it was not known whether all the excess of TFA was eliminated. The second part consisted in the synthesis of the intermediate oxadiazole **29**, first through the addition of hydroxylamine on compound **27** to form carboximidamide compound **28**. The 1,2,4-oxadiazole was formed by reaction of **28** with chloroacetyl chloride in the presence of the hindered base DIPEA. Finally, a $SN_2$ reaction between both intermediates **26** and **29** provided the expected compound **22**. As the stability of compound **29** is not known, it was used in the last reaction freshly synthesized compared to compound **26** which is in the form of a salt and should not deteriorate. Compound **22** was obtained as a sticky oil, which rendered further manipulations difficult. Therefore, a change of the physical state should be accomplished by modulating the physical and chemical properties of the molecule. Salification assays of compound **22** were carried out and the results are presented in the next Part II.

## 2. ACTIVATOR COMPOUNDS OF UCH-L1

UCH-L1 is a protein that represents 2% of the total neuronal proteins in the brain. Studies showed that several mutations altering the enzymatic activity were associated with PD and that downregulation of its activity in this disease was related to the idiopathic form of the disease.[52,110,121] In the literature inhibitors of UCH-L1 have mostly been studied up until now but finding activators can lead to a therapeutic pathway in PD.

### 2.1 Virtual screening of hUCH-L1

The purpose of this study is to screen a chemical library in order to identify new potential activators of hUCH-L1. In that respect, we applied the selective optimization of side activities (SOSA) approach. It consists of using old drugs or candidates for the generation of novel leads towards a target that is different from its original one.[172] This process is less time consuming and more cost efficient as the approved drugs have accessible bioavailability and toxicity data that does not need to be reproduced.[173] This approach is becoming well-known as it is an alternative approach of high throughput screening. For that reason, a screening of a virtual database was performed to find compounds that could interact with the targeted protein hUCH-L1. The ZINC drug chemical library was selected as it contains commercially available compounds.[174,175] Compounds that came out of the virtual screening were first ranked according to their GOLD score (**Figure 12**). Among them, a series of potential candidates was retrieved.

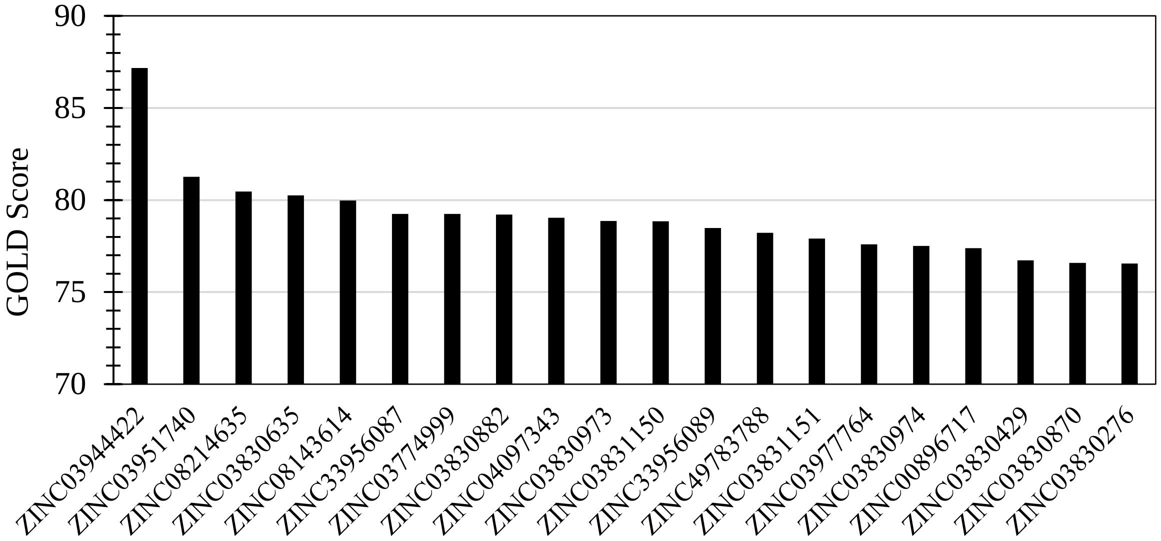

**Figure 12** –Virtual screening results of ZINC database within the active site of hUCH-L1. Top 20 best ranked molecules based on the GOLD score.

The top two molecules, presented in **Figure 13**, are Ritonavir and Lopinavir with GOLD scores of 87.17 and 81.26, respectively. Of all the molecules within the database, it is interesting that the two highest ranked compounds have the same target and mode of action: Ritonavir and Lopinavir are peptidomimetic molecules that act as HIV protease inhibitors. Knowing that hUCH-L1 is a protease and its substrate is a protein, these two compounds are likely to interact with hUCH-L1. Their influence on the enzymatic activity was therefore tested as a priority (**Figure 14**).

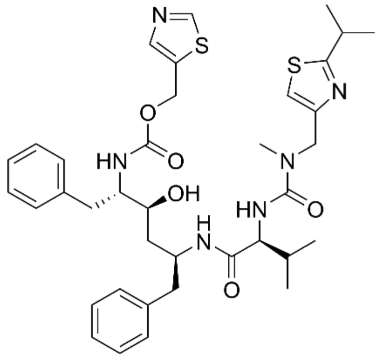

**Ritonavir, 30**

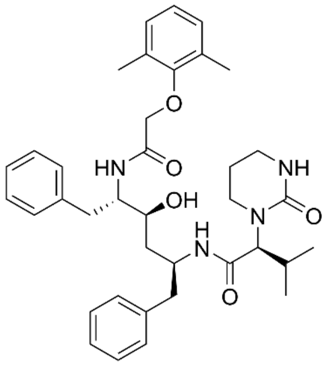

**Lopinavir, 31**

**Figure 13** - Compounds from virtual screening of ZINC database within the active site of hUCH-L1. Top 2 best ranked molecules based on the GOLD score.

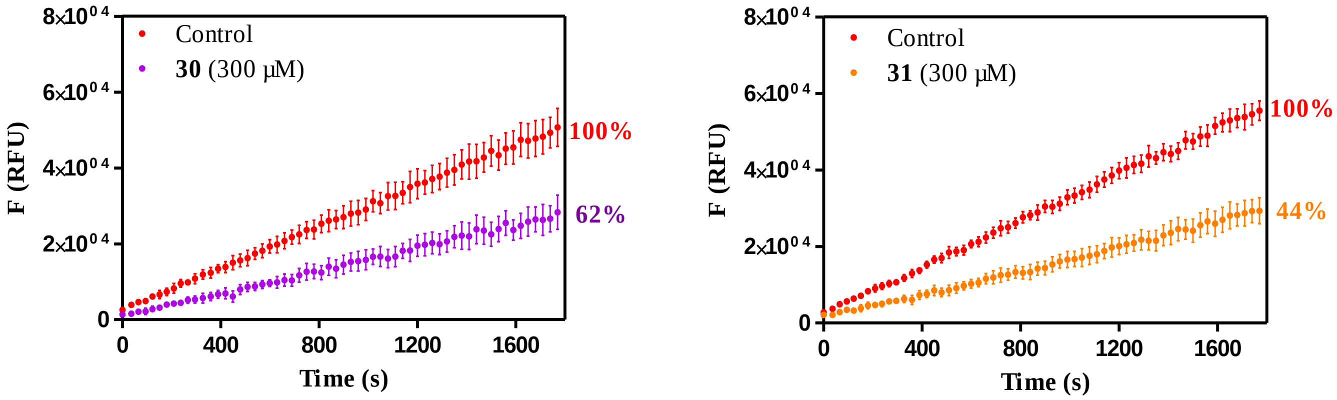

**Figure 14** - Enzymatic activity of hUCH-L1 in the presence of Ritonavir **30** (left) and Lopinavir **31** (right) at 300 µM. No modulator (control) was defined as 100% activity.

The molecules were first tested at 300 µM in order to study their modulation. The two tested compounds turned out to be inhibitors and not activators. Ritonavir and Lopinavir are potentially interesting as they inhibit and the remaining enzymatic activity is 62% and 44% respectively at 300 µM. Preliminary additional experiments showed an $IC_{50}$ of around 200-300 µM.

The virtual screening results showed that the highest ranked molecules based on the GOLD score are only large systems. Thus, the size of the ligands is an additional parameter that can be considered. For this purpose, a ranking based on the ligand efficiency (LE) value, defined as the GOLD score divided by the number of heavy atoms (all atoms except the hydrogen one) is represented in **Figure 15**. This analysis demonstrated that small ligands preferentially show the highest LE values. Thus, both parameters were taken into account and the plot of the GOLD score vs LE in **Figure 16** allowed to identify additional candidates.

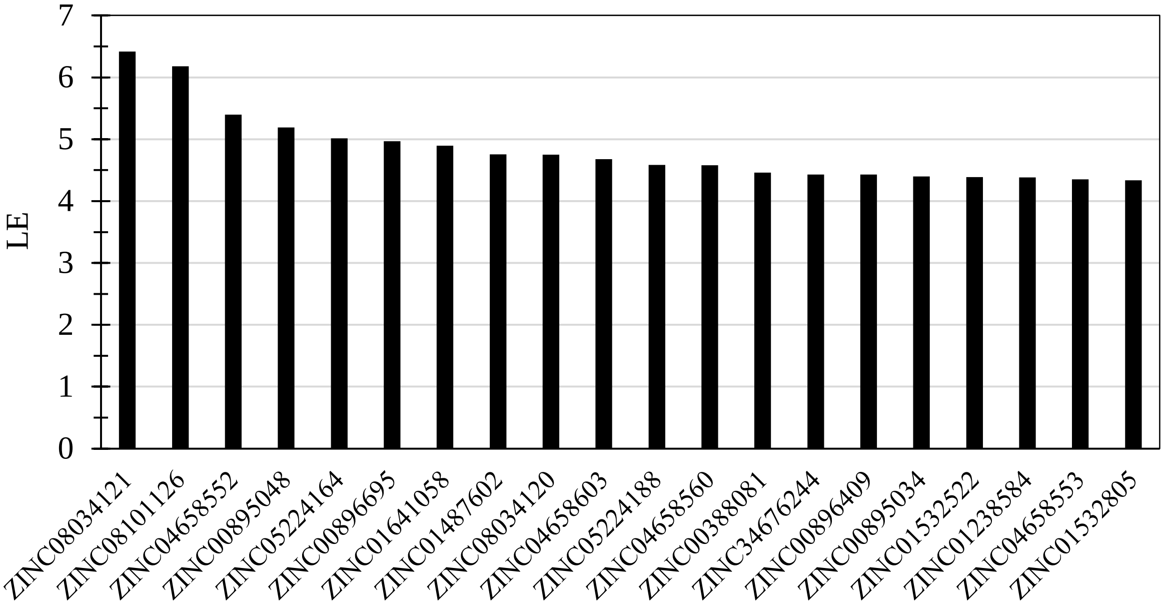

**Figure 15** - Results of the virtual screening of ZINC database within the active site of hUCH-L1. Top 20 best ranked molecules based on the LE.

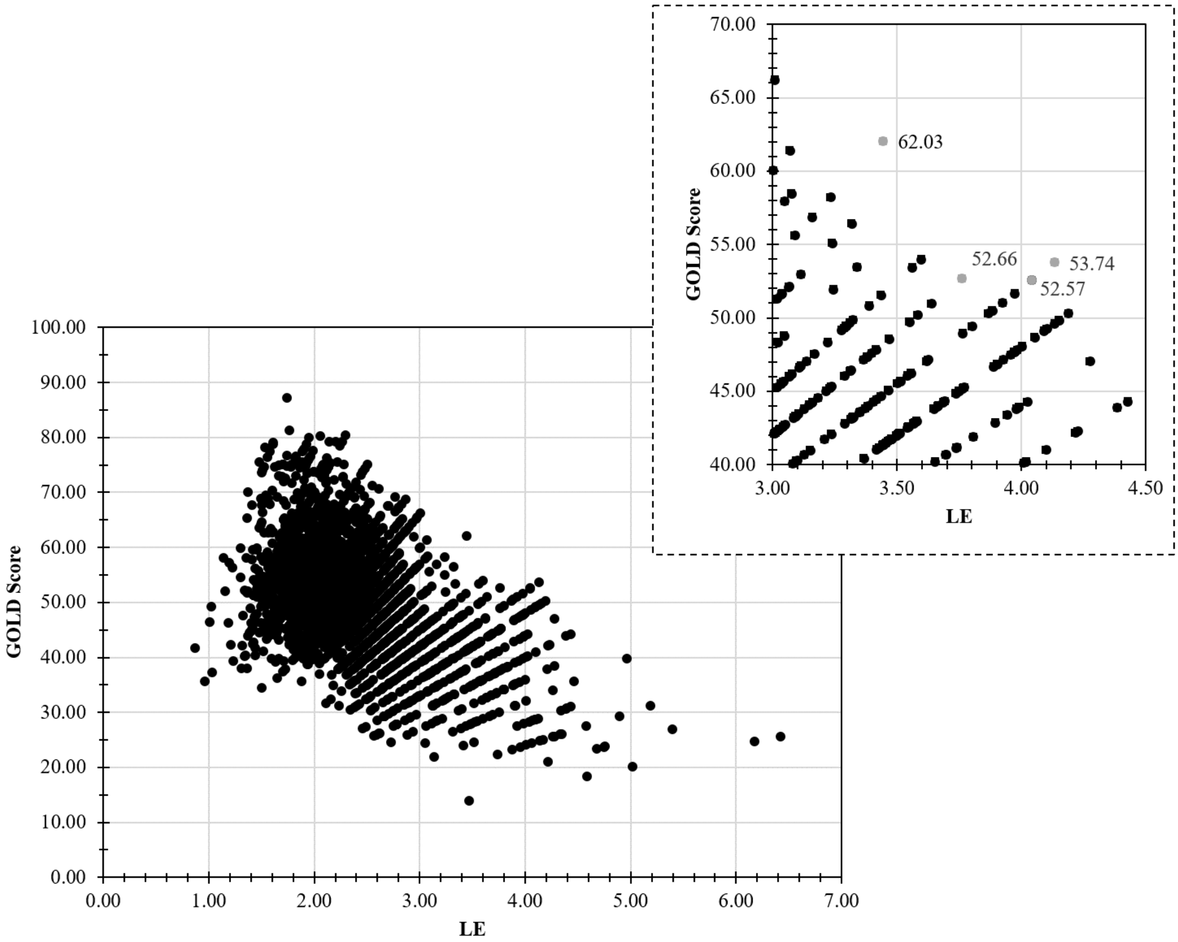

**Figure 16** - Results of the virtual screening of ZINC database within the active site of hUCH-L1, based on the GOLD score and the LE.

Promising compounds taking into account the GOLD and LE score are highlighted in the magnification in **Figure 16**. They correspond to Benserazide, L-DOPA, L-adrenaline and Levonordefrin (represented in **Figure 17**) with 62.03, 52.66, 53.74 and 52.57 as GOLD scores respectively.

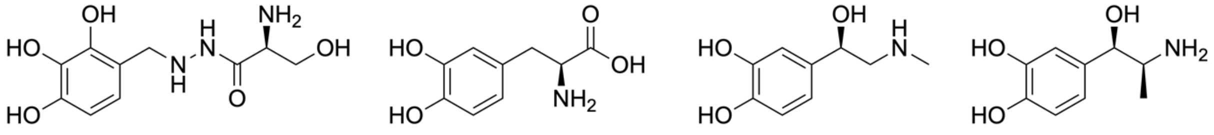

**Benserazide, 32** **L-DOPA, 33** **L-Adrenaline, 34** **Levonordefrin, 35**

**Figure 17** - Compounds from virtual screening of ZINC database within the active site of hUCH-L1. Compound selection based on the GOLD score and the LE parameter.

All four compounds (**32**-**35**) belong to or are derivatives of compounds from the catecholamine family, derivatives of the amino acid tyrosine. Benserazide **32** and L-DOPA **33** are already used as drugs in PD.[5] Benserazide **32** is an inhibitor of the DOPA decarboxylase converting L-DOPA to dopamine. In that respect, Benserazide is given as a supplement to L-DOPA in order to increase its half-life in the blood, thus to allow it to go through the BBB and be converted to dopamine in the brain which will alleviate the motor symptoms. L-DOPA **33** and L-adrenaline **34** (also known as epinephrine) are both present in the biosynthetic path of catecholamine. L-adrenaline is a neurotransmitter that is involved in the fight-or-flight response. The last molecule that came out of this screening is Levonordefrin **35**, also known as α-methyl-norepinephrine, a derivative of the catecholamine norepinephrine. It is used as a nasal decongestant and vasoconstrictor in dentistry.[176]

As L-DOPA **33** and L-adrenaline **34** are neurotransmitters they will certainly show important off-target activities. They will then not be selected for the further *in vitro* experiments with hUCH-L1. Furthermore, as Levonordefrin **35** is highly structurally similar to norepinephrine, it could also lead to an off-target activity. In that respect, benserazide was first chosen so as to study its potential effect on the hUCH-L1 enzymatic activity. The compound was firstly tested as a racemic mixture, as both S and R configurations have a high GOLD score (62.03 and 56.86, respectively) and LE (3.45 and 3.16 respectively). The data showed a modest-weak inhibitory activity (20%) of hUCH-L1 (**Figure 18**).

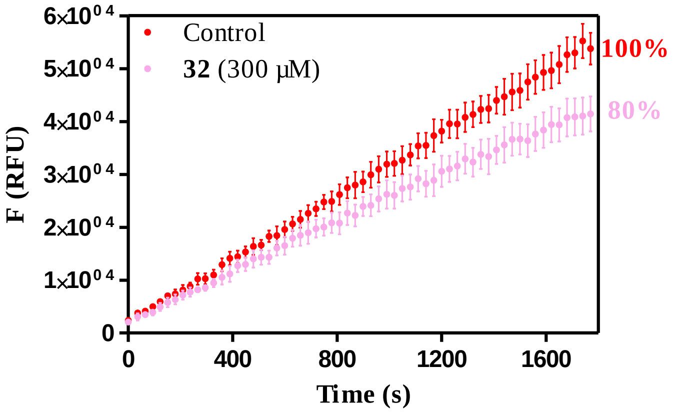

**Figure 18** - Enzymatic activity of hUCH-L1 in the presence Benserazide **32** at 300 µM. No modulator (control) was defined as 100% activity.

The precise function of UCH-L1 in PD remains unclear. Up till now, inhibitors of this protein are mostly studied in cancer applications as UCH-L1 is found to be upregulated in breast and colorectal cancer for instance.[128,131] On the other hand, in PD models inhibition of UCH-L1 activity by LDN-57444 demonstrated a clearance of aggregated α-synuclein.[177] Thus, these three inhibitors could be potentially interesting to open new paths in the study of inhibitors of UCH-L1 as therapeutic option in PD.

### 2.2 Alanylpiperidine derivatives as modulators of UCH-L1

Only one activator is described in the literature: ethyl 1-(N-(methylsulfonyl)-N-(p-tolyl)-alanyl)piperidine-4-carboxylate (**Figure 19**, compound **21**). It was discovered through *in silico* drug screening by Mitsui's group who revealed activation properties of this compound in UCH-L1 as the enzymatic activity was up to 111% at 63 µM.[149] This activator has been used as a starting molecule in this work. Derivatives of compound **21** were then investigated as potential activators. Several parts of compound **21** can be modulated: the tolyl group, the N-sulfonamide, the ester moiety and the methyl of the stereogenic center. The ester moiety was the first modulation selected in this work as to find potential activators. The ester was first replaced by a carboxyl group (**Figure 19**, compound **36**). A study was consequently conducted as to investigate the influence of such transformation. Compound **36** bears a carboxylic acid group which opens a possibility for co-crystallization and salification to modulate its physical and chemical properties.

Compounds **21** and **36** bear a stereogenic center. The compound with a S absolute configuration is derived from L-alanine (refered to as **(S)-21** or **(S)-36**) and the one with a R absolute configuration is derived from D-alanine (refered to as **(R)-21** or **(R)-36**).

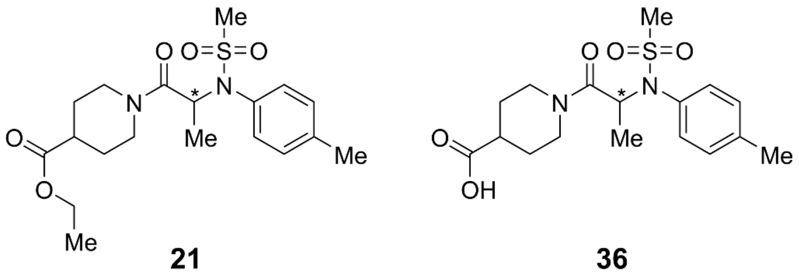

**21** **36**

**Figure 19** - Structure of ethyl 1-(N-(methylsulfonyl)-N-(p-tolyl)-alanyl)piperidine-4-carboxylate **21** and 1-(N-(methylsulfonyl)-N-(p-tolyl)-alanyl)piperidine-4-carboxylic acid **36** (ABXY-1).

### 2.2.1 Synthesis of compound 36

The synthesis of compound **36** was carried out starting from compound **21**. A small amount of the latter compound was acquired by our collaborators which allowed us to perform our preliminary studies on it. We were then able to synthesize compound **36** through a saponification reaction of **21** in the presence of LiOH (***Scheme 2***). The synthesis succeeded, with a high yield. Furthermore, compound **21** was obtained in a racemic mixture thus synthesis of compound **36** also yielded a racemic mixture.

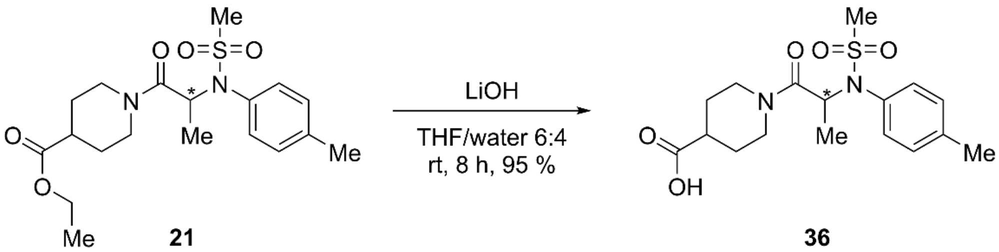

**Scheme 2** - Saponification reaction of compound **21**.

### 2.2.2 Structural study of compounds 21 and 36

Herein, we report the crystal structures of both compounds **21** and **36** as well as a survey on the interactions observed in compound **36**. These results were published in Acta Crystallographica Section E under the reference: Mambourg, K., Tumanov, N., Henon, G., Lanners, S., Garcia-Ladona, J., & Wouters, J. (2021). Crystal structures of two alanylpiperidine analogues. *Acta Crystallographica Section E: Crystallographic Communications*, 77(11), 1095-1098. The published version is included in Appendix H.

### Structural commentary

Both compounds **21** and **36** crystallize as colorless plate-like crystals but in different space groups. Compound **21** crystallizes in triclinic $P\bar{1}$ and compound **36** in monoclinic $P2_1/n$ space group. The asymmetric units are shown in **Figure 20**. Both compounds crystallize as a racemic mixture and have one molecule in the asymmetric unit in a similar conformation. The torsion angles of N1-C1-C2-N2 (atom numbering in **Figure 20**) is 156.2 (1)° and 153.5 (1)° for compounds **21** and **36** respectively. The only slight difference between both compounds is the geometry of N2. In compound **21**, the distance between N2 and the plane formed by C2, C3 and C7 is 0.114 Å compared to compound **36** where this distance is 0.014 Å. A more planar arrangement of N2 in compound **36** is noticed, probably caused by the crystal packing. Single-crystals represent the bulk samples as the powder patterns calculated from SCXRD data are similar to the experimental ones.

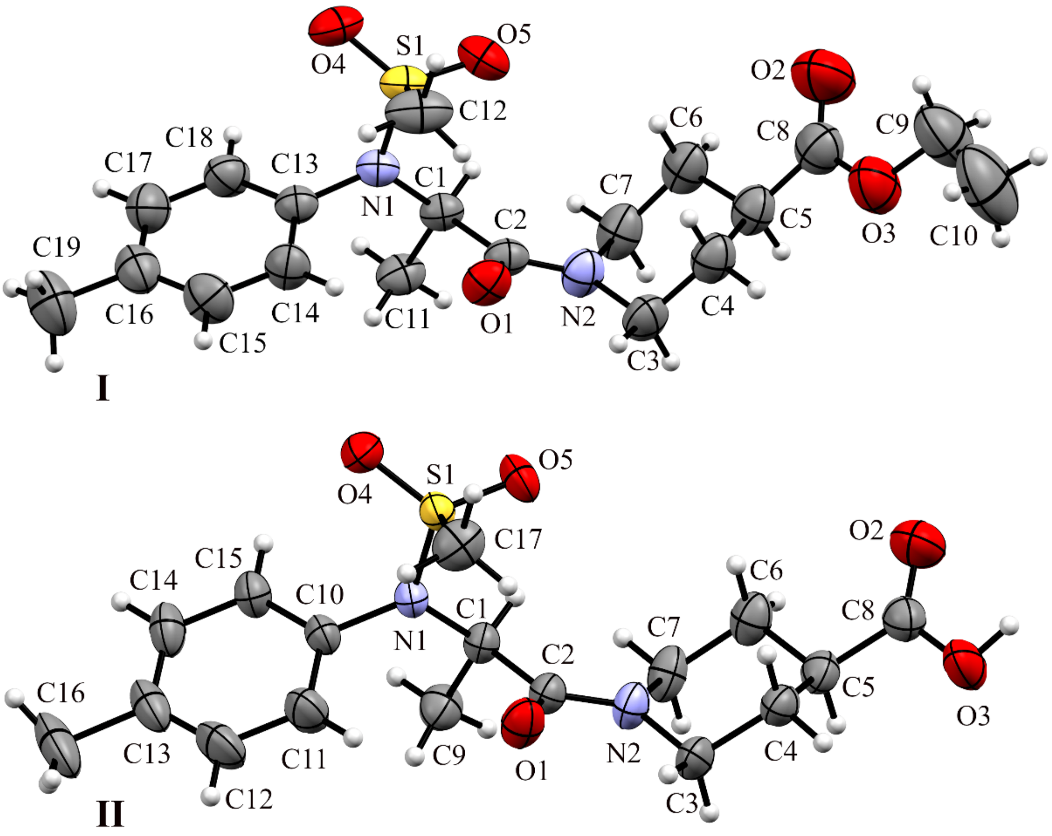

**Figure 20** - The asymmetric unit of the crystal structure for compound **21** (I) and compound **36** (II), with displacement ellipsoids drawn at the 50% probability level.

## Supramolecular features

As compound **21** does not have any strong hydrogen bond donor, only weak hydrogen bonds are observed in the crystal structure (**Table 3**). The amide oxygen O1 participates in the formation of two intramolecular hydrogen bonds ($S_1^1(7)$ motifs[178]). The oxygen atom O4 is inter-connected with a H12 of sulfonyl methyl of an adjacent molecule [d(H···O) 2.44 Å; **Table 3**] forming a $R_2^2(8)$ hydrogen bond motif along a axis (**Figure 21**). As compound **21** bears a tolyl moiety, π-π interactions were expected but not observed in this crystal packing.

**Table 3** - Hydrogen-bond geometry (Å,°) for **21**.

| D—H···A | D—H | H···A | D···A | D—H···A |
|---|---|---|---|---|
| C12—H12B···O1 | 0.96 | 2.50 | 3.210 (2) | 130.4 |
| C12—H12C···O4$^{i}$ | 0.96 | 2.44 | 3.376 (2) | 163.7 |
| C14—H14···O1 | 0.93 | 2.48 | 3.177 (2) | 132.3 |

Symmetry code: (i) –x, -y, -z+1

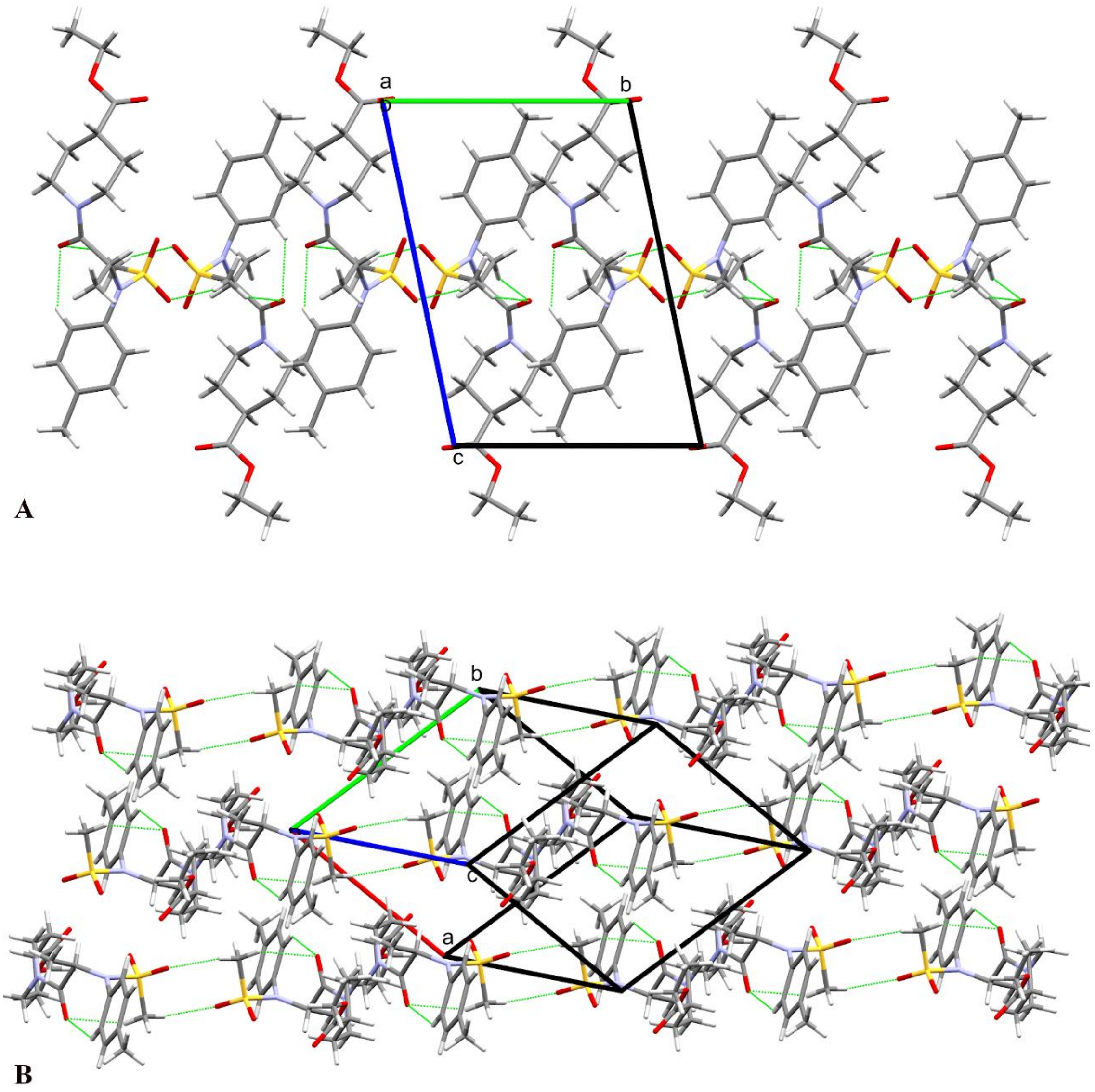

**Figure 21** - Crystal packing of compound **21** with hydrogen bonds highlighted in green (A) showing one layer of molecules, viewed down the a axis and (B) showing adjacent layers of molecules.

Compound **36** bearing a carboxylic moiety instead of an ester has an impact on the hydrogen bonds and thus on the crystal packing. In compound **36** a tubular arrangement (**Figure 22**) can be observed, that is different from compound **21**. In compound **36**, a hydrogen bond ring $R^2_2(24)$ formed by a strong hydrogen bond between H3 of the carboxylic acid group and O5 from an adjacent molecule [d(H···O) 1.88 (3) Å; **Table 4**] is observed. In addition, two intramolecular ($S^1_1(7)$ motifs) and one intermolecular ($R^2_2(10)$ motif) weak hydrogen bonds are detected. As in compound **21**, no π-π interactions are noticed in the crystal structure. In the crystal packing a dimer synthon is observed in both cases but for compound **21** it is ensured by weak hydrogen bonds contrary to compound **36** where the dimer is based on the strong hydrogen bond.

**Table 4** - Hydrogen-bond geometry (Å,°) for **36**.

| D—H⋯A | D—H | H⋯A | D⋯A | D—H⋯A |
|---|---|---|---|---|
| O3—H3⋯O5$^{i}$ | 0.960 (3) | 1.88 (3) | 2.7463 (15) | 161 (2) |
| C17—H17A⋯O1 | 0.96 | 2.48 | 3.144 (2) | 126.6 |
| C4—H4B⋯O2$^{i}$ | 0.97 | 2.52 | 3.471 (2) | 167.3 |
| C11—H11⋯O1 | 0.93 | 2.56 | 3.2558 (19) | 132.3 |

Symmetry code: (i) –x+2, -y+1, -z+1

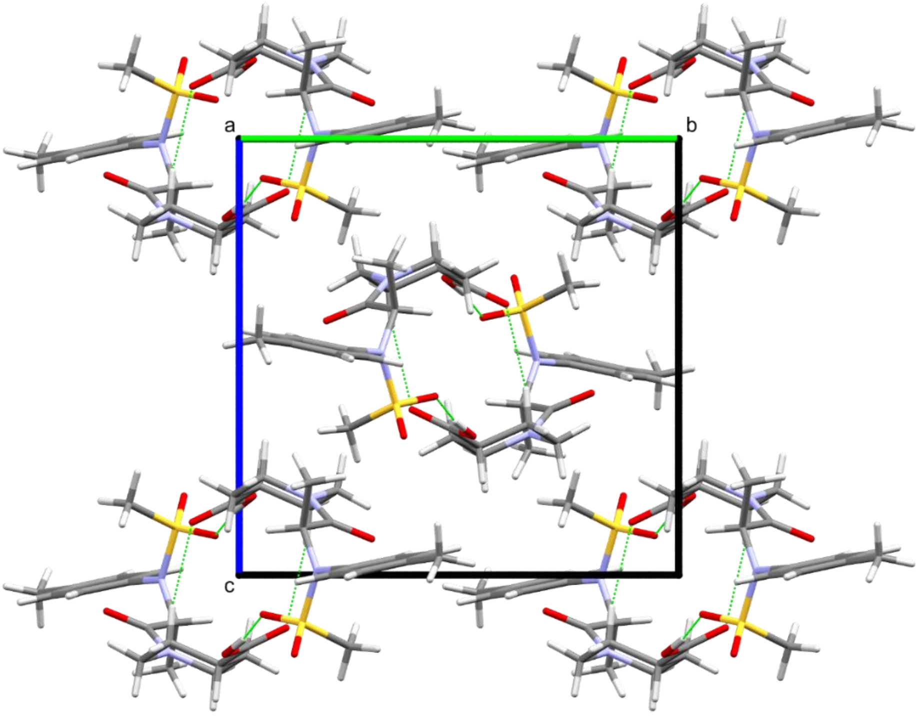

**Figure 22** - Crystal packing of compound **36** showing tubular arrangement viewed down the a axis. Hydrogen bonds are highlighted in green.

### Database survey

Searches on the Cambridge Structural Database[179] (CSD, Version 5.42, update September 2021) were carried out with the exact structures of compounds **21** and **36** and with substructures containing the significant fragments (alanylpiperidine with and without sulfonyl methyl and tolyl group). No comparable structures came out of this survey. A polymorph risk assessment based on the hydrogen bonds in the CSD was carried out. This statistical analysis allows us to estimate which atoms are the donors and the acceptors for hydrogen bonds in the crystal structure.[158,180] This quantifies the probability of hydrogen bond formation and thus the different probable polymorphs that can arise from a specific compound. The results are summarized in **Table 5**. A hydrogen bond interaction between two carboxylic groups is predicted with the highest probability. We did not observe the carboxylic dimer but rather this group interacting with one oxygen of the sulfonyl methyl. The analysis also predicts other plausible hydrogen bond networks (**Figure 23**), one that is statistically slightly more likely to be formed than the current one. This suggests that another potential polymorph can be obtained. Thus, we made a polymorph screening by several crystallization experiments of compound **36**. The recrystallization solvents that we tested were cyclohexane, toluene, ethyl acetate, chloroform, dichloromethane, acetone, acetonitrile, 2-propanol, ethanol and methanol. They all lead to the same polymorph.

**Table 5** - Hydrogen-bond propensity calculation for compound **36**.

| Donor | Acceptor | Propensity |
|---|---|---|
| O3 | O2 | 0.36 |
| O3 | O4 | 0.30 |
| O3 | O5 | 0.30 |

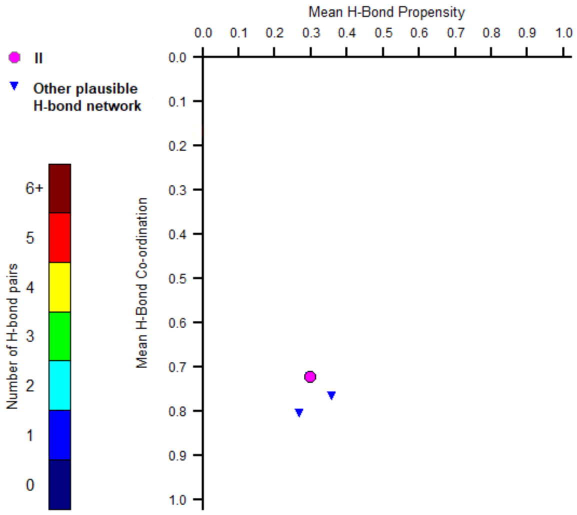

**Figure 23** - Hydrogen bond propensity chart for compound **36**.

### 2.2.3 Docking of compounds 21 and 36 in hUCH-L1

The interaction between compound **36** and *Homo sapiens* UCH-L1 (hUCH-L1) protein was first studied *in silico*. In order to characterize it, a docking of both compounds, **21** and **36**, was performed in hUCH-L1. As no information is given on whether the activator is interacting with the active site or with an allosteric site of the protein, both possibilities were investigated. Up until now, only two sites were characterized in the literature: the active site where the hydrolysis reaction of ubiquitinated proteins occurs and a distal site where the ubiquitin induces conformational changes within the protein.[108,119] Calculations were performed to predict and visualize possible protein-ligand binding sites of hUCH-L1 using SiteMap[181]. The predicted sites obtained are presented in **Figure 24** and their respective site scores are included in **Table 6**.

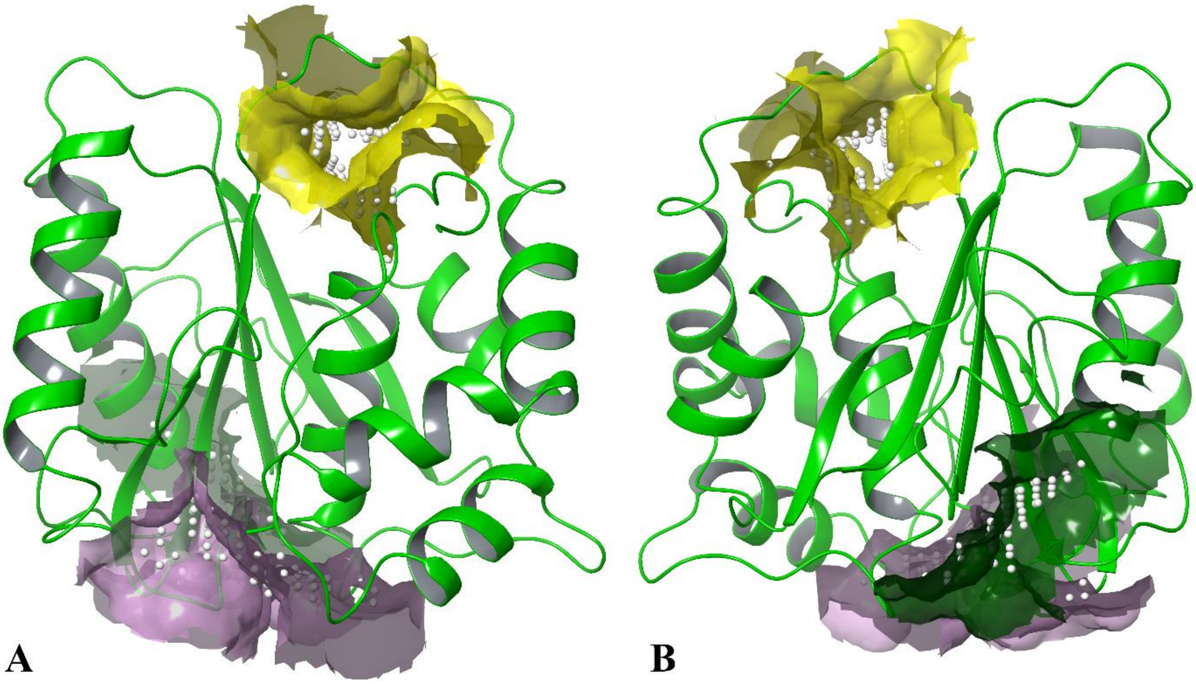

**Figure 24** - Structures of (A) “front” and (B) “back” of hUCH-L1 (PDB ID: 2ETL) in green ribbon representation. Sites from SiteMap calculations are represented as follows: in yellow the active site, in purple allosteric site n°1 and in green allosteric site n°2.

**Table 6** - SiteMap results of hUCH-L1 crystal structure (PDB ID: 2ETL). AS stands for allosteric site.

| | Site score | V (Å$^3$) |
|---|---|---|
| Active site | 1.035 | 337.5 |
| AS-1 | 0.952 | 308.0 |
| AS-2 | 0.643 | 105.0 |

SiteMap identified the active site with the highest score (1.035) and two additional allosteric sites (AS-1 and AS-2). The AS-1 is obtained with a score of 0.952, almost as high as the one of the active site of hUCH-L1. The results obtained with SiteMap were further corroborated with another software tool, PrankWeb, also predicting ligand binding areas.[182] It confirmed the active site and suggested also the presence of AS-1. SiteMap also highlighted AS-2 with a lower score of 0.643 that was not observed with PrankWeb. The active site and AS-1 were chosen for further investigation as high and similar scores were obtained.

Furthermore, in the predicted binding locations, the distal site was not included in the possible ligand accessible locations. As previously mentioned, the β-hairpin of the ubiquitin substrate present at this location causes a steric hindrance which induces a domino rearrangement of some amino acids in UCH-L1.[119] Thus, this is not a site per se as there is no space to fit a ligand.

Docking of compounds **21** and **36**, each in both configurations, was then performed in the active site and in AS-1. The docking results are depicted in **Figure 25** and **26**. It appears that the docking of the four compounds was successfully achieved in both sites, as interactions with the protein are observed. The glide score, corresponding to an approximation of the ligand binding-free energy, was used to rank the best poses obtained for each docking.[183] The binding-free energies are then calculated by MM-GBSA and are gathered in **Table 7.**

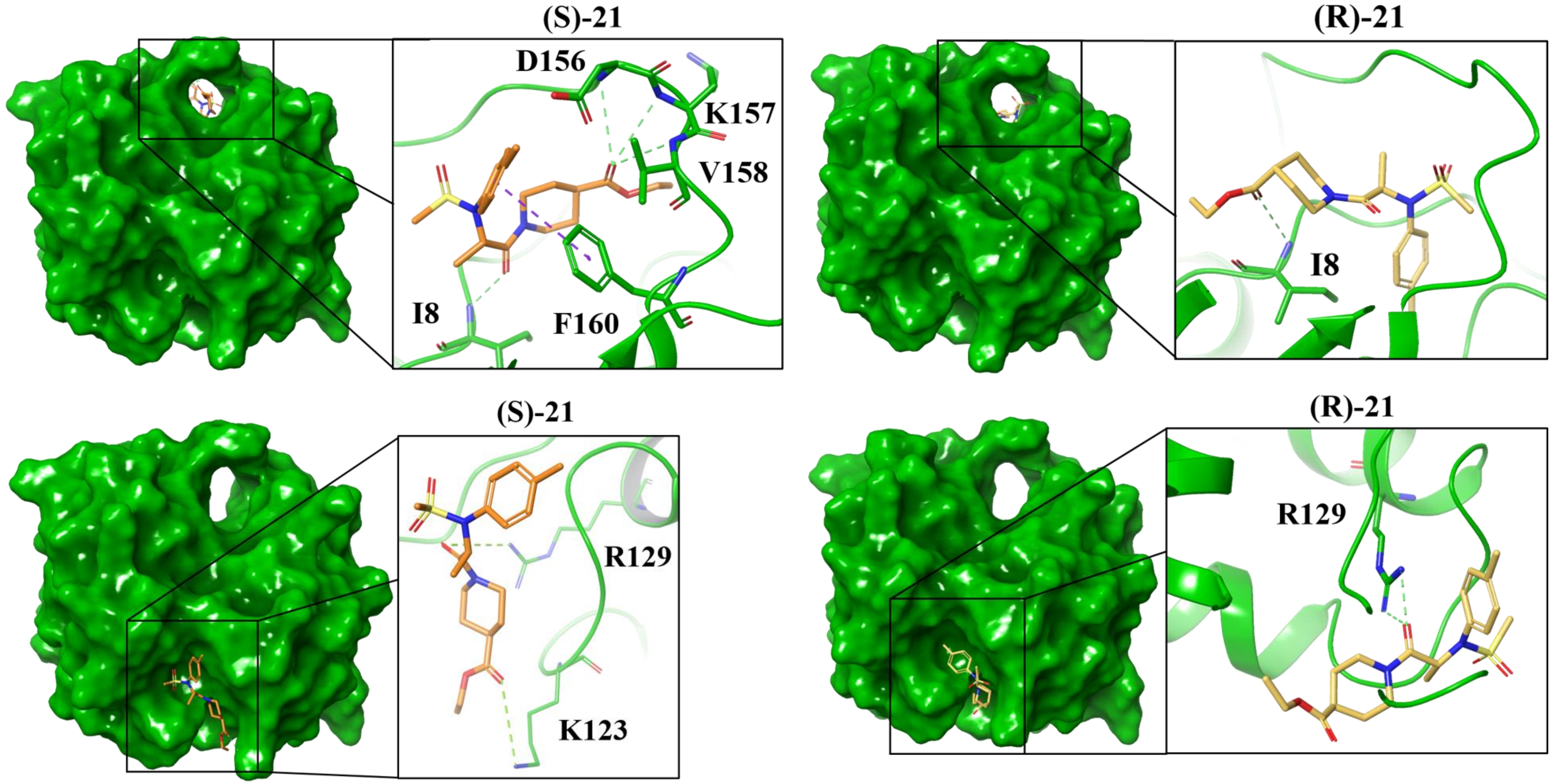

**Figure 25** - Docking results of **(S)-21** (orange) and **(R)-21** (yellow) in hUCH-L1 (represented as molecular surface in green) active site (top) and AS-1 (bottom). For each result interactions with hUCH-L1 are highlighted. Hydrogen atoms are not shown for clarity purpose. The best pose based on the glide score is presented for each situation.

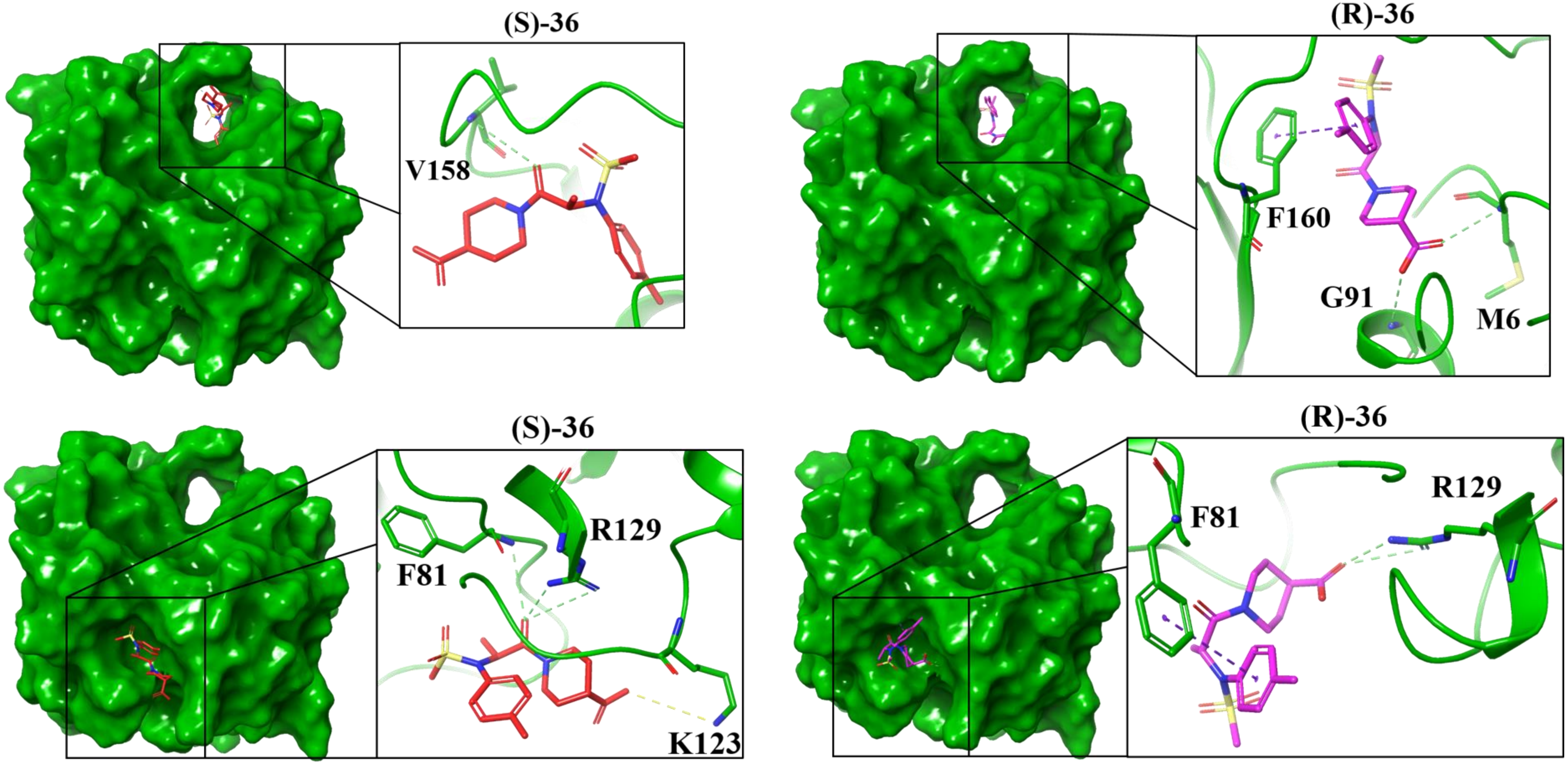

**Figure 26** -Docking results of **(S)-36** (red) and **(R)-36** (purple) in hUCH-L1 (represented as molecular surface in green) active site (top) and AS-1 (bottom). For each result interactions with hUCH-L1 are highlighted. Hydrogen atoms are not shown for clarity purpose. The best pose based on the glide score is presented for each situation.

**Table 7**- MM-GBSA calculations of the affinity between hUCH-L1 and the compounds **21** and **36**.

| | $\Delta G_{binding}$ [kcal/mol] | | | |
|---|---|---|---|---|
| | **(S)-21** | **(R)-21** | **(S)-36** | **(R)-36** |
| Active site | -26.7 | -21.9 | -20.5 | -6.3 |
| AS-1 | -22.7 | -27.6 | -22.8 | -25.0 |

The docking of compound **21** in the active and the allosteric sites generates 5 kcal/mol differences between S and R configurations (**Table 7**). For compound **36**, the docking in the active site demonstrated a difference of 14 kcal/mol contrary to the docking in the allosteric site that showed 3 kcal/mol difference between S and R configurations.

In order to quantify a significant difference in kcal/mol, a comparison of similar conformations from the docking of the same compound in the same protein was realized. The docking results of compound **36** in the allosteric site yielded several poses where a difference of 4 kcal/mol is observed between the three best ones, which are in a very similar conformation (see Appendix A). A difference of 4 kcal/mol was then assumed not significant in this work. Thus, the small difference observed for compound **21** (5 kcal/mol) was therefore not significant. In both configurations, compound **36** expresses a similar binding-free energy in the allosteric site. However, it is likely that the two enantiomers of compound **36** behave differently with this protein. Compound **36** show an *in silico* stereoselectivity at the active site and subsequently may have an effect on the activity of hUCH-L1.

Comparison of the binding-free energies between both docking sites, showed no significant differences for compound **21**. However, compound **36** does not display a similar behavior: in the allosteric site, the binding-free energies are in the same range as for compound **21**, but in the active site the binding-free energies of **(R)-36** are much lower than in the allosteric one. This allowed us to hypothesize that compound **36** interacts less with the active site.

Comparison of the docking conformations of compounds **21** and **36** in S and R configurations in the cavity showed that in the active site all four compounds are docked in the same place but with different conformations (see **Figure 27.A**). These poses were chosen considering the highest glide scores. Analysis of the top five poses obtained for each compound showed that they can display a similar conformation (**Figure 27.B**). For compounds **(S)-21** and **(R)-21** this pose is not insignificant because even if it does not correspond to the highest glide score it corresponds to the highest emodel score, another Maestro score function that is well-suited for comparing conformers.[183] Thus, these results lead us to the hypothesis that compounds **21** and **36** can interact in the same way at the active site of the hUCH-L1.

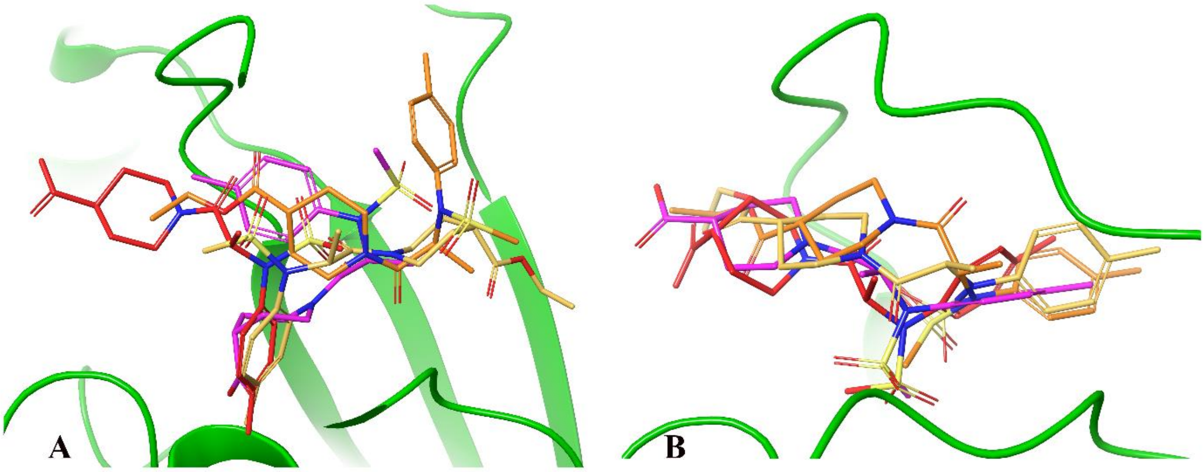

**Figure 27** - Docking poses of **(S)-21** (orange), **(R)-21** (yellow), **(S)-36** (red) and **(R)-36** (purple) in the active site of hUCH-L1 inactive form (PDB: 2ETL, in green). Hydrogen atoms are not shown for clarity purpose. A: The best poses based on the glide score are presented for each compound. B: Based on the glide score: pose 3 of **(S)-21**, pose 4 of **(R)-21** and poses 2 of **(S)-36** and **(R)-36** are presented.

The docking positions of compounds **21** and **36** at the active site showed interactions with Met6, Ile8 and Phe160 (**Figure 25** and **Figure 26**). These results are different from the one demonstrated by Mitsui's group, where an interaction with Cys90 was highlighted (enantiomer not specified).[149] They suggested that compound **21** operates as to open a binding pocket. However, the three amino acids identified were already highlighted by Boudreaux's group as important for the interaction between hUCH-L1 and its substrate.[184] They obtained the crystal structure of UbVMe substrate complexed to hUCH-L1 mimicking the intermediate position of the hydrolysis reaction of Ub with the targeted protein. The fact that the same interactions are observed in the docking of compounds **21** and **36** would mean that they are placed at the same place as the substrate. Since compound **21** has been described as an activating compound of hUCH-L1, it would not seem logical to block access to the substrate. Thus, the hypothesis that the substrate will rather go interact in the AS-1 is reinforced.

A superposition of each best pose, obtained with the glide score, of the docking conformations of compounds **21** and **36** in S and R configurations in the allosteric site AS-1 showed that they are placed in the same cavity but are in different conformations (**Figure 28**). Analysis of all poses yielded after docking in hUCH-L1 showed no similar conformation for all four compounds. In the AS-1, Arg129 and Lys123 appeared to be key amino acids as they interact with both compounds **21** and **36** (**Figure 25** and **26**).

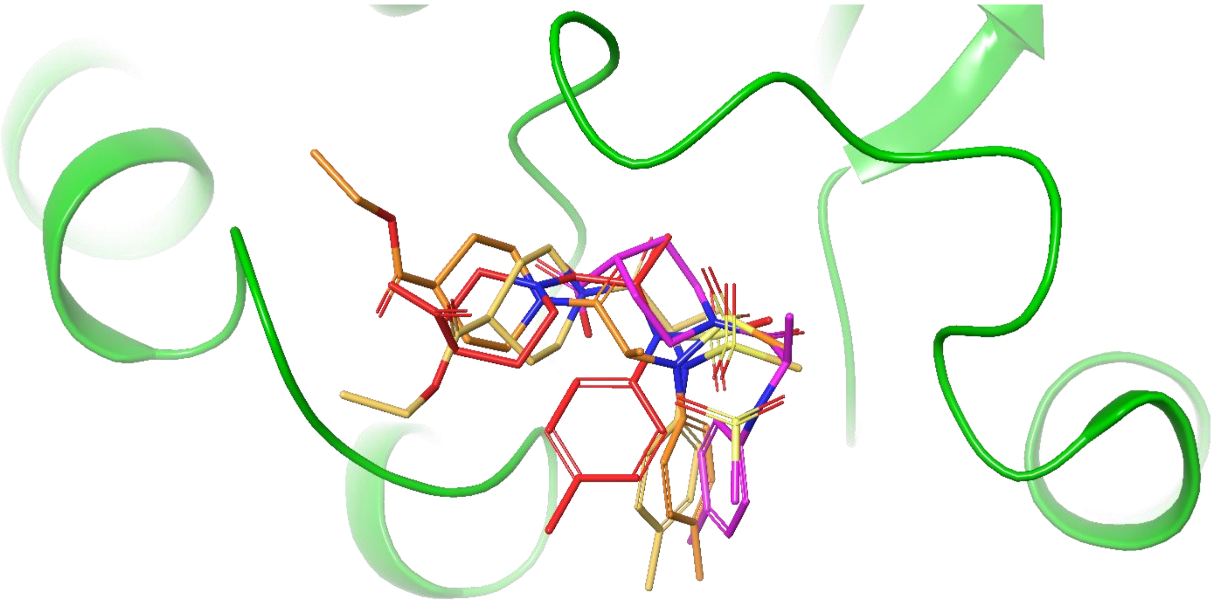

**Figure 28** - Docking poses of **(S)-21** (orange), **(R)-21** (yellow), **(S)-36** (red) and **(R)-36** (purple) in the AS-1 of hUCH-L1 inactive form (PDB: 2ETL, in green), defined by SiteMap. Hydrogen atoms are not shown for clarity purpose.

A comparison of the docking poses with the crystallographic structures obtained for both compounds **21** and **36** molecules showed that they are not in the same conformation as in the crystal structures. This could be explained by the docking parameters chosen. In this work, rigid docking calculations were carried out meaning that the ligand in flexible conformation is docked in a rigid protein with no flexibility allowed. These parameters were chosen as the active site is not significantly altered upon binding of the substrate and because it is also a low time-consuming method.

### 2.2.4 Influence of compound 36 on the enzymatic activity of hUCH-L1

Now that compound **36** was characterized and that its interaction with UCH-L1 was studied *in silico*, it is important to assess its influence *in vitro*. The enzymatic hydrolase activity of UCH-L1 was studied with Ub-Rho substrate. First, an optimization of the conditions (concentration of UCH-L1 and of the substrate) was carried out. Then, the hydrolase activity of UCH-L1 in the presence of compound **36** was performed and the results are provided in **Figure 29**.

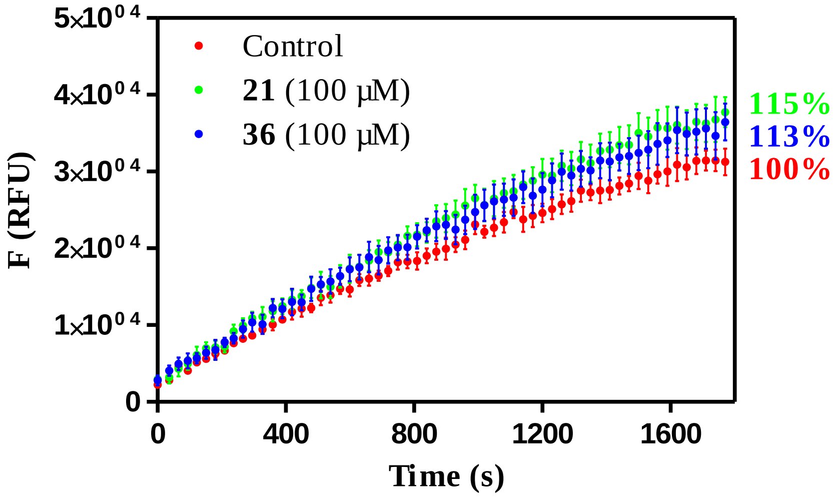

**Figure 29** - Enzymatic activity of hUCH-L1 in the presence of compounds **21** and **36** at 100 µM. No modulator (control) was defined as 100% activity.

Early analysis of *in vitro* activity of compound **21** at 100 µM showed 15% activation of hUCH-L1 enzymatic activity, which corroborates with the results from the literature (11% at 63 µM[149]). Compound **36** showed 13% of activation, very similar to compound **21**. It follows that modulating the ester part of compound **21** does not affect the enzymatic activation of hUCH-L1.

A deeper study of the hUCH-L1 enzymatic activity was then carried out with both compounds **21** and **36**. An $EC_{50}$ assessment was attempted for each compound with hUCH-L1 but solubility problems were encountered. Furthermore, at higher concentrations (200-300 µM), an inhibition of hUCH-L1 enzymatic activity was observed. Even though compounds that activate at lower concentration and inhibit at higher concentration exist, we do not think it is the case here. Indeed, during the experiment, precipitation of compound **21** and **36** in the well was observed. The precipitate compound forms aggregates that destabilized hUCH-L1 and led to a non-active protein.[185]

In the above context, we attempted a higher concentration of DMSO in the well to avoid the precipitation. The protein hUCH-L1 is tolerating, without interfering with the enzymatic activity, until 5% of DMSO but this was still not enough to avoid precipitation of compounds **21** and **36** at higher concentrations. Different biocompatible solvents such as glycerol, PEG at different molecular weight and DMF were then tested to solubilize compounds **21** and **36**.[186] None of these solvents improved the solubility. Thus, a modulation of the physical and chemical properties was further performed by salification trials on both compounds **21** and **36**. This process is presented in the next Part II.

## 3. CONCLUSION

We identified an agonist of the GLP-1R. To further study the 1,2,4-oxadiazole derivative **22**, its synthesis was carried out successfully. However, the compound was found to be a sticky oil and this physical state is rendered further characterization difficult. In order to perform further experiments with it, a modulation of the physical and chemical properties must be achieved.

A subsequent virtual screening of hUCH-L1 with commercially available compounds was performed. Based on the GOLD score and the LE parameter, six small molecules were identified in this study. We demonstrated that Ritonavir, Lopinavir and Benserazide are inhibitors of UCH-L1 enzymatic activity. These compounds did not turn out to be activators as expected. Nevertheless, they could be potentially interesting to open new paths in the understanding of UCH-L1 implication in PD.

Finally, the only compound described in the literature as activator of UCH-L1 was further studied as well as a derivative that was demonstrated a metabolite of compound **21**. We first highlighted *in silico* that compounds **21** and **36** interact with an allosteric site instead of the active site as described in the literature.[149] Indeed, in the active site, it was observed that the compounds interact with the protein in the same place as the substrate which should lead to an inhibition and not an activation of the protein. The docking results we have obtained for compound **21** in the allosteric site seem more adequate as this compound acts as an activator of hUCH-L1. Then, the synthesis of compound **36** starting from compound **21** was described. It allowed us to study further *in vitro* the behavior of these alanylpiperidine derivatives. We showed that compound **36** is an activator, in the same range of activation as compound **21**. Thus, we were able to demonstrate that the modulation of the ester moiety of compound **21** into a carboxylic acid does not affect the activation properties on hUCH-L1.

As the enzymatic essays were performed with the racemic mixture of compounds **21** and **36**, it should be interesting to test the enantiomers separately since a difference between both configurations were observed *in silico* for compounds **36**. A deeper study of the modulators **21** and **36** was not achieved as solubility problems were encountered. A modulation through salification of compound **36** must be done in order to improve the solubility.

# PART II:

# MODULATION OF THE PHYSICAL AND CHEMICAL PROPERTIES OF SMALL MOLECULES

In this chapter, modulation assays of the physical and chemical properties of the small molecules studied in the last sections were investigated. A change in the physical aspect of a 1,2,4-oxadiazole derivative was first performed. Then, alanylpiperidine derivatives were studied so as to solve the solubility problems that have been encountered previously.

## 1. 1,2,4-OXADIAZOLE DERIVATIVES AS AGONIST OF GLP-1R

As reported in last chapter, the synthesis of compound **22** yielded a sticky oil that rendered its handling difficult. This compound showed interesting *in vitro* properties regarding GLP-1R. In order to perform further studies, to characterize the molecule and the interaction with GLP-1R, a change of the physical state has to be achieved. In order to obtain a solid formulation of compound **22**, salification assays were performed. As compound **22** bears basic sites, acids were used to form a salt. This was achieved either through grinding or in solution, depending on the nature of the acid (solid or liquid). As a result, three cases are possible: (i) a salt, if there is deprotonation of the acid, (ii) a mixture, if there is no interaction between the two components and (iii) a co-crystal or co-amorphous system (CAM), if there are interactions between the two components. Some of the results were published in the patent under the reference (Appendix I): Wouters, J., Mambourg, K., Garcia-Ladona, J. Solid Formulation of a 1,2,4-oxadiazole derivative. **WO2021009355 A1** (2021).

### 1.1 Chloride salt

Chloride ions are one of the mostly used anionic counter ions for the formation of salts.[187] Thus, salification assays were first performed with hydrochloric acid. The compound obtained was initially a powder that turned out to be hygroscopic, as it rapidly became deliquiescent. An unstable solid when in contact with air humidity was obtained. Therefore, it was difficult to handle and no further characterization was possible on this sample. The hygroscopicity problem of chloride salts is known in the literature and thus, lately the chloride ion is replaced with other anions in order to overcome this complication.[187]

### 1.2 Screening of various acids

Salification assays were then performed by testing several acids available in the laboratory (***Figure 30***). The experiment was carried out for the liquid acids in ether solvent and for the solid acids through grinding of the two solids. The latter technique is actually very commonly used for the formation of salts.[188]

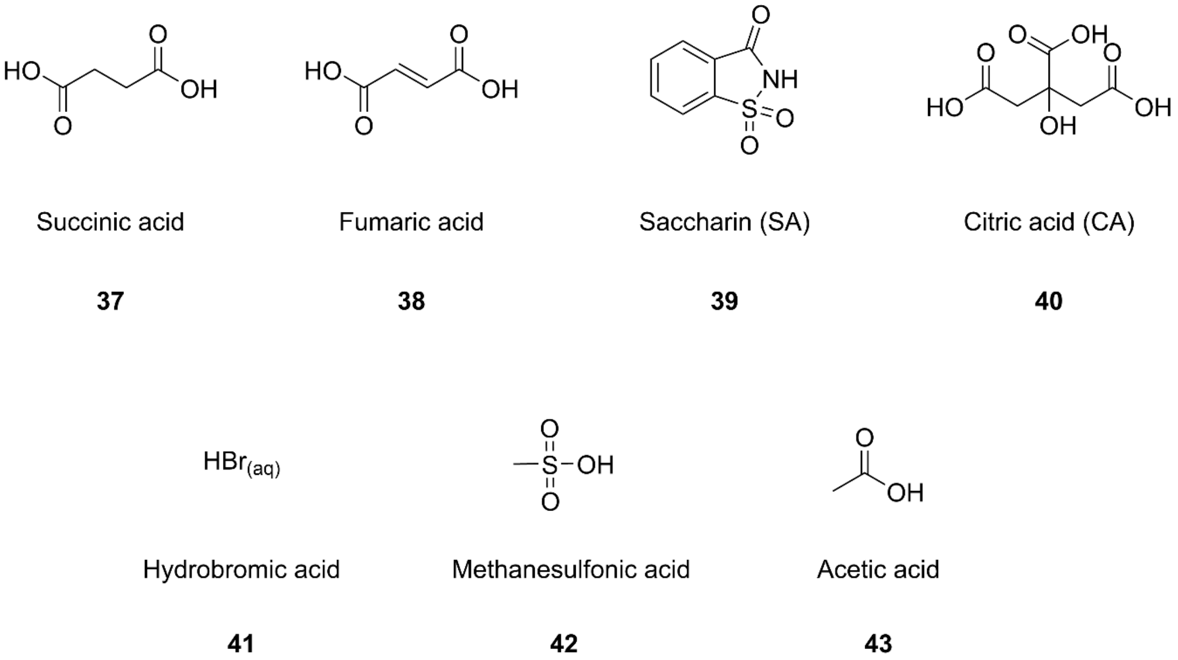

**Figure 30** - Structure of the acids (**37-40** are solid acids and **41-43** are liquid acids) used for salification assays of compound **22**.

In most of the cases (liquid and solid acids), the resuling sample was still obtained as a sicky oil but in some cases the compound turned out to be a hygroscopic solid. However, the use of citric acid (CA) and saccharin (SA) was benefical. When they were both tested with 1 equivalent (eq.) to compound **22**, a sticky oil was achieved. Nevertheless, using 2 eq. yielded a stable solid powder. For an easier understanding in the manuscript, the powder of compound **22** ground with 2 eq. of citric acid will be named **22_2CA** and compound **22** ground with 2 eq. of saccharin will be named **22_2SA**.

The two acids are interesting as both are used in pharamaceutical applications. Its low cost, large availability and its very low toxicity made citric acid a widely used molecule in pharmaceutical applications.[151,189] In addition, saccharin is a GRAS compound. It is not used as much as citric acid in the pharmaceutical industries but there are still several API saccharinates described in the literature.[190,191] Saccharin is an artificial sweetener, thus it can remove the bitter tastes of the API and therefore can be used in pediatric medications.[191]

Currently, there is still a controversy about the safety of saccharin.[192] Since it was discovered in 1879, it was linked to bladder cancer in rats and was thus banned 1970 by the Congress. Since then, after more than 30 human studies, no clear relationship in humans between saccharin intake and cancer was shown. Thus, in 2000, the National Toxicology Program of the National Institutes of Health removed saccharin from the carcinogen list.[193] In that respect, the use of saccharin in this work is justified.

### 1.3 Characterization of 22_2CA and 22_2SA

A characterization of the resulting compounds was carried out in order to study their physical and chemical properties and to compare them to the starting compounds.

First, depending on the grinding conditions, solid forms were obtained but with different composition for both samples. Indeed, the powder X-ray diffraction (PXRD) analyses showed the influence of the ball size (3 mm vs. 12 mm) during grinding. The powder patterns are represented in **Figure 31.A** for **22_2SA** and **Figure 31.B** for **22_2CA**. As compound **22** is an oil, a large broad peak is observed as it is not a crystalline but an amorphous compound.

The results for **22_2CA** and **22_2SA** ground with balls having a diameter of 3 mm showed the presence of an amorphous phase and the starting acid in the mixture. The amorphous phase could be (i) the amorphous compound **22**, meaning that no reaction had occurred upon grinding or (ii) an amorphous salt or CAM system. In the second hypothesis the system is not in 1:2 proportions (**22**:acid) as there is excess of acid. However, it was later discovered that the grinding with a ball having a 12 mm diameter instead of 3 mm yielded an amorphous phase without an excess of the acid. The hypothesis is that a new amorphous phase is completely formed contrary to the case with the 3 mm balls where there was an incomplete reaction. A second hypothesis is that saccharin and citric acid became amorphous upon grinding. However, grinding of both SA and CA alone in the same conditions showed no presence of amorphization in the powder pattern. In that respect, the new amorphous phase could be related to either an amorphous salt or a CAM system, depending on the interactions.

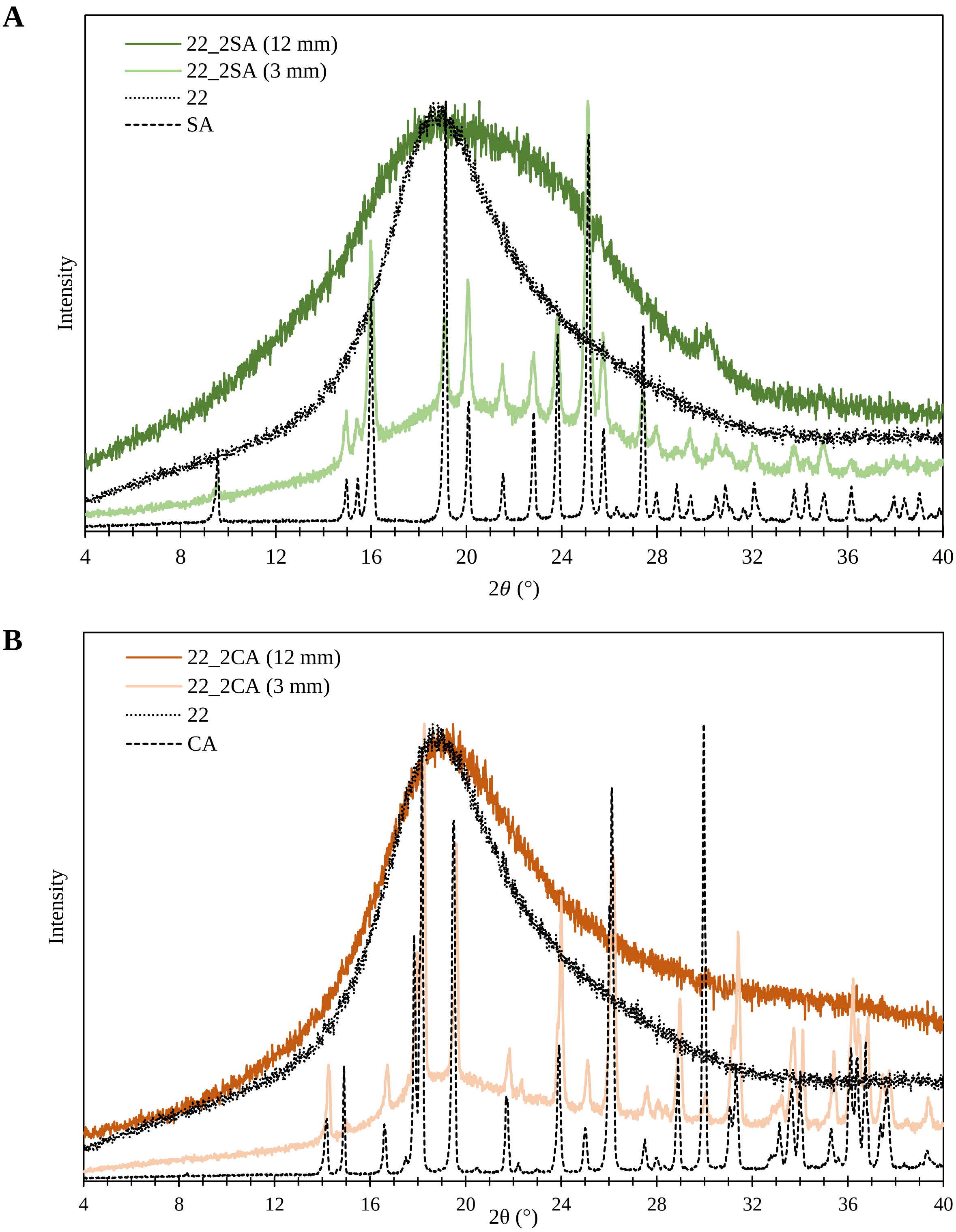

**Figure 31** - Powder patterns of (A) compound **22**, saccharin and **22_2SA**, ground either with a 3 mm or 12 mm ball and of (B) of compound **22**, citric acid and **22_2CA**, ground either with a 3 mm or 12 mm ball. The maximum intensity was normalized for better comparison.

Characterizations were then carried out to study the type of interactions taking place in **22_2CA** and **22_2SA**. For each powder $^{1}$H NMR and $^{13}$C NMR spectra were recorded. In all cases, no deterioration of the compounds and no significant difference of chemical shift of the carbon near the protonated nitrogen were observed. This is leading to a first hypothesis that a CAM system is formed and not an amorphous salt.

Infrared spectroscopy (IR) was then further applied. The vibrational frequency of specific bonds was examined in order to understand whether the resulting amorphous species **22_2CA** and **22_2SA** could be a salt. The major characteristic vibrational frequencies of the starting compounds are indicated in **Table 8** and the IR spectra for **22_2CA** and **22_2SA** are gathered in **Figure 32**.

**Table 8** - Major vibrational frequencies of compound **22**, saccharin and citric acid (s stands for stretching, b for bending, sym for symmetric and asym for asymmetric).

| Compound **22** | | Saccharin | | Citric acid | |
|---|---|---|---|---|---|
| Bond | Vibrational frequency [cm$^{-1}$] | Bond | Vibrational frequency [cm$^{-1}$] | Bond | Vibrational frequency [cm$^{-1}$] |
| $C_{Ar}$-H (s) | 2935 | N-H (s) | 3096 | (C)O-H (s) | 3494 |
| C-H (s) | 2800-2856 | C-H (s) | 2953 | (C=O)O-H (s) | 3288 |
| C-H (b) | 1416 | C=O (s) | 1716 | C=O (s) | 1743<br>1697 |
| C-N (s) | 1322 | C=C (s) | 1594 | C-O(H) (s) | 1138 |
| C-F (s) | 1116 | $SO_2$ (sym & asym s) | 1334<br>1174 | | |

Banerjee *et al.*[190] demonstrated that in saccharin salts, the C=O situated next to the deprotonated nitrogen of saccharin has a frequency of 1690 cm$^{-1}$ instead of 1720 cm$^{-1}$ (1716 cm$^{-1}$ in our conditions). In the IR spectra of **22_2SA** (**Figure 32.A**) a vibration peak at 1738 cm$^{-1}$ is noticed thus strongly suggesting that **22_2SA** is not in a salt form. However, there are interactions between the two components as a shift of the absorption peak is observed. Indeed, in the literature it is demonstrated that the frequency of C=O stretching shifts towards 1730 cm$^{-1}$ when saccharin is in interactions.[190,194] The absorption peak corresponding to the N-H stretching is not observed in **22_2SA** but a shift of the other characteristic absorption peaks is noticed. The appearance of these new peaks could be due to the interactions between compound **22** and saccharin.

Furthermore, for compound **22_2CA**, if a salt was formed with compound **22**, the citric acid moiety should have absorption peaks around 1570 and 1400 cm$^{-1}$ corresponding to the asymmetric and symmetric stretching of C=O from COO$^{-}$ instead of 1750 cm$^{-1}$ of the COOH.[195,196] Experimentally (**Figure 32.B**), vibrations at 1743 cm$^{-1}$ for citric acid and 1723 cm$^{-1}$ for **22_2CA** were observed. This leads us to believe that the mixture is not a salt and that there are interactions between the two compounds as a shift of the absorption peak is observed.[197] The (C=O)O-H stretching could be also considered but the absorption peaks in this area of the spectra are not strong and thus it is difficult to analyze them.

The results obtained with IR spectroscopy led to the hypothesis that species **22_2CA** and **22_2SA** are not an amorphous salt but a CAM system. Indeed, shifts of the vibrational peaks are observed, suggesting that the amorphous phase is presenting interactions, such as hydrogen bonds and Van der Waals interactions, between compound **22** and either citric acid or saccharin.

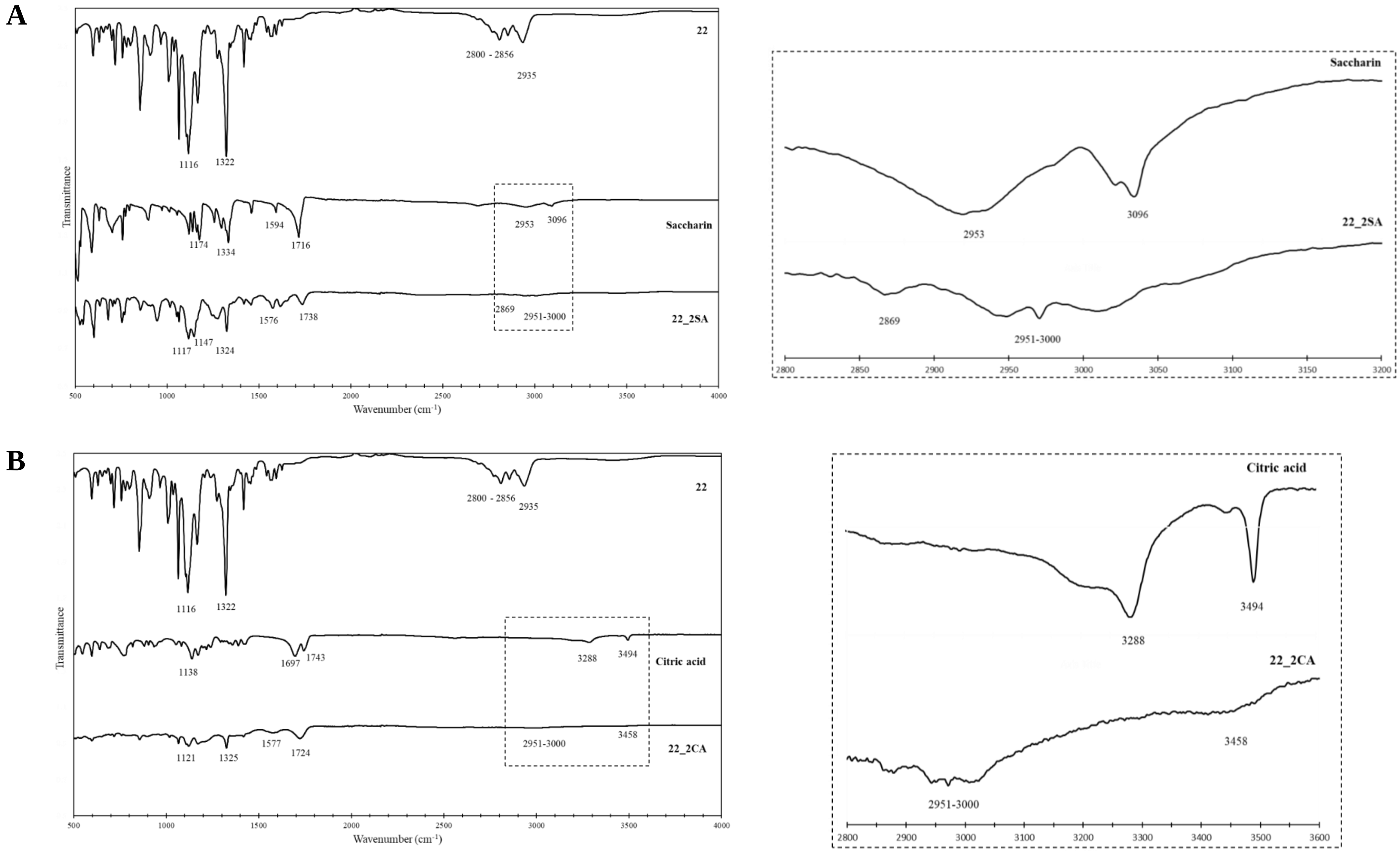

**Figure 32** - IR spectra of (A) compound **22**, saccharin and **22_2SA** (from top to bottom) and of (B) compound **22**, citric acid and **22_2CA** (from top to bottom). Both followed of a magnification in the 3000 cm$^{-1}$ regions.

The thermal behavior of **22_2CA** and **22_2SA** was then assessed. For that purpose, differential scanning calorimetry (DSC) analysis coupled to a thermogravimetric analysis (TGA) were performed (Appendix B). For both samples, an endothermic peak is observed around 50-60°C with **22_2CA** and around 60-65°C with **22_2SA**. It corresponds to the glass transition temperature ($T_g$) with an enthalpy relaxation. These results are consistent with the macroscopic observations made with a Kofler bench. An increase of the $T_g$ is observed for **22_2CA** and **22_2SA** compared to saccharin ($T_g$ of 20°C[198]) and citric acid ($T_g$ of 11°C[199]) meaning that a stabilization of the amorphous system has occurred.[161] Furthermore, the obtained DSC curve of **22_2CA** resembles the DSC curve of a CAM system with citric acid in the literature.[200] Beyond the $T_g$, the samples start to degrade at 140°C for **22_2CA**, 15°C below the degradation of citric acid (155°C) and at 210°C for **22_2SA**, 10°C below the degradation temperature of saccharin (220°C). These results reveal that the thermal behavior of both samples is indeed different form that of the two starting compounds (compound **22** and either citric acid or saccharin).

Furthermore, a verification of the hygroscopicity of both samples was carried out. As most of the salification experiments with various acids leads to hygroscopic compounds, a preliminary characterization of this specification was carried out. The samples were left in ambient air at room temperature (19 ±2°C) and relative humidity of 60 ± 5% for two weeks (**Figure 33**).

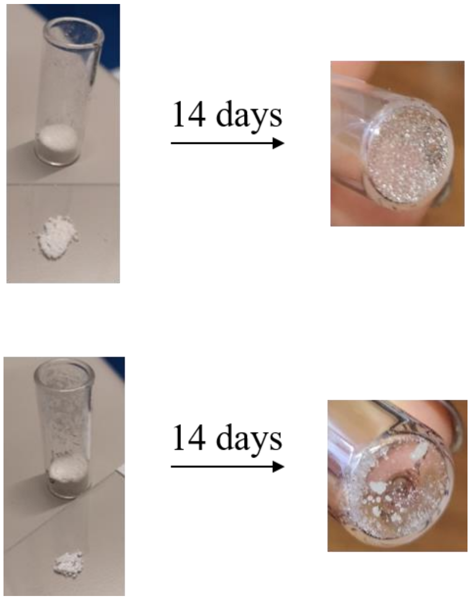

**Figure 33** - Pictures of **22_2CA** (top) and **22_2SA** (bottom) left at air for two weeks.

Both **22_2CA** and **22_2SA** behaved similarly: after a week, the powder started to become sticky and no changes are observed upon two weeks. In order to better characterize the hygroscopicity of both samples, dynamic vapor sorption (DVS) technique could be performed. The change in mass of the samples is analyzed over time and during the variation of the surrounding vapor concentration. This could allow us to study the quantity of water absorbed by the sample.

Finally, a morphological examination was performed. The surface of both samples **22_2SA** and **22_2CA** was investigated by $N_2$ physisorption and SEM imaging. This allowed to determine the porosity and the specific surface area of the samples. The specific surface area is a quite important parameter in the study of pharmacological compounds.[201,202] It was demonstrated that a high specific surface leads to a higher dissolution rate. A drug that dissolves fast can be rapidly absorbed within the gastrointestinal transit time.

The results obtained with $N_2$ physisorption analysis are gathered in **Figure 34** and the high magnification of the sample's surface obtained with SEM are represented in **Figure 35**.

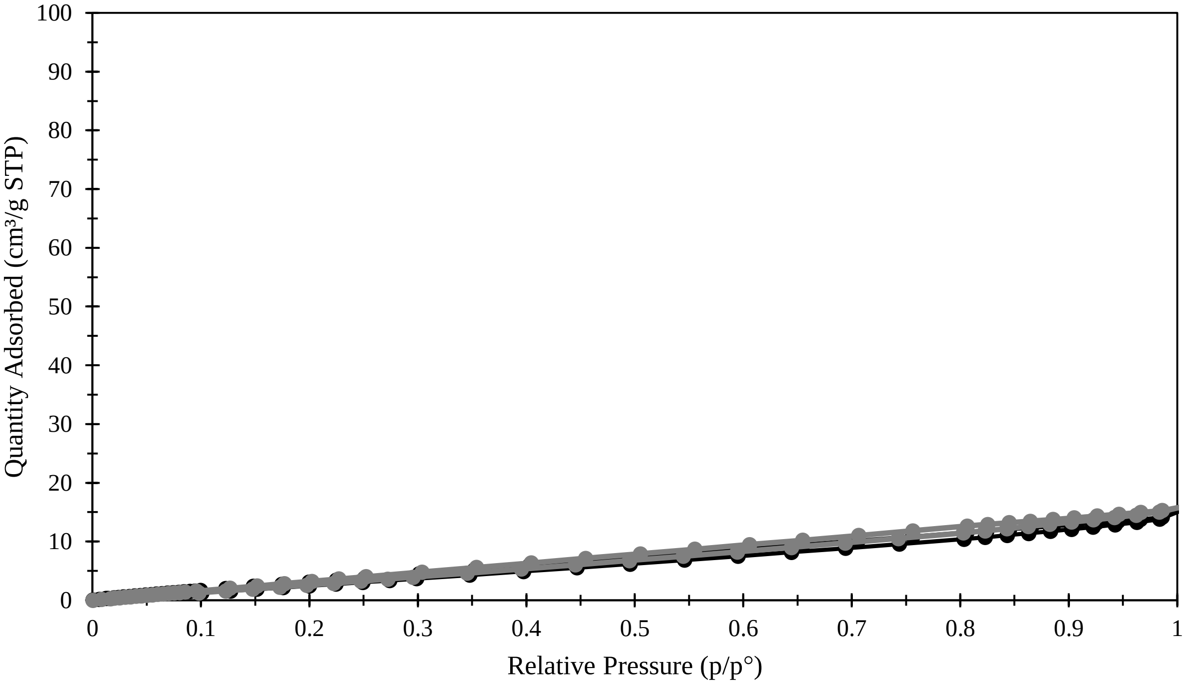

**Figure 34** - Nitrogen adsorption-desorption isotherms of **22_2SA** (black) and **22_2CA** (grey) samples.

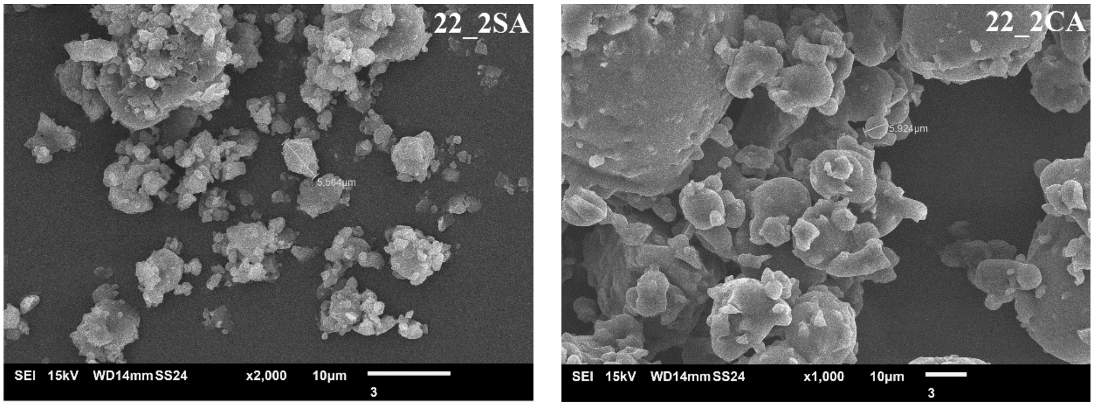

**Figure 35** - Pictures of **22_2SA** and **22_2CA** taken by a SEM.

The adsorption-desorption isotherms (**Figure 34**) of the samples show that the volume of absorbed $N_2$ is low over the entire relative pressure range with a slight increase towards high relative pressure. This isotherm (type 3) is indicative of a non-porous material and of the presence of a slight interparticle porosity. However, the small volume of nitrogen adsorbed (10 $cm^3/g$) could confirm that the detected porosity corresponds to interparticle porosity and not an intrinsic porosity of the analyzed material. The SEM pictures (**Figure 35**) show that the small interparticulate porosity is caused by agglomeration of the particles and not due to a porous nature of the material. Furthermore, the $N_2$ physisorption technique allowed us to determine the specific surface area of **22_2CA** and **22_2SA**. The results are gathered in **Table 9** and it showed that **22_2SA** and **22_2CA** have similar specific surface area.

**Table 9** - Different parameters obtained for **22_2SA** and **22_2CA** after $N_2$ physisorption. (n.d. not determined)

| | **SA** | **CA** | **22_2SA** | **22_2CA** |
|---|---|---|---|---|
| Specific surface area ($m^2/g$) | 10 | n.d. | 22 | 27 |
| Total pore volume ($cm^3/g$) | 0.011 | n.d. | 0.022 | 0.024 |
| Average pore width (nm) | 4.3 | n.d. | 4.3 | 4.3 |

The specific surface area is higher for **22_2SA** compared to saccharin (10 $m^2/g$). At first, the grinding was assumed to increase the specific surface area but after grinding of saccharin in the same conditions the specific surface area is slightly lower (7 $m^2/g$). The different parameters could not be recovered with the citric acid (before and after grinding) as the results were within the detectable limit of the device. Thus, the formation of **22_2SA** and **22_2CA** increases the specific surface area of the sample. Solubility assays should now be performed in order to quantify the impact of this specific surface area.

## 2. ALANYLPIPERIDINE DERIVATIVES AS MODULATORS OF UCH-L1

During the enzymatic activity assessment of compounds **21** and **36**, solubility problems were encountered. This caused complication in the *in vitro* study that was carried out. The solubility parameter is important in the development of new pharmaceutical molecules. Low solubility is unfavorable for the development of the drug as it limits its absorption in the body and can limit the oral bioavailability.[202] To enhance low-solubility issues of drugs, several approaches exist: (i) chemical modifications such as prodrugs or salt formation or (ii) formulation with cyclodextrins.[168,203–205] In this case, the chemical modifications approach will be carried out.

Compound **21** is actually a prodrug of compound **36**. Previous tests performed by Abaxys Therapeutics, the company we are collaborating with on this project, showed that compound **21** forms the metabolite **36** when conditions mimicking the liver are applied. The use of a prodrug is not suitable in this case as compound **21** has a problematic solubility. Additionally, compound **36** bears a carboxylic moiety which renders its transformation into a salt feasible. Therefore, in the remainder of this section, the second approach of salt and co-crystal formation will be performed.

### 2.1 Co-former and counter ion selection

There is a wide range of possible co-formers/counter ions that may form salts or co-crystals with the API **36**. In order to decide which co-former and counter ion to select, three criteria were considered: (i) H-bond propensity (HBP) or $\Delta pKa > 3$, (ii) biocompatibility and (iii) solubility. The followed decision pathway is represented in **Figure 36**. As there was only a small quantity of compound **21** purchased, and by extension a small quantity of compound **36**, only few salification and co-crystallization tests were possible to realize.

As mentioned earlier, compound **36** bears a carboxylic group meaning that basic molecules with a difference of pKa higher than 3 should be used to form a salt. Furthermore, the biocompatibility of the chosen counter ions must also be taken into consideration. A screening of the literature showed that the most commonly studied counter ion in the pharmaceutical sector for an acidic moiety is the sodium ion.[151] This screening also showed that amino acids are also a valuable choice to form pharmaceutical salts.[206] They present low toxicity and thus are included in the GRAS list.

They also present a good solubility in water and are affordable. Therefore, three amino acids - histidine, arginine and lysine - were selected.

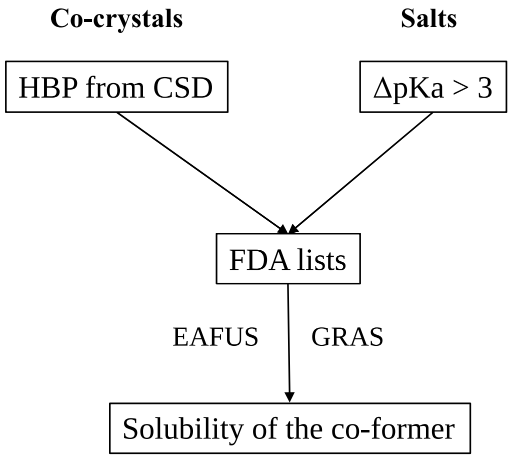

**Figure 36 -** Decision pathway used for the selection of co-former and counter ions in order to form a salt and/or co-crystals of compound **36**.

A co-crystal can also be formed with co-formers that interact with compound **36**. For that purpose, in order to determine which co-former can be interesting, the HBP method was used. It determines the probability of hydrogen bond formation between molecules included in the CSD and compound **36**. The co-crystal is more likely to be formed when the $\Delta_{propensity}$ is high. The limitation for a favorable prediction is $\Delta_{propensity} > 0.02$ and between -0.02 and 0.02, a gray area exists where the formation of the co-crystal is achieved with less certainty. A result under -0.02 is unfavorable to form a co-crystal between both species. The results highlighted 39 molecules that could potentially form hydrogen bonds with compound **36**, with a $\Delta_{propensity}$ score higher than -0.02. As the biocompatibility criterion also has to be taken into consideration, the molecules were further selected among the EAFUS and GRAS lists. Finally, as the aim is to modulate the solubility of compound **36**, the last criterion that has to be taken into account is the solubility of the co-former. Based on these three criteria, a total of 15 compounds could be potentially tested to form co-crystals with compound **36**. As only a small amount of compound **36** was available, a selection of three compounds attracted our attention in this list: caffeine, saccharin and citric acid. Caffeine was chosen because it was obtained with a high $\Delta_{propensity}$ score of 0.3. Saccharin and citric acid were selected because they were easily available in the laboratory and they showed interesting results with the 1,2,4-oxadiazole compound. The different co-formers that were selected for the salification and co-crystallization tests are represented in **Figure 37**. As they are all solid compounds, mechanochemistry was also used as a method to form salts or co-crystals.[188]

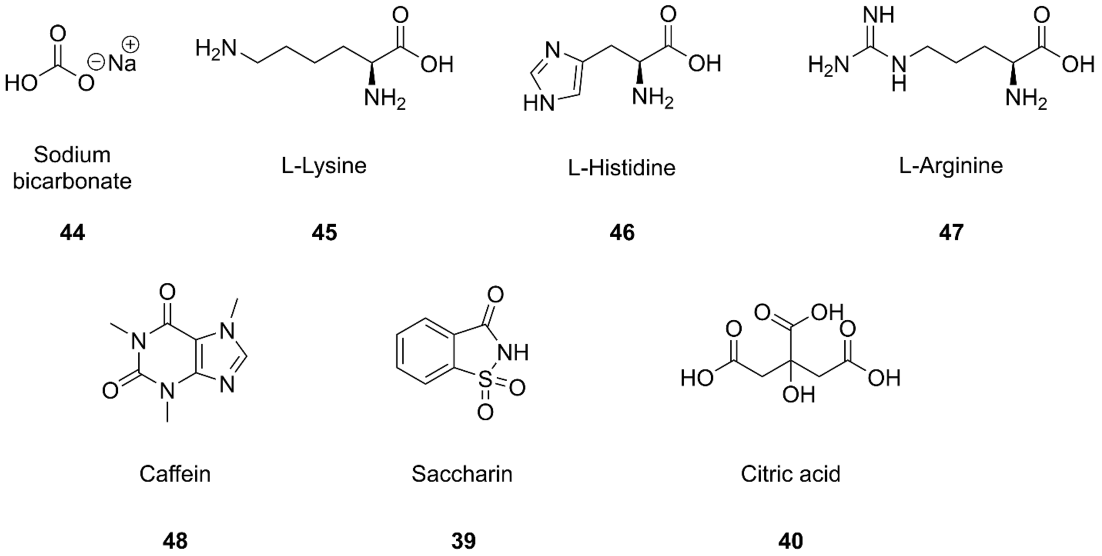

**Figure 37** - Structures of co-formers used for salification and co-crystallization of compound **36**.

### 2.2 Salification and co-crystallization of compound 36

The salification and co-crystallization assays were first performed without added solvent i.e. by neat grinding (NG). PXRD patterns of all ground powders were compared to the one of the starting materials and powders that are not leading to new diffraction pattern were further ground by liquid assisted grinding (LAG). All powders leading to new diffraction patterns were used in the crystallization experiment and were further characterized by thermal analysis. Similar powder patterns were obtained in all the cases compared to the starting reagents (Appendix C), except for the grinding of compound **36** with lysine (**36_Lys**) and sodium bicarbonate (**36_Na**), represented in **Figure 38.**

The grinding assays with sodium bicarbonate and lysine were performed in LAG with water and ethyl acetate respectively. In both cases, a powder was obtained and analyzed by PXRD. In the case of **36_Lys**, an amorphous phase is observed in the powder diffraction pattern, rendering the comparison of the peaks less simple than for **36_Na**. As a result of the LAG, a new crystalline phase was observed in both cases. Indeed, the appearance and disappearance of peaks (highlighted in grey in **Figure 38**) in the powder pattern of **36_Na** and **36_Lys** can be observed when compared to the two starting compounds. Therefore, recrystallization assays were carried out but no crystals suitable for SXRD were obtained for neither of the samples.

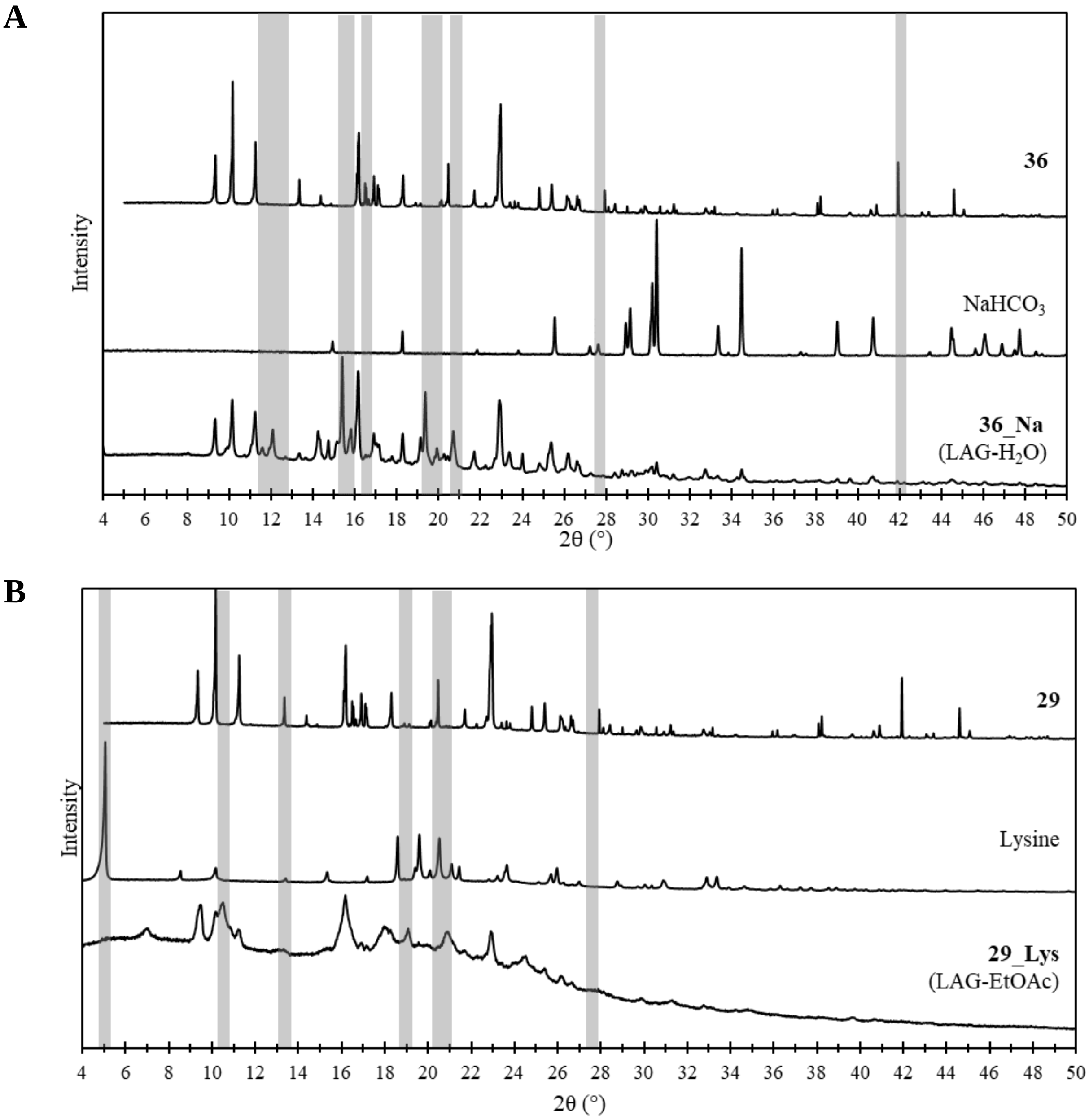

**Figure 38** -Normalized PXRD diffraction pattern of (A) **36**, sodium bicarbonate and **36_Na** (from top to bottom) and of (B) **36**, lysine and **36_Lys** (from top to bottom). In grey are highlighted the different peaks of **36_Na** and **36_Lys** compared to the starting reagents.

In order to confirm the presence of a new crystalline phase, the thermal behavior of **36_Na** and **36_Lys** was then examined (**Figure 39**). The thermal behaviors of the starting material are represented in Appendix D.

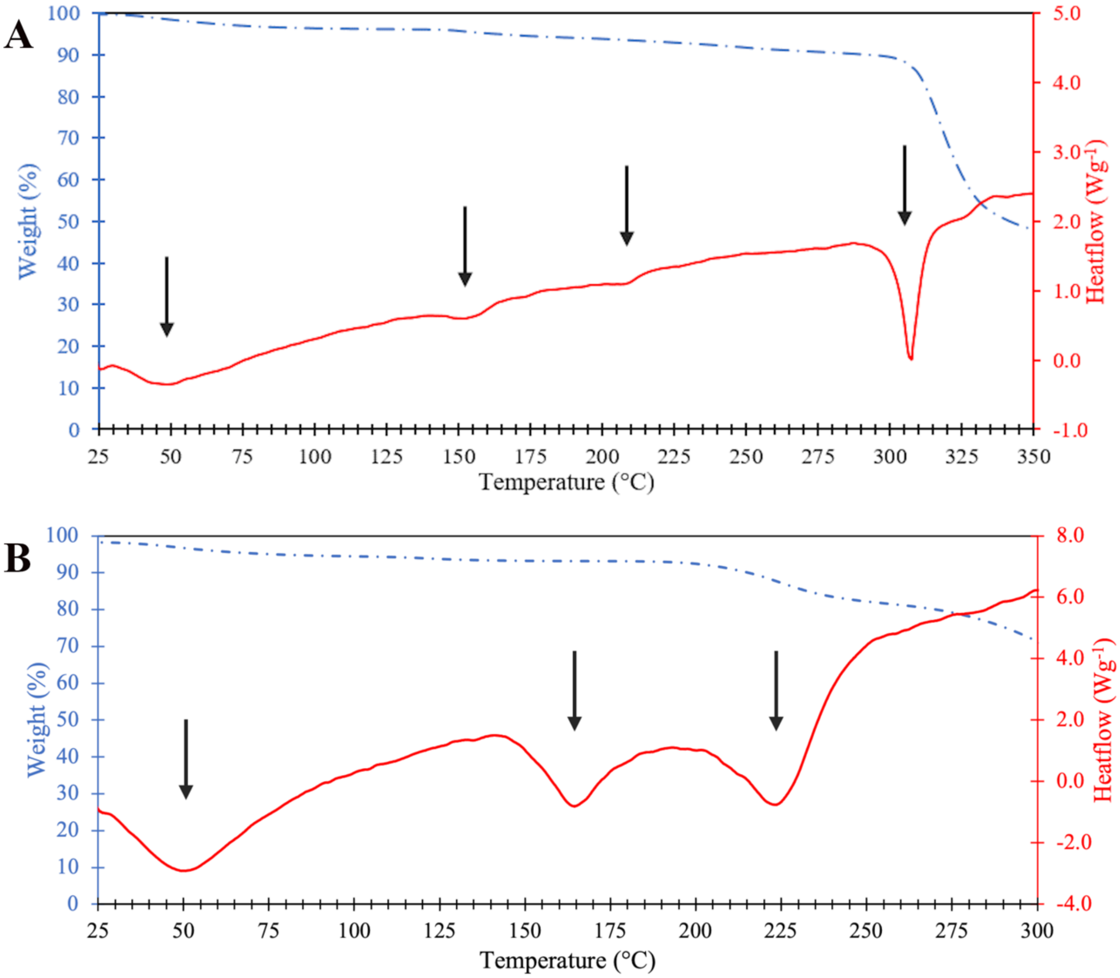

**Figure 39** - DSC and TGA thermograms of (A) **36_Na** and (B) **36_Lys**. The DSC curve is in red line and the TGA one in blue dotted line.

For **36_Na**, a first weight loss can be observed at 50°C accompanied by an endothermic peak. This is probably caused by the water solvent used for the LAG grinding but also by the evaporation of water molecules formed by the acid-base reaction between sodium bicarbonate and compound **36**:

$NaHCO_3$ + **36**H → **36**$^-$Na$^+$ + $H_2O$ + $CO_2$

Furthermore, the Eppendorf tube in which the grinding took place popped open at the end of the experiment which may be related to pressure build-up caused by the formation of $CO_2$ from the above-mentioned reaction. These observations can confirm that the salification of **36** was achieved, at least partially.

A second endothermic peak accompanied by a weight loss is seen around 155°C. It can be correlated with an evaporation of water molecules trapped in the crystalline packing or to the melting point of the remaining sodium bicarbonate.[207] In the second hypothesis, the salt formation is not in ratio 1:1 and sodium bicarbonate is still in excess. A small endothermic peak is also noticed at 220°C, corresponding to the melting temperature of compound **36**. Finally, a last endothermic peak seen at 305°C corresponds to the melting point of the sample. After the melting, a drastic loss of weight can confirm that a degradation of the sample has occurred. The loss observed between 300 and 350° is equivalent to 50%, which can correspond to the elimination of the sulfonamide moiety forming an acrylamide, known to arise in cooked food.[208]

These results suggest that there is an excess of compound **36** in addition to **36_Na** and thus the new crystalline phase is not in stoichiometry 1:1. Going back to the powder pattern of **36_Na** reveals that all the peaks of compound **36** are found in the pattern of **36_Na** except the peak situated at 42° that could still be due to background noise.

As for **36_Lys**, a first endothermic peak accompanied by a weight loss and correlated with the evaporation of water is seen at 50°C. Indeed, the starting reagent lysine was not totally anhydrous and thus in the DSC of lysine the same thermal behavior is observed (Appendix D). The endothermic peak at 165°C corresponds to the melting point of **36_Lys**. Then, a last endothermic peak at 224°C is observed in the DSC curve. It could correspond to both or one of the reagents, as the melting points of lysine and compound **36** are 223°C and 226°C respectively. During the crystallization assays of **36_Lys**, crystals of compound **36** were obtained. Thus, we can assume that the peak observed at 224°C is most likely related to the melting temperature of compound **36**. Furthermore, a degradation can be observed at a temperature higher than 225°C as the weight loss decreases.

Furthermore, a verification of the hygroscopicity of both samples was carried out. The samples **36_Lys** and **36_Na** were left in ambient air at room temperature (19±2°C) and relative humidity of 60±5% for two weeks. A solid acid was still observed for **36_Na** contrary to **36_Lys** which turned out to be deliquescent.

Thus, in both cases for **36_Lys** and **36_Na**, a new crystalline phase was obtained but with an excess of compound **36**. A further purification and/or grinding experiments with different ratios of the starting compounds should be performed. This was not possible to achieve as compound **36** was entirely used in order to generate the preliminary results. Once the new pure crystalline phase is obtained further characterization should be performed in order to study the type of interactions between both compounds and the hygroscopicity of each sample. Solubility assays should then be carried out and their results should be compared to the solubility of compounds **21** and **36**.

## 3. CONCLUSION

In conclusion, the physical and chemical properties of both small molecules studied in this work, the 1,2,4-oxadiazole derivative **22** and the alanylpiperidine derivative **36**, were modulated.

In the case of the GLP-1R agonist, the objective was to modulate the physical state for an easier handling. It was achieved by yielding a powder, through the formulation of a CAM system. Most of the grinding tests either led to deliquescent solids or did not lead to a change in the physical state. However, in the presence of citric acid or saccharin in 2 eq., a powder was obtained. Characterizations of the **22_2SA** and **22_2CA** powders were then performed: a thermal study by DSC/TGA, a structural characterization via PXRD, NMR and IR and finally morphological examination through $N_2$ physisorption and SEM. It can be concluded that a CAM system rather than an amorphous salt was formed in both **22_2CA** and **22_2SA** samples. This new formulation of compound **22** as a CAM system is rather interesting for pharmaceutical purposes as a major problem with new drugs is their solubility and therefore their bioavailability.[209,210] Thus, the amorphous phase confers the advantage to improve the solubility compared to the crystalline phase of the same compound. However, the amorphous phase is unstable as it can crystallize. For that purpose, CAM systems are used to stabilize the amorphous phase. This new formulation of compound **22** changed the physical state yielding a powder that was easy to handle, which can allow now to further perform *in vitro* and *in vivo* experiments on compound **22**.

Furthermore, these results look promising as in the literature saccharin and citric acid are already studied for modulation of the physical and chemical properties through CAM systems. Previous results reported an enhancement of the solubility, the dissolution rate and the physical stability when drug-drug CAM were prepared in combination with either saccharin (SA) or citric acid (CA).[200,211] Some examples such as Repaginide:SA[211]; Indomethacin:CA[212]; Paracetamol:CA[213] and acyclovir:CA[214] can be cited. Agonists of GLP-1R are studied already in different formulations, such as encapsulation and cyclodextrins,[215,216] thus for the first time a CAM system formulation is described for an agonist of GLP-1R.

Finally, Hossain's group studied the difference of NG and LAG on their ketoconazole – dicarboxylic acid system and observed that NG resulted in CAM systems whereas LAG generated co-crytals.[217] Thus, if the amorphous forms of **22_2SA** and **21_2CA** prove to be problematic later on, a grinding in LAG conditions could be performed so as to achieve a crystalline form of the mixture.

The objective of the salification and co-crystallization trials of compound **36** were to modulate its solubility. Two new crystalline phases were obtained upon grinding with lysine and sodium bicarbonate. For **36_Na**, the salt form is expected as water and $CO_2$ generated by the acid-base reaction were detected. The grinding with lysine yielded a new crystalline phase, compound **36_Lys**, but the determination of the salt or co-crystal formation was not achieved.

Further grinding assays should be performed in different ratios for both systems in order to obtain the pure salt or co-crystal. It was not possible in our case as amounts of compound **21**, and by extension **36**, were not sufficient for conducting further studies. Once the pure compounds will be characterized, their solubility should be assessed and compared to compounds **21** and **36**.

Finally, compounds **22_2SA**, **22_2CA** and **36_Lys** showed hygroscopicity properties after being left in ambient at air for two weeks. A deeper characterization of the hygroscopicity of all the compounds (including **36_Na**) should be performed using the dynamic vapor sorption (DVS) technique. This could allow us to study the quantity of water absorbed by each sample. This description is important for later formulations such as the excipient selection and packaging requirement to control the moisture penetration.[218]

# PART III:

---

# *DANIO RERIO* UCH-L1 AN ALTERNATIVE MODEL TOWARDS THE STUDY OF *HOMO SAPIENS* UCH-L1 MODULATORS

Zebrafish species (*Danio rerio*) are gaining in popularity as robust *in vivo* models for the use in the modeling of neurodegenerative diseases because of the accessibility of the embryos, their transparency allowing the use of non-invasive imaging and especially because of the genetic similarity with humans.[169,170] As UCH-L1 is related to neurodegenerative disease, zebrafish have been used as *in vivo* models to study UCH-L1.[169] As it was never described or studied in the literature, in this section we are interested in UCH-L1 from *Danio rerio* species in order to study the protein and to compare it to UCH-L1 from *Homo sapiens*.

## 1. SEQUENCE AND STRUCTURAL ANALYSIS OF HUMAN AND ZEBRAFISH UCH-L1 PROTEINS

UCH-L1 from *Danio rerio* species (zUCH-L1) has a length of 233 amino acids and a mass of 24659 Da. The amino acid sequence alignment of the hUCH-L1 and the zUCH-L1 orthologues is represented in **Figure 40**. The alignment shows a similarity of 79% and an identity of 66% between both sequences and a full conservation of the catalytic residues (Cys90, His161 and Asp176). Given this percentage of identity, building a 3D structure of zUCH-L1 is conceivable by comparative modeling.

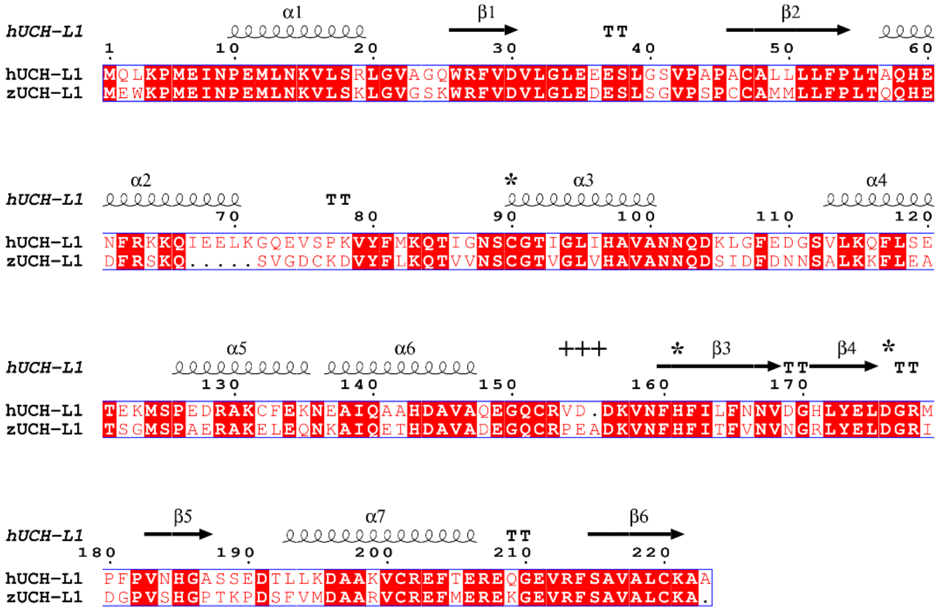

**Figure 40** - Sequence alignment of *Homo sapiens* (hUCH-L1) and *Danio rerio* (zUCH-L1) UCH-L1 proteins. Conserved residues between both species are highlighted in red background. Secondary structure elements from crystallographic structure 2ETL are represented in upper line: α-helices as springs, β-strands are rendered as arrows and strict β-turns as TT letters. The catalytic residues are highlighted by a star and the catalytic loop by a plus sign.

Homology modeling, based on two known structures of hUCH-L1, was used as a technique for this purpose. Both structures are represented in **Figure 41**. The first X-ray structure (PDB: 2ETL) seen in **Figure 41.A** corresponds to the inactive form where the distance between two residues from the catalytic triad Cys90 and His161 is 8 Å. The second, seen in **Figure 41.B**, is an X-ray structure of hUCH-L1 complexed with the ubiquitin vinyl methyl ester (UbVMe) substrate (PDB: 3KW5), that shows an active form of the protein. In the presence of a substrate, Boudreaux *et al.*[184] demonstrated that the distance between the above-mentioned catalytic residues is 4 Å due to a domino rearrangement, leading to an active form (represented in the Introduction of the thesis: **Figure 8**).

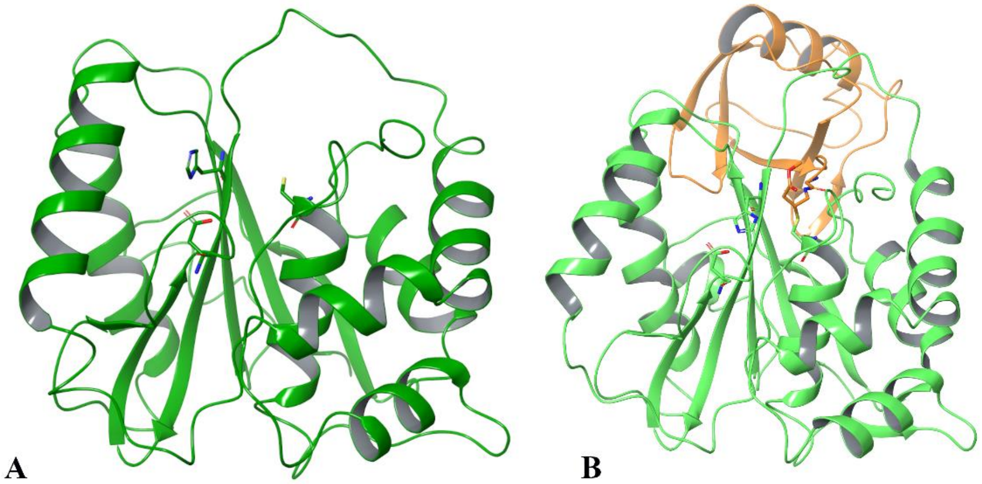

**Figure 41** – Secondary structures representation of (A) hUCH-L1 X-ray structure (PDB: 2ETL) and (B) hUCH-L1-UbVMe complex X-ray structure (PDB: 3KW5). UbVMe is shown in orange and the catalytic triad in sticks.

In that respect, we generated the homology models of zUCH-L1 for both forms in the presence (active form) or in the absence (inactive form) of ubiquitin (Ub): zUCH-L1(a) and zUCH-L1(i) respectively (**Figure 42)**. These models show a structure similar to that reported for the hUCH-L1. In order to measure the similarity between two protein structures, the estimated root-mean-square deviation (RMSD) can be calculated. For both homology models compared to the crystal structures, the RMSD values are 1.105 Å and 0.861 Å for zUCH-L1(i) and zUCH-L1(a) respectively.

Two main features are observed (**Figure 42**): (i) the presence of two lobes, one with five α-helices (right) and one with two α-helices and five β-strands (left) and (ii) a secondary structure helix-β-helix sandwich fold. Both active and inactive models reveal small structural differences in two important sites (the active and distal sites) compared to hUCH-L1 orthologue. In the homology models, the active site and its surrounding appear as in the originally reported hUCH-L1. However, a slightly different conformation of the loop above the catalytic cleft was noticed compared to the crystal structure of hUCH-L1. This is caused by an extra amino acid present in the loop of zUCH-L1 (see the sequence alignment in **Figure 40**). As the loop has been related to the substrate selection that can be ubiquitinated by hUCH-L1, this difference could have an impact on the effect of ligands in the active site.[108] In the distal site, the only difference in the homology models is the presence of a methionine (Met201) instead of a threonine (Thr205) in hUCH-L1 (**Figure 40** and **Figure 42**). This difference is located in the distal site, where there is an interaction with the

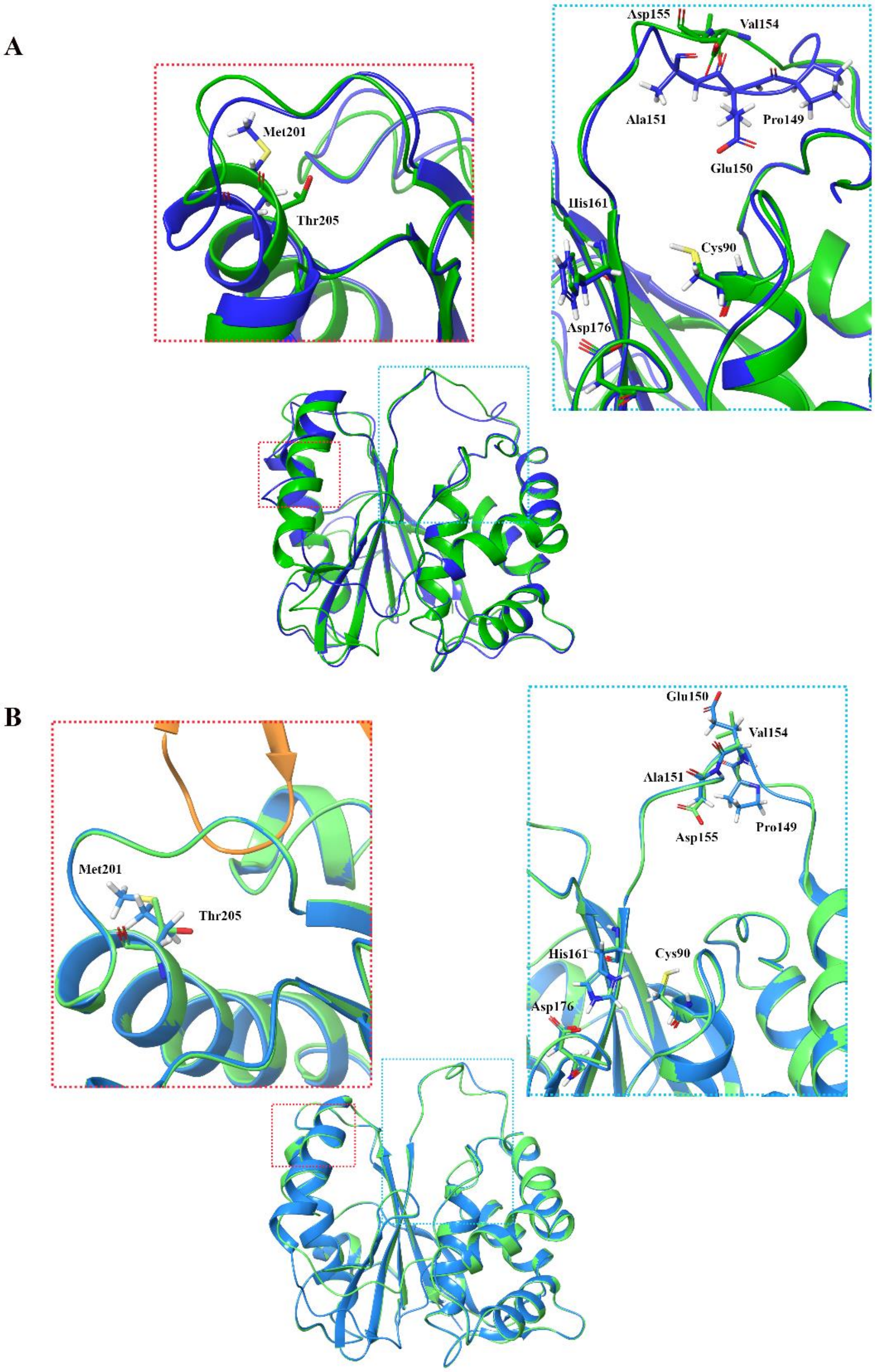

**Figure 42** - 3D structure of homology models zUCH-L1(i) and zUCH-L1(a). Secondary structure representation of the superposition between X-ray structure of (A) hUCH-L1 (2ETL in green) and homology model zUCH-L1(i) (from 2ETL, in blue) and (B) hUCH-L1-UbVMe complex (3KW5, hUCH-L1 in green and UbVMe in orange) and homology model zUCH-L1(a) (from 3KW5, in blue). Two magnifications are illustrated: the catalytic triad and the loop in light blue and the distal site in red. Residues of interest are represented in sticks.

ubiquitin substrate.[119] In order to ensure that this difference is not significant, a docking of the substrate was performed. Boudreaux's group[119] obtained the crystal structure of hUCH-L1 in the active form with the ubiquitin substrate linked to a vinyl methyl ester (VMe) group forming a thioether bond with Cys90 of hUCH-L1(**Figure 42.B**). For this purpose, the docking of UbVMe in zUCH-L1(a) was performed using the ZDOCK server.[219] As we are not interested in the covalent bond but in the position that the ubiquitin substrate takes in the protein zUCH-L1(a), the docking performed is mimicking the intermediate position before reaction of Cys90 with VMe forming the covalent bond. The results suggest that the substrate is positioned in the same way as in hUCH-L1 (**Figure 43**). Superposition of the docking pose in zUCH-L1(a) with hUCH-L1 crystal structure showed an RMSD of 1.025 Å. Despite the difference in amino acid, the β-hairpin of the UbVMe is placed in the distal site. This suggests that zUCH-L1 exhibits the same enzymatic function as hUCH-L1.

For both zUCH-L1 models, the quality of geometry, using PROCHECK[220], showed that 97% of the residues are placed in the "most favorable" and "favorable" regions of the Ramachandran plot and between 1 to 1.6% in the disallowed areas (Appendix E).

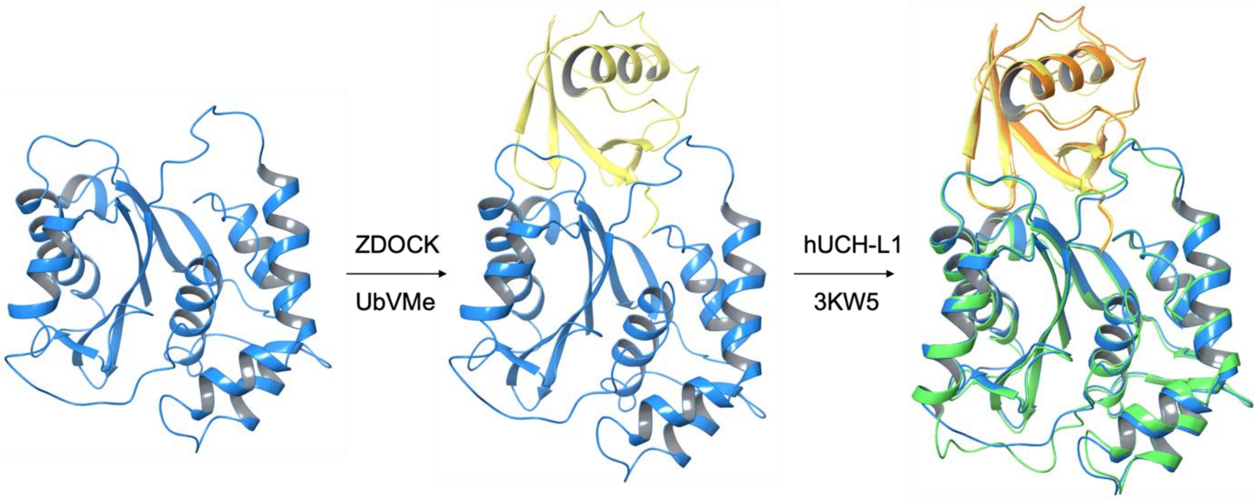

**Figure 43** - Representation of the methodology used to study the UbVMe substrate in the zUCH-L1(a) model. Starting from zUCH-L1(a) in light blue, protein-protein docking of UbVMe substrate was performed with ZDOCK server.[219] The first docking pose of UbVMe is shown in yellow. To this, superposition of X-ray structure hUCH-L1-UbVMe complex (3KW5, in green hUCH-L1 and in orange UbVMe) was performed.

## 2. DOCKING OF REFERENCE LIGANDS IN THE HUMAN AND ZEBRAFISH UCH-L1 PROTEINS

Three effective inhibitors (LDN-57444, LDN-91946 and TCID) and one activator were chosen as reference ligands (structures represented in **Figure 44**). The dockings were performed in both hUCH-L1 and zUCH-L1, at pH 7.4 thus LDN-91946 and TCID are deprotonated. LDN-57444 and LDN-91946 are described as competitive and uncompetitive inhibitors respectively in the literature,[123,143] thus the docking in the inactive and active form respectively was studied. For TCID and the activator no information is given, their docking was investigated in the inactive form of the enzymes.

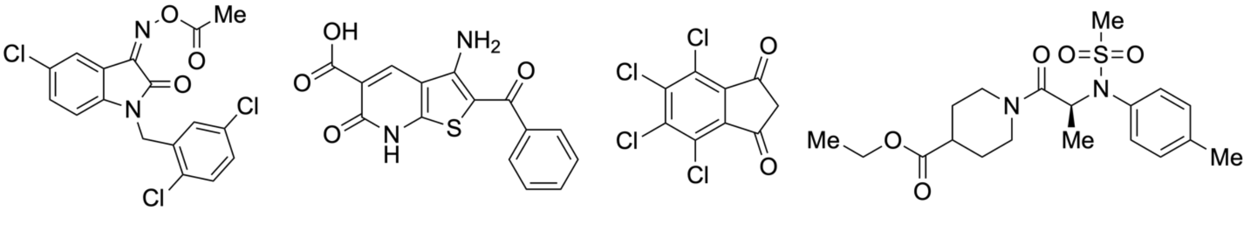

LDN-57444, **15** LDN-91946, **16** TCID, **17** **(S)-21**

**Figure 44** - Previously reported UCH-L1 ligands.

The docking pose locations of the reference ligands in 3D models of zUCH-L1 and hUCH-L1 (**Figure 45**) are different when comparing the inactive and active forms of zUCH-L1. In zUCH-L1(i) (**Figure 45.A,C-D**), the results indicate that for every obtained pose, the ligands favored interactions near the active site. However, in zUCH-L1(a) (**Figure 45.B**), the compound LDN-91946 is docked further forward from the active site as it is hindered by the substrate UbVMe. The locations of the docking poses are also different when comparing the same ligand in both orthologues. The results for the compounds **15, 17 & 21** (**Figure 45.A,C-D**) in zUCH-L1(i) show that the ligands are right above the active site whereas in hUCH-L1, the ligands are well inside the structure. Additionally, the docking poses obtained for compound **16** (**Figure 45.B**) in both orthologues are also different.

Docking results for the activator **21** and inhibitor TCID **17** (**Figure 45.C-D**) show that, in hUCH-L1, both compounds interact with Ile8 and LDN-57444 **15** interacts with the catalytic site. In zUCH-L1, the three ligands show an interaction with the amino acids from the α-helix next to the catalytic site. A second interaction with Cys85 from the catalytic triad is observed for compounds **17** and **21**. As the docking poses are different between both orthologues, no retained interactions are observed.

Mitsui’s group described an interaction between the activator **21** and Cys90 of hUCH-L1.[149] The docking results obtained in hUCH-L1 did not show this interaction because this compound is observed in different conformations from Mitsui’s results. As a different program was used by this group, a slight difference in the results is not surprising. However, it is comforting to observe the interaction with Cys90 in the docking results of activator **21** in zUCH-L1. It reinforces the idea that zUCH-L1 should have a similar behavior than hUCH-L1.

Docking results for LDN-91946 **16** (**Figure 45.B**), in both human and zebrafish proteins, did not indicate interactions with the catalytic site and show different interactions between docking results in both orthologues.

As mentioned before, the loop above the active site in the homology model is in a slightly different conformation compared to the one in the hUCH-L1. To ensure that it is not only the homology model built by Maestro that gives this loop conformation, the homology models of zUCH-L1 were also built with the SWISS-MODEL web service[221] for comparison. A different conformation of the loop is still observed compared to the model obtained with Maestro and the crystallographic structure of hUCH-L1. This disparity in the modeling of the loop may be caused by the lack of secondary structures in it. In addition, the docking of the reference compounds was also performed with the SWISS-MODEL homology model in order to study if the loop conformation has an impact on the localization of the docking positions. No significant differences were observed. The second investigation of the loop was focused on Glu150, that is pointing in the tunnel above the catalytic site in zUCH-L1(i) (**Figure 42**). The assumption made is that the hindrance caused by this amino acid is blocking the ligands forward compared to the poses obtained with hUCH-L1. To ensure this hypothesis, a conformer of zUCH-L1(i) was generated with Glu150 pointing in the opposite direction (RMSD: 1.145Å compared to hUCH-L1 inactive form, Appendix F) and the docking of LDN-57444 was conducted in zUCH-L1(i) “open form”. The two best poses obtained are positioned as in hUCH-L1, further inside the tunnel (Appendix F). The remaining three poses are placed similarly in zUCH-L1(i). These results clearly suggest that the ligands are interacting in the same way in both proteins.

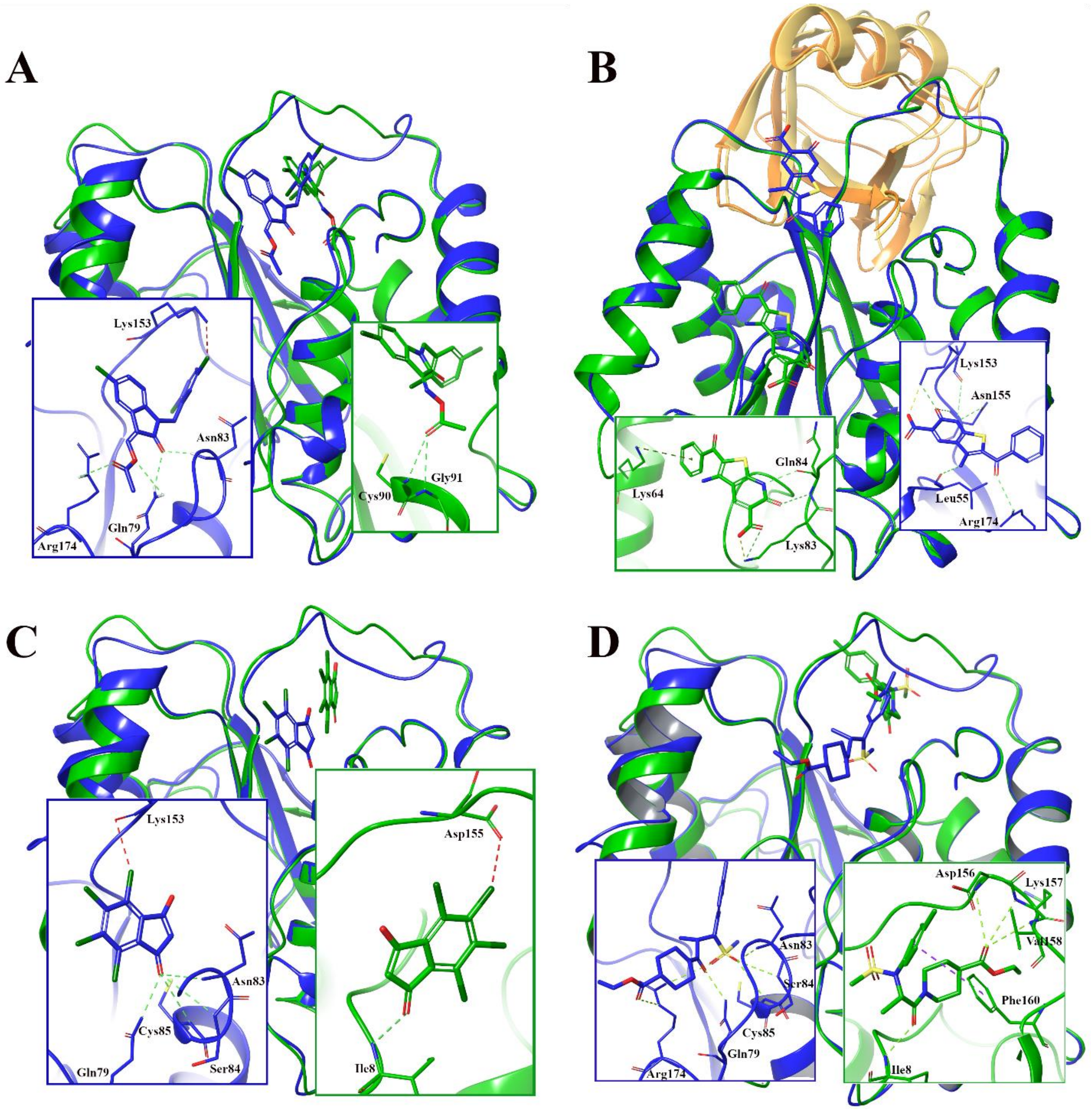

**Figure 45** - Superposition of docking results of previously reported UCH-L1 ligands in 3D homology model of zUCH-L1 in blue secondary structure representation with UbVMe in yellow (A,C-D: zUCH-L1(i) and B: zUCH-L1(a)) and crystallographic structure hUCH-L1 in green ribbon representation with UbVMe in orange (A,C-D: 2ETL and B: 3KW5). For each result, interactions with the protein are highlighted. (A) LDN-57444 **15**, (B) LDN-91946 **16**, (C) TCID **17** and (D) Activator **(S)-21**: in green corresponds to the docking pose in hUCH-L1 and in blue corresponds to the docking pose in zUCH-L1.

In order to evaluate the ligand-protein affinity through the binding-free energy, MM-GBSA calculations on the docking poses for each compound (LDN-57444 **15**, LDN-91946 **16**, TCID **17** and activator **21**) in both forms of hUCH-L1 and zUCH-L1 proteins (**Table 10**) were carried out. A higher affinity of LDN-57444 **15** for the inactive forms of hUCH-L1 and zUCH-L1 proteins is observed. This is consistent with the results that LDN-5744 is a competitive inhibitor.[123] LDN-91946 expressed a higher affinity for the active forms of hUCH-L1 and zUCH-L1, which is consistent with the uncompetitive characteristic of the inhibitor.[143] TCID has a similar behavior in both forms of the proteins and activator **21** showed higher affinity in the inactive forms of hUCH-L1 and zUCH-L1. Furthermore, if the binding-free energies for each compound in the forms studied for the docking are compared, a ranking can be realized. A higher affinity is observed for LDN-57444 inhibitor compared to the other ligands (around -40 kcal/mol). This substantiates that it is one of the most potent inhibitors of UCH-L1. Activator **21** showed an affinity of around -30 kcal/mol, slightly higher than TCID and LDN-91946 with binding-free energy in the same range, around -25 kcal/mol. A comparison between both species (in each form separately) for the same ligand reveals similar binding-free energies ($\Delta G_{binding}$) with slight differences. A difference of 4 kcal/mol was judged to be not significant as for each ligand the $\Delta G_{binding}$ is differing of ~4 kcal/mol between each pose obtained (Appendix A).

**Table 10** – MM-GBSA calculations of the affinity between the two studied proteins (hUCH-L1 and zUCH-L1 in both inactive and active forms) and the reference ligands: LDN-57444 **15**, LDN-91946 **16**, TCID **17** and activator **(S)-21.**

| | $\Delta G_{binding}$ [kcal/mol] | | | |
|---|---|---|---|---|
| | Inactive form | | Active form | |
| | hUCH-L1 | zUCH-L1 | hUCH-L1 | zUCH-L1 |
| LDN-57444 **15** | **-38.9** | **-41.0** | -26.3 | -30.3 |
| LDN-91946 **16** | -17.9 | -20.1 | **-25.0** | **-24.0** |
| TCID **17** | **-20.4** | **-28.3** | -20.6 | -24.0 |
| Activator **(S)-21** | **-26.7** | **-27.9** | -20.6 | -21.2 |

It can be concluded that a limitation of the homology model is the modeling of a loop with different amino acids as there is no secondary structural elements. In that respect, it will be interesting to conduct molecular dynamic simulation of this loop in order to find its preferential position or to obtain the crystal structure of zUCH-L1. Furthermore, the disparity in the loop has no significant impact on the binding-free energies when comparing zUCH-L1 homology models to the hUCH-L1 crystal structures. zUCH-L1 proteins show a behavior similar to that of hUCH-L1 regarding the same ligands. It allowed us to assume that both hUCH-L1 and zUCH-L1 proteins should have a similar behavior *in vitro* in the presence of the same ligands.

## 3. RECOMBINANT EXPRESSION AND PURIFICATION OF ZUCH-L1

Considering that zUCH-L1 has shown a similar performance *in silico* compared to the human analogue, *in vitro* enzymatic activities were carried out. For that purpose, zUCH-L1 protein was produced in *E. coli.* and purified with a GST-tag, allowing to follow a similar purification protocol as described in the literature.[108] During the purification process, zUCH-L1 showed similar elution profile compared to hUCH-L1 (Appendix G). The cleavage of the GST-tag allowed a near full removal of contaminants. The SDS-PAGE gel with fractions for every step of the process is represented in **Figure 46**.

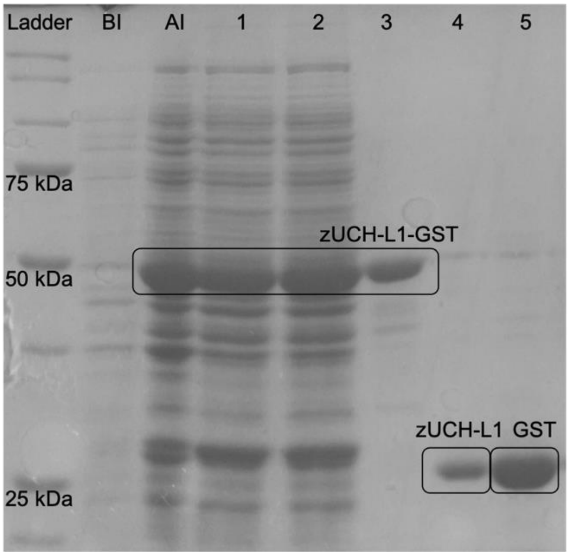

**Figure 46** - SDS-PAGE gel of every step in the production and purification of zUCH-L1 with coomassie stain. Different amounts of protein were loaded in each well. BI: before induction, AI: after induction with 0.5 M IPTG, 1 and 2: Flow through from purification of zUCH-L1-GST by GSTrap, 3: protein fraction collected after purification by GSTrap, 4: protein fraction collected after cleavage of GST-tag by PreScission protease 5: GST tag and contaminant collected after cleavage of zUCH-L1-GST.

## 4. ACTIVITY OF RECOMBINANT ZUCH-L1

The analysis of zUCH-L1 mediated DUB activity using Ub-Rho substrate, showed a saturable kinetic with constants similar to hUCH-L1. The plot of the initial velocity against substrate concentration is shown in **Figure 47** for zUCH-L1 and hUCH-L1. The kinetic parameters that came out of fitting the Michaelis-Menten equation to the experimental data are reported in **Table 11**. The kinetic analysis of zUCH-L1, compared to the human protein, showed a slightly lower affinity for the Ub substrate. The turnover number $k_{cat}$ is five times higher for zUCH-L1 compared to hUCH-L1. This tends to indicate that zUCH-L1 is converting more substrate into the product per seconds compared to the hUCH-L1. The Michaelis-Menten constant $K_m$ obtained for hUCH-L1 is very similar to the ones reported in the literature.[222–224] However, $k_{cat}$ values of hUCH-L1 in the literature showed a difference of 5 to 10-fold with our experimental conditions. The difference in the results can be due to the specific conditions that were used in this work compared to the ones detailed in the literature.

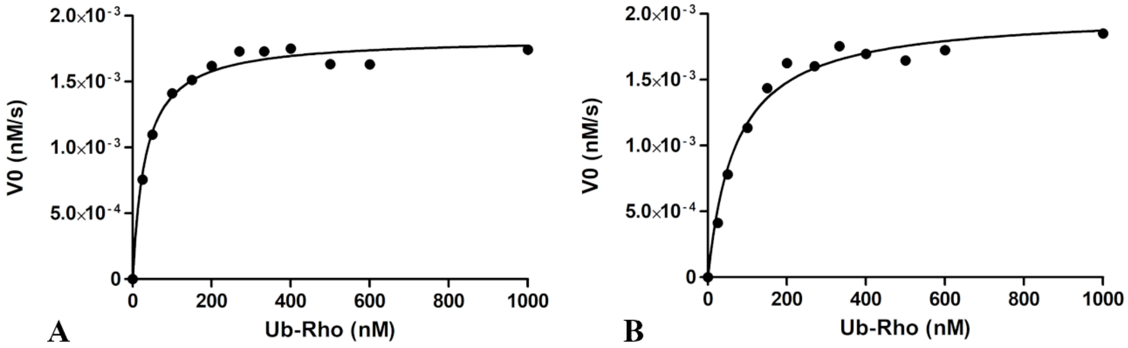

**Figure 47** – Variation of the initial velocity as a function of Ub-Rho concentration. Best fit Michaelis-Menten equation is shown as a solid line (results for one experiment performed in triplicates): (A) zUCH-L1 and (B) hUCH-L1.

**Table 11** - Kinetic parameters of hUCH-L1 and zUCH-L1 for the hydrolysis of Ub-Rho110. Comparison to the kinetic parameters obtained by Case *et al.*[222], Boudreaux *et al*.[224] and Luchansky *et al*.[223] of hUCH-L1 hydrolysis of Ub-AMC.

| | | $K_m$ [nM] | $V_{max}$ [nM/s] | $k_{cat}$ [$s^{-1}$] | $k_{cat}/K_m$ [$s^{-1}$ µ$M^{-1}$] |
|---|---|---|---|---|---|
| **zUCH-L1** | Our work | 71.2 ± 9.5 | 20.0 ± 6.2x$10^{-5}$ | 0.010 ± 3.1x$10^{-4}$ | 0.14 |
| **hUCH-L1** | Our work | 31.9 ± 3.6 | 18.3 ± 3.4x$10^{-5}$ | 0.0018 ± 3.4x$10^{-5}$ | 0.05 |
| | Literature[222–224] | 35-47 | - | 0.01-0.03 | 0.29-0.74 |

## 5. EFFECT OF UCH-L1 REFERENCE LIGANDS *IN VITRO*

*In vitro* assays of zUCH-L1 and hUCH-L1 using LDN-57444 **15**, LDN-91946 **16** and TCID **17** revealed dose-dependent inhibitory activities (**Figure 48.A-B)**. The estimated inhibition constant ($K_{i,app}$) and $IC_{50}$ values for each compound in both proteins are reported in **Table 12**.

The results in **Table 12** show similar $K_i$ of the same ligands in both proteins. These results support the idea that both proteins have a similar behavior when interacting with ligands. Furthermore, the $K_{i,app}$ estimated values obtained in hUCH-L1 are in the same range as the ones in the literature. The small differences can be correlated to the different approaches used to calculate the $K_i$. In this work, the inhibition constants were estimated whereas in the literature, these constants were measured experimentally. Interestingly, a stronger inhibition for TCID was also achieved in our experimental condition in hUCH-L1. In fact, $IC_{50}$ values were used in the literature in order to describe TCID inhibition, values that are strongly influenced by experimental conditions. In this work, $K_i$ values were estimated so as to characterize inhibition.

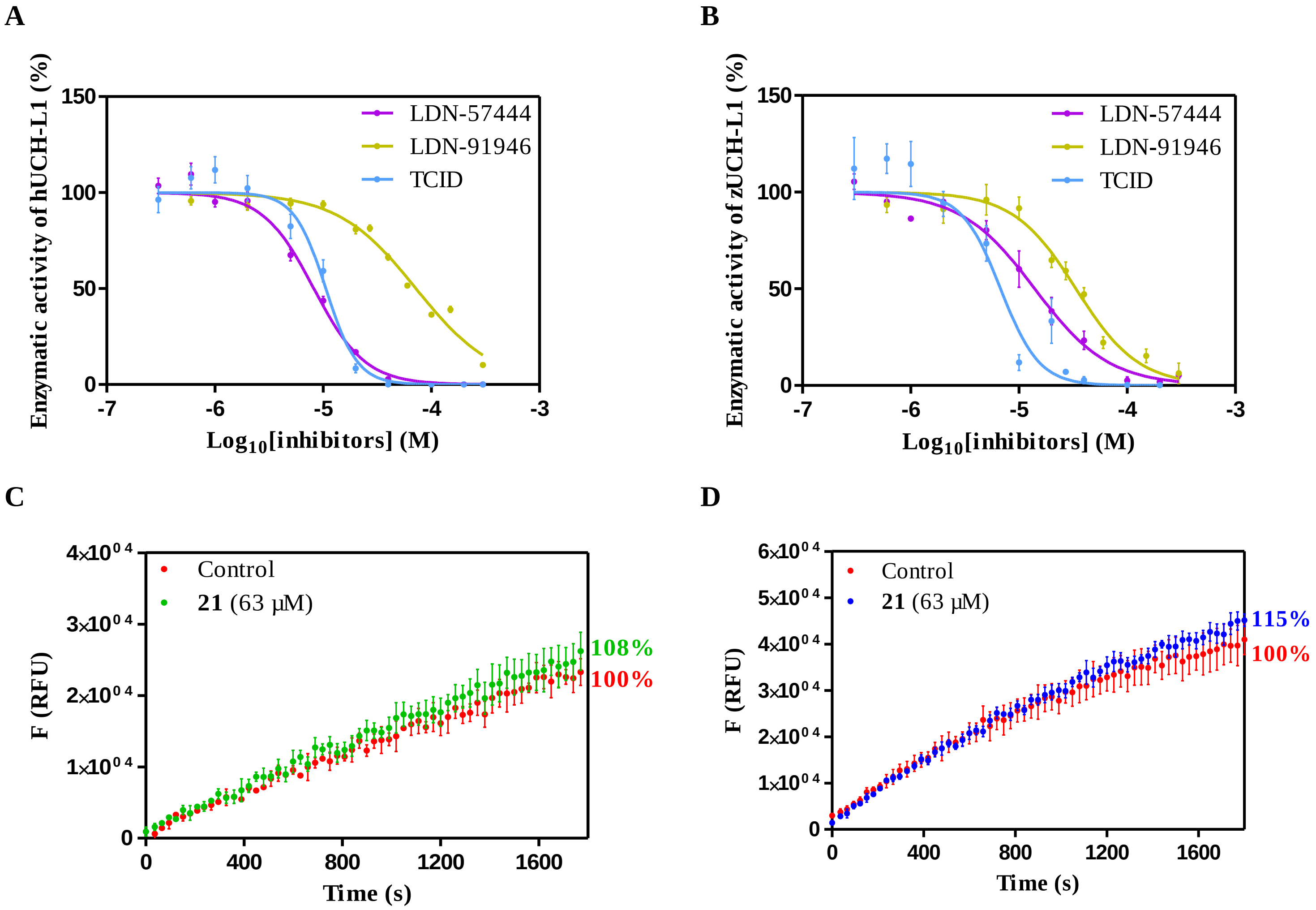

**Figure 48** - Dose response curves of inhibitors LDN-57444 **15**, LDN-91946 **16** and TCID **17** in (A) hUCH-L1 and (B) in zUCH-L1. Hydrolase activity of hUCH-L1 (C) and zUCH-L1 (D) in the presence of activator **21** at 63 µM. No inhibitor (control) was defined as 100% activity.

**Table 12** - Effect of compounds LDN-57444 **15**, LDN-91946 **16**, TCID **17** and activator **21** on the hydrolase activity of zUCH-L1 and hUCH-L1. Results are compared to the one described in the literature for hUCH-L1.

| | $IC_{50}$ (µM) | | $K_{i,\ app}$ (µM) | | Literature |
|---|---|---|---|---|---|
| | zUCH-L1 | hUCH-L1 | zUCH-L1 | hUCH-L1 | hUCH-L1 |
| LDN-57444 **15** | 14.6± 1.9 | 7.7± 0.6 | 8.6± 1.1 | 3.0± 0.2 | $K_i$ measured: 400 nM[123] |
| LDN-91946 **16** | 62.5± 13.6 | 66.7± 6.0 | 13.2± 1.3 | 41.0± 3.6 | $K_i$ measured: 3-90 µM[143] |
| TCID **17** | 5.3± 0.6 | 10.2± 0.9 | 3.1± 0.3 | 3.4± 0.3 | $IC_{50}$: 75 µM[123] |
| Activator **21** | 115% 63 µM | 108% 63 µM | - | | 111% at 63 µM[149] |

The incubation of recombinant hUCH-L1 and zUCH-L1 with 63 µM of compound **21** demonstrated a stimulatory effect on their protease activity (**Figure 48.C-D**). Results of enzymatic assays of hUCH-L1 in the presence of compound **21** are consistent with hUCH-L1 results already described in the literature by Mitsui *et al*. (111%[149] vs 108% in this work, at the same concentration). Compound **21** was here tested as a racemic mixture. It will be interesting to further investigate the enzymatic activity of each enantiomer separately. Indeed, one of the stereoisomers may have the desired beneficial effects, while the other may lead to undesirable side effects.[225] A well-known example is thalidomide. The compound was sold as a racemic mixture but it turned out that (S)-thalidomide has teratogenic effects.[226]

## 6. CONCLUSION

In conclusion, we have characterized zUCH-L1 protein for the first time and we have demonstrated to behave similarly as hUCH-L1 regarding the same ligands. A structural homology model was built for both inactive and active forms of zUCH-L1. It allowed us to study the docking of four reference ligands compared to the docking in the crystal structures of hUCH-L1 in the active and inactive forms. MM-GBSA calculations allowed us then to compare the binding free-energy of each compound in both proteins. The results showed that zUCH-L1 has a similar behavior *in silico* regarding the same ligands compared to the hUCH-L1 protein. The same ligands were then studied *in vitro* on both proteins. They showed once again a similar action regarding different kind of modulators: inhibitors and an activator. In this section, we were able to demonstrate that zUCH-L1 is a good alternative model to hUCH-L1. These results support that zebrafish is a potential good *in vivo* model to study UCH-L1 ligands.

It will be now interesting to study *in vivo* the behavior of these four modulators in zebrafish models.

# GENERAL CONCLUSIONS AND OUTLOOKS

The aim of this work was to study activators of UCH-L1 and an agonist of GLP-1R. They were synthesized and their physical and chemical properties were investigated. A further study of UCH-L1 activators in interaction with the protein was also carried out.

In the case of GLP-1R, our objective was to identify and study small molecules that activate the receptor as a therapeutic target of PD. The first objective was achieved as we identified compound **22** as a new agonist of GLP-1R. This 1,2,4-oxadiazole derivative is not insignificant as a compound bearing this 1,2,4-oxadiazole scaffold is already known as agonist of GLP-1R.[105]

As to perform further *in vitro* and *in vivo* studies, the synthesis of compound **22** was successfully achieved (**Figure 49**). However, the final physical state of the compound (a sticky oil) rendered its handling and further characterization difficult. For that purpose, a formulation of this compound into a CAM system was achieved by grinding it with saccharin or citric acid. CAM systems show common properties with co-crystals; in both systems, intermolecular interactions between the API and the co-former such as hydrogen bonds, π-π stacking, or van der Waals interactions are formed. The difference between co-crystals and CAM systems is that the latter is an amorphous solid that does not have a long-range order in the arrangement of the component. Both systems are nevertheless used in order to modulate the properties of the API, such as the physical stability and the dissolution rate.[200,227] The advantage of the amorphous phase is the higher solubility that can be obtained compared to the crystal structure of the same compound. This new formulation of compound **22** offers a solid compound that is now easy to handle, will facilitate the deeper characterizations and allow the *in vitro* and *in vivo* studies to be performed. Several formulations of peptide agonists of GLP-1R, such as encapsulation or complexation with cyclodextrins, were already tested in order to improve the properties of the latter.[215,216] However, the CAM formulation is a first in the study of GLP-1R agonist and most importantly offers interesting properties regarding bioavailability since superior dissolution profiles are usually reached.

This project allowed us to highlight a novel agonist of GLP-1R. In order to ensure that the powder formulation do not impact the biological properties of compound **22** regarding GLP-1R activation, a biological evaluation should be performed. Furthermore, the stability should still be characterized in order to ensure that the amorphous phase does not tend to crystallize.

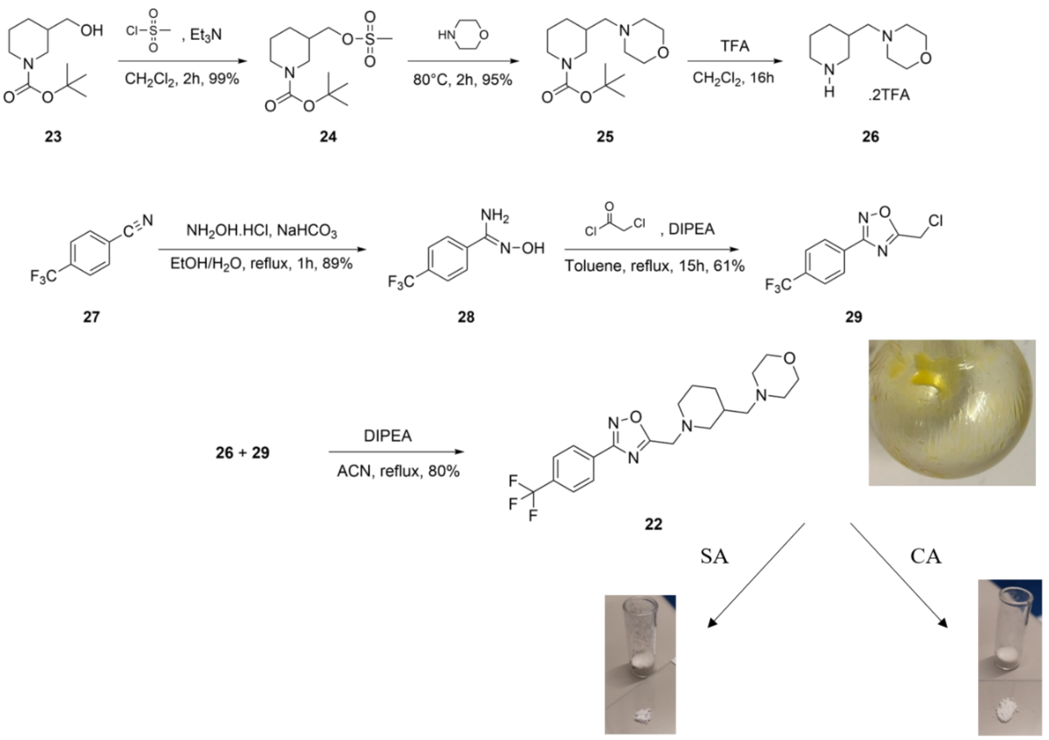

**Figure 49** - Synthesis and CAM formulation of the 1,2,4-oxadiazole derivative **22** with saccharin (SA) and citric acid (CA).

The second objective was to identify and study small molecules that activate UCH-L1 as a therapeutic target of PD. For that purpose, two approaches were investigated: (i) a virtual screening of UCH-L1 as to identify new scaffolds that could enhance the enzymatic activity and (ii) the study of the only compound described in the literature as an activator if this enzyme.

The virtual screening performed on UCH-L1 showed three compounds potentially interacting with the protein: Ritonavir, Lopinavir and Benserazide. After an *in vitro* evaluation, we demonstrated for the first time that these compounds are inhibitors of UCH-L1. These results did not allow us to achieve our objective of identifying new activators. However, they are still interesting in regards to a therapeutic strategy in PD[177].

Furthermore, the results of the virtual screening displayed four catecholamine-derived compounds. It may therefore be interesting in future work to study catecholamine derivatives as potential modulators of hUCH-L1.

The second class of molecules that we investigated were alanylpiperidine compounds as activators of UCH-L1 (**Figure 50**). The study focused on compound **21**, the only activator described in the literature[149] and its derivatives. The synthesis of compound **36** through a saponification reaction was achieved starting from compound **21**. Then, most importantly, we demonstrated that compound **36** is an activator of UCH-L1. The objective of identifying new activator compounds of UCH-L1 was achieved. The study of these two compounds **21** and **36** proved that the change of the ester group into a carboxylic acid does not impact UCH-L1 enzymatic activity. Furthermore, we demonstrated that these activators interact with an allosteric site instead of the active site as described in the literature for compound **21**.[149] Indeed, the *in silico* interactions in the active site are similar to the ones observed in the crystal structure of hUCH-L1 with the suicide substrate UbVMe.[184] This suggests that compounds **21** and **36** are not interacting in the active site otherwise they would have shown an inhibitory activity as they block the substrate and its hydrolysis. The allosteric site was highlighted *in silico* and demonstrated that both compounds are placed in the same position and thus interact with the same amino acids (Lys123 and Arg129) in the pocket.

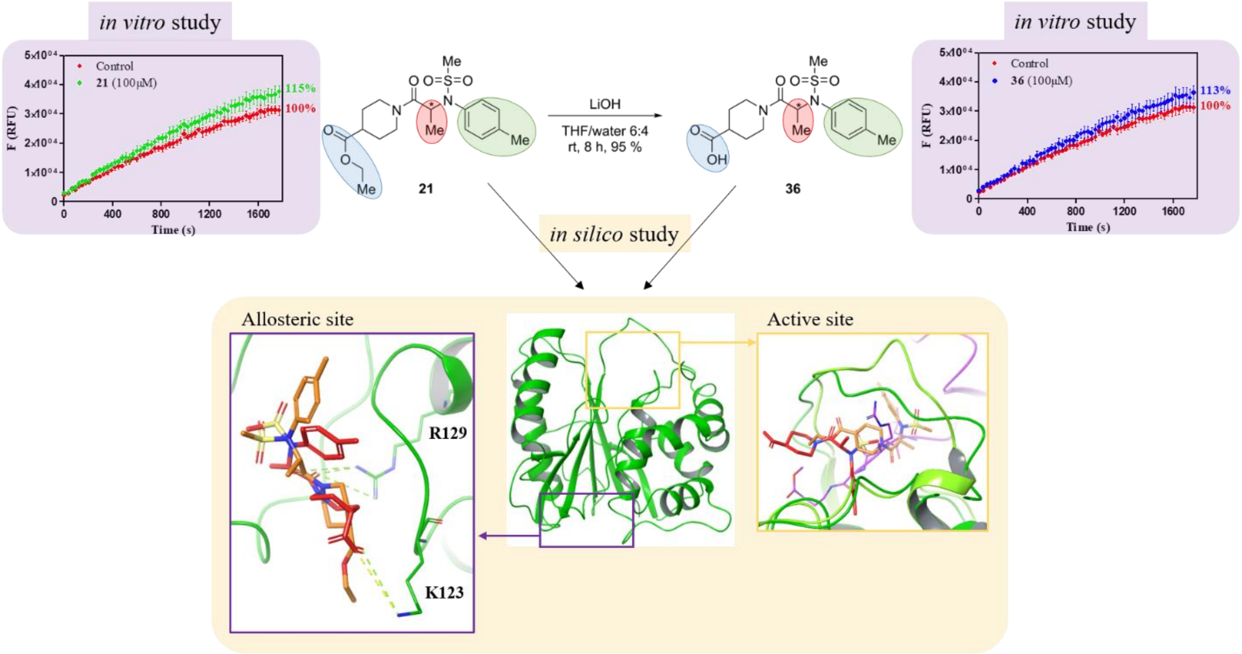

**Figure 50** - The *in vitro* and *in silico* results of compounds **21** and **36** and the synthesis reaction of the latter.

Crystallizing the complex composed of molecules **21** or **36** and hUCH-L1 may confirm the position in which the molecules interact within the protein. The result can then be compared with those of the *in silico* studies performed in this work. Preliminary attempts were already carried out. Potential co-crystals were obtained in condition with hUCH-L1 and molecule **36** but presented a poor diffraction pattern.

As the activator and its analogue are chiral compounds, it would be interesting to study each enantiomer separately in order to assess their influence on the activity of UCH-L1. Indeed, a stereoisomer can have the desired beneficial effects while the other can lead to undesired side effects, such as a different expected affinity towards the proteins. The best-known example is the thalidomide incident.[228] In the purpose of obtaining the enantiomers separately, either asymmetric synthesis of the desired compound can be carried out or at the end of the synthesis, chiral resolution can be used to separate the two enantiomers. Compared to the asymmetric synthesis approach, the disadvantage of the chiral resolution is the 50% yield of each enantiomer. Separating enantiomers can also be done by either crystallization in the form of enantiomerically pure crystals or conducting a reaction with a chiral compound so as to form diastereoisomers that can be easily separated by conventional physical and chemical characterizations.

Furthermore, based on the docking results obtained for compounds **21** and **36** (in both cavities and for both configurations), three parts of the alanylpiperidine derivative interacting with UCH-L1 protein were identified (**Figure 50**). This highlights the possible substitution sites as to obtain other derivatives of compounds **21** or **36** with regards of finding new activator compounds.

Depending on the configuration of compounds **21** and **36**, different poses and interactions are observed. Thus, the asymmetric center is the first part that can be highlighted (**Figure 50**, in red). Then, the tolyl group was shown to interact with Phe residues through π-π stacking (**Figure 50**, highlighted in green). Finally, the ester or carboxylic acid moiety can also interact through hydrogen bonds with Arg, Lys and the main peptide chain (**Figure 50**, highlighted in blue). These three highlighted parts can be modulated to change the interactions with the protein and thus the enzymatic behavior. In the presence of a carboxylic moiety, an easier functionalization of this functional group can be performed. In order to decide which part to functionalize and which functional group to choose, the fragment-based drug design approach can be used as a means to obtain derivatives of compounds **21** or **36**. It consists in the identification of small fragments that can bind with the target to obtain a high activity.[229] Then, according to the selected small fragments, the final compounds can either be synthesized or bought. In the first case, the synthesis of compound **21** would allow us to modulate the final compound easily as only the starting molecule bearing the desired function should be changed. In that respect, a preliminary trial of this synthesis was conducted. Continuing the procedure is therefore necessary as much as evaluating the cost efficiency of such a procedure. Buying the desired derivatives from Aurora[230] is another practical alternative to the synthesis.

The objective was also to modulate the physical and chemical properties of the identified activators as a potential therapy in PD. In that respect, the solubility is an essential parameter during the development of pharmaceutical drugs. It was stated that between 70 to 90% of drug candidates under development display a low solubility causing a low bioavailability of the drug.[209,210] However, solubility problems were encountered when a further characterization of the enzymatic activity of hUCH-L1 in the presence of both compounds **21** and **36** was performed. Hence, the improvement of the solubility is essential in order to study the exact behavior of compounds **21** and **36** but also in general during the development of an API. A common way to improve the solubility and dissolution rate of drug candidates is through salification. The equivalent to salt formation for non-ionizable drugs is co-crystallization. The modulation of the physical and chemical properties was assessed by salification experiments conducted on compound **36** since it bears a carboxylic acid moiety. Mechanochemistry has proven to be a method of choice in our case as it is increasingly used in salification assays.[188,231] We obtained two new crystalline phases with two counter ions: lysine and sodium bicarbonate.

In the case of **36_Na**, in view of the $CO_2$ loss, salt formation (or its partial formation) is suggested. In the case of **36_Lys**, a new crystalline phase similar to the one of compound **36** is observed in the powder pattern. The objective was not completely achieved, as the solubility of compound **36** should be now assessed to ensure these new crystalline phases are interesting regarding the development of a pharmaceutical drug.

The counter ions chosen are however interesting regarding to pharmaceutical application, sodium being the most widely used counter ion for acidic molecules in oral formulations. They usually show a high solubility in water.[232] Lysine is also highly used in salt formation compared to other basic amino acids. It is used in salts with different therapeutic agents, such as antibiotics, analgesic and anti-inflammatory compounds. Ibuprofen and Voltaren Gel® are common examples of known drugs of sodium and lysine salts.[233] Furthermore, it was demonstrated that between 2002 and 2006 15% of the injectable salts were in lysine salt form while the sodium salt was used for oral and parenteral formulation.[151,233] Thus, depending on the type of counter ion used, different administration routes can be possible.

Several characterizations should be performed as to allow the further study of these compounds. For **36_Lys**, the new crystalline phase can simply be a polymorph of **36** in ethyl acetate. In that perspective, a verification of compound **36** ground in the LAG solvent can be performed. The similarity in the powder pattern can also come from an excess of compound **36** in the sample. This suggests that the salt or co-crystal resulting from the new powder pattern is not in 1:1 ratio (**36**: lysine). Supplementary experiments should be performed with several ratios of both reagents. This was not possible in this work as the quantity of compound **21** and therefore **36** was not sufficient for further experiments. Once the salt or co-crystal is obtained without excess of compound **36**, solubility experiments should be performed. If a better solubilization is obtained, the deeper enzymatic characterization will then be carried out.

Furthermore, the hygroscopicity of both compounds should be assessed by DVS as **36_Lys** was found to be deliquescent after two weeks.

Finally, the last chapter was dedicated to the study of *Danio rerio* UCH-L1 (zUCH-L1) as an aim to test the UCH-L1 modulators in zebrafish *in vivo* models. We described zUCH-L1 protein for the first time (**Figure 51**). We started with an *in silico* study and since the crystal structure of the protein is not known, a homology model was obtained starting from the crystal structures of *Homo sapiens* UCH-L1 (hUCH-L1) in the active and inactive form. It allowed us to perform docking of selected reference ligands and to compare the results obtained with hUCH-L1. The protein production and purification were carried out in the same conditions as the one described for hUCH-L1.[123] This allows us to describe the enzymatic activity of zUCH-L1 *in vitro* by testing the same reference ligands as the one studied *in silico*. We demonstrated *in silico* and *in vitro* a similar behavior of zUCH-L1 against the same reference ligands compared to hUCH-L1. Up till now, zUCH-L1 was not characterized in the literature, thus these results allowed us to strengthen the use of zebrafish *in vivo* models in the study of UCH-L1 enzymatic activity.

Supplementary characterizations of zUCH-L1 can be performed so as to compare it further to hUCH-L1. These characterizations can include the study of the oligomeric states and their different enzymatic activities. As a monomeric form, hUCH-L1 was shown to function as a deubiquitinase. However, at high concentration the protein dimerizes showing a ligase activity with a reduced hydrolase activity. Furthermore, the crystallization of zUCH-L1 must be performed as it will allow us to confirm or refute the structure of the homology model. In the meantime, a study of the loop above the catalytic site can be performed by molecular dynamics. It will allow to study further its position in zUCH-L1 which can impact the docking results. Finally, *in vivo* testing of the reference ligands and the new activator **36** on zebrafish model constitutes the most important perspective of this work. It will allow us to validate the obtained *in vitro* results and understand the experimental behavior of these activators in living models.

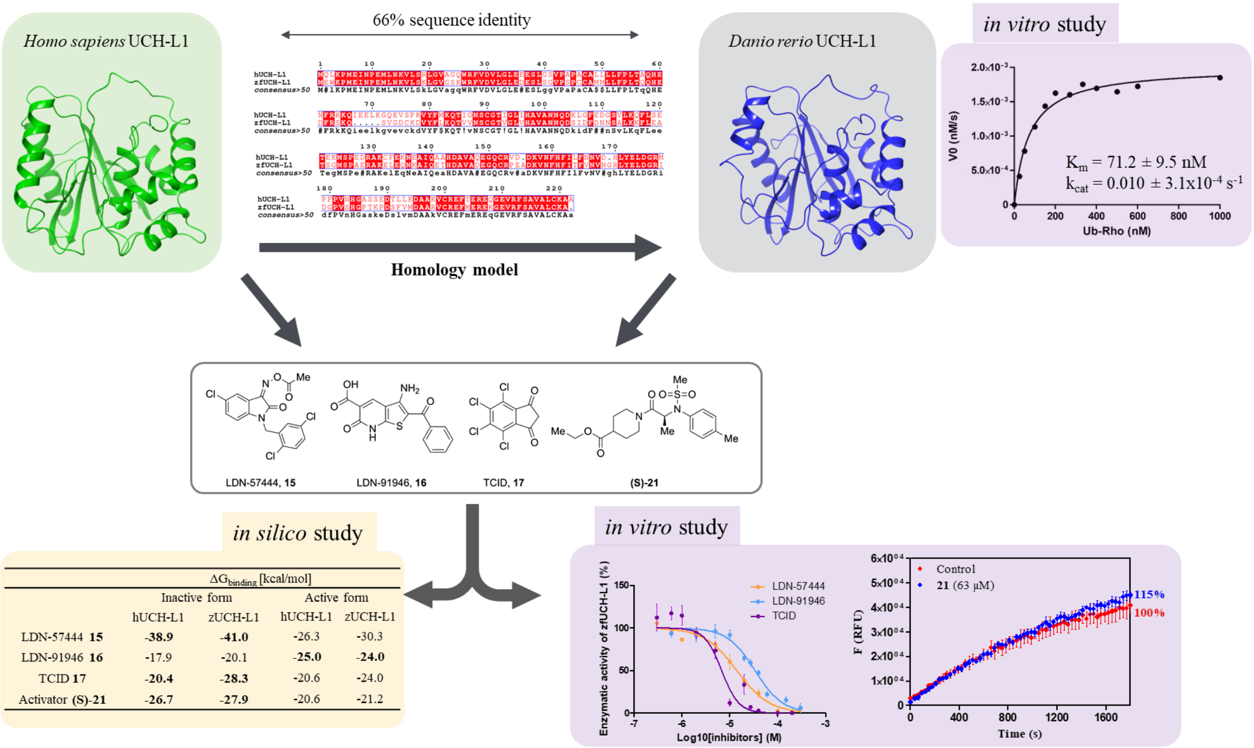

| | $\Delta G_{binding}$ [kcal/mol] | | | |
|---|---|---|---|---|
| | Inactive form | | Active form | |
| | hUCH-L1 | zUCH-L1 | hUCH-L1 | zUCH-L1 |
| LDN-57444 **15** | **-38.9** | **-41.0** | -26.3 | -30.3 |
| LDN-91946 **16** | -17.9 | -20.1 | **-25.0** | **-24.0** |
| TCID **17** | **-20.4** | **-28.3** | -20.6 | -24.0 |
| Activator **(S)-21** | **-26.7** | **-27.9** | -20.6 | -21.2 |

**Figure 51** - Homology modeling of *Danio rerio* UCH-L1 based on the sequence alignment with *Homo sapiens* UCH-L1. Results of the Michaelis-Menten analysis of zUCH-L1 and of the *in silico* and *in vitro* studies performed with compounds **15**, **16**, **17** and **21**.

At the end of this work small molecules were studied first in regards to GLP-1R. We characterized a new agonist of GLP-1R. The modulation of its physical and chemical properties to a CAM system allowed to change the physical state of the compound, yielding a powder that was easy to handle. That formulation opens now the possibility to new studies and further characterizations as GLP-1R agonist. Furthermore, in the study of small molecules as therapeutic option in PD, activators of UCH-L1 were investigated. We were able to demonstrate a new compound with activation properties regarding UCH-L1 enzymatic activity. This compound was shown to interact with an allosteric site in UCH-L1 described for the first time. As an aim to study the modulators in zebrafish *in vivo* models, the protein UCH-L1 of this species was characterized for the first time and even demonstrated to behave similarly to hUCH-L1. These results confirm the use of zebrafish models for further studies.

# EXPERIMENTAL SECTION

## 1. SOLVENTS AND CHEMICALS

Compounds LDN-57999 **15**, LDN-91946 **16**, TCID **17** and Activator **21** were purchased from Evotec SE or obtained by Abaxys Therapeutics S.A. All solvents and reagents used in protein production, purification, enzymatic reactions and synthesis were purchased from MilliporeSigma/Merck KGaA, Fisher Scientific International Inc, TCI and Tebu-bio. They were used without any further purification.

## 2. CHARACTERIZATION

### 2.1. $^1$H NMR and $^{13}$C NMR spectroscopy

The NMR spectra were obtained either with JEOL JNM 400 MHz or 500 MHz or with a Bruker Avance 500 MHz ($^1$H NMR at 500 MHz or 400 MHz and $^{13}$C NMR at 100 MHz or 126 MHz). The samples were prepared by dilution in deuterated solvent in a standard quartz tube (5 mm) at room temperature (18-22°C). Spectra were resolved with JEOL's Delta software. Chemical shifts ($\delta$), calibrated from the deuterated solvent, are given in ppm and the coupling constant ($J$) in Hertz (Hz). The multiplicity is noted as follows: s (singulet), d (doublet), t (triplet), q (quadruplet), dd (double doublet), dt (double triplet), m (multiplet) and br (broad). Assignment to protons was accomplished by H-H correlation COSY and assignment of carbon through H-C correlation HMQC and HMBC.

### 2.2. Infrared spectroscopy

IR spectra were recorder either on a Bruker tensor 27 equipped with a Specac attenuated total reflection (ATR) accessory, or with a Perkin Elmer "Spectrum two" Fourrier transform infrared spectrometer (FT-IR) also coupled to ATR technique. Wavenumbers ($\bar{\nu}$) are given in cm$^{-1}$.

### 2.3. Chromatography

Thin layer chromatography (TLC) was performed with aluminum-backed 2 mm thick Merck silica gel 60 $F_{254}$ plates. The compounds were detected under UV light at 254 nm or $KMnO_4$ solution (3 g of $KMnO_4$, 20 g of $K_2CO_3$, 5 mL NaOH 5 % and 300 mL of water). The retention factor $R_f$ was determined by dividing the distance of the product spot by the distance of the reference spot. Flash purification chromatography columns were performed under pressure using Davisil silica gel (40-63 µm particles size). The ratio of the different solvents is expressed in volume.

### 2.4. Powder X-ray diffraction (PXRD)

PXRD data were collected at room temperature on a Panalytical X'Pert Pro diffractometer (Bragg−Brentano geometry, X'Celerator detector), using Cu Kα radiation (λ = 1.54184 Å) at 45 kV and 30 mA. Each sample was collected at 2θ angles from 4 and 40° with a step size of 0.0167°.

### 2.5. Single-crystal X-ray diffraction (SCXRD)

Selected crystals were mounted on Oxford Diffraction Gemini Ultra R diffractometer using Mo $K_\alpha$ radiation (λ=0.71073 Å) with Ruby CCD detector at 295(2) K. Analytical absorption correction was performed with *CrysAlis PRO*[234], based on expressions derived by Clark & Reid[235]. Structures were solved using SHELXT[236] and refined with SHELXL[237] within OLEX2[238] and SHELXLE[239]. Non-hydrogen atoms were refined anisotropically. All H atoms, except one of the -OH group in **36**, were refined using a riding model, with C—H = 0.93 (aromatic), 0.96 (methyl) or 0.98 Å (tertiary carbon). Coordinates of the hydrogen atom of the -OH group were refined. The isotropic atomic displacement parameters of the hydrogen atoms were set at 1.5 Ueq of the parent atom for the methyl and alcohol groups, and at 1.2 Ueq otherwise.

### 2.6. Thermal properties assessment

The thermal properties were assessed by DSC coupled to a TGA on a Mettler Toledo TGA/DSC 3+ apparatus. Solid samples (mass about 5-10 mg) were placed in 100 µL aluminum sample pans. The analysis was performed from 25 to 300°C (or 350°C) at a scanning rate of 5 or 10°C/min using nitrogen (60 mL/min) as purge gas. The results were analyzed with STARe software (version 16.20).

### 2.7. LC-MS

High-performance liquid chromatography (HPLC) couplet to mass spectrometry (MS) was performed with an Agilent 1200LC-MSD VL apparatus (compounds **22-29**) or with HPLC alliance Waters 2695 (Compounds **21** and **36**). LC separation was achieved for compounds **22-29** with an Eclipse XDB-C18 column (5 µm, 4.6 mm x 15 mm) with a guard column (5 µm, 4.6 mm x 12.5 mm) or for compounds **21** and **36** with a Waters Xbridge C18 column (3.5 µm, 2 mm x 50 mm). A gradient mobile of water/acetonitrile from 95:5 to 5:95 was used with (for compounds **22-29**) or without (compounds **21** and **36**) 0.1% ammonium hydroxide and 0.1 formic acid. MS analysis was conducted with an electrospray ionization (ESI) source. Spectra were acquired in positive and negative ionization mode with UV/Vis detector.

### 2.8. Elemental analysis

Elemental analysis (C, N, H) was performed with Perkin Elmer 2400 apparatus. The analyses were performed by V. Charles (PC2 platform - UNamur).

### 2.9. Nitrogen physisorption

Isotherms of nitrogen absorption and desorption were recorded at -196°C (liquid nitrogen) with a volumetric adsorption analyzer Micromeritics 3Flex. The specific surface was calculated with Brunauer-Emmett-Teller (BET) method in the relative pressure of 0.05 – 0.25. Before the measure, all samples were degassed at 60°C, 0.1 Torr during 8 h.

### 2.10. Scanning electron microscopy (SEM)

SEM images were carried out on a JEOL JSM-6010LV at 15 kV with SEI detector to study the morphology of the sample surface.

## 3. BIOINFORMATICS TOOLS AND COMPUTATIONAL DETAILS

### 3.1. Sequence alignment and homology modeling

Sequence alignment was performed using ESprint web site and the identity and similarity parameters were obtained from EMBOSS Needle.[240,241] The homology models were build using Prime application of Maestro version 2019-1 (Schrödinger LLC).[242] The template used for the homology models of zUCH-L1 are hUCH-L1 crystal structures from the inactive (PDB entry: 2ETL, chain A) and active forms (PDB entry: 3KW5, chain A). The obtained models were named as zUCH-L1(i) and zUCH-L1(a), respectively. For all homology models, the quality of geometry was validated by the online server PROCHECK.[220]

### 3.2. Docking

For both proteins (hUCH-L1 and zUCH-L1 models), the methodology for docking of reference ligands is the same. The proteins were prepared with Protein Preparation Wizard workflow using OPLS3e force fields within Maestro suite.[242,243] Binding sites were determined with SiteMap tool of the Maestro version 2019-1 (Schrödinger LLC).[181] It was run to detect up to 5 top-ranked binding sites with at least 15 site points per site using a standard grid method. All compounds were prepared with LigPrep tool generating possible states at pH 7.4, retaining specific chirality using OPLS3e force field within Maestro suite.[243–245] The docking location was confined in a box of 10 Å around the catalytic triad (hUCH-L1: Cys90, His161 and Asp176; zUCH-L1: Cys85, His157 and Asp172). Docking was performed in Maestro Glide tool using Ligand Docking with Extra Precision.[183,246] The top docking poses were assessed at first through the glide score and for each docking, the first pose is the retained one. MM-GBSA calculations were performed for the retained docking poses with Maestro Prime tool using VSGB solvation and OPLS3e force field.[243,247]

The docking protein-protein of UbVMe (PDB entry: 3KW5, chain B) with homology model zUCH-L1(a) was performed with ZDOCK online server.[219] The best scored pose was then prepared through Protein Preparation Wizard from Maestro version 2019-1 (Schrödinger LLC).

### 3.3. Virtual screening

Virtual screening was performed using Genetic Optimization for Ligand Docking, GOLD, software (CCDC, Cambridge, UK).[248] The crystal structure of hUCH-L1 (PDB entry: 2ETL, chain A) was prepared by removing water and Cl ions. The binding site was defined around Cys90 within a 10 Å sphere. The database ZINC was used as an input library.[174] A subset of this chemical library was selected with compounds that are approved by the FDA (around 3000 molecules). The protonation state of all compounds was fixed at pH 7.0. A total of 10 docking solution were generated using the GOLD score.[249]

## 4. RECOMBINANT UCH-L1 EXPRESSION AND PURIFICATION

Plasmid of hUCH-L1 was a gift from C. Das group (Purdue University, USA) and plasmid of zUCH-L1 was bought on GenScript. Both proteins, hUCH-L1 and zUCH-L1, have a GST-UCH-L1 DNA construct in pGEX-6p-1 vectors. Each plasmid was transformed in *Escherichia coli* strain Rosetta (DE3) BL21 competent cells. Transformed cells were grown in LB medium with ampicillin (100 mg/mL) and chloramphenicol (34 mg/mL) at 37°C overnight. After reaching an optical density of 0.6, protein expression was inducted at 20°C for 20 hours by addition of IPTG 0.2 mM for hUCH-L1 and 0.5 mM for zUCH-L1. Cells were harvested by centrifugation (30 min, 4°C, 5000 rpm) and were lysed by sonication (20 MHz, 10 cycles of 30 seconds sonication and 30 seconds resting) in a lysis buffer (PBS pH 7.4 with lysozyme 10 µg/mL). The lysate was centrifuged (1 h, 4°C, 10000 rpm) and the supernatant was filtered with 0.45 µm and 0.22 µm filters. The protein was then purified using Glutathione Sepharose resin (GE Healthcare), following the manufacture's protocol. Fractions that contained the desired protein were mixed and dialyzed against Tris.HCl 50 mM pH 7.5, NaCl 150 mM, DTT 1 mM and EDTA 1 mM overnight. Cleavage of GST tag was performed with PreScission protease 1 µL/100 µg of tagged protein. The protein was then again purified using Glutathione Sepharose resin (GE Healthcare), following the manufacture's protocol. The proteins were aliquoted into small volume and stored at -80°C. The fractions collected from the purifications were followed by SDS-PAGE.

## 5. ENZYMATIC ACTIVITIES

The enzymatic activity of UCH-L1 was evaluated through hydrolysis reaction of a ubiquitin substrate couplet to Rhodamine 110 (**Figure 52**). The fluorescence of the released Rhodamine110 is then monitored.

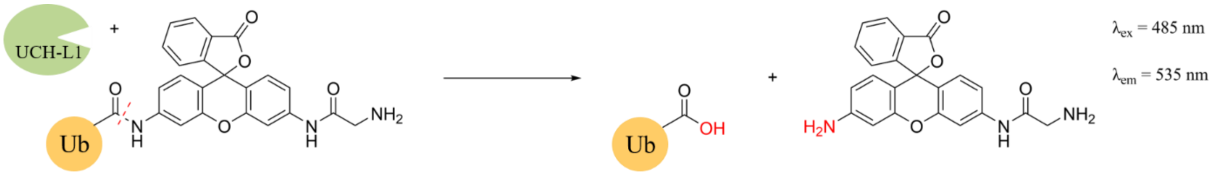

**Figure 52** - Representation of Ub-Rho110 assay to evaluate the enzymatic activity of UCH-L1. Illustration adapted from Hassiepen *et al.*[250]

### 5.1. UCH-L1 kinetic studies

Enzymatic reactions were performed in black 96-well immuno plates (ThermoFisher 7605) in a final reaction volume of 100 µL. The protein was diluted in reaction buffer (Tris.HCl 50 mM pH 7.4, EDTA 1 mM, DTT 1 mM and BSA 0.1 mg/mL) and 15 µL are added in the wells as to reach a final concentration of 1.0 nM/well (hUCH-L1) and 0.2 nM/well (zUCH-L1). Enzymatic activity assays were performed with an increasing final concentration of Ub-Rho ranging from 4 µM to 100 nM. The reaction is then read immediately after substrate addition for 30 minutes at 25°C using SpectraMax iD3 (Molecular Device, 485 nm/535 nm). Michaelis-Menten parameters were determined by plotting the reaction rate against the concentration of substrate Ub-Rho and fitting Michaelis-Menten curve (GraphPad, San Diego, California, USA, version 5.04). The apparent inhibitor constant ($K_{i,app}$) was calculated through the server $IC_{50}$-to-$K_{i}$.[251] Values of $K_{cat}$ were calculated from $V_{max}$ values using Rhodamine 110 calibration curve to convert units of fluorescence to molarity (**Figure 53**).

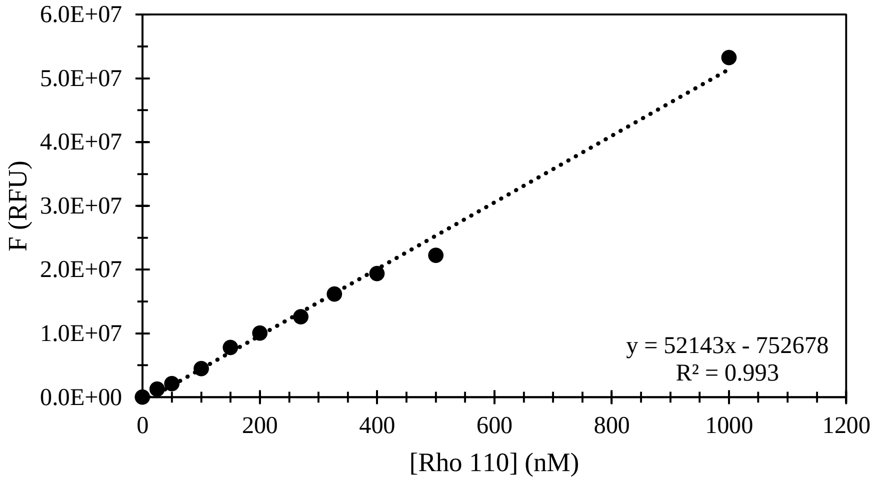

**Figure 53** - Calibration curve of the fluorescence against different concentration of Rhodamine110.

### 5.2. UCH-L1 modulators assays

In order to verify the tendency of the *in silico* results, kinetic studies of UCH-L1 enzymatic activity were performed in the presence of the four reference compounds. Reactions were performed in black 96-well immuno plates (ThermoFisher 7605) in a final reaction volume of 100 µL. The protein was diluted in reaction buffer (Tris.HCl 50 mM pH 7.4, EDTA 1 mM, DTT 1 mM and BSA 0.1 mg/mL) and 15 µL are added in the wells for a final concentration of 1.0 nM/well (hUCH-L1) and 0.2 nM/well (zUCH-L1). Then, 100% DMSO (3 µL) or diluted inhibitor (3 µL) with increasing final concentration ranging from 0.3 µM to 300 µM are added to the wells. Assays for the activators **21** and **36** were performed at a fixed concentration of 63 µM. The protein with the ligand is incubated for 15 minutes at 25°C. The reaction is initiated by the addition of the substrate Ub-Rho, 25 µL is added in the wells for a final concentration of 50 nM per well. The reaction is then read immediately after substrate addition for 30 minutes at 25°C using SpectraMax iD3 (Molecular Device, 485 nm/535 nm). $IC_{50}$ values were determined by fitting a four parameters dose-response curve to a plot of UCH-L1 enzymatic activity in percentage against the reference compound concentration (GraphPad, San Diego, California, USA, version 5.04).

# 6. ALANYLPIPERIDINE DERIVATIVES

## 6.1. Synthesis and crystallization

*Ethyl 1-(N-(methylsulfonyl)-N-(p-tolyl)-alanyl)piperidine-4-carboxylate* ***21***

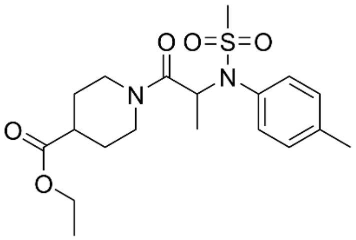

$C_{19}H_{28}N_2O_5S$

MW= 396.50 g.mol$^{-1}$

The product was crystallized by slow evaporation from non-anhydrous ethyl acetate, which provided colorless plate-like crystals suitable for SCXRD. Crystal data, data collection and structure refinement details of compound **21** are summarized in **Table 13**.

**TLC**: $R_f \approx$ 0.9(Cy/EtOAc/$CH_3COOH$: 4.5/4.5/1)

**$^1$H-NMR** ($CDCl_3$): 7.53 (t, $J_1$=7.5, 1H, $CH_{arom}$), 7.33 (d, $J_1$=7.5, 1H, $CH_{arom}$), 7.20 (d, $J_1$=8.0 2H, $CH_{arom}$), 5.35-5.29 (m, 1H, $C_\alpha H$), 4.41-4.26 (m, 1H, ½$CH_2N_{pip}$), 4.18-4.13 (m, 2H, $CH_2N_{pip}$), 4.06-3.93 (m, 1H, ½$CH_2N_{pip}$), 3.34-3.18 (m, 1H, $CH_{pip}$), 2.93 (s, 3H, $SO_2Me$), 3.00-2.82 (m, 1H, $CH_{pip}$), 2.62-3.51 (m, 2H, $OCH_2$), 2.31 (s, 3H, PheMe), 2.06-1.90 (m, 2H, $CH_{2pip}$), 1.77-1.62 (m, 1H, $CH_{2pip}$), 1.26 (m, 3H, $CH_2Me$), 1.14 (m, 3H, $C_\alpha Me$).
**$^{13}$C-NMR** ($CDCl_3$): 169.1 ($\underline{C}OOEt$), 168.7 (($\underline{C}$=O)N), 139.1 ($C_{Ar}$), 133.2 ($C_{Ar}$), 132.3 ($2C_{Ar}$), 129.9 ($2C_{Ar}$), 60.9 ($O\underline{C}H_2CH_3$), 54.3 ($C_\alpha H$), 45.7 ($CH_{pip}$), 45.1 ($CH_{pip}$), 41.8 ($CH_{pip}$), 39.1 ($SO_2\underline{C}H_3$), 28.7 ($CH_{pip}$), 28.0 ($CH_{pip}$), 21.3 ($Phe\underline{C}H_3$), 17.8 ($C_\alpha\underline{C}H_3$), 14.3 ($CH_2Me$)
**LC-MS** (ESI+): for $[M+H]^+$ calculated 397.18 and found 397.5
**Mp:** 169.9 °C
**Elemental analysis**: calculated: C 57.56%; H 7.12%; N 7.07% and found: C 57.35%; H 7.04%; N 7.12%

**Table 13** - Experimental details.

| | **21** |
|---|---|
| **Crystal data** | |
| Chemical formula | $C_{19}H_{28}N_2O_5S$ |
| $M_r$ | 396.49 |
| Crystal system, space group | Triclinic, $P\bar{1}$ |
| Temperature (K) | 295 |
| *a*, *b*, *c* (Å) | 8.5368 (6), 9.6594 (6), 13.5173 (12) |
| α, β, γ (°) | 75.947 (6), 79.302 (6), 74.554 (5) |
| *V* (Å$^3$) | 1033.47 (14) |
| *Z* | 2 |
| Radiation type | Mo *K*α |
| M (mm$^{-1}$) | 0.19 |
| Crystal size (mm) | 0.79 x 0.18 x 0.05 |
| **Data collection** | |
| Diffractometer | Oxford Diffraction Xcalibur, Gemini Ultra R |
| Absorption correction | Analytical<br>*CrysAlis PRO*[234], based on expressions derived by Clark & Reid[235]. |
| $T_{\min}$, $T_{\max}$ | 0.923, 0.991 |
| No. of measured, independent and observed [$I > 2\sigma(I)$] reflections | 13200, 6870, 4304 |
| $R_{\text{int}}$ | 0.026 |
| $(\sin \theta/\lambda)_{\max}$ (Å$^{-1}$) | 0.762 |
| **Refinement** | |
| $R[F^2 > 2\sigma(F^2)]$, $wR(F^2)$, $S$ | 0.054, 0.158, 1.02 |
| No. of reflections | 6870 |
| No. of parameters | 248 |
| H-atom treatment | H-atom parameters constrained |
| $\Delta\rho_{\max}$, $\Delta\rho_{\min}$ (e Å$^{-3}$) | 0.34, -0.37 |

Computer programs: *CrysAlis PRO*[234], SHELXT 2014[236], *SHELXL* 2016[237], *Mercury*[252], *publCIF*[253] .

*1-(N-(methylsulfonyl)-N-(p-tolyl)-alanyl)piperidine-4-carboxylic acid* ***36***

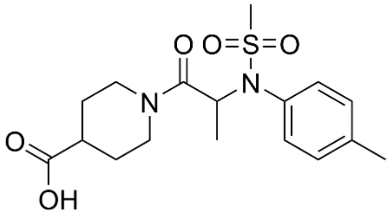

$C_{17}H_{24}N_2O_5S$

MW= 368.45 g.mol$^{-1}$

**Operating procedure:**

In a round bottom flask, compound **21** (405.1 mg, 1.02 mmol, 1.0 eq) dissolved in 8 mL of THF was added to a solution of LiOH (81.9 mg, 3.40 mmol, 3.4 eq) dissolved in 5 mL of water. The mixture was stirred at room temperature for 8 h. The resulting mixture was washed with ether. The aqueous phase was then acidified with HCl 37% to a pH of 2 and extracted with dichloromethane. The combined organic phases were dried over anhydrous $Na_2SO_4$ and concentrated under vacuum to yield 351.0 mg of a white solid. The product was crystallized by slow evaporation from methanol, which provided colorless plate-like crystals suitable for SCXRD.

**Yield**: 93%

**TLC**: $R_f \approx$ 0.56 (Cy/EtOAc 5/5+ 10% acetic acid)

**$^1$H-NMR** ($(CD_3)_2SO$): 12.32 (s, 1H, COOH), 7.39 (d, 2H, *J*=8.0, $CH_{Ar}$), 7.20 (d, 2H, *J*=8.0, $CH_{Ar}$), 5.20 (s, 1H, $C_\alpha H$), 4.03 - 3.15 (m, 4H, $2CH_2N_{pip}$), 2.96 (s, 3H, $SO_2Me$), 2.79 (m, 1H, $CH_{pip}$), 2.31 (s, 3H, $PheCH_3$), 1.83-1.36 (m, 4H, $2CH_{2pip}$), 1.03 (d, *J*=7.0, 3H, $C_\alpha Me$)

**$^{13}$C-NMR** ($(CD_3)_2SO$): 169.1 ($\underline{C}OOH$), 168.7 (($\underline{C}$=O)N), 138.2 ($C_{Ar}$), 133.5 ($C_{Ar}$), 132.0 ($2C_{Ar}$), 129.4 ($2C_{Ar}$), 53.3 ($C_\alpha H$), 44.5 ($2CH_{pip}$), 41.3 ($CH_{pip}$), 40.2 ($SO_2\underline{C}H_3$), 28.5 ($2CH_{pip}$), 20.7 ($Phe\underline{C}H_3$), 16.8 ($C_\alpha \underline{C}H_3$)

**Mp:** 223.1 °C

**IR:** $\bar{\nu}$ (cm$^{-1}$) 3268, 2936, 1736, 1640, 1316, 1142, 1121

**Elemental analysis**: calculated: C 55.44%; H 6.57%; N 7.60%; determined: C 55.33%; H 6.84%; N 7.47%

The product was crystallized by slow evaporation from non-anhydrous ethyl acetate, which provided colorless plate-like crystals suitable for SCXRD. Crystal data, data collection and structure refinement details of **36** are summarized in **Table 14**.

**Table 14** - Experimental details.

| | **36** |
|---|---|
| **Crystal data** | |
| Chemical formula | $C_{17}H_{24}N_2O_5S$ |
| $M_r$ | 368.44 |
| Crystal system, space group | Monoclinic, $P2_1/n$ |
| Temperature (K) | 295 |
| $a$, $b$, $c$ (Å) | 12.1013 (2), 12.3092 (2), 12.4348 (3) |
| α, β, γ (°) | 90, 100.546 (2), 90 |
| $V$ (Å$^3$) | 1820.97 (6) |
| $Z$ | 4 |
| Radiation type | Mo $K\alpha$ |
| M (mm$^{-1}$) | 0.21 |
| Crystal size (mm) | 0.77 x 0.18 x 0.11 |
| **Data collection** | |
| Diffractometer | Oxford Diffraction Xcalibur, Gemini Ultra R |
| Absorption correction | Analytical<br>*CrysAlis PRO*[234], based on expressions derived by Clark & Reid[235]. |
| $T_{min}$, $T_{max}$ | 0.882, 0.980 |
| No. of measured, independent and observed [$I > 2\sigma(I)$] reflections | 29518, 6284, 4779 |
| $R_{int}$ | 0.026 |
| $(\sin \theta/\lambda)_{max}$ (Å$^{-1}$) | 0.761 |
| **Refinement** | |
| $R[F^2 > 2\sigma(F^2)]$, $wR(F^2)$, $S$ | 0.043, 0.126, 1.02 |
| No. of reflections | 6284 |
| No. of parameters | 232 |
| H-atom treatment | H atoms treated by a mixture of independent and constrained refinement |
| $\Delta\rho_{max}$, $\Delta\rho_{min}$ (e Å$^{-3}$) | 0.29, -0.29 |

Computer programs: *CrysAlis PRO*[234], SHELXT 2014[236], *SHELXL* 2016[237], *Mercury*[252], *publCIF*[253] .

### 6.2. Salification of compound 36

The grinding conditions with $NaHCO_3$ were beforehand optimized as only small amount of compound **36** was in our possession. The optimization was carried out with diclofenac as it is also bearing a carboxylic acid and that was well studied in the laboratory. In that respect, the frequency, the grinding ball and the solvent were optimized with this system before applying the optimal conditions in the system with the alanylpiperidin derivative **36**.

***36_Na***

**Operating procedure:** In a 2 mL Eppendorf tube, **36** (1.0 eq), sodium bicarbonate (1.0 eq), two of 3 mm and seven of 2 mm stainless steel grinding balls were added. The Eppendorf tube was then placed in the grinding machine (Retsch MM 400 Mixer Mill apparatus), equipped with two grinding jars. The grinding was then performed for 90 min at 30 Hz. The grinding was with 20 µL of water.

**Aspect**: White solid

**Mp** : 305°C

***36_Lys***

**Operating procedure:** In a 2 mL Eppendorf tube, **36** (1.0 eq), lysin (1.0 eq), two of 3 mm and seven of 2 mm stainless steel grinding balls were added. The Eppendorf tube was then placed in the grinding machine (Retsch MM 400 Mixer Mill apparatus), equipped with two grinding jars. The grinding was then performed for 90 min at 20 Hz. The grinding was with 20 µL of ethyl acetate.

**Aspect**: White solid

**Mp** : 165°C

# 7. 1,2,4-OXADIAZOLE DERIVATIVE

## 7.1. Synthesis of compound 22

*Synthesis of tert-butyl 3-{[(methylsulfonyl)oxy]methyl}piperidine-1-carboxylate (**24**)*

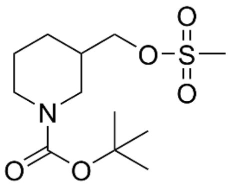

$C_{12}H_{23}NO_5S$

MW= 299.38 g.mol$^{-1}$

**Operating procedure:**

Triethylamine (0.98 mL, 7.03 mmol, 1.5 eq) was added dropwise to a solution of the piperidine (1.00 g, 4.65 mmol, 1.0 eq) in 7.5 mL of anhydrous dichloromethane at 0°C under argon atmosphere. The reaction mixture was stirred at rt for 15 min and then methanesulfonyl chloride (0.43 mL, 5.55 mmol, 1.2 eq) was added slowly at 0°C. The reaction mixture was stirred for 2 h at rt. The residue was then filtrated and the solid was washed with dichloromethane. The organic phases were washed with brine, dried over $MgSO_4$ and the solvent was evaporated under reduced pressure in order to yield 1.314 g of **24** as a yellow oil.

**Yield**: 93%

**TLC** : $R_f$ = 0.66 (DCM/EtOAc: 9/1)

**$^1$H-NMR** ($CDCl_3$): δ 4.05-4.13 (m, 2H, $CH_2N_{pip}$), 3.92 (d, *J*=13.2, 1H, 1/2$CH_2N_{pip}$), 3.78-3.84 (dt, $J_1$=4.4, $J_2$=13.2, 1H, 1/2$CH_2N_{pip}$), 3.02 (s, 3H, $CH_3$), 2.89-2.96 (m, 1H, 1/2$CH_2$OMs), 2.77-2.82 (dd, $J_1$=13.2, $J_2$=9.6, 1H, 1/2$CH_2$OMs), 1.92-2.00 (m, 1H, 1/2$CH_{2,pip}$), 1.79-1.86 (m, 1H, 1/2$CH_{2,pip}$), 1.63-1.71 (m, 1H, 1/2$CH_{2,pip}$), 1.46 (s, 9H, 3$CH_3$), 1.41-1.53 (m, 1H, 1/2$CH_{2,pip}$), 1.25-1.36 (m, 1H, 1/2$CH_{2,pip}$)

Spectral data in agreement with the literature reference.[171]

*Synthesis of tert-butyl 3-(morpholin-4-ylmethyl)piperidine-1-carboxylate (**25**)*

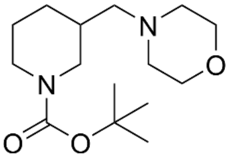

$C_{15}H_{28}N_2O_3$

MW= 284.40 g.mol$^{-1}$

**Operating procedure:**

A solution of **24** (1.262 mg, 4.30 mmol) and morpholine (5.0 ml, 0.8 ml/mmol) was heated at 80°C for 2 h under argon atmosphere. The reaction mixture was evaporated and the residue was dissolved with ethyl acetate. The organic solution was washed with water and brine, dried over $Na_2SO_4$, filtered and the solvent was removed under reduced pressure to yield 1.15 g of **25** as a yellow oil.

**Yield**: 94%

**TLC** : Rf ≈ 0.30 (Cy/EtOAc: 1/1)

**$^1$H-NMR** ($CDCl_3$): δ (ppm) 4.08 (s, 1H, 1/2$CH_2N_{pip}$), 3.94 (d, *J*=17.6, 1H, 1/2$CH_2N_{pip}$), 3.70 (s, 4H, 2$CH_2O_{morph}$), 2.78 (t, *J*=13.2, 1H, 1/2$CH_2N_{pip}$), 2.36-2.43 (m, 5H, 1/2$CH_2N_{pip}$, 2$CH_2N_{morph}$), 2.15 (m, 2H, $CH_{2,morph}$), 1.80-1.61 (m, 3H, $CH_{2,pip,}$ CH), 1.45 (s, 10H, 3$CH_3$, 1/2$CH_{2,pip}$), 1.09 (m, 1H, 1/2$CH_{2,pip}$).

**$^{13}$C-NMR** ($CDCl_3$): δ (ppm) 155.0 (C=O), 79.3 ($\underline{C}(CH_3)_3$), 67.2 (2$CH_2O_{morph}$), 62.4 ($CH_{2,morph}$), 54.2 (2$CH_2N_{morph}$), 52.2 ($CH_2N_{pip}$), 45.0 ($CH_2N_{pip}$), 33.2 (CH), 29.6 ($CH_{2,pip}$), 28.6 (3$CH_3$), 24.9 ($CH_{2,pip}$).

**LC-MS** (ESI+): for $[M+H]^+$ calculated 285.21 and found 285.2

**Mp**: 58-59 °C

**IR**: $\bar{\nu}$ (cm$^-$) 2975, 2936, 1689, 1365, 1271, 1167, 1125

*Synthesis of 3-(morpholin-4-ylmethyl)piperidinium trifluoroacetate (**26**)*

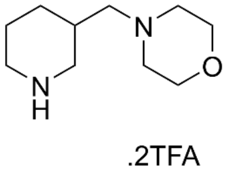

$C_{14}H_{22}F_6N_2O_5$

MW= 412.33 g.mol$^{-1}$

**Operating procedure:**

Trifluoroacetic acid (TFA) (6.0 ml, 87.4 mmol, 19 eq) was added to a solution of **25** (1.150 g, 4.04 mmol) in anhydrous dichloromethane (77 mL) under argon atmosphere. The reaction mixture was stirred at rt for 17 h. Then, the solvent was removed under reduced pressure. The excess of TFA was removed by azeotropic distillation with dichloromethane (x2), toluene and the resulting residue was dried under vacuum to afford the trifluoroacetate salt **26** as a brown solid (2.171 g).

**TLC** : 0.10 (Cy/EtOAc: 1/1)

**$^1$H-NMR** (methanol-*d4*): δ 4.00-3.88 (m, 4H, $2CH_2O_{morph}$), 3.54 (d, *J*=12.8, 1H, $1/2CH_2N_{pip}$), 3.40 (d, *J*=12.8, 1H, $1/2CH_2N_{pip}$), 3.21-3.40 (m, 4H, $2CH_2N_{morph}$), 3.11-3.19 (dd, $J_1$=2.8, $J_2$=6.8, 2H, $CH_{2,morph}$), 2.94 (td, $J_1$=12.4, $J_2$= 3.2, 1H, $1/2CH_2N_{pip}$), 2.79 (t, *J*=12.4, 1H, $1/2CH_2N_{pip}$), 2.30-2.40 (m, 1H, CH), 1.95-2.02 (m, 2H, $CH_{2,pip}$), 1.72-1.84 (m, 1H, $1/2CH_{2,pip}$), 1.33-1.44 (m, 1H, $1/2CH_{2,pip}$).

**$^{13}$C-NMR** (methanol-*d4*): 64.8 ($2CH_2O_{morph}$), 60.7 ($CH_{2,morph}$), 53.7 ($2CH_2N_{pip}$), 47.3 ($CH_2N_{pip}$), 44.9 ($CH_2N_{pip}$), 30.2 (CH), 27.7 ($CH_{2,pip}$), 22.7 ($CH_{2,pip}$).

**Mp**: 343.15 K

**IR**: ν̄ (cm$^-$) 3431, 1670, 1455, 1432, 1200, 1171, 1130

*Synthesis of N-hydroxy-4-(trifluoromethyl)benzenecarboximidamide (**28**)*

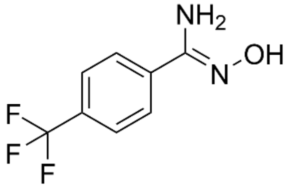

$C_8H_7F_3N_2O$

MW= 204.15 g.mol$^{-1}$

**Operating procedure:**

4-Trifluoromethylbenzonitrile (1.004 g, 5.88 mmol, 1.0 eq) in 22 mL of ethanol was added to hydroxylamine hydrochloride (2.444 g, 35.2 mmol, 6.0 eq) and sodium hydrogen carbonate (1.485 g, 17.7 mmol, 3.0 eq) in 22 mL of water. The mixture was stirred at 100°C for 1 h. Then, the solvents were evaporated from the cooled mixture under reduced pressure and ice-cold water was poured on the residue. The precipitate was collected by filtration, washed with cooled water and dried to yield **28** 1.06 g of as a light blue powder.

**Yield**: 89%

**TLC** : 0.54 (Cy/AcOEt: 1/1)

**$^1$H-NMR** ($(CD_3)_2SO$): δ 9.93 (s, 1H, OH), 7.90 (d, 2H, *J*=8.0, 2CH$_{ar}$), 7.74 (d, 2H, *J*=8.0, 2CH$_{ar}$), 6.00 (s, 2H, NH$_2$)

Spectral data in agreement with the literature reference.[254]

*Synthesis of 5-(chloromethyl)-3-[4-(trifluoromethyl)phenyl]-1,2,4-oxadiazole (**29**)*

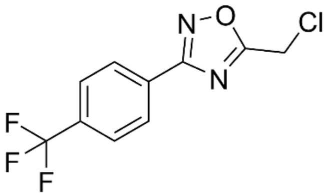

$C_{10}H_6ClF_3N_2O$

MW= 262.62 g.mol$^{-1}$

**Operating procedure:**

Benzamidoxime **28** (860 mg, 4.21 mmol, 1.0 eq) and *N*,*N*-diisopropylethylamine (DIPEA) (1.2 mL, 6.32 mmol, 1.5 eq) in 27 mL of anhydrous toluene were added to a solution of chloroacetyl chloride (0.44 mL, 5.53 mmol, 1.3 eq) in 5 mL of anhydrous toluene at 0°C under argon atmosphere. The mixture was stirred at reflux for 2 h. Then, the solvent was evaporated from the cooled mixture. The resulting residue was then purified by flash column chromatography (Cy to Cy:EtOAc, 9:1) to yield 671.0 mg of **29** as a yellow oil.

**Yield**: 61%

**TLC** : 0.75 (Cy/EtOAc: 3/1)

**$^1$H-NMR** ($CDCl_3$): δ 8.17 (d, *J*=8.2, 2H, $2CH_{Ar}$), 7.71 (d, *J*=8.2, 2H, $2CH_{Ar}$), 4.72 (s, 2H, $CH_2$).

**$^{13}$C-NMR** ($CDCl_3$): 175.0 (C(O)=N), 168.1 (C(N)=N), 133.4 ($\underline{C}CF_3$), 129.7 ($C_{Ar}$), 128.0 ($2CH_{Ar}$), 126.1 ($2CH_{Ar}$), 123.8 ($CF_3$), 33.4 ($CH_2$)

Spectral data in agreement with the literature reference.[255]

### *Synthesis of 4-{[1-({3-[4-(trifluoromethyl)phenyl]-1,2,4-oxadiazol-5-yl}methyl) piperidin-3-yl]methyl}morpholine* ***22***

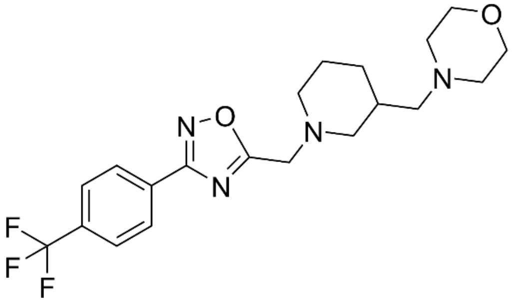

$C_{20}H_{25}F_3N_4O_2$

MW= 410.44 g.mol$^{-1}$

**Operating procedure:**

DIPEA (2.7 mL, 15.5 mmol, 6.1 eq) and **26** (1.580 g, 3.83 mmol, 1.5 eq) were added to a solution of **29** (671 mg, 2.55 mmol, 1.0 eq) in 27 mL of anhydrous acetonitrile under argon atmosphere. The reaction mixture was stirred at reflux for 2 h. Then, the solvent was evaporated from the cooled mixture. The residue was dissolved in ethyl acetate and washed with brine. The organic layer was dried over $Na_2SO_4$, filtered and the solvent was evaporated under reduced pressure. The residue was purified by flash column chromatography (DCM to DCM:MeOH, 98:2) to yield 40.9 mg of compound **22** as a pale yellow syrup.

**Yield**: 48%

**TLC** : 0.67 (DCM/MeOH: 9/1)

**$^1$H-NMR** (($CD_3$)$_2$SO): 8.22 (d, 2H, *J*=8.0, 2$CH_{Ar}$), 7.95 (d, 2H, *J*=8.0, 2$CH_{Ar}$), 3.98 (dd, 2H, $J_1$=15.0, $J_2$=23.0, $CH_{2,pip}$), 3.52 (m, 4H, 2$CH_2O_{morph}$), 2.93 (d, 1H, *J*=9.0, 1/2$CH_2N_{pip}$), 2.78 (d, 1H, *J*=10.0, 1/2$CH_2N_{pip}$), 2.62 (m, 4H, 2$CH_2N_{morph}$), 2.36-2.23 (m, 3H, $CH_{2morph}$, 1/2$CH_2N_{pip}$), 1.88 (t, 1H, *J*=10.0, 1/2$CH_2N_{pip}$), 1.79 (s br, 1H, CH), 1.65-1.58 (m, 2H, $CH_{2pip}$),1.52-1.43 (m, 1H, 1/2$CH_{2pip}$), 0.89-0.81 (m, 1H, 1/2$CH_{2pip}$).

**$^{13}$C-NMR** (($CD_3$)$_2$SO): δ 177.8 (C(O)=N), 166.5 (C(N)=N), 130.0 (q, $\underline{C}CF_3$), 127.9 (2$CH_{Ar}$), 126.2 (2$CH_{Ar}$), 125.2 (q, $C_{Ar}$), 122.5 (q, $CF_3$), 66.2 (2$CH_2O_{morph}$), 62.3 ($CH_{2morph}$), 57.6 ($CH_2N_{pip}$), 53.7 (2$CH_2N_{morph}$), 53.3 ($CH_2N_{pip}$), 52.7 ($CH_{2pip}$), 32.6 (CH), 28.3 ($CH_{2pip}$), 24.5 ($CH_{2pip}$).

**LC-MS** (ESI+): for $[M+H]^+$ calculated 411.20 and found 411.2

**IR**: $\bar{\nu}$ (cm$^{-}$) 2935, 2800, 2856, 1416, 1322, 1116

### 7.2. Salification of compound 22

*Synthesis of **22_Cl***

A 2 M HCl in $Et_2O$ (3 mL/mmol) solution was added dropwise to a solution of the free amine **22** in anhydrous $Et_2O$ (6 mL/mmol) under argon atmosphere. For 3 h, the mixture was allowed to stand. The hydrochloride salt can be isolated by evaporation of the solvent and followed by drying under vacuum to yield an off-white solid which in contact with humidity of the air became rapidly deliquescent.

**Mp**: 206-207°C

**Elemental analysis**: calculated: C 46.25%; H 6.02%; N 10.79%; determined: C 46.47%; H 5.99%; N 10.91%

*Synthesis of **22_2CA***

In a grinding jar, **22** (201 mg, 0.490 mmol, 1.0 eq), citric acid (188 mg, 0.976 mmol, 2.0 eq), and a grinding ball (Zirconium oxide, 12 mm of diameter) were added. The jar was then placed in the grinding machine (Retsch Mixer Mill 400), equipped with another grinding jar~~s~~. The dry grinding was then performed for 90 min at 30 Hz to afford an off-white solid.

**$^1$H-NMR** ($(CD_3)_2SO$): δ 8.23 (d, 2H, $J$=8.2, $2CH_{Ar}$), 7.95 (d, 2H, $J$=8.2, $2CH_{Ar}$), 4.02 (dd, 2H, $J_1$=23.0, $J_2$=15.0, $CH_{2pip}$), 3.66 (m, 4H, $2CH_2O_{morph}$), 2.92 (d, 1H, $J$=9.0, $1/2CH_2N_{pip}$), 2.78 (d, 1H, $J$=9.0, $1/2CH_2N_{pip}$), 2.72 (d, 4H, $J$=15.5, $2{*}CH_{2CA}$), 2.62 (m, 8H, $2{*}CH_{2CA}$, $2CH_2N_{morph}$), 2.38-2.45 (m, 2H, $CH_{2morph}$), 2.22 (t, 1H, $J$=9.0, $1/2CH_2N_{pip}$), 1.96 (t, 1H, $J$=9.0, $1/2CH_2N_{pip}$), 1.90 (s br, 1H, CH), 1.66-1.45 (m, 3H, $1/2CH_{2pip}$, $CH_{2pip}$), 0.89-0.97 (m, 1H, $1/2CH_{2pip}$).

**$^{13}$C-NMR** ($(CD_3)_2SO$): δ 177.8 (C(O)=N), 175.0 ($2COOH_{CA}$), 171.4 ($4COOH_{CA}$), 166.6 (C(N)=N), 130.0 (q, $\underline{C}CF_3$), 128.0 ($2CH_{Ar}$), 126.2 ($2CH_{Ar}$), 125.0 (q, $C_{Ar}$), 122.8 (q, $CF_3$), 72.3 ($2C(OH)_{CA}$), 65.2 ($2CH_2O_{morph}$), 61.3 ($CH_{2morph}$), 57.1 ($CH_2N_{pip}$), 53.0 ($2CH_2N_{morph}$), 52.6 ($CH_2N_{pip}$, $CH_{2pip}$), 43.0 ($4CH_{2,CA}$), 31.9 (CH), 28.1 ($CH_{2pip}$), 24.2 ($CH_{2pip}$).

**$T_g$:** 55-57 °C (degradation from 140°C)

**IR**: $\bar{\nu}$ ($cm^-$) 3458, 2951-3000, 1724, 1577, 1325, 1121

**Elemental analysis**: calculated: C 48.37%; H 5.20%; N 7.05%; determined: C 47.32%; H 5.09%; N 6.55%

*Synthesis of **22_2SA***

In a grinding jar, **22** (150 mg, 0.365 mmol, 1.0 eq), saccharin (135 mg, 0.737 mmol, 2.0 eq), and a grinding ball (Zirconium oxide, 12 mm of diameter) were added. The jar was then placed in the grinding machine (Retsch Mixer Mill 400), equipped with another grinding jar~~s~~. The dry grinding was then performed for 90 min at 30 Hz to afford an off-white solid.

**$^{1}$H-NMR** ($(CD_3)_2SO$): 8.22 (d, 2H, *J*=8.2, 2$CH_{Ar}$), 7.96 (d, 2H, *J*=8.2, 2$CH_{Ar}$), 7.89 (d, *J*=7.0, 6.4, 2H, $CH_{Ar,Sacc}$), 7.79-7.73 (m, 6H, $CH_{Ar,sacc}$), 4.20 (s, 2H, $CH_{2,pip}$), 3.82 (s br , 4H, 2$CH_2O_{moprh}$), 3.23 (s br, 3H, 2$CH_2N_{moprh}$), 3.07-3.03 (m, 3H, 1/2$CH_2N_{pip}$, $CH_{2morph}$), 2.91 (s, 1H, 1/2$CH_2N_{pip}$), 2.44 (t, 1H, 1/2$CH_2N_{pip}$), 2.25 (t, 1H, 1/2$CH_2N_{pip}$), 2.14 (s br, 1H, CH), 1.73-1.69 (m, 3H, 1/2$CH_{2pip}$, $CH_{2pip}$), 1.08 (d, 1H, *J*=10.0, 1/2$CH_{2pip}$)

**$^{13}$C-NMR** ($(CD_3)_2SO$): δ 176.6 (C(O)=N), 166.6 (C(N)=N), 164.7 ($C{=}O_{sacc}$), 142.5 ($C_{Ar,sacc}$), 133.2 ($C_{Ar,sacc}$), 133.1 ($C_{Ar,sacc}$), 131.7 ($\underline{C}CF_3$), 131.4 ($C_{Ar}$), 129.9 (2$CH_{Ar}$), 128.0 ($C_{Ar,sacc}$), 126.4 (2$CH_{Ar}$), 124.9 (q, $CF_3$), 123.6 ($C_{Ar,sacc}$), 120.1 ($C_{Ar,sacc}$), 63.2 (2$CH_2O_{morph}$), 59.1 ($CH_{2morph}$), 55.8 ($CH_2N_{pip}$), 52.4 ($CH_2N_{pip}$), 51.9 ($CH_{2pip}$), 51.7 (2$CH_2N_{morph}$), 29.9 (CH), 26.9 ($CH_{2pip}$), 23.0 ($CH_{2pip}$)

**$T_g$:** 62-63 °C (degradation from 210°C)
**Elemental analysis**: calculated: C 52.57%; H 4.54%; N 10.82%; determined: C 51.25%; H 4.52%; N 10.35%
**IR**: $\bar{\nu}$ (cm$^{-}$) 3951-3000, 2869, 1738, 1576, 1324, 1147, 1117

# REFERENCES

1. Poewe, W. *et al.* Parkinson Disease. *Nat. Rev. Dis. Prim.* **3**, 17013 (2017).
2. Draoui, A. *et al.* Parkinson's Disease : Moving Forward Accreditations The Story of Parkinson's Disease. *Plant Arch.* **22**, 733–745 (2021).
3. Cacabelos, R. Parkinson's Disease: From Pathogenesis to Pharmacogenomics. *Int. J. Mol. Sci.* **18**, 551 (2017).
4. Koziorowski, D. *et al.* Mechanisms of Neurodegeneration in Various Forms of Parkinsonism—Similarities and Differences. *Cells* **10**, 656 (2021).
5. Singh, S. & Joshi, N. *Pathology, Prevention and Therapeutics of Neurodegenerative Disease*. *Pathology, Prevention and Therapeutics of Neurodegenerative Disease* (Springer Singapore, 2019).
6. Draoui, A., El Hiba, O., Aimrane, A., El Khiat, A. & Gamrani, H. Parkinson's Disease: From Bench to Bedside. *Rev. Neurol. (Paris).* **176**, 543–559 (2020).
7. Parkinson, J. An Essay on the Shaking Palsy. *Sherwood, Neely and Jones* (1817).
8. Prasad, E. M. & Hung, S.-Y. Current Therapies in Clinical Trials of Parkinson's Disease: A 2021 Update. *Pharmaceuticals* **14**, 717 (2021).
9. Alexander, G. E. Biology of Parkinson's Disease: Pathogenesis and Pathophysiology of a Multisystem Neurodegenerative Disorder. *Dialogues Clin. Neurosci.* **6**, 259–280 (2004).
10. Hirsch, L., Jette, N., Frolkis, A., Steeves, T. & Pringsheim, T. The Incidence of Parkinson's Disease: A Systematic Review and Meta-Analysis. *Neuroepidemiology* **46**, 292–300 (2016).
11. Calabrese, V. P. *et al.* Projected Number of People with Parkinson Disease in the Most Populous Nations, 2005 Through 2030. *Neurology* **69**, 223–224 (2007).
12. Brady, S., Siegel, G., Albers, R. W. & Price, D. L. *Basic Neurochemistry: Principles of Molecular, Cellular, and Medical Neurobiology.* (Elsevier, 2012).
13. Charvin, D., Medori, R., Hauser, R. A. & Rascol, O. Therapeutic Strategies for Parkinson Disease: Beyond Dopaminergic Drugs. *Nat. Rev. Drug Discov.* **17**, 804–822 (2018).
14. Kaya, Z. B. & Atilla, P. An Overview of Alpha Synuclein Protein and Its Role in Parkinson's disease. *Acta Medica Cordoba.* 1–10 (2021).
15. Pan-Montojo, F. & Reichmann, H. Considerations on the Role of Environmental Toxins in Idiopathic Parkinson's Disease Pathophysiology. *Transl. Neurodegener.* **3**, 10 (2014).
16. Vila, M. & Przedborski, S. Targeting Programmed Cell Death in Neurodegenerative Diseases. *Nat. Rev. Neurosci.* **4**, 365–375 (2003).
17. Franco, R., Rivas-Santisteban, R., Navarro, G., Pinna, A. & Reyes-Resina, I. Genes Implicated in Familial Parkinson's Disease Provide a Dual Picture of Nigral Dopaminergic Neurodegeneration with Mitochondria Taking Center Stage. *Int. J. Mol. Sci.* **22**, 4643 (2021).
18. Ferreira, M. & Massano, J. An Updated Review of Parkinson's Disease Genetics and

Clinicopathological Correlations. *Acta Neurol. Scand.* **135**, 273–284 (2017).

19. Polymeropoulos, M. H. Mutation in the Alpha-Synuclein Gene Identified in Families with Parkinson's Disease. *Science.* **276**, 2045–2047 (1997).

20. Greggio, E., Bisaglia, M., Civiero, L. & Bubacco, L. Leucine-Rich Repeat Kinase 2 and Alpha-Synuclein: Intersecting Pathways in the Pathogenesis of Parkinson's Disease? *Mol. Neurodegener.* **6**, 1–10 (2011).

21. Quinn, P. M. J., Moreira, P. I., Ambrósio, A. F. & Alves, C. H. PINK1/PARKIN Signalling in Neurodegeneration and Neuroinflammation. *Acta Neuropathol. Commun.* **8**, 189 (2020).

22. Dawson, T. M. & Dawson, V. L. The Role of Parkin in Familial and Sporadic Parkinson's Disease. *Mov. Disord.* **25**, S32–S39 (2010).

23. Ariga, H. *et al.* Neuroprotective Function of DJ-1 in Parkinson's Disease. *Oxid. Med. Cell. Longev.* **2013**, 1–9 (2013).

24. Bonifati, V. Mutations in the DJ-1 Gene Associated with Autosomal Recessive Early-Onset Parkinsonism. *Science.* **299**, 256–259 (2003).

25. Di Fonzo, A. *et al.* Comprehensive Analysis of the LRRK2 Gene in Sixty Families with Parkinson's Disease. *Eur. J. Hum. Genet.* **14**, 322–331 (2006).

26. Gilks, W. *et al.* A Common Mutation in Idiopathic Parkinson's Disease. *Lancet* **365**, 415–416 (2005).

27. Nalls, M. A. *et al.* Large-Scale Meta-Analysis of Genome-Wide Association Data Identifies Six New Risk Loci for Parkinson's Disease. *Nat. Genet.* **46**, 989–993 (2014).

28. Mata, I. F., Wedemeyer, W. J., Farrer, M. J., Taylor, J. P. & Gallo, K. A. LRRK2 in Parkinson's Disease: Protein Domains and Functional Insights. *Trends Neurosci.* **29**, 286–293 (2006).

29. Bonifati, V., Oostra, B. A. & Heutink, P. Linking DJ-1 to Neurodegeneration Offers Novel Insights for Understanding the Pathogenesis of Parkinson's Disease. *J. Mol. Med.* **82**, 163–174 (2004).

30. About Parkinson's Disease. https://www.genome.gov/Genetic-Disorders/Parkinsons-Disease (2014) Accessed on the 31 August 2021.

31. Langston, J., Ballard, P., Tetrud, J. & Irwin, I. Chronic Parkinsonism in Humans Due to a Product of Meperidine-Analog Synthesis. *Science.* **219**, 979–980 (1983).

32. Ali, S. F., David, S. N., Newport, G. D., Cadet, J. L. & Slikker, W. MPTP-Induced Oxidative Stress and Neurotoxicity are Age-Dependent: Evidence From Measures of Reactive Oxygen Species and Striatal Dopamine Levels. *Synapse* **18**, 27–34 (1994).

33. Jenner, P. Parkinson's Disease, Pesticides and Mitochondrial Dysfunction. *Trends Neurosci.* **24**, 245–246 (2001).

34. Cersosimo, M. G. & Koller, W. C. The Diagnosis of Manganese-Induced Parkinsonism. *Neurotoxicology* **27**, 340–346 (2006).

35. Ball, N., Teo, W.-P., Chandra, S. & Chapman, J. Parkinson's Disease and the Environment. *Front. Neurol.* **10**, (2019).

36. Coon, S. *et al.* Whole-Body Lifetime Occupational Lead Exposure and Risk of Parkinson's Disease. *Environ. Health Perspect.* **114**, 1872–1876 (2006).

37. Mappin-Kasirer, B. *et al.* Tobacco Smoking and the Risk of Parkinson Disease. *Neurology* **94**, e2132–e2138 (2020).

38. Ren, X. & Chen, J.-F. Caffeine and Parkinson's Disease: Multiple Benefits and Emerging Mechanisms. *Front. Neurosci.* **14**, 1–12 (2020).

39. Blesa, J., Trigo-Damas, I., Quiroga-Varela, A. & Jackson-Lewis, V. R. Oxidative Stress and Parkinson's Disease. *Front. Neuroanat.* **9**, (2015).

40. Brieger, K., Schiavone, S., Miller, J. & Krause, K. Reactive Oxygen Species: From Health to Disease. *Swiss Med. Wkly.* **142**, 1–14 (2012).

41. Blesa, J., Trigo-Damas, I., Quiroga-Varela, A. & Jackson-Lewis, V. R. Oxidative Stress and Parkinson's Disease. *Front. Neuroanat.* **9**, (2015).

42. Block, M. L., Zecca, L. & Hong, J.-S. Microglia-Mediated Neurotoxicity: Uncovering the Molecular Mechanisms. *Nat. Rev. Neurosci.* **8**, 57–69 (2007).

43. Kempuraj, D. *et al.* Neuroinflammation Induces Neurodegeneration. *J. Neurol. Neurosurg. spine* **1**, 1–15 (2016).

44. Hickman, S., Izzy, S., Sen, P., Morsett, L. & El Khoury, J. Microglia in Neurodegeneration. *Nat. Neurosci.* **21**, 1359–1369 (2018).

45. Nelson, D. L. & Cox, M. M. *Lehninger Principles of Biochemistry*. (Macmillan Higher Education : Basingstoke, 2017, 2017).

46. Kemp, M. Recent Advances in the Discovery of Deubiquitinating Enzyme Inhibitors. in *Progress in Medicinal Chemistry* vol. 55 149–192 (Elsevier, 2016).

47. Mevissen, T. E. T. & Komander, D. Mechanisms of Deubiquitinase Specificity and Regulation. *Annu. Rev. Biochem.* **86**, 159–192 (2017).

48. Amer-Sarsour, F., Kordonsky, A., Berdichevsky, Y., Prag, G. & Ashkenazi, A. Deubiquitylating Enzymes in Neuronal Health and Disease. *Cell Death Dis.* **12**, 120 (2021).

49. Abdul Rehman, S. A. *et al.* MINDY-1 Is a Member of an Evolutionarily Conserved and Structurally Distinct New Family of Deubiquitinating Enzymes. *Mol. Cell* **63**, 146–155 (2016).

50. Collins, G. A. & Goldberg, A. L. The Logic of the 26S Proteasome. *Cell* **169**, 792–806 (2017).

51. Kitada, T. *et al.* Mutations in the Parkin Gene Cause Autosomal Recessive Juvenile Parkinsonism. *Nature* **392**, 605–608 (1998).

52. Leroy, E. *et al.* The Ubiquitin Pathway in Parkinson's Disease. *Nature* **395**, 451–452 (1998).

53. Tanaka, Y. *et al.* Inducible Expression of Mutant α-Synuclein Decreases Proteasome Activity and Increases Sensitivity to Mitochondria-Dependent Apoptosis. *Hum. Mol. Genet.* **10**, 919–926 (2001).

54. de Dreu, M. J., van der Wilk, A. S. D., Poppe, E., Kwakkel, G. & van Wegen, E. E. H. Rehabilitation, Exercise Therapy and Music in Patients with Parkinson's Disease: a Meta-Analysis of the Effects of Music-Based Movement Therapy on Walking Ability, Balance and Quality of Life. *Parkinsonism Relat. Disord.* **18**, S114–S119 (2012).

55. Shen, X., Wong-Yu, I. S. K. & Mak, M. K. Y. Effects of Exercise on Falls, Balance, and Gait Ability in Parkinson's Disease. *Neurorehabil. Neural Repair* **30**, 512–527 (2016).

56. Syed, N., Bertoni, J. & Bhatti, D. Deep Brain Stimulation for Parkinson's Disease in Pakistan: Current Status, Opportunities and Challenges. *J. Pak. Med. Assoc.* **70**, 1–18 (2020).

57. Higuchi, Y., Matsuda, S. & Serizawa, T. Gamma Knife Radiosurgery in Movement Disorders: Indications and Limitations. *Mov. Disord.* **32**, 28–35 (2017).

58. Xu, Y. *et al.* Safety and Efficacy of Magnetic Resonance Imaging-Guided Focused Ultrasound Neurosurgery for Parkinson's Disease: a Systematic Review. *Neurosurg. Rev.* **44**, 115–127 (2021).

59. Barker, R. A., Barrett, J., Mason, S. L. & Björklund, A. Fetal Dopaminergic Transplantation Trials and the Future of Neural Grafting in Parkinson's Disease. *Lancet Neurol.* **12**, 84–91 (2013).

60. Abbott, A. Levodopa: the Story So Far. *Nature* **466**, S6–S7 (2010).

61. Galimberti, D. & Scarpini, E. *Neurodegenerative Diseases: Clinical Aspects, Molecular Genetics and Biomarkers*. (Springer International Publishing, 2018).

62. Antonini, A., Tolosa, E., Mizuno, Y., Yamamoto, M. & Poewe, W. H. A Reassessment of Risks and Benefits of Dopamine Agonists in Parkinson's Disease. *Lancet Neurol.* **8**, 929–937 (2009).

63. Tompson, D. & Vearer, D. Steady-State Pharmacokinetic Properties of a 24-hour Prolonged-Release Formulation of Ropinirole: Results of Two Randomized Studies in Patients with Parkinson's Disease. *Clin. Ther.* **29**, 2654–2666 (2007).

64. Zhang, Z. *et al.* Roles of Glutamate Receptors in Parkinson's Disease. *Int. J. Mol. Sci.* **20**, 1–17 (2019).

65. Hopkins, C. R., Lindsley, C. W. & Niswender, C. M. mGluR4-Positive Allosteric Modulation as Potential Treatment for Parkinson's Disease. *Future Med. Chem.* **1**, 501–513 (2009).

66. Vijayakumar, D. & Jankovic, J. Drug-Induced Dyskinesia, Part 1: Treatment of Levodopa-Induced Dyskinesia. *Drugs* **76**, 759–777 (2016).

67. Schwab, R. S. Amantadine in the Treatment of Parkinson's Disease. *J. Am. Med. Assoc.* **208**, 1168 (1969).

68. Carrera, I., Fernandez-Novoa, L., Sampedro, C. & Cacabelos, R. Neuroprotective Effect of Atremorine in an Experimental Model of Parkinson's Disease. *Curr. Pharm. Des.* **23**, 1710–1720 (2017).

69. Cacabelos, R. *et al.* Atremorine in Parkinson's Disease: From Dopaminergic Neuroprotection to Pharmacogenomics. *Med. Res. Rev.* **41**, 2841–2886 (2021).

70. Poewe, W., Seppi, K., Marini, K. & Mahlknecht, P. New Hopes for Disease Modification in Parkinson's Disease. *Neuropharmacology* **171**, 108085 (2020).

71. Vijiaratnam, N., Simuni, T., Bandmann, O., Morris, H. R. & Foltynie, T. Progress Towards Therapies for Disease Modification in Parkinson's Disease. *Lancet Neurol.* **20**, 559–572 (2021).

72. Paolini Paoletti, F., Gaetani, L. & Parnetti, L. The Challenge of Disease-Modifying Therapies in Parkinson's Disease: Role of CSF Biomarkers. *Biomolecules* **10**, 335 (2020).

73. Holst, J. J., Burcelin, R. & Nathanson, E. Neuroprotective Properties of GLP-1: Theoretical and Practical Applications. *Curr. Med. Res. Opin.* **27**, 547–558 (2011).

74. Hölscher, C. Novel Dual GLP-1/GIP Receptor Agonists Show Neuroprotective Effects in Alzheimer's and Parkinson's Disease Models. *Neuropharmacology* **136**, 251–259 (2018).

75. Tai, J., Liu, W., Li, Y., Li, L. & Hölscher, C. Neuroprotective Effects of a Triple GLP-1/GIP/Glucagon Receptor Agonist in the APP/PS1 Transgenic Mouse Model of Alzheimer's Disease. *Brain Res.* **1678**, 64–74 (2018).

76. McIntyre, R. S. *et al.* The Neuroprotective Effects of GLP-1: Possible Treatments for Cognitive Deficits in Individuals with Mood Disorders. *Behav. Brain Res.* **237**, 164–171 (2013).

77. Grieco, M. *et al.* Glucagon-Like Peptide-1: A Focus on Neurodegenerative Diseases. *Front. Neurosci.* **13**, 1–7 (2019).

78. Athauda, D. & Foltynie, T. The Glucagon-Like Peptide 1 (GLP) Receptor as a Therapeutic Target in Parkinson's Disease: Mechanisms of Action. *Drug Discov. Today* **21**, 802–818 (2016).

79. Li, Y. *et al.* GLP-1 Receptor Stimulation Preserves Primary Cortical and Dopaminergic Neurons in Cellular and Rodent Models of Stroke and Parkinsonism. *Proc. Natl. Acad. Sci.* **106**, 1285–1290 (2009).

80. Kastin, A. J. & Akerstrom, V. Entry of Exendin-4 Into Brain is Rapid But May Be Limited at High Doses. *Int. J. Obes.* **27**, 313–318 (2003).

81. Sharma, A. N. *et al.* GLP-1 Receptor Agonist Liraglutide Reverses Long-Term Atypical Antipsychotic Treatment Associated Behavioral Depression and Metabolic Abnormalities in Rats. *Metab. Brain Dis.* **30**, 519–527 (2015).

82. Nassar, N. N., Al-Shorbagy, M. Y., Arab, H. H. & Abdallah, D. M. Saxagliptin: A Novel Antiparkinsonian Approach. *Neuropharmacology* **89**, 308–317 (2015).

83. Kim, S., Moon, M. & Park, S. Exendin-4 Protects Dopaminergic Neurons by Inhibition of

Microglial Activation and Matrix Metalloproteinase-3 Expression in an Animal Model of Parkinson's Disease. *J. Endocrinol.* **202**, 431–439 (2009).

84. Holst, J. J. & Gromada, J. Role of Incretin Hormones in the Regulation of Insulin Secretion in Diabetic and Nondiabetic Humans. *Am. J. Physiol. Metab.* **287**, E199–E206 (2004).

85. Deacon, C. F., Johnsen, A. H. & Holst, J. J. Degradation of Glucagon-Like Peptide-1 by Human Plasma in Vitro Yields an N-terminally Truncated Peptide that is a Major Endogenous Metabolite in Vivo. *J. Clin. Endocrinol. Metab.* **80**, 952–957 (1995).

86. Campbell, J. E. & Drucker, D. J. Pharmacology, Physiology, and Mechanisms of Incretin Hormone Action. *Cell Metab.* **17**, 819–837 (2013).

87. Wei, Y. & Mojsov, S. Tissue-specific Expression of the Human Receptor for Glucagon-Like Peptide-I: Brain, Heart and Pancreatic Forms Have the Same Deduced Amino Acid Sequences. *FEBS Lett.* **358**, 219–224 (1995).

88. Jazayeri, A. *et al.* Crystal Structure of the GLP-1 Receptor Bound to a Peptide Agonist. *Nature* **546**, 254–258 (2017).

89. American Diabetes Association. 2. Classification and Diagnosis of Diabetes: Standards of Medical Care in Diabetes - 2021. *Diabetes Care* **44**, S15–S33 (2021).

90. St Onge, E., Miller, S., Clements, E., Celauro, L. & Barnes, K. The Role of Glucagon-Like Peptide-1 Receptor Agonists in the Treatment of Type 2 Diabetes. *J. Transl. Intern. Med.* **5**, 79–89 (2017).

91. Hansen, K. B., Knop, F. K., Holst, J. J. & Vilsbøll, T. Treatment of Type 2 Diabetes with Glucagon-Like Peptide-1 Receptor Agonists. *Int. J. Clin. Pract.* **63**, 1154–1160 (2009).

92. Tibaldi, J. M. Incorporating Incretin-Based Therapies into Clinical Practice for Patients with Type 2 Diabetes. *Adv. Ther.* **31**, 289–317 (2014).

93. Lau, J. *et al.* Discovery of the Once-Weekly Glucagon-Like Peptide-1 (GLP-1) Analogue Semaglutide. *J. Med. Chem.* **58**, 7370–7380 (2015).

94. Hunter, K. & Hölscher, C. Drugs Developed to Treat Diabetes, Liraglutide and Lixisenatide, Cross the Blood Brain Barrier and Enhance Neurogenesis. *BMC Neurosci.* **13**, 33 (2012).

95. Scheen, A. J., Charpentier, G., Östgren, C. J., Hellqvist, Å. & Gause-Nilsson, I. Efficacy and Safety of Saxagliptin in Combination with Metformin Compared with Sitagliptin in Combination with Metformin in Adult Patients with Type 2 Diabetes Mellitus. *Diabetes. Metab. Res. Rev.* **26**, 540–549 (2010).

96. Nauck, M. A. Unraveling the Science of Incretin Biology. *Am. J. Med.* **122**, S3–S10 (2009).

97. Gilbert, M. P. & Pratley, R. E. GLP-1 Analogs and DPP-4 Inhibitors in Type 2 Diabetes Therapy: Review of Head-to-Head Clinical Trials. *Front. Endocrinol. (Lausanne).* **11**, 1–13 (2020).

98. Frias, J. P. *et al.* The Sustained Effects of a Dual GIP/GLP-1 Receptor Agonist, NNC0090-2746, in Patients with Type 2 Diabetes. *Cell Metab.* **26**, 343–352 (2017).

99. Yang, X. *et al.* Novel Small Molecule Glucagon-Like Peptide-1 Receptor Agonist S6 Stimulates Insulin Secretion From Rat Islets. *Front. Pharmacol.* **12**, 1–10 (2021).

100. Sloop, K. W. *et al.* Novel Small Molecule Glucagon-Like Peptide-1 Receptor Agonist Stimulates Insulin Secretion in Rodents and From Human Islets. *Diabetes* **59**, 3099–3107 (2010).

101. Knudsen, L. B. *et al.* Small-Molecule Agonists for the Glucagon-Like Peptide 1 Receptor. *Proc. Natl. Acad. Sci.* **104**, 937–942 (2007).

102. Wootten, D. *et al.* Modulation of the Glucagon-Like Peptide-1 Receptor Signaling by Naturally Occurring and Synthetic Flavonoids. *J. Pharmacol. Exp. Ther.* **336**, 540–550 (2011).

103. Morris, L. C. *et al.* Discovery of ( S )-2-Cyclopentyl- N -((1-isopropylpyrrolidin2-yl)-9-methyl-1-oxo-2,9-dihydro-1 H -pyrrido[3,4- b ]indole-4-carboxamide (VU0453379): A Novel, CNS Penetrant Glucagon-Like Peptide 1 Receptor (GLP-1R) Positive Allosteric Modulator (PAM). *J. Med. Chem.* **57**, 10192–10197 (2014).

104. Biernacki, K. *et al.* Novel 1,2,4-Oxadiazole Derivatives in Drug Discovery. *Pharmaceuticals* **13**, 111 (2020).

105. De Fonseca, A. F. R., Cuevas, M. R., Ortiz, L. O., Decara Del Olmo, J. M. & Alonso, M. 1,2,4-Oxadiazole Derivatives as Drugs Modulating the GLP-1 Peptide Receptor. US 2014/0031347 A1.

106. Jackson, P. & Thompson, R. J. The Demonstration of New Human Brain-Specific Proteins by High-Resolution Two-Dimensional Polyacrylamide Gel Electrophoresis. *J. Neurol. Sci.* **49**, 429–438 (1981).

107. Bishop, P., Rocca, D. & Henley, J. M. Ubiquitin C-Terminal Hydrolase L1 (UCH-L1): Structure, Distribution and Roles in Brain Function and Dysfunction. *Biochem. J.* **473**, 2453–2462 (2016).

108. Das, C. *et al.* Structural Basis for Conformational Plasticity of the Parkinson's Disease-Associated Ubiquitin Hydrolase UCH-L1. *Proc. Natl. Acad. Sci.* **103**, 4675–4680 (2006).

109. Bilguvar, K. *et al.* Recessive Loss of Function of the Neuronal Ubiquitin Hydrolase UCHL1 Leads to Early-Onset Progressive Neurodegeneration. *Proc. Natl. Acad. Sci.* **110**, 3489–3494 (2013).

110. Choi, J. *et al.* Oxidative Modifications and Down-Regulation of Ubiquitin Carboxyl-Terminal Hydrolase L1 Associated with Idiopathic Parkinson's and Alzheimer's Diseases. *J. Biol. Chem.* **279**, 13256–13264 (2004).

111. Contu, V. R. *et al.* Endogenous Neurotoxic Dopamine Derivative Covalently Binds to Parkinson's Disease-Associated Ubiquitin C-Terminal Hydrolase L1 and Alters its Structure and Function. *J. Neurochem.* **130**, 826–838 (2014).

112. Liu, Z. *et al.* Membrane-Associated Farnesylated UCH-L1 Promotes Alpha-Synuclein Neurotoxicity and is a Therapeutic Target for Parkinson's Disease. *Proc. Natl. Acad. Sci.* **106**, 4635–4640 (2009).

113. Ross, C. A. & Poirier, M. A. Protein Aggregation and Neurodegenerative Disease. *Nat. Med.* **10**, S10–S17 (2004).

114. Xia, Q. Proteomic Identification of Novel Proteins Associated with Lewy Bodies. *Front. Biosci.* **Volume**, 3850 (2008).

115. Bradbury, J. M. & Thompson, R. J. Immunoassay of the Neuronal and Neuroendocrine Marker PGP 9.5 in Human Tissues. *J. Neurochem.* **44**, 651–653 (1985).

116. Kwon, J. *et al.* Developmental Regulation of Ubiquitin C-Terminal Hydrolase Isozyme Expression During Spermatogenesis in Mice. *Biol. Reprod.* **71**, 515–521 (2004).

117. Caballero, O. L. *et al.* Interaction and Colocalization of PGP9.5 with JAB1 and p27Kip1. *Oncogene* **21**, 3003–3010 (2002).

118. Lowe, J., McDermott, H., Landon, M., Mayer, R. J. & Wilkinson, K. D. Ubiquitin Carboxyl-Terminal Hydrolase (PGP 9.5) is Selectively present in Ubiquitinated Inclusion Bodies Characteristic of Human Neurodegenerative Diseases. *J. Pathol.* **161**, 153–160 (1990).

119. Boudreaux, D. A., Maiti, T. K., Davies, C. W. & Das, C. Ubiquitin Vinyl Methyl Ester Binding Orients the Misaligned Active Site of the Ubiquitin Hydrolase UCHL1 Into Productive Conformation. *Proc. Natl. Acad. Sci.* **107**, 9117–9122 (2010).

120. Osaka, H. *et al.* Ubiquitin Carboxy-Terminal Hydrolase L1 Binds to and Stabilizes Monoubiquitin in Neuron. *Hum. Mol. Genet.* **12**, 1945–58 (2003).

121. Liu, Y., Fallon, L., Lashuel, H. A., Liu, Z. & Lansbury, P. T. The UCH-L1 Gene Encodes Two Opposing Enzymatic Activities that Affect α-Synuclein Degradation and Parkinson's Disease Susceptibility. *Cell* **111**, 209–218 (2002).

122. Walters, B. J. *et al.* Differential Effects of USP14 and UCH-L1 on the Ubiquitin Proteasome System and Synaptic Activity. *Mol. Cell. Neurosci.* **39**, 539–548 (2008).

123. Liu, Y. *et al.* Discovery of Inhibitors that Elucidate the Role of UCH-L1 Activity in the H1299 Lung Cancer Cell Line. *Chem. Biol.* **10**, 837–846 (2003).

124. Papa, L. *et al.* UCH-L1 is a Novel Biomarker for severe Traumatic Brain Injury in Human. *Crit. Care Med.* **38**, 138–44 (2010).

125. Wang, K. K. W., Kobeissy, F. H., Shakkour, Z. & Tyndall, J. A. Thorough Overview of Ubiquitin C-Terminal hydrolase-L1 and Glial Fibrillary Acidic Protein as Tandem Biomarkers Recently Cleared by US Food and Drug Administration for the Evaluation of Intracranial Injuries Among Patients with Traumatic Brain Injury. *Acute Med. Surg.* **8**, (2021).

126. Liu, H. *et al.* Role of UCHL1 in Axonal Injury and Functional Recovery After Cerebral Ischemia. *Proc. Natl. Acad. Sci. U. S. A.* **116**, 4643–4650 (2019).

127. Gong, Z. *et al.* UCHL1 Inhibition Attenuates Cardiac Fibrosis via Modulation of Nuclear Factor-κB Signaling in Fibroblasts. *Eur. J. Pharmacol.* **900**, 174045 (2021).

128. Hussain, S., Bedekovics, T., Chesi, M., Bergsagel, P. L. & Galardy, P. J. UCHL1 is a Biomarker of Aggressive Multiple Myeloma Required for Disease Progression. *Oncotarget*

**6**, 40704–40718 (2015).

129. Mao, R. *et al.* Ubiquitin C-Terminal Hydrolase L1 Promotes Expression of Programmed Cell Death-Ligand 1 in Non-Small-Cell Lung Cancer Cells. *Cancer Sci.* **111**, 3174–3183 (2020).

130. Shimada, Y. *et al.* Ubiquitin C-Terminal Hydrolase-L1 has Prognostic Relevance and is a Therapeutic Target for High-Grade Neuroendocrine Lung Cancers. *Cancer Sci.* **111**, 610–620 (2020).

131. Ma, Y. *et al.* Proteomic Profiling of Proteins Associated with Lymph Node Metastasis in Colorectal Cancer. *J. Cell. Biochem.* **110**, 1512–1519 (2010).

132. Zhong, J. *et al.* UCHL1 Acts as a Colorectal Cancer Oncogene via Activation of the β-Catenin/TCF Pathway Through its Deubiquitinating Activity. *Int. J. Mol. Med.* **30**, 430–436 (2012).

133. Tezel, E., Hibi, K., Nagasaka, T. & Nakao, A. PGP9.5 as a Prognostic Factor in Pancreatic Cancer. *Clin. Cancer Res.* **6**, 4764–4767 (2000).

134. Mondal, M., Conole, D., Nautiyal, J. & Tate, E. W. UCHL1 as a Novel Target in Breast Cancer: Emerging Insights From Cell and Chemical Biology. *Br. J. Cancer* 1–10 (2021).

135. Liu, S. *et al.* Deubiquitinase Activity Profiling Identifies UCHL1 as a Candidate Oncoprotein That Promotes TGFβ-Induced Breast Cancer Metastasis. *Clin. Cancer Res.* **26**, 1460–1473 (2020).

136. Jang, M. J., Baek, S. H. & Kim, J. H. UCH-L1 Promotes Cancer Metastasis in Prostate Cancer Cells Through EMT Induction. *Cancer Lett.* **302**, 128–135 (2011).

137. Messick, T. E. *et al.* Structural Basis for Ubiquitin Recognition by the Otu1 Ovarian Tumor Domain Protein. *J. Biol. Chem.* **283**, 11038–11049 (2008).

138. Tangri, A. *et al.* Deubiquitinase UCHL1 Maintains Protein Homeostasis through the PSMA7–APEH–Proteasome Axis in High-grade Serous Ovarian Carcinoma. *Mol. Cancer Res.* **19**, 1168–1181 (2021).

139. Goto, Y. *et al.* UCHL1 Provides Diagnostic and Antimetastatic Strategies due to its Deubiquitinating Effect on HIF-1α. *Nat. Commun.* **6**, 6153 (2015).

140. Liu, H. *et al.* The Point Mutation UCH-L1 C152A Protects Primary Neurons Against Cyclopentenone Prostaglandin-Induced Cytotoxicity: Implications for Post-Ischemic Neuronal Injury. *Cell Death Dis.* **6**, e1966 (2015).

141. Graham, S. Modification of Ubiquitin C-Terminal Hydrolase L1 by Reactive Lipid species: Role in Neural Regeneration and Diseases of Aging. *Neural Regen. Res.* **11**, 908–909 (2016).

142. Jara, J. H., Frank, D. D. & Özdinler, P. H. Could Dysregulation of UPS be a Common Underlying Mechanism for Cancer and Neurodegeneration? Lessons from UCHL1. *Cell Biochem. Biophys.* **67**, 45–53 (2013).

143. Mermerian, A. H., Case, A., Stein, R. L. & Cuny, G. D. Structure–Activity Relationship,

Kinetic Mechanism, and Selectivity for a New Class of Ubiquitin C-Terminal Hydrolase-L1 (UCH-L1) Inhibitors. *Bioorg. Med. Chem. Lett.* **17**, 3729–3732 (2007).

144. Davies, C. W. *et al.* The Co-Crystal Structure of Ubiquitin Carboxy-Terminal Hydrolase L1 (UCHL1) with a Tripeptide Fluoromethyl Ketone (Z-VAE(OMe)-FMK). *Bioorg. Med. Chem. Lett.* **22**, 3900–3904 (2012).

145. Jones, A. *et al.* Novel Compounds. US 2020/0369658 A1.

146. Jones, A. *et al.* Novel Compounds. WO 2016/046530 A1.

147. Panyain, N. *et al.* Discovery of a Potent and Selective Covalent Inhibitor and Activity-Based Probe for the Deubiquitylating Enzyme UCHL1, with Antifibrotic Activity. *J. Am. Chem. Soc.* **142**, 12020–12026 (2020).

148. Krabill, A. D. *et al.* Ubiquitin C-Terminal Hydrolase L1: Biochemical and Cellular Characterization of a Covalent Cyanopyrrolidine-Based Inhibitor. *ChemBioChem* **21**, 712–722 (2020).

149. Mitsui, T. *et al.* Identification of a Novel Chemical Potentiator and Inhibitors of UCH-L1 by in Silico Drug Screening. *Neurochem. Int.* **56**, 679–686 (2010).

150. Bhowmik, A., Khan, R. & Ghosh, M. K. Blood Brain Barrier: A Challenge for Effectual Therapy of Brain Tumors. *Biomed Res. Int.* **2015**, 1–20 (2015).

151. Paulekuhn, G. S., Dressman, J. B. & Saal, C. Trends in Active Pharmaceutical Ingredient Salt Selection Based on Analysis of the Orange Book Database. *J. Med. Chem.* **50**, 6665–6672 (2007).

152. Martins, I. C. B. *et al.* Enhancing Adamantylamine Solubility Through Salt Formation: Novel Products Studied by X-Ray Diffraction and Solid-State NMR. *Cryst. Growth Des.* **19**, 1860–1873 (2019).

153. Stahl, H. P. Salts of the Active Substance Rasagiline. WO 2008/019871.

154. Bolla, G. & Nangia, A. Pharmaceutical Cocrystals: Walking the Talk. *Chem. Commun.* **52**, 8342–8360 (2016).

155. Harmsen, B. & Leyssens, T. Dual-Drug Chiral Resolution: Enantiospecific Cocrystallization of ( S )-Ibuprofen Using Levetiracetam. *Cryst. Growth Des.* **18**, 441–448 (2018).

156. Childs, S. L., Stahly, G. P. & Park, A. The Salt−Cocrystal Continuum: The Influence of Crystal Structure on Ionization State. *Mol. Pharm.* **4**, 323–338 (2007).

157. Sarkar, N. & Aakeröy, C. B. Evaluating Hydrogen-Bond Propensity, Hydrogen-Bond Coordination and Hydrogen-Bond Energy as Tools for Predicting the Outcome of Attempted Co-Crystallisations. *Supramol. Chem.* **32**, 81–90 (2020).

158. Galek, P. T. A., Allen, F. H., Fábián, L. & Feeder, N. Knowledge-Based H-Bond Prediction to Aid Experimental Polymorph Screening. *CrystEngComm* **11**, 2634 (2009).

159. Karagianni, A., Kachrimanis, K. & Nikolakakis, I. Co-Amorphous Solid Dispersions for

Solubility and Absorption Improvement of Drugs: Composition, Preparation, Characterization and Formulations for Oral Delivery. *Pharmaceutics* **10**, 98 (2018).

160. Narala, S. *et al.* Pharmaceutical Co-Crystals, Salts, and Co-Amorphous Systems: A Novel Opportunity of Hot-Melt Extrusion. *J. Drug Deliv. Sci. Technol.* **61**, 102209 (2021).

161. Chavan, R. B., Thipparaboina, R., Kumar, D. & Shastri, N. R. Co Amorphous Systems: A Product Development Perspective. *Int. J. Pharm.* **515**, 403–415 (2016).

162. Newman, A., Chen, C. & Sanrame, C. Salt and Cocrystal Screening. in *Early Drug Development: Bringing a Preclinical Candidate to the Clinic* 229–270 (2018).

163. Mohammad, M. A., Alhalaweh, A. & Velaga, S. P. Hansen Solubility Parameter as a Tool to Predict Cocrystal Formation. *Int. J. Pharm.* **407**, 63–71 (2011).

164. Saal, C. & Becker, A. Pharmaceutical Salts: A Summary on Doses of Salt Formers From the Orange Book. *Eur. J. Pharm. Sci.* **49**, 614–623 (2013).

165. Do, J.-L. & Friščić, T. Mechanochemistry: A Force of Synthesis. *ACS Cent. Sci.* **3**, 13–19 (2017).

166. Friščić, T. & Jones, W. Recent Advances in Understanding the Mechanism of Cocrystal Formation via Grinding. *Cryst. Growth Des.* **9**, 1621–1637 (2009).

167. Trask, A. V. & Jones, W. Crystal Engineering of Organic Cocrystals by the Solid-State Grinding Approach. in *Topics in Current Chemistry* vol. 254 41–70 (2005).

168. Solares-Briones, M. *et al.* Mechanochemistry: A Green Approach in the Preparation of Pharmaceutical Cocrystals. *Pharmaceutics* **13**, 790 (2021).

169. Kooij, R. *et al.* Small-Molecule Activity-Based Probe for Monitoring Ubiquitin C-Terminal Hydrolase L1 (UCHL1) Activity in Live Cells and Zebrafish Embryos. *J. Am. Chem. Soc.* **142**, 16825–16841 (2020).

170. Bandmann, O. & Burton, E. A. Genetic Zebrafish Models of Neurodegenerative Diseases. *Neurobiol. Dis.* **40**, 58–65 (2010).

171. Magano, J., Waldo, M., Greene, D. & Nord, E. The Synthesis of (S)-5-Fluoro-1-(2-fluorophenyl)-3-(piperidin-3-ylmethoxy)-1 H -indazole, a Norepinephrine/Serotonin Reuptake Inhibitor for the Treatment of Fibromyalgia. *Org. Process Res. Dev.* **12**, 877–883 (2008).

172. Handler, N., Wolkerstorfer, A. & Buschmann, H. Selective Optimization of Side Activities: An Alternative and Promising Strategy for Lead Generation. in *Lead Generation: Methods, Strategies and Case Studies* 221–258 (2016).

173. Wermuth, C. G. Selective Optimization of Side Activities: the SOSA Approach. *Drug Discov. Today* **11**, 160–164 (2006).

174. Irwin, J. J. & Shoichet, B. K. ZINC - A Free Database of Commercially Available Compounds for Virtual Screening. *J. Chem. Inf. Model.* **45**, 177–182 (2005).

175. Sterling, T. & Irwin, J. J. ZINC 15 – Ligand Discovery for Everyone. *J. Chem. Inf. Model.*

**55**, 2324–2337 (2015).

176. Morton, I. K. M. & Hall, J. M. *Concise Dictionary of Pharmacological Agents*. (Springer Netherlands, 1999).

177. Cartier, A. E. *et al.* Differential Effects of UCHL1 Modulation on Alpha-Synuclein in PD-Like Models of Alpha-Synucleinopathy. *PLoS One* **7**, e34713 (2012).

178. Etter, M. C., MacDonald, J. C. & Bernstein, J. Graph-Set Analysis of Hydrogen-Bond Patterns in Organic Crystals. *Acta Crystallogr. Sect. B Struct. Sci.* **46**, 256–262 (1990).

179. Groom, C. R., Bruno, I. J., Lightfoot, M. P. & Ward, S. C. The Cambridge Structural Database. *Acta Crystallogr. Sect. B Struct. Sci. Cryst. Eng. Mater.* **72**, 171–179 (2016).

180. Chemburkar, S. R. *et al.* Dealing with the Impact of Ritonavir Polymorphs on the Late Stages of Bulk Drug Process Development. *Org. Process Res. Dev.* **4**, 413–417 (2000).

181. Schrödinger Release 2021-3: SiteMap, Schrödinger, LLC, New York, NY, 2021.

182. Jendele, L., Krivak, R., Skoda, P., Novotny, M. & Hoksza, D. PrankWeb: a Web Server for Ligand Binding Site Prediction and Visualization. *Nucleic Acids Res.* **47**, W345–W349 (2019).

183. Halgren, T. A. *et al.* Glide: A New Approach for Rapid, Accurate Docking and Scoring. 2. Enrichment Factors in Database Screening. *J. Med. Chem.* **47**, 1750–1759 (2004).

184. Boudreaux, D. A., Maiti, T. K., Davies, C. W. & Das, C. Ubiquitin Vinyl Methyl Ester Binding Orients the Misaligned Active Site of the Ubiquitin Hydrolase UCHL1 Into Productive Conformation. *Proc. Natl. Acad. Sci.* **107**, 9117–9122 (2010).

185. Seidler, J., McGovern, S. L., Doman, T. N. & Shoichet, B. K. Identification and Prediction of Promiscuous Aggregating Inhibitors among Known Drugs. *J. Med. Chem.* **46**, 4477–4486 (2003).

186. Papaneophytou, C. P., Mettou, A. K., Rinotas, V., Douni, E. & Kontopidis, G. A. Solvent Selection for Insoluble Ligands, a Challenge for Biological Assay Development: A TNF-α/SPD304 Study. *ACS Med. Chem. Lett.* **4**, 137–141 (2013).

187. Berge, S. M., Bighley, L. D. & Monkhouse, D. C. Pharmaceutical Salts. *J. Pharm. Sci.* **66**, 1–19 (1977).

188. Hasa, D. *et al.* Drug Salt Formation via Mechanochemistry: The Case Study of Vincamine. *Mol. Pharm.* **10**, 211–224 (2013).

189. Nangare, S., Vispute, Y., Tade, R., Dugam, S. & Patil, P. Pharmaceutical Applications of Citric Acid. *Futur. J. Pharm. Sci.* **7**, 54 (2021).

190. Banerjee, R., Bhatt, P. M., Ravindra, N. V. & Desiraju, G. R. Saccharin Salts of Active Pharmaceutical Ingredients, Their Crystal Structures, and Increased Water Solubilities. *Cryst. Growth Des.* **5**, 2299–2309 (2005).

191. Bhatt, P. M., Ravindra, N. V., Banerjee, R. & Desiraju, G. R. Saccharin as a Salt Former. Enhanced Solubilities of Saccharinates of Active Pharmaceutical Ingredients. *Chem.*

*Commun.* 1073 (2005).

192. Singh, Z. Toxicological Aspects of Saccharin. *Food Biol.* **2**, 4–7 (2013).

193. FDA. Additional Information about High-Intensity Sweeteners Permitted for Use in Food in the United States. https://www.fda.gov/food/food-additives-petitions/additional-information-about-high-intensity-sweeteners-permitted-use-food-united-states Accessed on the 21 December 2021.

194. Lin, H.-L., Zhang, G.-C. & Lin, S.-Y. Real-Time Co-Crystal Screening and Formation Between Indomethacin and Saccharin via DSC analytical Technique or DSC–FTIR Microspectroscopy. *J. Therm. Anal. Calorim.* **120**, 679–687 (2015).

195. Barth, A. The Infrared Absorption of Amino Acid Side Chains. *Prog. Biophys. Mol. Biol.* **74**, 141–173 (2000).

196. Mesallati, H., Conroy, D., Hudson, S. & Tajber, L. Preparation and Characterization of Amorphous Ciprofloxacin-Amino Acid Salts. *Eur. J. Pharm. Biopharm.* **121**, 73–89 (2017).

197. Lin, H.-L., Hsu, P.-C. & Lin, S.-Y. Theophylline–Citric Acid Co-Crystals Easily Induced by DSC–FTIR Microspectroscopy or Different Storage Conditions. *Asian J. Pharm. Sci.* **8**, 19–27 (2013).

198. Mahlin, D. & Bergström, C. A. S. Early Drug Development Predictions of Glass-Forming Ability and Physical Stability of Drugs. *Eur. J. Pharm. Sci.* **49**, 323–332 (2013).

199. Lu, Q. & Zografi, G. Properties of Citric Acid at the Glass Transition. *J. Pharm. Sci.* **86**, 1374–1378 (1997).

200. Ali, A. M. A., Ali, A. A. & Maghrabi, I. A. Clozapine-Carboxylic Acid Plasticized Co-Amorphous Dispersions: Preparation, Characterization and Solution Stability Evaluation. *Acta Pharm.* **65**, 133–146 (2015).

201. Chu, K. R., Lee, E., Jeong, S. H. & Park, E.-S. Effect of Particle Size on the Dissolution Behaviors of Poorly Water-Soluble Drugs. *Arch. Pharm. Res.* **35**, 1187–1195 (2012).

202. Di, L. & Kerns, E. H. *Drug-Like Properties*. (Elsevier, 2016).

203. Fleisher, D., Bong, R. & Stewart, B. H. Improved Oral Drug Delivery: Solubility Limitations Overcome by the Use of Prodrugs. *Adv. Drug Deliv. Rev.* **19**, 115–130 (1996).

204. Kang, J., Kumar, V., Yang, D., Chowdhury, P. R. & Hohl, R. J. Cyclodextrin Complexation: Influence on the Solubility, Stability, and Cytotoxicity of Camptothecin, an Antineoplastic Agent. *Eur. J. Pharm. Sci.* **15**, 163–170 (2002).

205. Stella, V. J. & Rajewski, R. A. Cyclodextrins: Their Future in Drug Formulation and Delivery. *Pharmaceutical Research* vol. 14 556–567 (1997).

206. Tilborg, A., Norberg, B. & Wouters, J. Pharmaceutical Salts and Cocrystals Involving Amino Acids: A brief StructuralOoverview of the State-of-Art. *Eur. J. Med. Chem.* **74**, 411–426 (2014).

207. Widmann, G. *et al.* Interpreting TGA Curves. *User Com.* **2**, (2001).

208. Friedman, M. & Mottram, D. *Chemistry and Safety of Acrylamide in Food*. (Springer, 2005).

209. Thayer, A. M. Finding Solutions. *Chem. Eng. News Arch.* **88**, 13–18 (2010).

210. Di, L., Fish, P. V. & Mano, T. Bridging Solubility Between Drug Discovery and Development. *Drug Discov. Today* **17**, 486–495 (2012).

211. Gao, Y., Liao, J., Qi, X. & Zhang, J. Coamorphous Repaglinide–Saccharin with Enhanced Dissolution. *Int. J. Pharm.* **450**, 290–295 (2013).

212. Lu, Q. & Zografi, G. Phase Behavior of Binary and Ternary Amorphous Mixtures Containing Indomethacin, Citric Acid, and PVP. *Pharm. Res.* **15**, 1202–6 (1998).

213. Hoppu, P., Jouppila, K., Rantanen, J., Schantz, S. & Juppo, A. M. Characterisation of Blends of paracetamol and Citric Acid. *J. Pharm. Pharmacol.* **59**, 373–381 (2010).

214. Masuda, T. *et al.* Cocrystallization and Amorphization Induced by Drug–Excipient Interaction Improves the Physical Properties of Acyclovir. *Int. J. Pharm.* **422**, 160–169 (2012).

215. DeYoung, M. B., MacConell, L., Sarin, V., Trautmann, M. & Herbert, P. Encapsulation of Exenatide in Poly-(d,l-Lactide-Co-Glycolide) Microspheres Produced an Investigational Long-Acting Once-Weekly Formulation for Type 2 Diabetes. *Diabetes Technol. Ther.* **13**, 1145–1154 (2011).

216. Park, H., Ha, E.-S. & Kim, M.-S. Complexation of Exenatide and Cyclodextrin: An Approach for the Stabilization and Sustained Release of Exenatide in PLGA Microsphere. *Carbohydr. Polym.* **266**, 118169 (2021).

217. Hossain, M. R., Biswas, H., Raihan Dider, A. & Degadwala, S. Design and Implementation of Smart Energy Meter System with GSM Module. *Int. J. Sci. Res. Sci. Technol.* 51–60 (2020).

218. Newman, A. W., Reutzel-Edens, S. M. & Zografi, G. Characterization of the "Hygroscopic" Properties of Active Pharmaceutical Ingredients. *J. Pharm. Sci.* **97**, 1047–1059 (2008).

219. Pierce, B. G. *et al.* ZDOCK Server: Interactive Docking Prediction of Protein-Protein Complexes and Symmetric Multimers. *Bioinformatics* **30**, 1771–1773 (2014).

220. Laskowski, R. A., MacArthur, M. W., Moss, D. S. & Thornton, J. M. PROCHECK: a Program to Check the Stereochemical Quality of Protein Structures. *J. Appl. Crystallogr.* **26**, 283–291 (1993).

221. Waterhouse, A. *et al.* SWISS-MODEL: Homology Modelling of Protein Structures and Complexes. *Nucleic Acids Res.* **46**, W296–W303 (2018).

222. Case, A. & Stein, R. L. Mechanistic Studies of Ubiquitin C-Terminal Hydrolase L1. *Biochemistry* **45**, 2443–2452 (2006).

223. Luchansky, S. J., Lansbury, P. T. & Stein, R. L. Substrate Recognition and Catalysis by UCH-L1. *Biochemistry* **45**, 14717–14725 (2006).

224. Boudreaux, D. A., Chaney, J., Maiti, T. K. & Das, C. Contribution of Active Site Glutamine to Rate Enhancement in Ubiquitin C-Terminal Hydrolases. *FEBS J.* **279**, 1106–1118 (2012).

225. Mc.Conathy, J. & Owens, M. J. Stereochemistry in Drug Action. *Prim. Care Companion J. Clin. Psychiatry* **05**, 70–73 (2003).

226. Vargesson, N. Thalidomide-Induced Teratogenesis: History and Mechanisms. *Birth Defects Res. Part C Embryo Today Rev.* **105**, 140–156 (2015).

227. Wu, W., Wang, Y., Löbmann, K., Grohganz, H. & Rades, T. Transformations Between Co-Amorphous and Co-Crystal Systems and Their Influence on the Formation and Physical Stability of Co-Amorphous Systems. *Mol. Pharm.* **16**, 1294–1304 (2019).

228. Nakanishi, T. *et al.* Chiral Discrimination Between Thalidomide Enantiomers Using a Solid Surface with Two-Dimensional Chirality. *Chirality* **16**, S36–S39 (2004).

229. Wolfgang, J. & Erlanson, D. A. *Fragment-based Approaches in Drug Discovery*. (Wiley-VCH, 2006).

230. Aurora Fine Chemicals. https://aurorafinechemicals.com/ Accessed on the 22 December 2021.

231. Trask, A. V., Haynes, D. A., Motherwell, W. D. S. & Jones, W. Screening for Crystalline Salts via Mechanochemistry. *Chem. Commun.* 51–53 (2006).

232. Nievergelt, P. P., Babor, M., Čejka, J. & Spingler, B. A High Throughput Screening Method for the Nano-Crystallization of Salts of Organic Cations. *Chem. Sci.* **9**, 3716–3722 (2018).

233. Gupta, D., Bhatia, D., Dave, V., Sutariya, V. & Varghese Gupta, S. Salts of Therapeutic Agents: Chemical, Physicochemical, and Biological Considerations. *Molecules* **23**, 1719 (2018).

234. Rigaku OD (2018). CrysAlis PRO. Rigaku Oxford Diffraction, Yarnton, England.

235. Clark, R. C. & Reid, J. S. The Analytical Calculation of Absorption in Multifaceted Crystals. *Acta Crystallogr. Sect. A Found. Crystallogr.* **51**, 887–897 (1995).

236. Sheldrick, G. M. SHELXT – Integrated Space-Group and Crystal-Structure Determination. *Acta Crystallogr. Sect. A Found. Adv.* **71**, 3–8 (2015).

237. Sheldrick, G. M. Crystal Structure Refinement with SHELXL. *Acta Crystallogr. Sect. C Struct. Chem.* **71**, 3–8 (2015).

238. Dolomanov, O. V., Bourhis, L. J., Gildea, R. J., Howard, J. A. K. & Puschmann, H. OLEX2 : A Complete Structure Solution, Refinement and Analysis Program. *J. Appl. Crystallogr.* **42**, 339–341 (2009).

239. Hübschle, C. B., Sheldrick, G. M. & Dittrich, B. ShelXle : A Qt Graphical User Interface for SHELXL. *J. Appl. Crystallogr.* **44**, 1281–1284 (2011).

240. Needleman, S. B. & Wunsch, C. D. A General Method Applicable to the Search for Similarities in the Amino Acid Sequence of Two Proteins. *J. Mol. Biol.* **48**, 443–453 (1970).

241. Robert, X. & Gouet, P. Deciphering Key Features in Protein Structures with the New

ENDscript Server. *Nucleic Acids Res.* **42**, W320–W324 (2014).

242. Schrödinger Release 2021-3:Maestro, Schrödinger, LLC, New York, NY, 2021.

243. Harder, E. *et al.* OPLS3: A Force Field Providing Broad Coverage of Drug-like Small Molecules and Proteins. *J. Chem. Theory Comput.* **12**, 281–296 (2016).

244. Schrödinger Release 2021-3: LigPrep, Schrödinger, LLC, New York, NY, 2021.

245. Madhavi Sastry, G., Adzhigirey, M., Day, T., Annabhimoju, R. & Sherman, W. Protein and Ligand Preparation: Parameters, Protocols, and Influence on Virtual Screening Enrichments. *J. Comput. Aided. Mol. Des.* **27**, 221–234 (2013).

246. Friesner, R. A. *et al.* Extra Precision Glide: Docking and Scoring Incorporating a Model of Hydrophobic Enclosure for Protein-Ligand Complexes. *J. Med. Chem.* **49**, 6177–6196 (2006).

247. Li, J. *et al.* The VSGB 2.0 Model: A Next Generation Energy Model for High Resolution Protein Structure Modeling. *Proteins Struct. Funct. Bioinforma.* **79**, 2794–2812 (2011).

248. Jones, G., Willett, P. & Glen, R. C. Molecular Recognition of Receptor Sites Using a Genetic Algorithm with a Description of Desolvation. *J. Mol. Biol.* **245**, 43–53 (1995).

249. Liebeschuetz, J. W., Cole, J. C. & Korb, O. Pose Prediction and Virtual Screening Performance of GOLD Scoring Functions in a Standardized Test. *J. Comput. Aided. Mol. Des.* **26**, 737–748 (2012).

250. Hassiepen, U. *et al.* A Sensitive Fluorescence Intensity Assay for Deubiquitinating Proteases Using Ubiquitin-Rhodamine110-Glycine as Substrate. *Anal. Biochem.* **371**, 201–207 (2007).

251. Cer, R. Z., Mudunuri, U., Stephens, R. & Lebeda, F. J. IC50-to-Ki: a Web-Based Tool for Converting IC50 to Ki Values for Inhibitors of Enzyme Activity and Ligand Binding. *Nucleic Acids Res.* **37**, W441–W445 (2009).

252. Macrae, C. F. *et al.* Mercury 4.0 : From Visualization to Analysis, Design and Prediction. *J. Appl. Crystallogr.* **53**, 226–235 (2020).

253. Westrip, S. P. publCIF : Software for Editing, Validating and Formatting Crystallographic Information Files. *J. Appl. Crystallogr.* **43**, 920–925 (2010).

254. Threadgill, M. D. *et al.* Tankyrase Inhibitors. WO 2014/087165 Al.

255. Dürüst, Y., Karakuş, H., Kaiser, M. & Tasdemir, D. Synthesis and Anti-Protozoal Activity of Novel Dihydropyrrolo[3,4-d][1,2,3]triazoles. *Eur. J. Med. Chem.* **48**, 296–304 (2012).

# APPENDICES

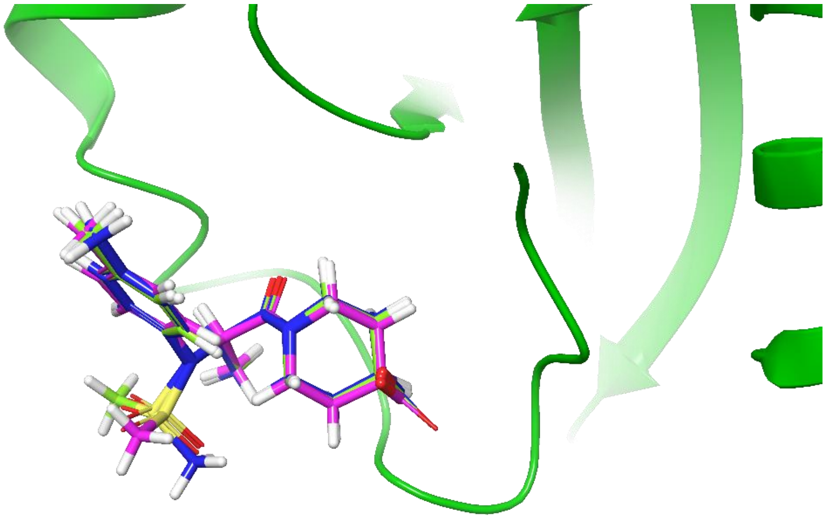

**Figure 54** - Docking poses of **(R)-36** in the allosteric site of hUCH-L1 inactive form (PDB: 2ETL). Representation of pose 1, 2 and 3 in pink, blue and green respectively.

**Table 15** -Raking based on the glide score of top 3 poses obtained for the docking of **(R)-36** in the AS-1 of hUCH-L1 inactive form, defined by SiteMap. Values of $\Delta G_{binding}$ were obtained by MM-GBSA calculations.

| Pose number | Color | $\Delta G_{binding}$ [kcal/mol] |
|---|---|---|
| 1 | Pink | -20.0 |
| 2 | Blue | -19.5 |
| 3 | Green | -23.0 |

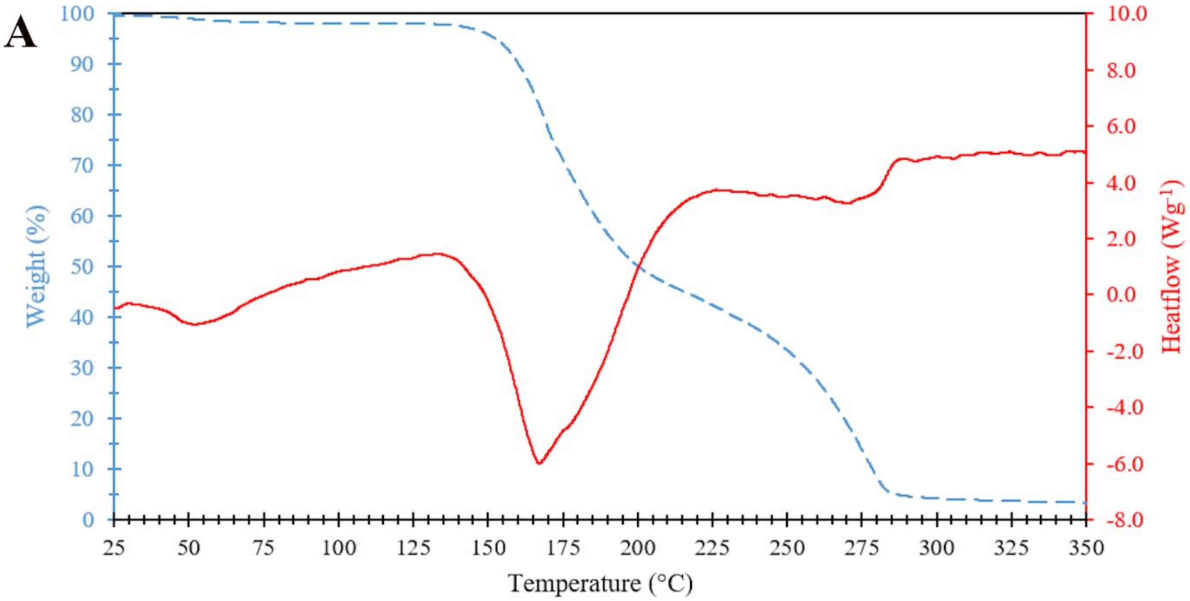

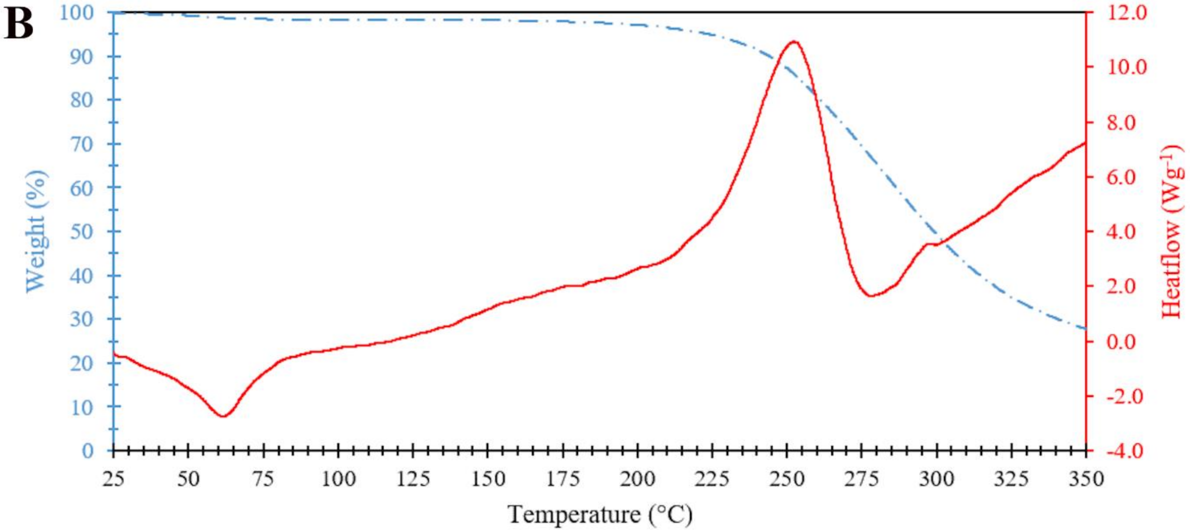

**Figure 55** - DSC/ TGA curves of compound (A) **22_2CA** and (B) **22_2SA**. The DSC curve is in red line and the TGA one in blue dotted line.

## APPENDIX C

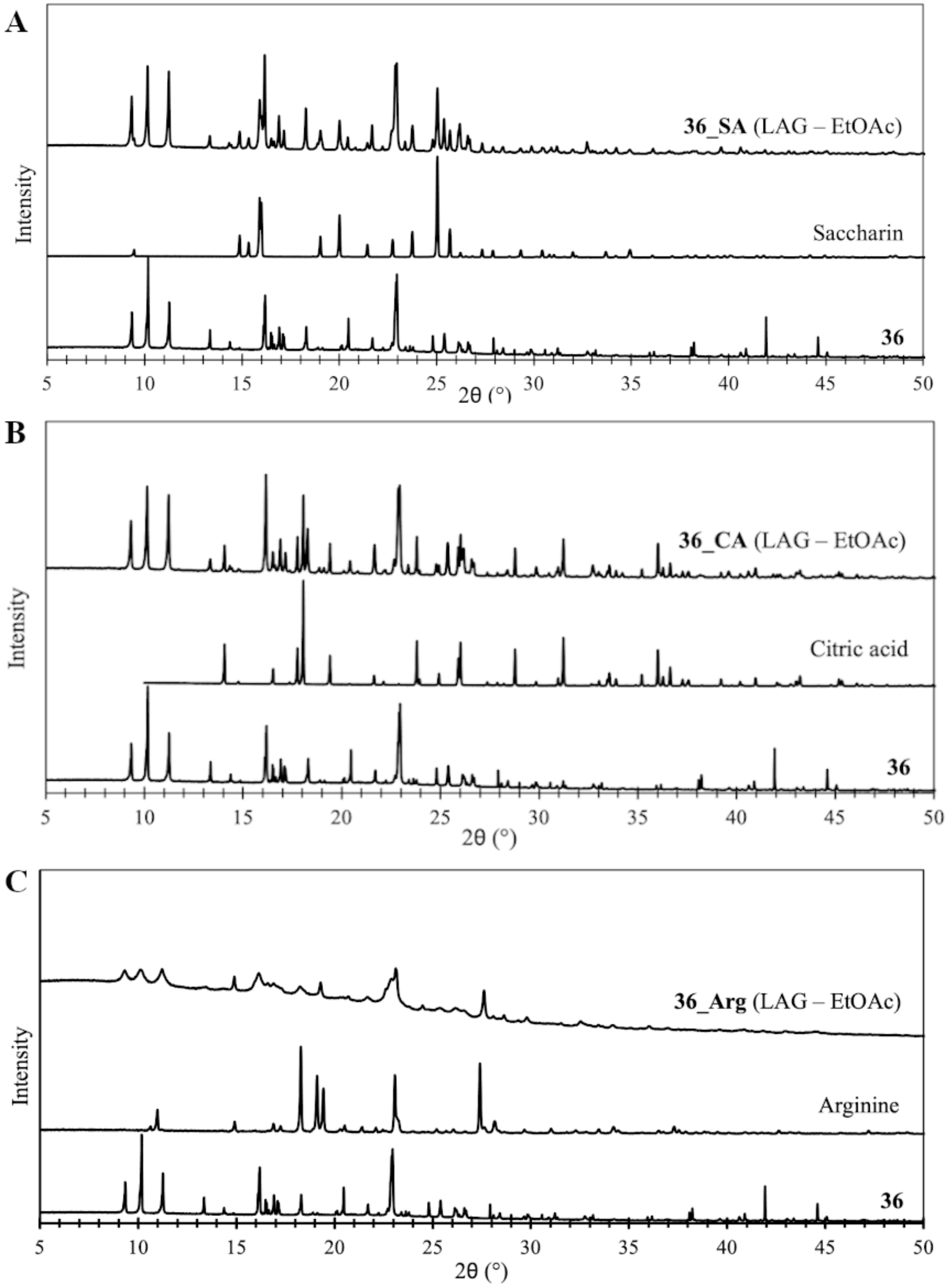

**Figure 56** - PXRD diffraction pattern of (A) **36_SA**, saccharin and **36** (from top to bottom), of (B) **36_CA**, citric acid and **36** (from top to bottom) and (C) **36_Arg**, arginine and **36** (from top to bottom).

## APPENDIX C

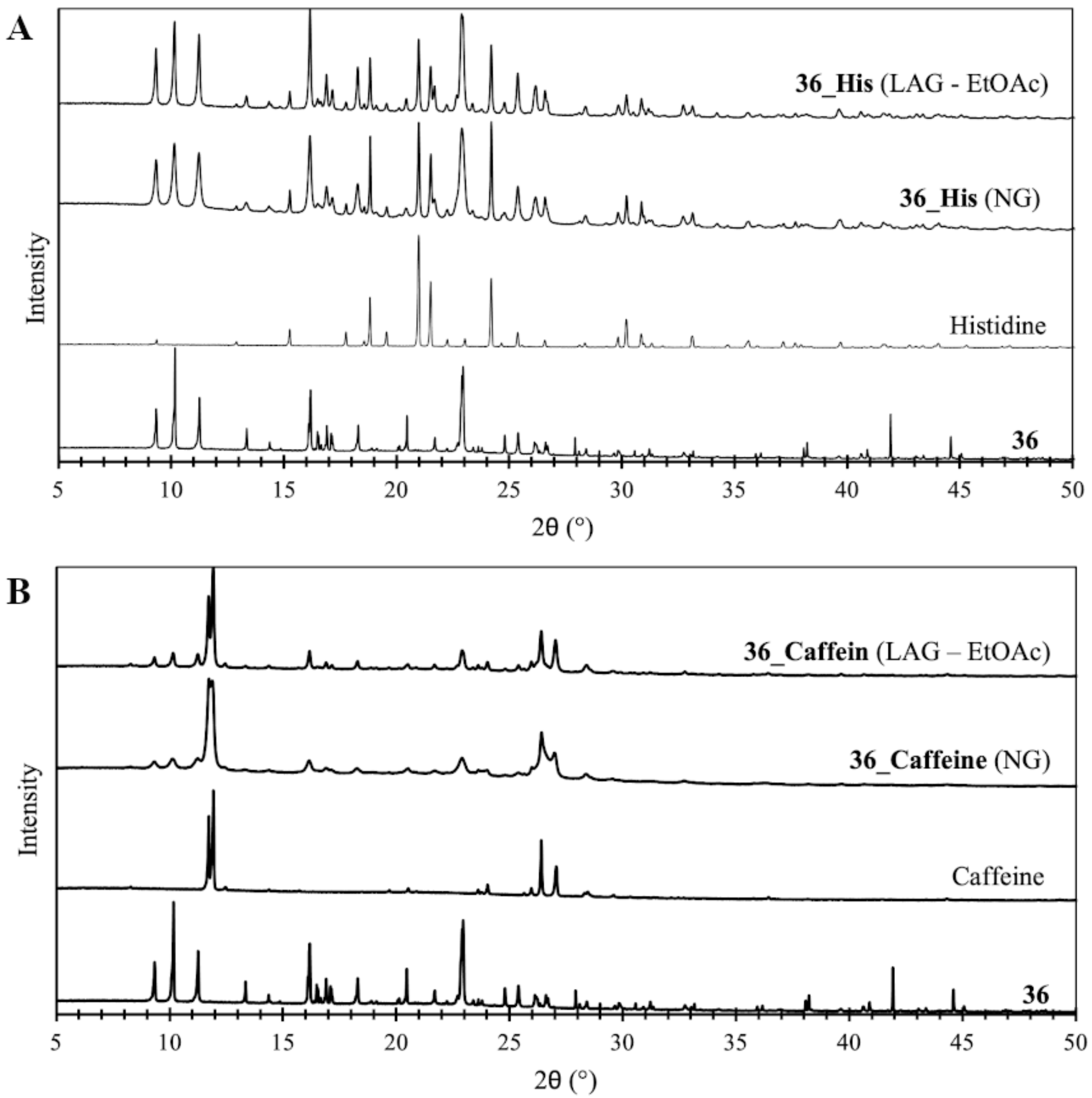

**Figure 57** - PXRD diffraction pattern of (A) **36_His**, histidine and **36** (from top to bottom) and of (B) **36_Caffeine**, caffeine and **36** (from top to bottom).

## APPENDIX D

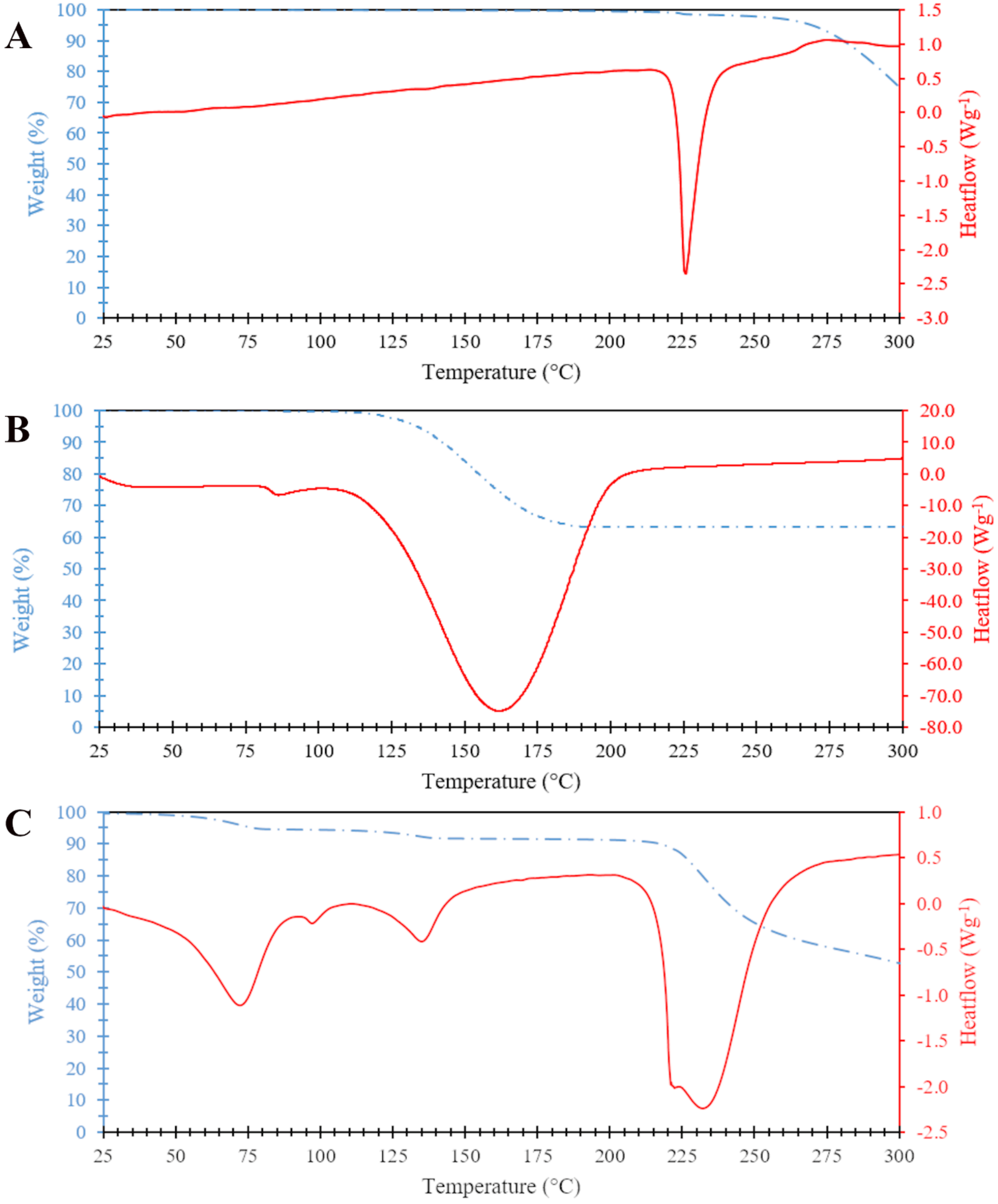

**Figure 58** - DSC/ TGA curves of compound **36**, sodium bicarbonate and lysine (from top to bottom). The DSC curve is in red line and the TGA one in blue dotted line

# APPENDIX E

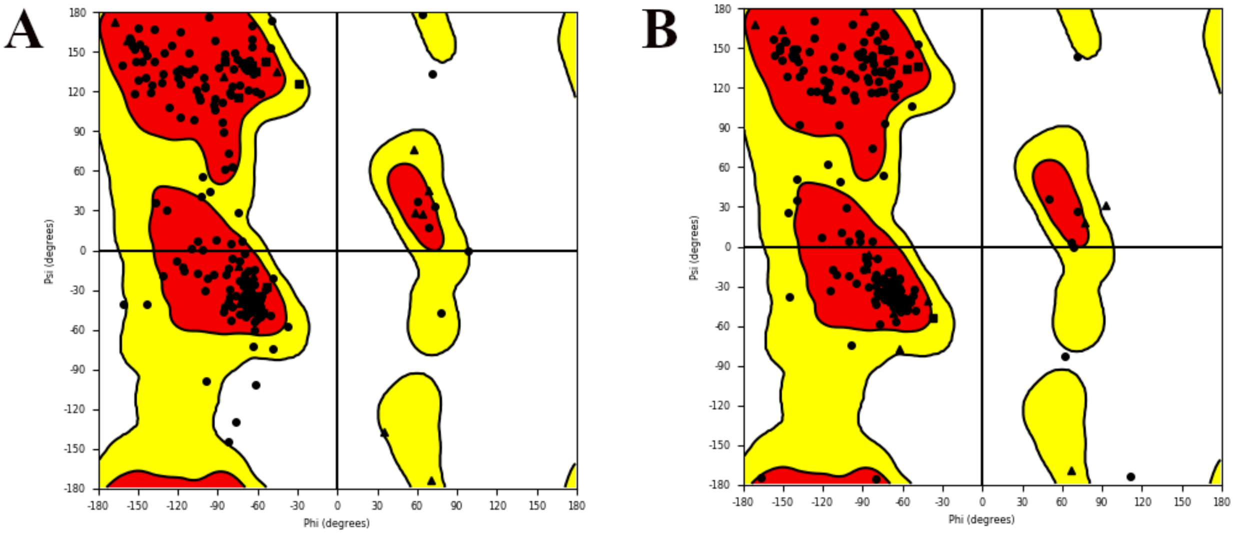

**Figure 59** - Ramachandran plot for both zUCH-L1 models (A) zUCH-L1(i) and (B) zUCH-L1(a). Glycines are plotted as triangles, prolines are plotted as squares, all other residues are plotted as circles. The red, yellow and white regions are the favored, the allowed and the disallowed regions respectively.

**Table 16** - List of amino acids that are in the disallowed regions of zUCH-L1(i) and zUCH-L1(a) homology models.

| **zUCH-L1(i)** | **zUCH-L1(a)** |
|---|---|
| Phe103 | Cys71 |
| Asp152 | Asp152 |
| Lys65 | Ser24 |
| Glu35 | |

## APPENDIX F

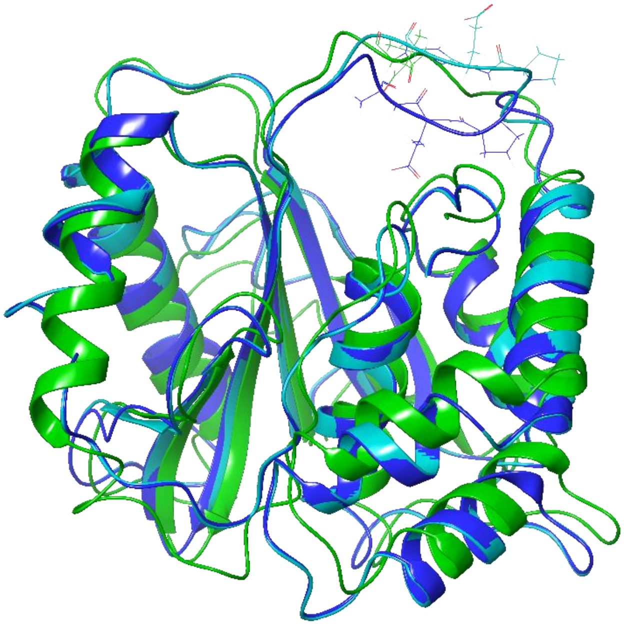

**Figure 60** – Superposition of 3D structures in secondary structure representation of hUCH-L1 inactive form (green), zUCH-L1(i) (dark blue) and zUCH-L1(i) "open form" (light blue). Residues of interest are represented in sticks.

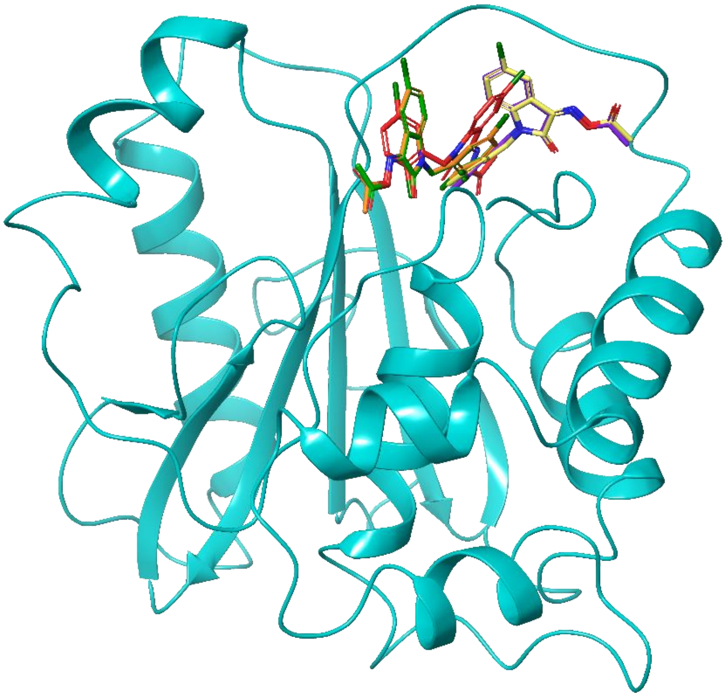

**Figure 61** - Docking results of LDN-57444 in zUCH-L1(i) in "open form". Protein in secondary structure representation and LDN-57444 for poses 1 to 5 in purple, yellow, orange, green and red respectively. Hydrogen atoms are not shown for clarity purpose.

## APPENDIX G

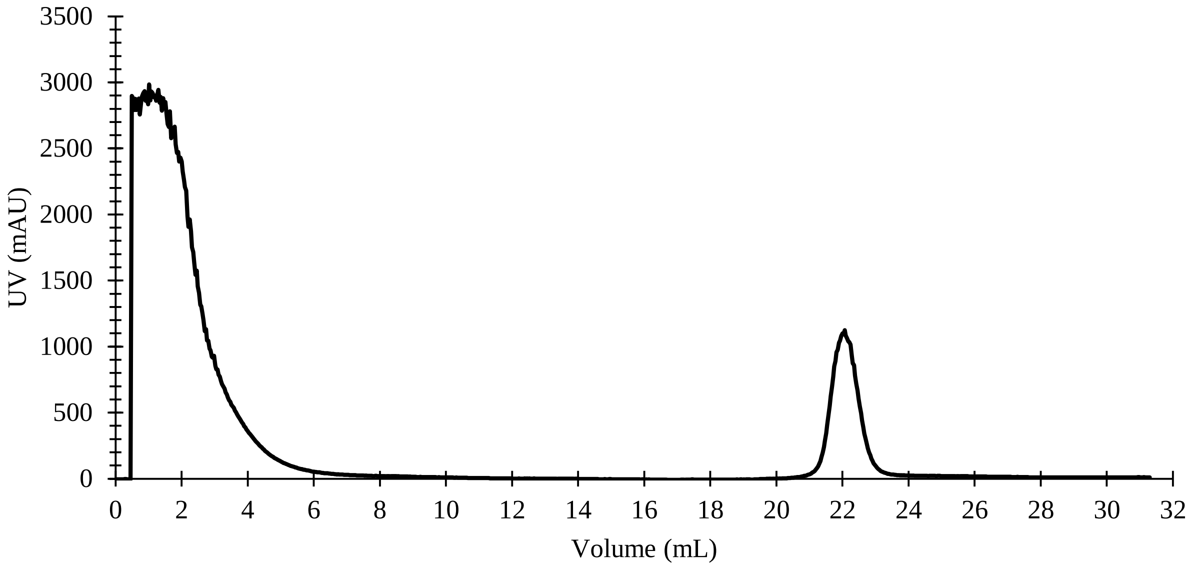

**Figure 62** - Elution profile of zUCH-L1-GST by GSTrap. At 16 mL, buffer A (PBS, pH 7.4) was eluted with buffer B (Tris.HCl 50 mM, NaCl 500 mM, DTT 1 mM, GSH 20 mM, pH 8.0).

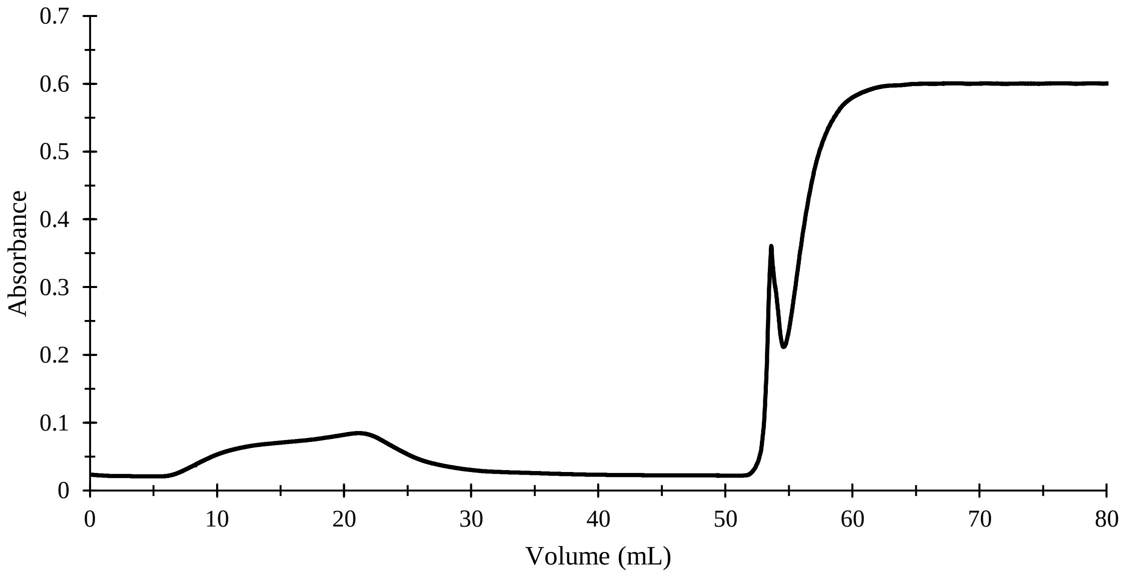

**Figure 63** - Elution profile of zUCH-L1 by GSTrap. At 50 mL, buffer A (Tris.HCl 50 mM, NaCl 150 mM, DTT 1 mM, EDTA 1 mM, pH 7.4) was eluted with buffer B (Tris.HCl 50 mM, NaCl 500 mM, GSH 20 mM, pH 8.0).

# APPENDIX H

research communications

Acta Cryst E
CRYSTALLOGRAPHIC COMMUNICATIONS

ISSN 2056-9890

# Crystal structures of two alanylpiperidine analogues

**Kalina Mambourg,[a]* Nikolay Tumanov,[a] Gilles Henon,[a] Steve Lanners,[a] Javier Garcia-Ladona[b] and Johan Wouters[a]**

[a]Department of Chemistry, University of Namur, Rue de Bruxelles 61, Namur 5000, Belgium, and [b]Abaxys Therapeutics, Rue du Berceau 91, Villers-la-Ville 1495, Belgium. *Correspondence e-mail: kalina.mambourg@unamur.be

Received 30 September 2021
Accepted 7 October 2021

Edited by L. Van Meervelt, Katholieke Universiteit Leuven, Belgium

**Keywords:** crystal structure; UCH-L1 activator; alanylpiperidine derivatives; polymorph risk assessment.

**CCDC references**: 2114340; 2114339

**Supporting information**: this article has supporting information at journals.iucr.org/e

The structure of ethyl 1-[*N*-(4-methylphenyl)-*N*-(methylsulfonyl)alanyl]-piperidine-4-carboxylate, $C_{19}H_{28}N_2O_5S$, **I**, a compound of interest as activator of Ubiquitin C-terminal Hydrolase-L1 (UCH-L1), was determined by single-crystal X-ray diffraction (SCXRD) analysis. In order to find new activators, a derivative of compound **I**, namely, 1-[*N*-(4-methylphenyl)-*N*-(methylsulfonyl)-alanyl]piperidine-4-carboxylic acid, $C_{17}H_{24}N_2O_5S$, **II**, was studied. The synthesis and crystal structure are also reported. Despite being analogues, different crystal packings are observed. Compound **II** bears a carboxylic group, which favors a strong hydrogen bond. A polymorph risk assessment was carried out to study interactions in compound **II**.

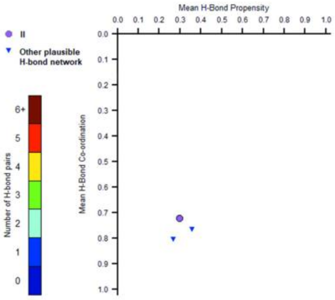

## 1. Chemical context

Ubiquitin C-terminal Hydrolase-L1 is a deubiquitinase that represents 2% of the neuronal soluble proteins in the brain and is involved in the neuropathogenesis of neurodegenerative diseases. Studies have shown that several mutations have an impact on the hydrolase activity of UCH-L1 (Leroy *et al.*, 1998; Maraganore *et al.*, 1999) and that its down-regulation is associated with idiopathic Parkinson's disease (Choi *et al.*, 2004). Finding potentiators of UCH-L1 could be a therapeutic pathway for these diseases (Mitsui *et al.*, 2010). Ethyl 1-[*N*-(methylsulfonyl)-*N*-(*p*-tolyl)-alanyl]piperidine-4-carboxylate was discovered through *in silico* drug screening as an activator of UCH-L1, with a hydrolase activity up to 111% at 63 μ*M* (Mitsui *et al.*, 2010). We studied the only known activator in the literature, compound **I**. Derivatives of compound **I** were then investigated as potential activators and compound **II** was obtained after a saponification. Compound **II** bears a carboxylic acid group, which opens up the possibility for co-crystallization and salification in order to modulate the physicochemical properties, such as the solubility. We report the crystal structures of these two compounds as well as a survey of the interactions observed in compound **II**.

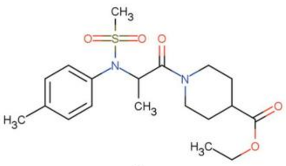

I

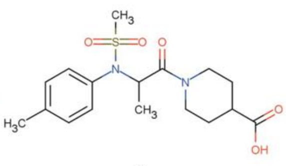

II

## 2. Structural commentary

Both compounds crystallize as colorless plate-like crystals but in different space groups. Compound **I** crystallizes in the

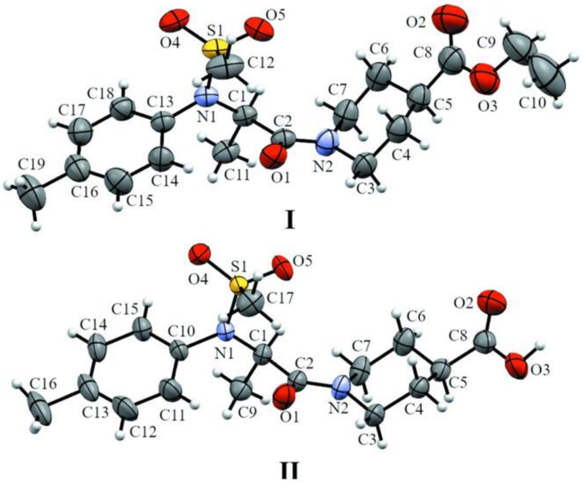

Figure 1
The asymmetric units of compounds **I** and **II**, with displacement ellipsoids drawn at the 50% probability level.

Table 1
Hydrogen-bond geometry (Å, °) for compound **I**.

| $D$—H$\cdots A$ | $D$—H | H$\cdots A$ | $D\cdots A$ | $D$—H$\cdots A$ |
|---|---|---|---|---|
| C12—H12$B\cdots$O1 | 0.96 | 2.50 | 3.210 (2) | 130 |
| C12—H12$C\cdots$O4$^{\rm i}$ | 0.96 | 2.44 | 3.376 (2) | 164 |
| C14—H14$\cdots$O1 | 0.93 | 2.48 | 3.177 (2) | 132 |

Symmetry code: (i) $-x, -y, -z+1$.

Table 2
Hydrogen-bond geometry (Å, °) for compound **II**.

| $D$—H$\cdots A$ | $D$—H | H$\cdots A$ | $D\cdots A$ | $D$—H$\cdots A$ |
|---|---|---|---|---|
| O3—H3$\cdots$O5$^{\rm i}$ | 0.90 (3) | 1.88 (3) | 2.7463 (15) | 161 (2) |
| C17—H17$A\cdots$O1 | 0.96 | 2.48 | 3.144 (2) | 127 |
| C4—H4$B\cdots$O2$^{\rm i}$ | 0.97 | 2.52 | 3.471 (2) | 167 |
| C11—H11$\cdots$O1 | 0.93 | 2.56 | 3.2558 (19) | 132 |

Symmetry code: (i) $-x+2, -y+1, -z+1$.

triclinic $P\overline{1}$ space groups and compound **II** in the monoclinic $P2_1/n$ space group. The asymmetric units are shown in Fig. 1. Both compounds crystallize as a racemic mixture and have one molecule in the asymmetric unit in a similar conformation. The torsion angle N1—C1—C2—N2 is 156.2 (1) and −153.5 (1)° for **I** and **II** respectively. The only slight difference between the two compounds is the geometry of N2. In compound **I**, the distance between N2 and the plane formed by C2, C3 and C7 is 0.114 (2) Å whereas in compound **II** this distance is 0.014 (2) Å. A more planar arrangement of N2 in compound **II** is noticed, probably caused by the crystal packing. Single crystals represent the bulk samples as the powder patterns calculated from SCXRD data are similar to the experimental ones.

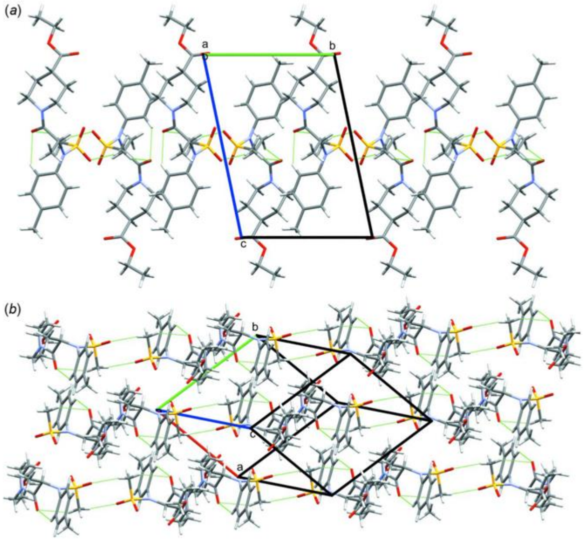

Figure 2
Crystal packing of **I** with hydrogen bonds highlighted in green (*a*) showing one layer of molecules, viewed down the *a* axis and (*b*) showing adjacent layers of molecules.

## 3. Supramolecular features

As compound **I** does not have any strong hydrogen-bond acceptors, only weak hydrogen bonds are observed in the crystal structure (see Table 1). The amide oxygen atom O1 participates in the formation of two intramolecular hydrogen bonds [$S^1_1(7)$ motifs; Etter *et al.*, 1990]. The oxygen atom O4 is inter-connected with atom H12*C* of the sulfonyl methyl of an adjacent molecule [$d$(H$\cdots$O) 2.44 Å; Table 1], forming an $R^2_2(8)$ hydrogen bond motif along the *a*-axis direction (Fig. 2). As compound **I** bears a tolyl moiety, π–π interactions were expected but were not observed in this crystal packing.

Compound **II** bearing a carboxylic moiety instead of an ester has an impact on the hydrogen bonds and thus on the

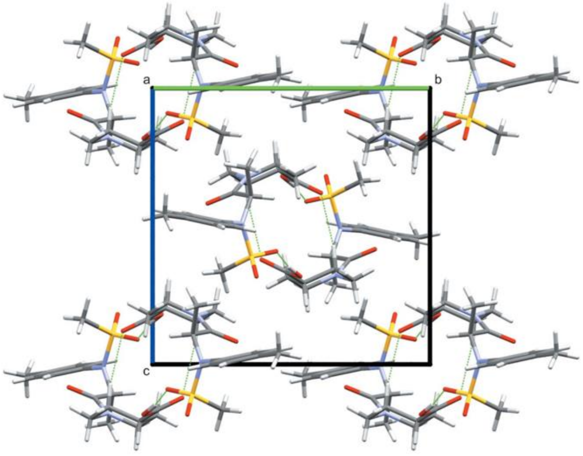

Figure 3
Crystal packing of **II** showing the tubular arrangement viewed down the *a* axis. Hydrogen bonds are highlighted in green.

**Table 3**
Hydrogen-bond propensity calculation for compound **II**.

| Donor | Acceptor | Propensity |
|---|---|---|
| O3 | O2 | 0.36 |
| O3 | O4 | 0.30 |
| O3 | O5 | 0.30 |

crystal packing. In compound **II**, a tubular arrangement (Fig. 3) can be observed, which is different from that of compound **I**. In compound **II**, a hydrogen-bonded ring with an $R_2^2(24)$ motif is formed by a strong hydrogen bond between H3 of the carboxylic acid group and O5 from an adjacent molecule [$d(\text{H}\cdots\text{O})$ 1.88 (3) Å; Table 2]. In addition, two intramolecular [$S_1^1(7)$ motifs] and one intermolecular [$R_2^2(10)$ motif] weak hydrogen bonds are detected. As in compound **I**, no $\pi$–$\pi$ interactions are noticed in the crystal structure. A dimer synthon is observed in the crystal packing in both cases, but for compound **I** it is ensured by weak hydrogen bonds in contrast to compound **II** where the dimer is based on strong hydrogen bonds.

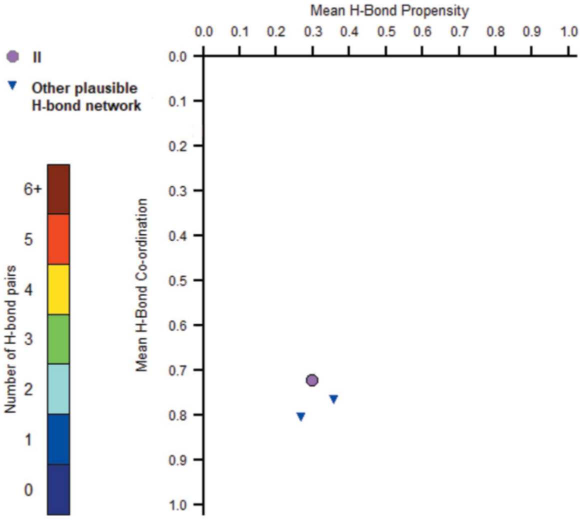

**Figure 4**
Hydrogen-bond propensity chart for compound **II**.

## 4. Database survey

Searches of the Cambridge Structural Database (CSD, version 5.42, update September 2021; Groom *et al.* 2016) were carried out with the exact structures of compounds **I** and **II** and with substructures containing the significant fragments (alanyl-piperidine with and without the sulfonyl methyl and tolyl group). No comparable structures came out of this survey.

A polymorph risk assessment based on the hydrogen bonds in the CSD was carried out. This statistical analysis allows us to estimate which atoms are the donors and the acceptors for hydrogen bonds in the crystal structure (Chemburkar *et al.*, 2000; Galek *et al.*, 2007). This quantifies the probability of hydrogen-bond formation and thus the different probable polymorphs that can arise from a specific compound. The results are summarized in Table 3. A hydrogen-bonding interaction between two carboxylic groups is predicted with the highest probability. We did not observe the carboxylic dimer but rather this group interacting with one oxygen of the sulfonyl methyl. The analysis also predicts other plausible hydrogen-bonded networks (Fig. 4), one that is statistically slightly more likely to be formed than the current one. This suggests that another potential polymorph could be obtained. Thus, we undertook a polymorph screening by several crystallization experiments of compound **II**. The recrystallization solvents that we tested were cyclohexane, toluene, ethyl acetate, chloroform, dichloromethane, acetone, acetonitrile, 2-propanol, ethanol and methanol. They all lead to the same polymorph.

## 5. Synthesis and crystallization

**Compound I:** This was purchased from Evotech (Hamburg, Germany). The product was crystallized by slow evaporation from non-anhydrous ethyl acetate, which provided colorless plate-like crystals suitable for SCXRD. M.p. 442.2 K

**Compound II:** In a round-bottom flask, compound **I** (405.1 mg, 1.02 mmol, 1.0 eq) dissolved in 8 mL of THF was added to a solution of LiOH (81.9 mg, 3.40 mmol, 3.4 eq) dissolved in 5 mL of water. The mixture was stirred at room temperature for 8 h. The resulting mixture was washed with ether. The aqueous phase was then acidified with HCl 37% to a pH of 2 and extracted with dichloromethane. The combined organic phases were dried over anhydrous $Na_2SO_4$ and concentrated under vacuum to yield a white solid (351.0 mg, 93%). The product was crystallized by slow evaporation from methanol, which provided colorless plate-like crystals suitable for SCXRD. $^1$H NMR (DMSO): 12.32 (*s*, 1H, carboxylic acid), 7.39 (*d*, 2H, $\text{CH}_{\text{arom}}$), 7.20 (*d*, 2H, $\text{CH}_{\text{arom}}$), 5.20 (*s*, 1H, $\text{CH}_{\alpha}$), 4.03–3.15 (*m*, 4H, $\text{CH}_{\text{pip}}$), 2.96 (*s*, 3H, $\text{CH}_{\text{SO2Me}}$), 2.79 (*m*, 1H, $\text{CH}_{\text{pip}}$), 2.31 (*s*, 3H, $\text{CH}_{\text{PheMe}}$), 1.83–1.36 (*m*, 4H, $\text{CH}_{\text{pip}}$), 1.03 (*d*, 3H, $\text{CH}_{\alpha\text{Me}}$) $^{13}$C NMR (DMSO): 169.1, 168.7, 138.2, 133.5, 132.0, 129.4, 53.3, 44.5, 41.3, 28.5, 20.7, 16.8. M.p. 496.2 K

## 6. Refinement

Crystal data, data collection and structure refinement details are summarized in Table 4. All H atoms, except one of the -OH group in **II**, were refined using a riding model, with C—H = 0.93 (aromatic), 0.96 (methyl) or 0.98 Å (tertiary carbon). Coordinates of the hydrogen atom of the -OH group were refined. The isotropic atomic displacement parameters of the H atoms were set at $1.5U_{\text{eq}}$ of the parent atom for the methyl and alcohol groups, and at $1.2U_{\text{eq}}$ otherwise.

## Acknowledgements

This work was performed on XRD equipment from the PC2 platform at UNamur and PXRD equipment has been funded

Table 4
Experimental details.

| | I | II |
|---|---|---|
| Crystal data | | |
| Chemical formula | $C_{19}H_{28}N_2O_5S$ | $C_{17}H_{24}N_2O_5S$ |
| $M_r$ | 396.49 | 368.44 |
| Crystal system, space group | Triclinic, $P\bar{1}$ | Monoclinic, $P2_1/n$ |
| Temperature (K) | 295 | 295 |
| $a, b, c$ (Å) | 8.5368 (6), 9.6594 (6), 13.5173 (12) | 12.1013 (2), 12.3092 (2), 12.4348 (3) |
| $\alpha, \beta, \gamma$ (°) | 75.947 (6), 79.302 (6), 74.554 (5) | 90, 100.546 (2), 90 |
| $V$ (Å$^3$) | 1033.47 (14) | 1820.97 (6) |
| $Z$ | 2 | 4 |
| Radiation type | Mo $K\alpha$ | Mo $K\alpha$ |
| $\mu$ (mm$^{-1}$) | 0.19 | 0.21 |
| Crystal size (mm) | 0.79 × 0.18 × 0.05 | 0.77 × 0.18 × 0.11 |
| Data collection | | |
| Diffractometer | Oxford Diffraction Xcalibur, Gemini Ultra R | Oxford Diffraction Xcalibur, Gemini Ultra R |
| Absorption correction | Analytical [*CrysAlis PRO* (Rigaku OD, 2018), based on expressions derived by Clark & Reid (1995)] | Analytical [*CrysAlis PRO* (Rigaku OD, 2018), based on expressions derived by Clark & Reid (1995)] |
| $T_{min}$, $T_{max}$ | 0.923, 0.991 | 0.882, 0.980 |
| No. of measured, independent and observed [$I > 2\sigma(I)$] reflections | 13200, 6870, 4304 | 29518, 6284, 4779 |
| $R_{int}$ | 0.026 | 0.026 |
| $(\sin \theta/\lambda)_{max}$ (Å$^{-1}$) | 0.762 | 0.761 |
| Refinement | | |
| $R[F^2 > 2\sigma(F^2)]$, $wR(F^2)$, $S$ | 0.054, 0.158, 1.02 | 0.043, 0.126, 1.02 |
| No. of reflections | 6870 | 6284 |
| No. of parameters | 248 | 232 |
| H-atom treatment | H-atom parameters constrained | H atoms treated by a mixture of independent and constrained refinement |
| $\Delta\rho_{max}$, $\Delta\rho_{min}$ (e Å$^{-3}$) | 0.34, −0.38 | 0.29, −0.29 |

Computer programs: *CrysAlis PRO* (Rigaku OD, 2018), *SHELXT2014* (Sheldrick, 2015*a*), *SHELXL2016* (Sheldrick, 2015*b*), *Mercury* (Macrae *et al.*, 2020) and *publCIF* (Westrip, 2010).

by FRS–FNRS. The authors thank Laurie Bodard for her help on the polymorph risk assessment.

## References

Chemburkar, S. R., Bauer, J., Deming, K., Spiwek, H., Patel, K., Morris, J., Henry, R., Spanton, S., Dziki, W., Porter, W., Quick, J., Bauer, P., Donaubauer, J., Narayanan, B. A., Soldani, M., Riley, D. & McFarland, K. (2000). *Org. Process Res. Dev.* **4**, 413–417.

Choi, J., Levey, A. I., Weintraub, S. T., Rees, H. D., Gearing, M., Chin, L. S. & Li, L. (2004). *J. Biol. Chem.* **279**, 13256–13264.

Clark, R. C. & Reid, J. S. (1995). *Acta Cryst.* A**51**, 887–897.

Etter, M. C., MacDonald, J. C. & Bernstein, J. (1990). *Acta Cryst.* B**46**, 256–262.

Galek, P. T. A., Fábián, L., Motherwell, W. D. S., Allen, F. H. & Feeder, N. (2007). *Acta Cryst.* B**63**, 768–782.

Groom, C. R., Bruno, I. J., Lightfoot, M. P. & Ward, S. C. (2016). *Acta Cryst.* B**72**, 171–179.

Leroy, E., Boyer, R., Auburger, G., Leube, B., Ulm, G., Mezey, E., Harta, G., Brownstein, M. J., Jonnalagada, S., Chernova, T., Dehejia, A., Lavedan, S., Gasser, T., Steinbach, P. J., Wilkinson, K. D. & Polymeropoulos, M. H. (1998). *Nature*, **395**, 451–452.

Macrae, C. F., Sovago, I., Cottrell, S. J., Galek, P. T. A., McCabe, P., Pidcock, E., Platings, M., Shields, G. P., Stevens, J. S., Towler, M. & Wood, P. A. (2020). *J. Appl. Cryst.* **53**, 226–235.

Maraganore, D. M., Farrer, M. J., Hardy, J. A., Lincoln, S. J., McDonnell, S. K. & Rocca, W. A. (1999). *Neurology*, **53**, 1858–1858.

Mitsui, T., Hirayama, K., Aoki, S., Nishikawa, K., Uchida, K., Matsumoto, T., Kabuta, T. & Wada, K. (2010). *Neurochem. Int.* **56**, 679–686.

Rigaku OD (2018). *CrysAlis PRO*. Rigaku Oxford Diffraction, Yarnton, England.

Sheldrick, G. M. (2015*a*). *Acta Cryst.* A**71**, 3–8.

Sheldrick, G. M. (2015*b*). *Acta Cryst.* C**71**, 3–8.

Westrip, S. P. (2010). *J. Appl. Cryst.* **43**, 920–925.

# APPENDIX H

# supporting information

*Acta Cryst.* (2021). E**77** [https://doi.org/10.1107/S2056989021010392]

## Crystal structures of two alanylpiperidine analogues

**Kalina Mambourg, Nikolay Tumanov, Gilles Henon, Steve Lanners, Javier Garcia-Ladona and Johan Wouters**

### Computing details

For both structures, data collection: *CrysAlis PRO* (Rigaku OD, 2018); cell refinement: *CrysAlis PRO* (Rigaku OD, 2018); data reduction: *CrysAlis PRO* (Rigaku OD, 2018); program(s) used to solve structure: SHELXT2014 (Sheldrick, 2015a); program(s) used to refine structure: *SHELXL2016* (Sheldrick, 2015b); molecular graphics: *Mercury* (Macrae *et al.*, 2020); software used to prepare material for publication: *publCIF* (Westrip, 2010).

### Ethyl 1-[*N*-(4-methylphenyl)-*N*-(methylsulfonyl)alanyl]piperidine-4-carboxylate (I)

*Crystal data*

$C_{19}H_{28}N_2O_5S$
$M_r = 396.49$
Triclinic, $P\overline{1}$
$a = 8.5368\ (6)$ Å
$b = 9.6594\ (6)$ Å
$c = 13.5173\ (12)$ Å
$\alpha = 75.947\ (6)°$
$\beta = 79.302\ (6)°$
$\gamma = 74.554\ (5)°$
$V = 1033.47\ (14)$ Å$^3$
$Z = 2$
$F(000) = 424$
$D_x = 1.274$ Mg m$^{-3}$
Mo $K\alpha$ radiation, $\lambda = 0.71073$ Å
Cell parameters from 3246 reflections
$\theta = 2.4–30.5°$
$\mu = 0.19$ mm$^{-1}$
$T = 295$ K
Plate, colorless
0.79 × 0.18 × 0.05 mm

*Data collection*

Oxford Diffraction Xcalibur, Gemini Ultra R diffractometer
Radiation source: fine-focus sealed X-ray tube
Graphite monochromator
Detector resolution: 10.3712 pixels mm$^{-1}$
$\omega$ scans
Absorption correction: analytical [CrysAlisPro (Rigaku OD, 2018), based on expressions derived by Clark & Reid (1995)]
$T_{min} = 0.923$, $T_{max} = 0.991$
13200 measured reflections
6870 independent reflections
4304 reflections with $I > 2\sigma(I)$
$R_{int} = 0.026$
$\theta_{max} = 32.8°$, $\theta_{min} = 2.2°$
$h = -12 \rightarrow 10$
$k = -13 \rightarrow 14$
$l = -20 \rightarrow 19$

*Refinement*

Refinement on $F^2$
Least-squares matrix: full
$R[F^2 > 2\sigma(F^2)] = 0.054$
$wR(F^2) = 0.158$
$S = 1.02$
6870 reflections
248 parameters
0 restraints
Primary atom site location: dual
Secondary atom site location: dual
Hydrogen site location: mixed
H-atom parameters constrained
$w = 1/[\sigma^2(F_o^2) + (0.0633P)^2 + 0.1206P]$ where $P = (F_o^2 + 2F_c^2)/3$
$(\Delta/\sigma)_{max} < 0.001$
$\Delta\rho_{max} = 0.34$ e Å$^{-3}$
$\Delta\rho_{min} = -0.37$ e Å$^{-3}$

*Special details*

**Geometry**. All esds (except the esd in the dihedral angle between two l.s. planes) are estimated using the full covariance matrix. The cell esds are taken into account individually in the estimation of esds in distances, angles and torsion angles; correlations between esds in cell parameters are only used when they are defined by crystal symmetry. An approximate (isotropic) treatment of cell esds is used for estimating esds involving l.s. planes.

*Fractional atomic coordinates and isotropic or equivalent isotropic displacement parameters (Å²)*

| | *x* | *y* | *z* | $U_{\rm iso}$*/$U_{\rm eq}$ |
|---|---|---|---|---|
| S1 | 0.21006 (5) | 0.11226 (4) | 0.49970 (3) | 0.04597 (14) |
| O1 | 0.20546 (16) | 0.42592 (12) | 0.58010 (10) | 0.0542 (3) |
| O2 | 0.2688 (3) | −0.0438 (2) | 1.00683 (16) | 0.1150 (8) |
| O3 | 0.1551 (3) | 0.16259 (18) | 1.06193 (12) | 0.0894 (5) |
| O4 | 0.21136 (17) | 0.03480 (13) | 0.42186 (11) | 0.0618 (4) |
| O5 | 0.25664 (18) | 0.02943 (13) | 0.59697 (11) | 0.0624 (4) |
| N1 | 0.33461 (16) | 0.22121 (13) | 0.45549 (10) | 0.0404 (3) |
| N2 | 0.3882 (2) | 0.31933 (16) | 0.69243 (11) | 0.0543 (4) |
| C1 | 0.4352 (2) | 0.24222 (16) | 0.52607 (12) | 0.0407 (3) |
| H1 | 0.484975 | 0.145601 | 0.564865 | 0.049* |
| C2 | 0.3309 (2) | 0.33501 (16) | 0.60307 (13) | 0.0435 (4) |
| C3 | 0.2942 (3) | 0.4081 (2) | 0.76676 (14) | 0.0622 (5) |
| H3A | 0.212739 | 0.487753 | 0.733487 | 0.075* |
| H3B | 0.367076 | 0.450568 | 0.791143 | 0.075* |
| C4 | 0.2099 (3) | 0.3155 (2) | 0.85723 (15) | 0.0598 (5) |
| H4A | 0.126979 | 0.283509 | 0.834039 | 0.072* |
| H4B | 0.155721 | 0.374364 | 0.908049 | 0.072* |
| C5 | 0.3330 (3) | 0.1809 (2) | 0.90679 (14) | 0.0595 (5) |
| H5 | 0.409068 | 0.216659 | 0.934903 | 0.071* |
| C6 | 0.4334 (3) | 0.0960 (2) | 0.82547 (15) | 0.0631 (5) |
| H6A | 0.517049 | 0.016237 | 0.856466 | 0.076* |
| H6B | 0.362540 | 0.054116 | 0.798864 | 0.076* |
| C7 | 0.5139 (3) | 0.1963 (2) | 0.73772 (15) | 0.0617 (5) |
| H7A | 0.590425 | 0.233317 | 0.763271 | 0.074* |
| H7B | 0.574515 | 0.141684 | 0.685678 | 0.074* |
| C8 | 0.2494 (3) | 0.0852 (2) | 0.99538 (17) | 0.0714 (6) |
| C9 | 0.0650 (4) | 0.0879 (3) | 1.1529 (2) | 0.1069 (10) |
| H9A | 0.004626 | 0.029494 | 1.132728 | 0.128* |
| H9B | 0.140898 | 0.023064 | 1.198758 | 0.128* |
| C10 | −0.0456 (5) | 0.1958 (4) | 1.2040 (2) | 0.1357 (14) |
| H10A | 0.012297 | 0.263307 | 1.213528 | 0.204* |
| H10B | −0.091589 | 0.148539 | 1.269779 | 0.204* |
| H10C | −0.131975 | 0.248210 | 1.163132 | 0.204* |
| C11 | 0.5719 (2) | 0.31422 (19) | 0.46630 (14) | 0.0503 (4) |
| H11A | 0.636931 | 0.256036 | 0.418334 | 0.075* |
| H11B | 0.639730 | 0.321567 | 0.513158 | 0.075* |
| H11C | 0.525388 | 0.410564 | 0.429625 | 0.075* |
| C12 | 0.0118 (2) | 0.2217 (2) | 0.5200 (2) | 0.0700 (6) |
| H12A | −0.017746 | 0.283965 | 0.455966 | 0.105* |

| | | | | |
|---|---|---|---|---|
| H12B | 0.008836 | 0.280954 | 0.568219 | 0.105* |
| H12C | −0.064229 | 0.159986 | 0.546811 | 0.105* |
| C13 | 0.3206 (2) | 0.31143 (16) | 0.35381 (13) | 0.0431 (4) |
| C14 | 0.2231 (2) | 0.45197 (18) | 0.33966 (14) | 0.0543 (4) |
| H14 | 0.166814 | 0.491483 | 0.396039 | 0.065* |
| C15 | 0.2097 (3) | 0.5336 (2) | 0.24101 (16) | 0.0641 (5) |
| H15 | 0.144679 | 0.628604 | 0.232086 | 0.077* |
| C16 | 0.2899 (3) | 0.4784 (2) | 0.15543 (15) | 0.0617 (5) |
| C17 | 0.3898 (3) | 0.3385 (2) | 0.17173 (16) | 0.0675 (6) |
| H17 | 0.447572 | 0.299605 | 0.115395 | 0.081* |
| C18 | 0.4060 (3) | 0.25519 (19) | 0.26953 (14) | 0.0569 (5) |
| H18 | 0.474265 | 0.161520 | 0.278607 | 0.068* |
| C19 | 0.2674 (4) | 0.5688 (3) | 0.04839 (17) | 0.0908 (8) |
| H19A | 0.162225 | 0.569619 | 0.032294 | 0.136* |
| H19B | 0.351973 | 0.526722 | −0.000565 | 0.136* |
| H19C | 0.273737 | 0.667492 | 0.045582 | 0.136* |

*Atomic displacement parameters (Å$^2$)*

| | $U^{11}$ | $U^{22}$ | $U^{33}$ | $U^{12}$ | $U^{13}$ | $U^{23}$ |
|---|---|---|---|---|---|---|
| S1 | 0.0381 (2) | 0.0362 (2) | 0.0636 (3) | −0.00995 (16) | −0.00197 (19) | −0.01207 (17) |
| O1 | 0.0444 (7) | 0.0491 (6) | 0.0645 (8) | 0.0048 (5) | −0.0079 (6) | −0.0194 (5) |
| O2 | 0.157 (2) | 0.0689 (11) | 0.1072 (15) | −0.0226 (12) | 0.0015 (14) | −0.0131 (10) |
| O3 | 0.1050 (15) | 0.0800 (10) | 0.0695 (10) | −0.0174 (10) | 0.0144 (9) | −0.0133 (8) |
| O4 | 0.0598 (9) | 0.0532 (7) | 0.0829 (9) | −0.0212 (6) | −0.0043 (7) | −0.0280 (6) |
| O5 | 0.0629 (9) | 0.0520 (7) | 0.0669 (8) | −0.0211 (6) | −0.0053 (7) | 0.0039 (6) |
| N1 | 0.0352 (7) | 0.0367 (6) | 0.0492 (7) | −0.0082 (5) | −0.0054 (6) | −0.0089 (5) |
| N2 | 0.0541 (10) | 0.0534 (8) | 0.0517 (8) | 0.0017 (7) | −0.0076 (7) | −0.0191 (6) |
| C1 | 0.0333 (8) | 0.0376 (7) | 0.0507 (9) | −0.0047 (6) | −0.0051 (7) | −0.0119 (6) |
| C2 | 0.0389 (9) | 0.0382 (7) | 0.0527 (9) | −0.0075 (6) | −0.0036 (7) | −0.0114 (6) |
| C3 | 0.0761 (15) | 0.0538 (10) | 0.0557 (11) | −0.0053 (10) | −0.0049 (10) | −0.0226 (8) |
| C4 | 0.0598 (13) | 0.0600 (11) | 0.0568 (11) | −0.0007 (9) | −0.0072 (9) | −0.0214 (9) |
| C5 | 0.0600 (13) | 0.0647 (11) | 0.0542 (11) | −0.0060 (9) | −0.0145 (9) | −0.0170 (8) |
| C6 | 0.0635 (14) | 0.0587 (10) | 0.0620 (12) | 0.0094 (9) | −0.0241 (10) | −0.0167 (9) |
| C7 | 0.0490 (12) | 0.0749 (12) | 0.0598 (11) | 0.0038 (9) | −0.0152 (9) | −0.0247 (9) |
| C8 | 0.0784 (17) | 0.0663 (13) | 0.0668 (13) | −0.0071 (11) | −0.0187 (12) | −0.0122 (10) |
| C9 | 0.114 (3) | 0.0948 (18) | 0.0859 (19) | −0.0194 (18) | 0.0136 (18) | 0.0053 (15) |
| C10 | 0.125 (3) | 0.143 (3) | 0.092 (2) | −0.013 (2) | 0.033 (2) | 0.009 (2) |
| C11 | 0.0363 (9) | 0.0539 (9) | 0.0644 (11) | −0.0139 (7) | −0.0001 (8) | −0.0200 (8) |
| C12 | 0.0332 (10) | 0.0571 (11) | 0.1202 (19) | −0.0110 (8) | 0.0035 (11) | −0.0288 (11) |
| C13 | 0.0396 (9) | 0.0410 (8) | 0.0493 (9) | −0.0094 (7) | −0.0059 (7) | −0.0105 (6) |
| C14 | 0.0528 (11) | 0.0484 (9) | 0.0554 (10) | 0.0016 (8) | −0.0105 (9) | −0.0109 (8) |
| C15 | 0.0567 (13) | 0.0568 (11) | 0.0695 (13) | 0.0007 (9) | −0.0188 (10) | −0.0030 (9) |
| C16 | 0.0607 (13) | 0.0713 (12) | 0.0540 (11) | −0.0235 (10) | −0.0112 (10) | −0.0024 (9) |
| C17 | 0.0791 (16) | 0.0693 (12) | 0.0534 (11) | −0.0223 (11) | 0.0062 (10) | −0.0168 (9) |
| C18 | 0.0627 (13) | 0.0471 (9) | 0.0573 (11) | −0.0109 (8) | 0.0035 (9) | −0.0143 (8) |
| C19 | 0.092 (2) | 0.1060 (19) | 0.0624 (14) | −0.0224 (16) | −0.0167 (14) | 0.0085 (13) |

*Geometric parameters (Å, º)*

| | | | |
|---|---|---|---|
| S1—O5 | 1.4285 (14) | C7—H7A | 0.9700 |
| S1—O4 | 1.4286 (13) | C7—H7B | 0.9700 |
| S1—N1 | 1.6278 (13) | C9—C10 | 1.428 (4) |
| S1—C12 | 1.7526 (19) | C9—H9A | 0.9700 |
| O1—C2 | 1.227 (2) | C9—H9B | 0.9700 |
| O2—C8 | 1.188 (3) | C10—H10A | 0.9600 |
| O3—C8 | 1.324 (3) | C10—H10B | 0.9600 |
| O3—C9 | 1.462 (3) | C10—H10C | 0.9600 |
| N1—C13 | 1.445 (2) | C11—H11A | 0.9600 |
| N1—C1 | 1.476 (2) | C11—H11B | 0.9600 |
| N2—C2 | 1.346 (2) | C11—H11C | 0.9600 |
| N2—C3 | 1.464 (2) | C12—H12A | 0.9600 |
| N2—C7 | 1.466 (2) | C12—H12B | 0.9600 |
| C1—C11 | 1.519 (2) | C12—H12C | 0.9600 |
| C1—C2 | 1.537 (2) | C13—C14 | 1.380 (2) |
| C1—H1 | 0.9800 | C13—C18 | 1.381 (2) |
| C3—C4 | 1.516 (3) | C14—C15 | 1.382 (3) |
| C3—H3A | 0.9700 | C14—H14 | 0.9300 |
| C3—H3B | 0.9700 | C15—C16 | 1.379 (3) |
| C4—C5 | 1.535 (3) | C15—H15 | 0.9300 |
| C4—H4A | 0.9700 | C16—C17 | 1.384 (3) |
| C4—H4B | 0.9700 | C16—C19 | 1.514 (3) |
| C5—C8 | 1.514 (3) | C17—C18 | 1.381 (3) |
| C5—C6 | 1.526 (3) | C17—H17 | 0.9300 |
| C5—H5 | 0.9800 | C18—H18 | 0.9300 |
| C6—C7 | 1.521 (3) | C19—H19A | 0.9600 |
| C6—H6A | 0.9700 | C19—H19B | 0.9600 |
| C6—H6B | 0.9700 | C19—H19C | 0.9600 |
| | | | |
| O5—S1—O4 | 118.43 (8) | O2—C8—O3 | 123.4 (2) |
| O5—S1—N1 | 106.30 (8) | O2—C8—C5 | 125.1 (2) |
| O4—S1—N1 | 108.16 (8) | O3—C8—C5 | 111.50 (18) |
| O5—S1—C12 | 108.50 (11) | C10—C9—O3 | 108.7 (2) |
| O4—S1—C12 | 107.33 (10) | C10—C9—H9A | 110.0 |
| N1—S1—C12 | 107.71 (8) | O3—C9—H9A | 110.0 |
| C8—O3—C9 | 119.1 (2) | C10—C9—H9B | 110.0 |
| C13—N1—C1 | 122.65 (12) | O3—C9—H9B | 110.0 |
| C13—N1—S1 | 117.57 (11) | H9A—C9—H9B | 108.3 |
| C1—N1—S1 | 118.92 (10) | C9—C10—H10A | 109.5 |
| C2—N2—C3 | 119.21 (16) | C9—C10—H10B | 109.5 |
| C2—N2—C7 | 126.42 (15) | H10A—C10—H10B | 109.5 |
| C3—N2—C7 | 112.45 (15) | C9—C10—H10C | 109.5 |
| N1—C1—C11 | 110.73 (13) | H10A—C10—H10C | 109.5 |
| N1—C1—C2 | 111.57 (13) | H10B—C10—H10C | 109.5 |
| C11—C1—C2 | 109.61 (12) | C1—C11—H11A | 109.5 |
| N1—C1—H1 | 108.3 | C1—C11—H11B | 109.5 |

| | | | |
|---|---|---|---|
| C11—C1—H1 | 108.3 | H11A—C11—H11B | 109.5 |
| C2—C1—H1 | 108.3 | C1—C11—H11C | 109.5 |
| O1—C2—N2 | 121.94 (15) | H11A—C11—H11C | 109.5 |
| O1—C2—C1 | 120.33 (15) | H11B—C11—H11C | 109.5 |
| N2—C2—C1 | 117.58 (15) | S1—C12—H12A | 109.5 |
| N2—C3—C4 | 110.73 (15) | S1—C12—H12B | 109.5 |
| N2—C3—H3A | 109.5 | H12A—C12—H12B | 109.5 |
| C4—C3—H3A | 109.5 | S1—C12—H12C | 109.5 |
| N2—C3—H3B | 109.5 | H12A—C12—H12C | 109.5 |
| C4—C3—H3B | 109.5 | H12B—C12—H12C | 109.5 |
| H3A—C3—H3B | 108.1 | C14—C13—C18 | 119.67 (16) |
| C3—C4—C5 | 111.24 (18) | C14—C13—N1 | 121.20 (15) |
| C3—C4—H4A | 109.4 | C18—C13—N1 | 119.13 (14) |
| C5—C4—H4A | 109.4 | C13—C14—C15 | 119.47 (17) |
| C3—C4—H4B | 109.4 | C13—C14—H14 | 120.3 |
| C5—C4—H4B | 109.4 | C15—C14—H14 | 120.3 |
| H4A—C4—H4B | 108.0 | C16—C15—C14 | 122.01 (18) |
| C8—C5—C6 | 112.44 (17) | C16—C15—H15 | 119.0 |
| C8—C5—C4 | 111.67 (19) | C14—C15—H15 | 119.0 |
| C6—C5—C4 | 110.22 (16) | C15—C16—C17 | 117.39 (18) |
| C8—C5—H5 | 107.4 | C15—C16—C19 | 120.6 (2) |
| C6—C5—H5 | 107.4 | C17—C16—C19 | 122.0 (2) |
| C4—C5—H5 | 107.4 | C18—C17—C16 | 121.65 (19) |
| C7—C6—C5 | 110.66 (16) | C18—C17—H17 | 119.2 |
| C7—C6—H6A | 109.5 | C16—C17—H17 | 119.2 |
| C5—C6—H6A | 109.5 | C13—C18—C17 | 119.76 (17) |
| C7—C6—H6B | 109.5 | C13—C18—H18 | 120.1 |
| C5—C6—H6B | 109.5 | C17—C18—H18 | 120.1 |
| H6A—C6—H6B | 108.1 | C16—C19—H19A | 109.5 |
| N2—C7—C6 | 109.70 (17) | C16—C19—H19B | 109.5 |
| N2—C7—H7A | 109.7 | H19A—C19—H19B | 109.5 |
| C6—C7—H7A | 109.7 | C16—C19—H19C | 109.5 |
| N2—C7—H7B | 109.7 | H19A—C19—H19C | 109.5 |
| C6—C7—H7B | 109.7 | H19B—C19—H19C | 109.5 |
| H7A—C7—H7B | 108.2 | | |

| | | | |
|---|---|---|---|
| O5—S1—N1—C13 | 176.09 (11) | C2—N2—C7—C6 | −103.4 (2) |
| O4—S1—N1—C13 | 47.92 (13) | C3—N2—C7—C6 | 60.5 (2) |
| C12—S1—N1—C13 | −67.78 (14) | C5—C6—C7—N2 | −57.7 (2) |
| O5—S1—N1—C1 | −14.24 (14) | C9—O3—C8—O2 | −2.2 (4) |
| O4—S1—N1—C1 | −142.40 (12) | C9—O3—C8—C5 | −179.8 (2) |
| C12—S1—N1—C1 | 101.89 (14) | C6—C5—C8—O2 | 6.3 (4) |
| C13—N1—C1—C11 | −25.36 (19) | C4—C5—C8—O2 | 130.8 (3) |
| S1—N1—C1—C11 | 165.51 (11) | C6—C5—C8—O3 | −176.2 (2) |
| C13—N1—C1—C2 | 97.02 (16) | C4—C5—C8—O3 | −51.7 (3) |
| S1—N1—C1—C2 | −72.11 (15) | C8—O3—C9—C10 | −171.3 (3) |
| C3—N2—C2—O1 | 3.0 (3) | C1—N1—C13—C14 | −76.6 (2) |
| C7—N2—C2—O1 | 165.98 (18) | S1—N1—C13—C14 | 92.68 (17) |

| | | | |
|---|---|---|---|
| C3—N2—C2—C1 | 178.66 (15) | C1—N1—C13—C18 | 103.66 (19) |
| C7—N2—C2—C1 | −18.4 (3) | S1—N1—C13—C18 | −87.07 (18) |
| N1—C1—C2—O1 | −28.1 (2) | C18—C13—C14—C15 | 1.3 (3) |
| C11—C1—C2—O1 | 94.89 (19) | N1—C13—C14—C15 | −178.45 (17) |
| N1—C1—C2—N2 | 156.17 (14) | C13—C14—C15—C16 | 0.7 (3) |
| C11—C1—C2—N2 | −80.81 (18) | C14—C15—C16—C17 | −2.1 (3) |
| C2—N2—C3—C4 | 106.1 (2) | C14—C15—C16—C19 | 177.7 (2) |
| C7—N2—C3—C4 | −59.1 (2) | C15—C16—C17—C18 | 1.7 (3) |
| N2—C3—C4—C5 | 54.5 (2) | C19—C16—C17—C18 | −178.1 (2) |
| C3—C4—C5—C8 | −178.38 (17) | C14—C13—C18—C17 | −1.7 (3) |
| C3—C4—C5—C6 | −52.6 (2) | N1—C13—C18—C17 | 178.02 (17) |
| C8—C5—C6—C7 | 179.54 (18) | C16—C17—C18—C13 | 0.2 (3) |
| C4—C5—C6—C7 | 54.2 (2) | | |

*Hydrogen-bond geometry (Å, º)*

| *D*—H···*A* | *D*—H | H···*A* | *D*···*A* | *D*—H···*A* |
|---|---|---|---|---|
| C12—H12*B*···O1 | 0.96 | 2.50 | 3.210 (2) | 130 |
| C12—H12*C*···O4$^{i}$ | 0.96 | 2.44 | 3.376 (2) | 164 |
| C14—H14···O1 | 0.93 | 2.48 | 3.177 (2) | 132 |

Symmetry code: (i) −*x*, −*y*, −*z*+1.

## 1-[*N*-(4-methylphenyl)-*N*-(methylsulfonyl)alanyl]piperidine-4-carboxylic acid (II)

### *Crystal data*

$C_{17}H_{24}N_2O_5S$
$M_r = 368.44$
Monoclinic, $P2_1/n$
$a = 12.1013$ (2) Å
$b = 12.3092$ (2) Å
$c = 12.4348$ (3) Å
$\beta = 100.546$ (2)°
$V = 1820.97$ (6) Å$^3$
$Z = 4$

$F(000) = 784$
$D_x = 1.344$ Mg m$^{-3}$
Mo *Kα* radiation, $\lambda = 0.71073$ Å
Cell parameters from 8359 reflections
$\theta = 2.7–31.5°$
$\mu = 0.21$ mm$^{-1}$
$T = 295$ K
Plate, colorless
0.77 × 0.18 × 0.11 mm

### *Data collection*

Oxford Diffraction Xcalibur, Gemini Ultra R diffractometer
Radiation source: fine-focus sealed X-ray tube
Graphite monochromator
Detector resolution: 10.3712 pixels mm$^{-1}$
*ω* scans
Absorption correction: analytical [CrysAlisPro (Rigaku OD, 2018), based on expressions derived by Clark & Reid (1995)]

$T_{min} = 0.882$, $T_{max} = 0.980$
29518 measured reflections
6284 independent reflections
4779 reflections with $I > 2\sigma(I)$
$R_{int} = 0.026$
$\theta_{max} = 32.7°$, $\theta_{min} = 2.2°$
$h = -18 \rightarrow 18$
$k = -18 \rightarrow 17$
$l = -17 \rightarrow 18$

### *Refinement*

Refinement on $F^2$
Least-squares matrix: full
$R[F^2 > 2\sigma(F^2)] = 0.043$
$wR(F^2) = 0.126$
$S = 1.02$

6284 reflections
232 parameters
0 restraints
Primary atom site location: dual
Secondary atom site location: dual

Hydrogen site location: difference Fourier map
H atoms treated by a mixture of independent and constrained refinement

$w = 1/[\sigma^2(F_o^2) + (0.0593P)^2 + 0.3685P]$
where $P = (F_o^2 + 2F_c^2)/3$
$(\Delta/\sigma)_{max} = 0.001$
$\Delta\rho_{max} = 0.29$ e Å$^{-3}$
$\Delta\rho_{min} = -0.29$ e Å$^{-3}$

*Special details*

**Geometry**. All esds (except the esd in the dihedral angle between two l.s. planes) are estimated using the full covariance matrix. The cell esds are taken into account individually in the estimation of esds in distances, angles and torsion angles; correlations between esds in cell parameters are only used when they are defined by crystal symmetry. An approximate (isotropic) treatment of cell esds is used for estimating esds involving l.s. planes.

*Fractional atomic coordinates and isotropic or equivalent isotropic displacement parameters (Å²)*

| | *x* | *y* | *z* | $U_{iso}$*/$U_{eq}$ |
|---|---|---|---|---|
| S1 | 0.58667 (2) | 0.35673 (2) | 0.60942 (2) | 0.03513 (9) |
| O1 | 0.68078 (9) | 0.19851 (8) | 0.41698 (10) | 0.0531 (3) |
| O2 | 1.04956 (12) | 0.60661 (11) | 0.37887 (13) | 0.0780 (4) |
| O3 | 1.13713 (10) | 0.46783 (11) | 0.31848 (13) | 0.0732 (4) |
| H3 | 1.195 (2) | 0.509 (2) | 0.352 (2) | 0.110* |
| O4 | 0.50845 (8) | 0.37442 (9) | 0.68112 (8) | 0.0479 (2) |
| O5 | 0.65804 (8) | 0.44541 (8) | 0.59029 (9) | 0.0501 (2) |
| N1 | 0.51748 (8) | 0.32221 (9) | 0.48974 (8) | 0.0344 (2) |
| N2 | 0.73982 (9) | 0.33804 (10) | 0.32395 (10) | 0.0447 (3) |
| C1 | 0.56084 (10) | 0.35539 (10) | 0.39054 (10) | 0.0359 (2) |
| H1 | 0.580679 | 0.432597 | 0.397240 | 0.043* |
| C17 | 0.67424 (14) | 0.24889 (13) | 0.66359 (13) | 0.0555 (4) |
| H17A | 0.726630 | 0.233560 | 0.616194 | 0.083* |
| H17B | 0.629402 | 0.185582 | 0.669483 | 0.083* |
| H17C | 0.714621 | 0.268508 | 0.734742 | 0.083* |
| C2 | 0.66661 (10) | 0.29079 (11) | 0.37903 (10) | 0.0392 (3) |
| C3 | 0.83897 (11) | 0.27729 (13) | 0.30503 (13) | 0.0488 (3) |
| H3A | 0.832698 | 0.263103 | 0.227419 | 0.059* |
| H3B | 0.842307 | 0.208002 | 0.342640 | 0.059* |
| C4 | 0.94599 (11) | 0.34095 (12) | 0.34608 (11) | 0.0427 (3) |
| H4A | 1.009763 | 0.302094 | 0.327725 | 0.051* |
| H4B | 0.957054 | 0.347251 | 0.425085 | 0.051* |
| C5 | 0.94003 (11) | 0.45455 (12) | 0.29524 (11) | 0.0438 (3) |
| H5 | 0.933185 | 0.446018 | 0.215935 | 0.053* |
| C6 | 0.83536 (12) | 0.51356 (12) | 0.31663 (13) | 0.0510 (3) |
| H6A | 0.841595 | 0.526101 | 0.394520 | 0.061* |
| H6B | 0.829392 | 0.583548 | 0.280182 | 0.061* |
| C7 | 0.73079 (12) | 0.44690 (14) | 0.27497 (12) | 0.0510 (4) |
| H7A | 0.665534 | 0.483641 | 0.292748 | 0.061* |
| H7B | 0.720557 | 0.440587 | 0.196007 | 0.061* |
| C8 | 1.04549 (13) | 0.51874 (13) | 0.33621 (12) | 0.0489 (3) |
| C9 | 0.47176 (12) | 0.34023 (14) | 0.28791 (12) | 0.0489 (3) |
| H9A | 0.458064 | 0.264097 | 0.275037 | 0.073* |
| H9B | 0.497692 | 0.371751 | 0.226417 | 0.073* |

| | | | | |
|---|---|---|---|---|
| H9C | 0.403409 | 0.375286 | 0.297628 | 0.073* |
| C10 | 0.42232 (10) | 0.25039 (10) | 0.48451 (10) | 0.0364 (2) |
| C11 | 0.43049 (14) | 0.14088 (12) | 0.46161 (15) | 0.0541 (4) |
| H11 | 0.498708 | 0.111490 | 0.451688 | 0.065* |
| C12 | 0.33581 (16) | 0.07526 (14) | 0.45357 (15) | 0.0641 (4) |
| H12 | 0.341460 | 0.001934 | 0.437384 | 0.077* |
| C13 | 0.23387 (13) | 0.11605 (14) | 0.46894 (12) | 0.0553 (4) |
| C14 | 0.22767 (12) | 0.22528 (14) | 0.49295 (13) | 0.0519 (4) |
| H14 | 0.159834 | 0.254119 | 0.504670 | 0.062* |
| C15 | 0.32057 (10) | 0.29283 (12) | 0.49995 (11) | 0.0423 (3) |
| H15 | 0.314406 | 0.366372 | 0.514958 | 0.051* |
| C16 | 0.13157 (17) | 0.0435 (2) | 0.45871 (17) | 0.0843 (7) |
| H16A | 0.085792 | 0.066468 | 0.509939 | 0.126* |
| H16B | 0.155060 | −0.030246 | 0.473939 | 0.126* |
| H16C | 0.088916 | 0.048332 | 0.385744 | 0.126* |

*Atomic displacement parameters (Å$^2$)*

| | $U^{11}$ | $U^{22}$ | $U^{33}$ | $U^{12}$ | $U^{13}$ | $U^{23}$ |
|---|---|---|---|---|---|---|
| S1 | 0.03062 (14) | 0.03481 (15) | 0.03976 (16) | −0.00400 (11) | 0.00588 (11) | −0.00067 (11) |
| O1 | 0.0514 (6) | 0.0410 (5) | 0.0722 (7) | 0.0074 (4) | 0.0248 (5) | 0.0058 (5) |
| O2 | 0.0771 (9) | 0.0640 (8) | 0.0943 (10) | −0.0098 (7) | 0.0193 (7) | −0.0239 (7) |
| O3 | 0.0402 (6) | 0.0697 (8) | 0.1097 (11) | −0.0137 (5) | 0.0139 (6) | −0.0303 (7) |
| O4 | 0.0448 (5) | 0.0571 (6) | 0.0436 (5) | −0.0033 (4) | 0.0129 (4) | −0.0075 (4) |
| O5 | 0.0436 (5) | 0.0481 (5) | 0.0563 (6) | −0.0190 (4) | 0.0033 (4) | 0.0010 (4) |
| N1 | 0.0293 (4) | 0.0375 (5) | 0.0373 (5) | −0.0058 (4) | 0.0082 (4) | −0.0016 (4) |
| N2 | 0.0353 (5) | 0.0490 (6) | 0.0530 (6) | 0.0044 (5) | 0.0171 (5) | 0.0037 (5) |
| C1 | 0.0321 (5) | 0.0382 (6) | 0.0387 (6) | −0.0001 (5) | 0.0102 (4) | 0.0020 (5) |
| C17 | 0.0548 (8) | 0.0583 (9) | 0.0515 (8) | 0.0155 (7) | 0.0051 (7) | 0.0093 (7) |
| C2 | 0.0345 (6) | 0.0428 (6) | 0.0414 (6) | 0.0005 (5) | 0.0103 (5) | −0.0025 (5) |
| C3 | 0.0366 (6) | 0.0525 (8) | 0.0609 (9) | 0.0005 (6) | 0.0184 (6) | −0.0099 (7) |
| C4 | 0.0360 (6) | 0.0486 (7) | 0.0450 (7) | 0.0029 (5) | 0.0114 (5) | −0.0049 (5) |
| C5 | 0.0388 (6) | 0.0551 (8) | 0.0387 (6) | −0.0029 (6) | 0.0107 (5) | 0.0008 (6) |
| C6 | 0.0493 (8) | 0.0481 (8) | 0.0591 (8) | 0.0065 (6) | 0.0190 (7) | 0.0149 (6) |
| C7 | 0.0397 (7) | 0.0658 (9) | 0.0499 (8) | 0.0079 (6) | 0.0147 (6) | 0.0195 (7) |
| C8 | 0.0490 (8) | 0.0517 (8) | 0.0469 (7) | −0.0062 (6) | 0.0107 (6) | −0.0010 (6) |
| C9 | 0.0407 (7) | 0.0635 (9) | 0.0411 (7) | 0.0017 (6) | 0.0039 (5) | 0.0014 (6) |
| C10 | 0.0327 (5) | 0.0359 (6) | 0.0404 (6) | −0.0076 (5) | 0.0059 (5) | 0.0002 (5) |
| C11 | 0.0499 (8) | 0.0397 (7) | 0.0735 (10) | −0.0066 (6) | 0.0131 (7) | −0.0083 (7) |
| C12 | 0.0713 (11) | 0.0434 (8) | 0.0759 (11) | −0.0228 (8) | 0.0088 (9) | −0.0078 (7) |
| C13 | 0.0513 (8) | 0.0660 (9) | 0.0443 (7) | −0.0296 (7) | −0.0026 (6) | 0.0081 (7) |
| C14 | 0.0316 (6) | 0.0692 (10) | 0.0534 (8) | −0.0112 (6) | 0.0038 (5) | 0.0085 (7) |
| C15 | 0.0320 (6) | 0.0447 (7) | 0.0500 (7) | −0.0045 (5) | 0.0066 (5) | 0.0028 (5) |
| C16 | 0.0732 (12) | 0.1026 (16) | 0.0695 (11) | −0.0573 (12) | −0.0065 (9) | 0.0100 (11) |

*Geometric parameters (Å, º)*

| | | | |
|---|---|---|---|
| S1—O4 | 1.4309 (10) | C5—C8 | 1.508 (2) |
| S1—O5 | 1.4385 (10) | C5—C6 | 1.5252 (19) |
| S1—N1 | 1.6249 (10) | C5—H5 | 0.9800 |
| S1—C17 | 1.7543 (15) | C6—C7 | 1.517 (2) |
| O1—C2 | 1.2300 (16) | C6—H6A | 0.9700 |
| O2—C8 | 1.2018 (19) | C6—H6B | 0.9700 |
| O3—C8 | 1.3269 (19) | C7—H7A | 0.9700 |
| O3—H3 | 0.90 (3) | C7—H7B | 0.9700 |
| N1—C10 | 1.4438 (15) | C9—H9A | 0.9600 |
| N1—C1 | 1.4834 (15) | C9—H9B | 0.9600 |
| N2—C2 | 1.3470 (17) | C9—H9C | 0.9600 |
| N2—C7 | 1.4677 (19) | C10—C15 | 1.3829 (18) |
| N2—C3 | 1.4688 (17) | C10—C11 | 1.3850 (19) |
| C1—C9 | 1.5238 (18) | C11—C12 | 1.390 (2) |
| C1—C2 | 1.5356 (17) | C11—H11 | 0.9300 |
| C1—H1 | 0.9800 | C12—C13 | 1.377 (3) |
| C17—H17A | 0.9600 | C12—H12 | 0.9300 |
| C17—H17B | 0.9600 | C13—C14 | 1.382 (2) |
| C17—H17C | 0.9600 | C13—C16 | 1.513 (2) |
| C3—C4 | 1.5198 (19) | C14—C15 | 1.3882 (18) |
| C3—H3A | 0.9700 | C14—H14 | 0.9300 |
| C3—H3B | 0.9700 | C15—H15 | 0.9300 |
| C4—C5 | 1.531 (2) | C16—H16A | 0.9600 |
| C4—H4A | 0.9700 | C16—H16B | 0.9600 |
| C4—H4B | 0.9700 | C16—H16C | 0.9600 |
| | | | |
| O4—S1—O5 | 118.24 (6) | C7—C6—C5 | 110.50 (13) |
| O4—S1—N1 | 108.76 (6) | C7—C6—H6A | 109.5 |
| O5—S1—N1 | 105.74 (6) | C5—C6—H6A | 109.5 |
| O4—S1—C17 | 107.33 (7) | C7—C6—H6B | 109.5 |
| O5—S1—C17 | 107.40 (7) | C5—C6—H6B | 109.5 |
| N1—S1—C17 | 109.13 (7) | H6A—C6—H6B | 108.1 |
| C8—O3—H3 | 105.0 (16) | N2—C7—C6 | 110.97 (12) |
| C10—N1—C1 | 122.13 (10) | N2—C7—H7A | 109.4 |
| C10—N1—S1 | 118.32 (8) | C6—C7—H7A | 109.4 |
| C1—N1—S1 | 119.22 (8) | N2—C7—H7B | 109.4 |
| C2—N2—C7 | 126.82 (11) | C6—C7—H7B | 109.4 |
| C2—N2—C3 | 119.62 (12) | H7A—C7—H7B | 108.0 |
| C7—N2—C3 | 113.53 (11) | O2—C8—O3 | 122.04 (15) |
| N1—C1—C9 | 111.04 (10) | O2—C8—C5 | 125.76 (15) |
| N1—C1—C2 | 111.26 (10) | O3—C8—C5 | 112.20 (13) |
| C9—C1—C2 | 109.42 (11) | C1—C9—H9A | 109.5 |
| N1—C1—H1 | 108.3 | C1—C9—H9B | 109.5 |
| C9—C1—H1 | 108.3 | H9A—C9—H9B | 109.5 |
| C2—C1—H1 | 108.3 | C1—C9—H9C | 109.5 |
| S1—C17—H17A | 109.5 | H9A—C9—H9C | 109.5 |

| | | | |
|---|---|---|---|
| S1—C17—H17B | 109.5 | H9B—C9—H9C | 109.5 |
| H17A—C17—H17B | 109.5 | C15—C10—C11 | 119.68 (12) |
| S1—C17—H17C | 109.5 | C15—C10—N1 | 119.04 (11) |
| H17A—C17—H17C | 109.5 | C11—C10—N1 | 121.26 (12) |
| H17B—C17—H17C | 109.5 | C10—C11—C12 | 119.43 (15) |
| O1—C2—N2 | 122.37 (12) | C10—C11—H11 | 120.3 |
| O1—C2—C1 | 120.17 (11) | C12—C11—H11 | 120.3 |
| N2—C2—C1 | 117.44 (11) | C13—C12—C11 | 121.70 (16) |
| N2—C3—C4 | 110.77 (12) | C13—C12—H12 | 119.1 |
| N2—C3—H3A | 109.5 | C11—C12—H12 | 119.1 |
| C4—C3—H3A | 109.5 | C12—C13—C14 | 118.04 (13) |
| N2—C3—H3B | 109.5 | C12—C13—C16 | 120.88 (18) |
| C4—C3—H3B | 109.5 | C14—C13—C16 | 121.08 (18) |
| H3A—C3—H3B | 108.1 | C13—C14—C15 | 121.38 (15) |
| C3—C4—C5 | 111.06 (12) | C13—C14—H14 | 119.3 |
| C3—C4—H4A | 109.4 | C15—C14—H14 | 119.3 |
| C5—C4—H4A | 109.4 | C10—C15—C14 | 119.76 (14) |
| C3—C4—H4B | 109.4 | C10—C15—H15 | 120.1 |
| C5—C4—H4B | 109.4 | C14—C15—H15 | 120.1 |
| H4A—C4—H4B | 108.0 | C13—C16—H16A | 109.5 |
| C8—C5—C6 | 111.72 (13) | C13—C16—H16B | 109.5 |
| C8—C5—C4 | 111.47 (12) | H16A—C16—H16B | 109.5 |
| C6—C5—C4 | 109.92 (11) | C13—C16—H16C | 109.5 |
| C8—C5—H5 | 107.9 | H16A—C16—H16C | 109.5 |
| C6—C5—H5 | 107.9 | H16B—C16—H16C | 109.5 |
| C4—C5—H5 | 107.9 | | |

| | | | |
|---|---|---|---|
| O4—S1—N1—C10 | −39.35 (11) | C8—C5—C6—C7 | −179.78 (12) |
| O5—S1—N1—C10 | −167.31 (9) | C4—C5—C6—C7 | −55.49 (15) |
| C17—S1—N1—C10 | 77.45 (11) | C2—N2—C7—C6 | 125.15 (15) |
| O4—S1—N1—C1 | 147.15 (9) | C3—N2—C7—C6 | −56.90 (16) |
| O5—S1—N1—C1 | 19.20 (11) | C5—C6—C7—N2 | 56.02 (16) |
| C17—S1—N1—C1 | −96.05 (11) | C6—C5—C8—O2 | −1.4 (2) |
| C10—N1—C1—C9 | 20.64 (16) | C4—C5—C8—O2 | −124.79 (17) |
| S1—N1—C1—C9 | −166.13 (9) | C6—C5—C8—O3 | 179.68 (13) |
| C10—N1—C1—C2 | −101.50 (13) | C4—C5—C8—O3 | 56.26 (17) |
| S1—N1—C1—C2 | 71.73 (12) | C1—N1—C10—C15 | −106.70 (14) |
| C7—N2—C2—O1 | 179.61 (14) | S1—N1—C10—C15 | 80.01 (14) |
| C3—N2—C2—O1 | 1.8 (2) | C1—N1—C10—C11 | 71.61 (17) |
| C7—N2—C2—C1 | 1.4 (2) | S1—N1—C10—C11 | −101.69 (14) |
| C3—N2—C2—C1 | −176.43 (12) | C15—C10—C11—C12 | 0.5 (2) |
| N1—C1—C2—O1 | 28.24 (17) | N1—C10—C11—C12 | −177.77 (14) |
| C9—C1—C2—O1 | −94.83 (15) | C10—C11—C12—C13 | −0.7 (3) |
| N1—C1—C2—N2 | −153.51 (11) | C11—C12—C13—C14 | 0.0 (3) |
| C9—C1—C2—N2 | 83.42 (15) | C11—C12—C13—C16 | 179.38 (17) |
| C2—N2—C3—C4 | −125.84 (14) | C12—C13—C14—C15 | 0.9 (2) |
| C7—N2—C3—C4 | 56.05 (17) | C16—C13—C14—C15 | −178.47 (15) |
| N2—C3—C4—C5 | −54.68 (15) | C11—C10—C15—C14 | 0.4 (2) |

# APPENDIX I

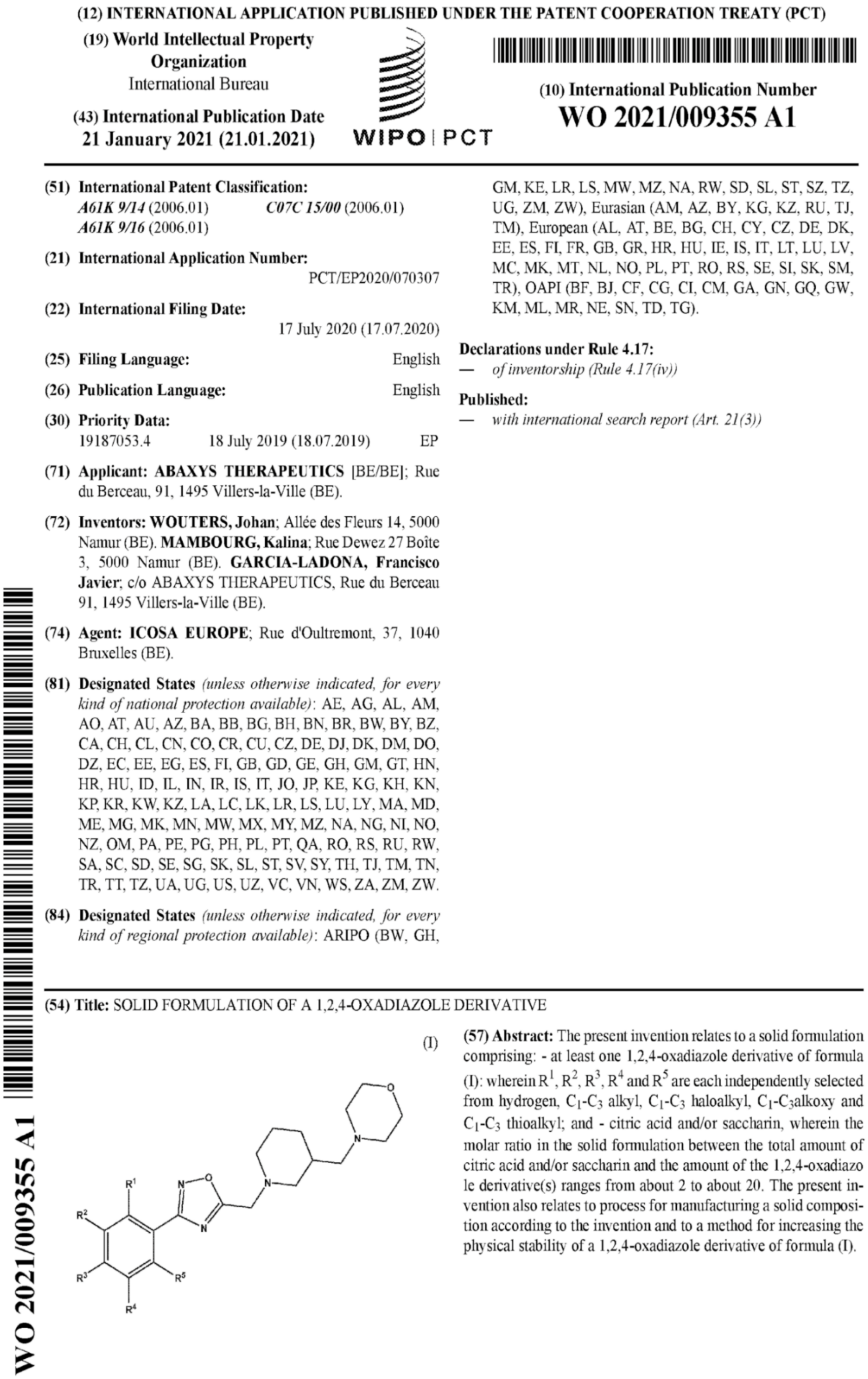

(12) INTERNATIONAL APPLICATION PUBLISHED UNDER THE PATENT COOPERATION TREATY (PCT)

(19) World Intellectual Property Organization
International Bureau

(43) International Publication Date
21 January 2021 (21.01.2021)

WIPO | PCT

(10) International Publication Number
WO 2021/009355 A1

(51) International Patent Classification:
*A61K 9/14* (2006.01) *C07C 15/00* (2006.01)
*A61K 9/16* (2006.01)

(21) International Application Number:
PCT/EP2020/070307

(22) International Filing Date:
17 July 2020 (17.07.2020)

(25) Filing Language: English

(26) Publication Language: English

(30) Priority Data:
19187053.4 18 July 2019 (18.07.2019) EP

(71) Applicant: **ABAXYS THERAPEUTICS** [BE/BE]; Rue du Berceau, 91, 1495 Villers-la-Ville (BE).

(72) Inventors: **WOUTERS, Johan**; Allée des Fleurs 14, 5000 Namur (BE). **MAMBOURG, Kalina**; Rue Dewez 27 Boîte 3, 5000 Namur (BE). **GARCIA-LADONA, Francisco Javier**; c/o ABAXYS THERAPEUTICS, Rue du Berceau 91, 1495 Villers-la-Ville (BE).

(74) Agent: **ICOSA EUROPE**; Rue d'Oultremont, 37, 1040 Bruxelles (BE).

(81) Designated States *(unless otherwise indicated, for every kind of national protection available)*: AE, AG, AL, AM, AO, AT, AU, AZ, BA, BB, BG, BH, BN, BR, BW, BY, BZ, CA, CH, CL, CN, CO, CR, CU, CZ, DE, DJ, DK, DM, DO, DZ, EC, EE, EG, ES, FI, GB, GD, GE, GH, GM, GT, HN, HR, HU, ID, IL, IN, IR, IS, IT, JO, JP, KE, KG, KH, KN, KP, KR, KW, KZ, LA, LC, LK, LR, LS, LU, LY, MA, MD, ME, MG, MK, MN, MW, MX, MY, MZ, NA, NG, NI, NO, NZ, OM, PA, PE, PG, PH, PL, PT, QA, RO, RS, RU, RW, SA, SC, SD, SE, SG, SK, SL, ST, SV, SY, TH, TJ, TM, TN, TR, TT, TZ, UA, UG, US, UZ, VC, VN, WS, ZA, ZM, ZW.

(84) Designated States *(unless otherwise indicated, for every kind of regional protection available)*: ARIPO (BW, GH, GM, KE, LR, LS, MW, MZ, NA, RW, SD, SL, ST, SZ, TZ, UG, ZM, ZW), Eurasian (AM, AZ, BY, KG, KZ, RU, TJ, TM), European (AL, AT, BE, BG, CH, CY, CZ, DE, DK, EE, ES, FI, FR, GB, GR, HR, HU, IE, IS, IT, LT, LU, LV, MC, MK, MT, NL, NO, PL, PT, RO, RS, SE, SI, SK, SM, TR), OAPI (BF, BJ, CF, CG, CI, CM, GA, GN, GQ, GW, KM, ML, MR, NE, SN, TD, TG).

**Declarations under Rule 4.17:**
— *of inventorship (Rule 4.17(iv))*

**Published:**
— *with international search report (Art. 21(3))*

(54) Title: SOLID FORMULATION OF A 1,2,4-OXADIAZOLE DERIVATIVE

(I)

(57) Abstract: The present invention relates to a solid formulation comprising: - at least one 1,2,4-oxadiazole derivative of formula (I): wherein $R^1$, $R^2$, $R^3$, $R^4$ and $R^5$ are each independently selected from hydrogen, $C_1$-$C_3$ alkyl, $C_1$-$C_3$ haloalkyl, $C_1$-$C_3$alkoxy and $C_1$-$C_3$ thioalkyl; and - citric acid and/or saccharin, wherein the molar ratio in the solid formulation between the total amount of citric acid and/or saccharin and the amount of the 1,2,4-oxadiazole derivative(s) ranges from about 2 to about 20. The present invention also relates to process for manufacturing a solid composition according to the invention and to a method for increasing the physical stability of a 1,2,4-oxadiazole derivative of formula (I).

WO 2021/009355 A1